Vicinal and Double Chemoselective Biofunctionalization of Polyoxazolines

Dissertation zur Erlangung des naturwissenschaftlichen Doktorgrades

der Julius-Maximilians-Universität Würzburg

vorgelegt von

Florian Pinzner

aus Schwabach

Würzburg 2020

Eingereicht bei der Fakultät für Chemie und Pharmazie am

_____

Gutachter*innen der schriftlichen Arbeit

1. Gutachter*in: _____

2. Gutachter*in: _____

Prüfer*innen des öffentlichen Promotionskolloquiums

1. Prüfer*in: _____

2. Prüfer*in: _____

3. Prüfer*in: _____

Datum des öffentlichen Promotionskolloquiums

_____

Doktorurkunde ausgehändigt am

_____

Wer etwas will, findet Wege,

wer nicht will, findet Gründe.

Die vorliegende Arbeit wurde in der Abteilung für Funktionswerkstoffe der Medizin und Zahnheilkunde, Julius-Maximilians-Universität Würzburg, Würzburg, Deutschland in der Zeit von April 2016 bis September 2020 unter der Leitung von Herrn Prof. Dr. Jürgen Groll angefertigt.

Table of Contents

List of Abbreviations and Symbols

°C	degree centigrade
Å	angstrom
AcOH	acetic acid
aff.	affinity
AIBN	2,2'-azo-bis(isobutyronitrile)
ATR	attenuated total reflection
Boc	*tert*-butyloxycarbonyl
bp	by-product
BSA	bovine serum albumin
ButenOx	2-butenyl-2-oxazoline
CaH_2	calcium hydride
cat.	catalyst
CD_3CN-*d3*	deuterated acetonitrile
$CHCl_3$	chloroform
*c*PrOx	2-cyclopropyl-2-oxazoline
CRD	carbohydrate recognition domain
CROP	cationic ring-opening polymerization
CsI_3	cesium triiodide
$CDCl_3$	deuterated chloroform
ConA	concanavalin A
conjug.	conjugate
COOH	carboxylic acid
Đ	dispersity
d	day
DCC	dicyclohexylcarbodiimide
DCM	dichloromethane
DCTB	*trans*-2-[3-(4-tert-Butylphenyl)-2-methyl-2-propenylidene] malononitrile
DecEnOx	2-decenyl-2-oxazoline
DLS	dynamic light scattering
DMF	dimethylformamide

DMAP	4-dimethylaminopyridine
DMPA	2,2-dimethoxy-2-phenylacetophenone
DMSO	dimethyl sulfoxide
D_2O	deuterated water
DTT	dithiothreitol
DVB	divinylbenzene
EDC	1-ethyl-3-(3-dimethylaminopropyl) carbodiimide
ee	enantiomeric excess
EP	equivalence point
EPR	enhanced permeability and retention
eq.	equivalents or equation
Et_2O	diethyl ether
EtOAc	ethyl acetate
exp.	experiment/experimental
FDA	U.S. Food and Drug Administration
FT	fourier-transform
funct.	functionalized
g	gram
Gal1	Recombinant Human Galectin-1
h	hour
HCl	hydrochloric acid
*i*PrOx	2-isopropyl-2-oxazoline
IR	infrared
Irgacure 2959	2-hydroxy-4'-(2-hydroxyethoxy)-2-methylpropiophenone
ITC	isothermal titration calorimetry
K_D	equilibrium dissociation constant
kDa	kilodalton
Lac*N*Ac	*N*-Acetyl-D-lactosamine
lit.	literature
LiOH	lithium hydroxide
LCROP	living cationic ring-opening polymerization

LCST	lower critical solution temperature
M	molar
MALDI-TOF	matrix-assisted laser desorption ionization – time of flight
max.	maximum
MBSA	3-mercapto benzyl sulfonate
MCR	multicomponent reaction
MeOH	methanol
MeOD	deuterated methanol
MeOx	2-methyl-2-oxazoline
$MgSO_4$	magnesium sulfate
mg	milligram
MHz	megahertz
min	minute
min.	minimum
mol.	molecular
mL	millilitre
M	molar concentration ($mol \cdot L^{-1}$)
M_n	number average molar mass
mmol	millimole
mol	mole
MPAA	4-mercapto phenylacetic acid
M_w	mass average molar mass
№	number
$NaNO_3$	sodium nitrate
NaN_3	sodium azide
NaOH	sodium hydroxide
NCL	native chemical ligation
NHS	*N*-hydroxysuccinimide
nm	nanometre
nM	nanomolar
NMR	nuclear magnetic resonance

NP	neutral point
*n*PrOx	2-*n*-propyl-2-oxazoline
PBS	phosphate-buffered saline
PE	polyethylene
PEG	polyethylene glycol
pHEMA	poly 2-hydroxyethyl methacrylate
PMeOx	poly(2-methyl-2-oxazoline)
P(MeOx-*co*-ButenOx)	poly(2-methyl-2-oxazoline-*co*-2-butenyl-2-oxazoline)
PNA	peanut agglutinin
P*n*BuOx	poly(2-*n*-butyl-2-oxazoline)
P*n*HpOx	poly(2-*n*-heptyl-2-oxazoline)
P*n*HxOx	poly(2-*n*-hexyl-2-oxazoline)
P*n*NonOx	poly(2-*n*-nonyl-2-oxazoline)
P*n*PeOx	poly(2-*n*-pentyl-2-oxazoline)
P*n*PrOx	poly(2-*n*-propyl-2-oxazoline)
POx	poly(2-oxazoline)
PP	polypropylene
ppm	parts per million
PPM	postpolymerization modification
PTFE	polytetrafluoroethylene
PVA	polyvinyl alcohol
PVP	polyvinylpyrrolidone
RCA	ricinus communis agglutinin
RT	room temperature
SAW	surface acoustic wave
SEC	size exclusion chromatography
SPR	surface plasmon resonance
TBD	triazabicyclodecene
TCEP	tris(2-carboxyethyl)phosphine
TFA	trifluoroacetic acid
theo.	theoretical

THF	tetrahydrofuran
THPP	*tris*(hydroxypropyl)phosphine
TLC	thin layer chromatography
TMDPO	(2,4,6-trimethylbenzoyl)diphenylphosphine oxide
*t*RNA	transfer ribonucleic acid
UV	ultraviolet
µg	microgram
µL	microlitre
µ	micrometre
µmol	micromole
V	volume
W	watt

Abbreviations of different signal shapes in NMR spectroscopy:

s	singlet
d	doublet
t	triplet
q	quartet
m	multiplet
dd	doublet of doublets
br.	broad
app.	apparent

Abbreviations of different signal shapes in IR spectroscopy:

w	weak
m	medium
s	strong
vs	very strong
br.	broad

Chapter 1

Introduction

Chapter 1 Introduction

In 1999, Williams defined a **biomaterial** as "a nonviable material used in a medical device, intended to interact with biological systems"[1]. Since then, the description of this term has continuously been updated, for example in 2007 by Park and Lakes as "any material to make devices to replace a part or a function of the body in a safe, reliable, economic, and physiologically acceptable manner"[2].

While, seen from a chronological point of view, a first goal for those materials was the need to be tolerated by living organisms, as it is the case for 'off-the-shelf' implant materials like titanium alloys, ceramics or basic thermoplastic polymers, the trend has shifted to more 'active' materials that interact with their environment in terms of cell recognition, specific protein adsorption or targeted cell binding and growth. The latest generation of **materials** are engineered to even have functional properties in terms of regulation of biological processes, degradation of the material or fighting infection after implantation.[3-4]

Fine-tuning the characteristic properties of such components is especially challenging as they are in contact with living matter and a lot of research has yet to be accomplished concerning those highly complex interactions. A promising advance in this field was the combination of synthetic polymers and biological polymers or substrates via *bioconjugation*, a process that focuses on combining two different materials, each one carrying complementary properties and functions. This can be achieved in manifold ways[5] – according to Koniev and Wagner[6], bioconjugation describes "a set of techniques allowing site-specific creation of a covalent link between a biomolecule and an exogenous moiety that endow it with desirable properties."[6]

'Classic' **synthetic polymers** such as polyesters, polypropylene (PP), polyethylene (PE) as well as polytetrafluoroethylene (PTFE) offer simple processability[7-8] and are usually biologically inactive and insoluble in water. On the other hand, polymers that shifted into focus for the design of bioactive or biomimetic materials are often hydrophilic, e.g. water soluble polymers,[9-10] with polyethylene glycol (PEG) as gold standard being one of the few candidates that has been implemented in medical applications.[11] Apart from PEG, other hydrophilic polymers are also under intensive investigations. One of the promising candidates as an alternative to PEG are polyoxazolines (POx)[11-13], which will be in focus of this work.

Biological molecules, which in general can be categorized into peptides and proteins, (poly)saccharides and polynucleotides[3] exhibit properties like biodegradability, usually low toxicity and low immunogenicity as well as specific recognition and binding attributes.[14-15] To put it in a nutshell, their interactions in biological systems make them ideal materials for biomedical applications.[16-18]

Combining both materials to achieve 'the best of both worlds' is thus an attractive goal. It has already been proven that conjugation of synthetic polymers to proteins significantly expands properties such as stability, circulation half-life and solubility[19-20] or even modulates protein activity[21-22]. This can for example lead to a more stable and efficient therapeutic[23-25] or an assembly for medical diagnostics.[26-30]

Simultaneously with developing new materials, however, it is crucial to obtain a genuine understanding of the underlying processes that are involved in material-tissue interactions. There is a great need to develop experimental settings that allow for the in-depth ***analysis*** of biochemical interactions, ideally in a controlled or isolated environment.

One example for such a system could be the recognition of enzymes or lectins and their respective substrates. It is conceivable to investigate suchlike systems by adhering the individual interaction partners to solid surfaces or matrices for precise and targeted measurement. Obviously, this fixation needs to be carried out in the most controlled way possible, with an accurate structural architecture and a thorough analysis of the conjugates.

It gets more complicated, when not only two, but multiple target moieties need to be positioned relatively to each other. While a lot of research focuses on the conjugation of two single components, in biological environments, one-fold interaction of two isolated binding partners exhibit only low binding affinities with values ranging in the millimolar scale, which is usually not sufficient enough to effectively mediate biological processes *in vivo*.[31] Especially in the field of saccharides, where multivalent recognition effects are responsible for the effectiveness of a binding event, there are a lot of effects involved that additionally affect affinity, such as synergistic effects or avidity. Yet, to date, little systems are available that allow for the distinct monitoring of those effects. Focus especially lies in the field of glycosides and polysaccharides[32-34], yet there are also some examples in the fields of peptides and polymers.[35-36] The overall demand for synthetic polymers with multiple side chain groups acting as multivalent ligands to increase avidity[33] is high.[37]

Most of such multivalent systems are based on the use of *similar* ligands. Multivalent materials however also allow for the introduction of *different* components with various functions to the basis material, for example if the carrier material is equipped with a drug molecule, a labelling marker and a targeting sequence all at the same time.[21, 38-39] Such multivalent ligand carriers are emerging as molecular imaging probes and diagnostic tools as well as therapeutic delivery vehicles in the field of autoimmune diseases, infectious diseases, cancer and inflammation[40-43].[44]

Compared to two-component conjugates, the complexity of design strategies and synthetic challenges are increased massively when three or more different compounds are conjugated. Limitations lie within aspects of chemoselectivity of the conjugation reactions, reactivity decline, control over ligand spacing and distance as well as steric hindrances.[22]

There are some approaches to conjugate three or more components - however, according to Espeel et al., "in literature, very few examples have been reported that provide the possibility of introducing more than one functionality at the same site."[45] Furthermore, most approaches attach the components at different sites of the polymer backbone and rely on a statistical distribution of ligands, which bears challenges in terms of product uniformity.[39]

Most recently, multicomponent reactions (MCR)[46-48] and more specifically, multistep conjugations relying on thiolactones as means for double post-polymerization modification[45, 49] have been used as a strategy in this field. Yet, although there are some examples of MCRs used for peptide conjugation in areas such as protein PEGylation, protein labelling and the synthesis of drug conjugates[50-51], only few polymers have since been used for this technique, with the main focus lying on (poly)saccharides[50, 52-53].[54]

The **aim of this work** was to provide a fundamental toolbox to create three-component polymer conjugates with a defined architecture, bearing two different biocomponents that can each interact with larger biological systems. These interactions were then extensively investigated in biomacromolecule recognition experiments.

Because there is still an immense need to fully understand these materials, focus lay on several challenges: General control over design, especially ligand distance and degree of functionalization, as well as control over rate of conjugation.

A target architecture that seemed conceivable for this aim was the fixation of two substrate-bearing functional 'arms' to one single point on a (polymer) surface/matrix, with the possibility to easily adjust/customize the length of the linker. To present knowledge, no polymer system with such an architecture has yet been developed and established.

Hydrophilic polyoxazoline polymers served as a basis material. As bioactive compounds, different peptide and saccharide moieties were evaluated. Control over the relative space between the ligands was obtained by attaching them vicinally at one binding site. This was implemented by a set of two well-established consecutive reactions: First, the Native Chemical Ligation, which is one of the major and commonly used methods in peptide ligation. It delivers a free thiol group directly at the binding

site between a thioester and a cysteine component. This thiol in turn can be used to chemoselectively attach an allyl component via the thiol-ene reaction, which is perceived as a very reliable click reaction. This work therefore explores an alternative in multistep conjugation techniques aiming to chemoselectively conjugate a hydrophilic polymer and two biological moieties. Reaction parameters and their impact on the outcome were monitored and evaluated throughout the whole reaction cascade.

Prior to this set of reactions, the relevant educts, namely thioester functionalized *polyoxazolines* needed to be synthesized. The inverse case: Coupling of thioester functionalized *peptides* and cysteine functionalized polymers[55], already exists. However, it is more feasible to instead equip polymers with the respective thioester functionality, since cysteine is one of the natural amino acids that already can easily be integrated into peptides.

The success of all cascade reaction steps leading to the final conjugation product were proven through recognition experiments with biomacromolecules, in this case, lectins. For this, specific affinity pairs of the respective binding partners were identified and the affinity difference between several conjugates, for example different derivates of saccharides and peptides and a combination of both peptides and saccharides was determined.

These experiments were realized by performing affinity measurements with surface acoustic wave (SAW) and surface plasmon resonance (SPR) spectroscopy and simultaneously served as proof of principle experiments for the feasibility of using such conjugates in biomedical applications. A specific design of the polymers, that allows for the attachment of the conjugates to the gold surface of the SAW and SPR devices, was needed for those methods and was implemented by using a strategy yielding novel double α as well as ω telechelic functionalized POx.

Furthermore, the degree of controlled functionalization at the end group as well at the side chain was investigated by comparing the conjugates resulting from both strategies.

For a content overview and a more detailed description of the approach that was pursued in order to realize the aim of this work, the reader is directed to Chapter 3 – The Approach of This Thesis.

Chapter 2

State of the Art: Hydrophilic Polymers as Biomaterials

Chapter 2 State of the Art: Hydrophilic Polymers as Biomaterials

Chapter 2.1 Biohybrid Polymers

Chapter 2.1.1 Polymer-Biomacromolecule Conjugates

Polymer peptide hybrid materials play an important role in biotechnological research, for example for drug delivery systems, implants or tissue engineering and in nanotechnology, for instance as biosensors or medical diagnostics.[30, 36, 56-57] Several review articles have described the synthesis and applications of polymer bioconjugates and hybrid biomaterials.[7-8, 26, 36, 44, 58-65]

Whereas peptides contribute to those hybrid conjugates with their (hierarchical) structural properties through non-covalent interactions, their self-organization functionality, low toxicity and low immunogenicity as well as specific recognition and binding attributes in biological systems,[14-15] which makes them ideal molecules for use as therapeutic agents or as molecular sensors and switches[16-18], polymers are biologically inactive and show resistance to enzymatic degradation, yet they can still be biocompatible and show a stealth effect, combined with a good processability.[7-8] Merging the properties of these compounds is an attractive strategy to synergistically combine the properties of both macromolecular families. It has already been proven that attachment of synthetic polymers to proteins significantly improves properties such as stability, biocompatibility and solubility[19-20] or even modulates protein activity[21].[26] One of the most prominent examples hereof is PEGylation, which is used to improve circulation half-life, stability or immunogenicity of therapeutic peptides[66] and has led to the development of several anticancer agents[17, 67]. In a work of Ding, Dong and Fong et al., stimuli responsive polymers such as thermo-responsive protein conjugates have also found application for selective protein isolation and affinity separation, used to facilitate protein purification or its easy recovery from a reaction mixture[68]. When treated with an external stimulus such as light, temperature or pH, the conjugates change their conformation and phase-separate from solution.[21, 69-70] If the stimulus is absent, the polymers are soluble again.[26, 61]

Chapter 2.1.1.1 *Architecture*

There are several different architectures of polymers and polymer conjugates[62] (see **figure 1**, top), the most common ones being the head-to-tail conjugate (see **figure 1** A), which is also called a telechelic functionalization of polymers. In this monovalent configuration, a peptide or other biomacromolecule is connected to a polymer at its chain-end. Then there are more complex, comb-shaped polymer conjugates, where the biomacromolecules are multivalently attached at the side-chain of the polymer backbone (see **figure 1** B). This configuration can be interesting for synergistic effects that will be described in chapter 2.1.2. The highest complexity and an even higher density of biomacromolecules is achieved in dendrimeric structures (see **figure 1** C).[62]

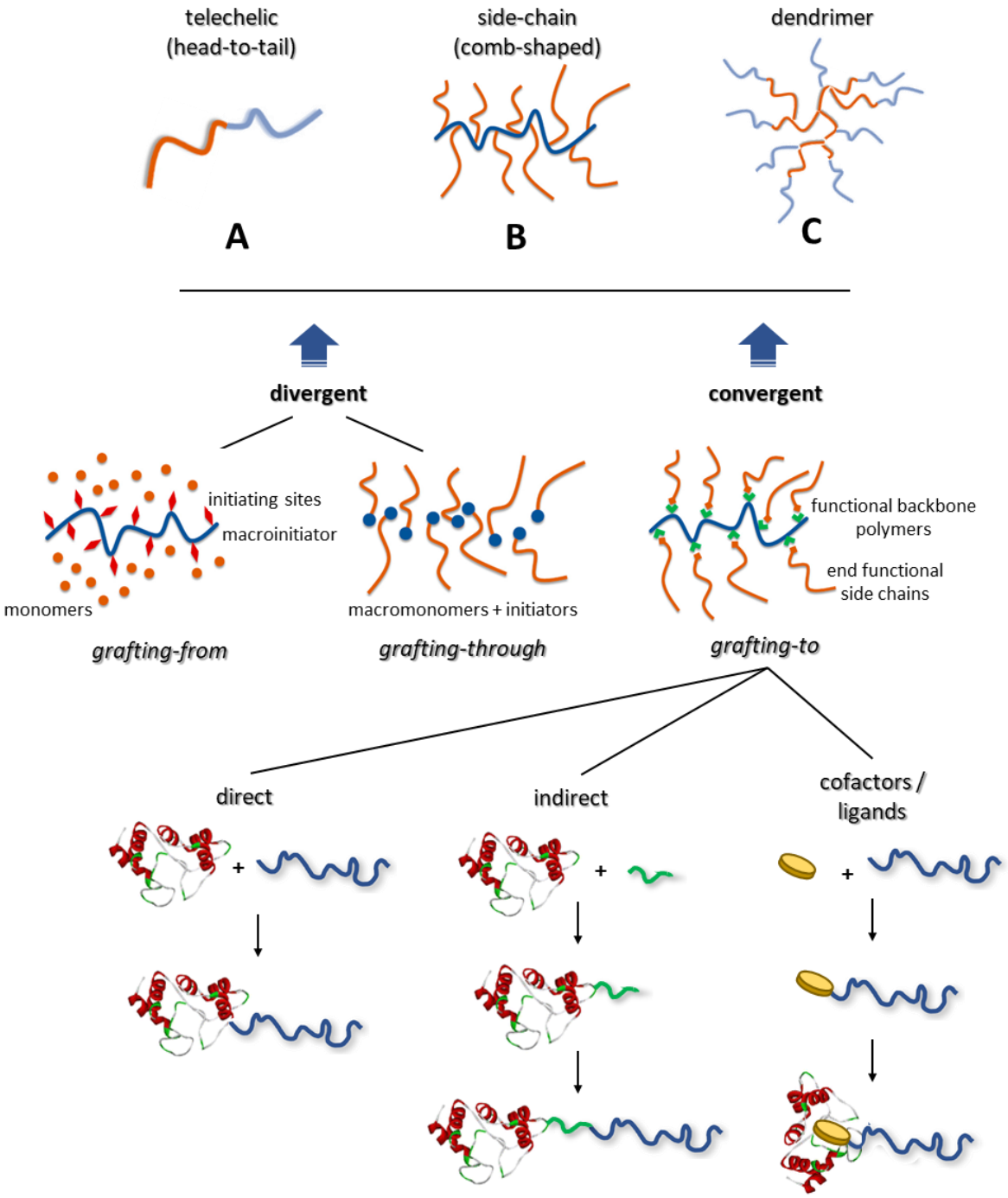

Figure 1: Top: Diverse architectures of polymer conjugates. Bottom: Different strategies in creating polymer conjugates: Divergent (*grafting-from* and *grafting-trough*) and convergent (*grafting-to*). The *grafting-to* approach can be done direct, indirect or via the use of cofactors/ligands. Adapted with permission from [71] and [61].

Chapter 2.1.1.2 *Synthetic Approaches for Peptide-Polymer Conjugates*

For the synthesis of peptide-polymer conjugates, there are several general approaches (see **figure 1**, bottom), whereas for each of the strategies explained hereafter, there exist solution phase as well as solid phase techniques[62]: There is the *divergent* approach, which is further subdivided into a *grafting-from* and *grafting-through* mechanism. By *grafting-from*, the hybrid material is synthesized from a peptide[72-73], respectively polymer[56-57] macroinitiator. The *grafting-through* technique, on the other

hand, polymerizes the hybrid materials from peptide- respectively polymer-functionalized (macro)monomers[74-75].[61]

In the *convergent* approach, which is also called the *grafting-to* method, both the polymer and peptide block are synthesized and functionalized separately and afterwards coupled together at one or multiple reactive sites. This can happen either *direct*[76-77], where both blocks are conjugated together without the use of a linker molecule, *indirect*[78-79], where a spacer molecule is first attached to the one partner and then linked to the other compound or via *cofactors or ligands*[80-81], that are attached to one of the blocks and show a specific affinity to the respective other one (see **figure 1**, bottom).[61]

Each method shows specific advantages or disadvantages. With the divergent approach, not only is the attachment of a small initiator molecule to a macromolecule easier than conjugation of two large macromolecules, but also a challenging removal of excess non-conjugated macromolecule is not necessary.[82] Still, the main drawback is that the macromolecule needs to be compatible with the polymerization conditions, since it is involved in all synthetic steps and synthesis of macromolecular initiators and monomers is not trivial.[62, 83]

The convergent approach on the other hand faces those exact difficulties of removing macromolecular starting materials and/or by-products from the desired conjugate and having reduced conversions due to limited accessibility of functional groups on macromolecules relative to small molecules.[8] Nevertheless, it allows for a broader range of functionalization and the lack of reactivity can be circumvented by using heterofunctional spacer molecules, for example in the indirect conjugation method.[61]

In this work, the approach that will be used for the synthesis of bioconjugates is the convergent grafting-to method, which will be further elucidated in chapter 2.1.3 - Chemical Coupling Strategies.

Chapter 2.1.2 Multivalency and Synergistic Effects

When it comes to interactions between biopolymers and biological systems, *multivalent* compounds are widely discussed in literature[34-35, 40, 84-88] since they are pivotal to a vast array of biological situations.

Chapter 2.1.2.1 *Key Terms*

When speaking of polymers or conjugates with multiple side chain functionalities and the concomitant structural attributes, a few key terms need to be defined and differentiated first:

Affinity is a biochemical parameter that indicates the degree of interaction between ligands and receptors.[40] The **equilibrium dissociation constant K_D**, which describes how tightly a ligand binds to a

particular protein or surface, can be used as a measure to quantify affinity. It can be determined by methods such as SPR[89], which measures association and dissociation rates of multivalent conjugates that are streamed over a receptor-laden surface or isothermal titration calorimetry (ITC)[90], which measures the enthalpy of binding events in solution.

Avidity is "the accumulated strength of multiple affinities summed up from multiple binding interactions and is commonly referred to as a functional affinity."[91] As such, avidity is distinct from affinity, with the latter only describing the strength of a single interaction.

Concerning multiple binding interactions, sometimes a **synergistic effect** can be observed, which occurs, when the combined power of several individual binding events is greater than the total power achieved by each event taking place separately.[92]

Synergistic effects can be a part of **cooperativity** phenomena, especially in the case of positive cooperativity. From a very theoretical point of view, cooperativity describes the "interplay of two or more interactions, so that the system as a whole behaves differently from expectations based on the properties of the individual interactions acting in isolation."[93] In practical terms, cooperativity occurs, as soon as the *affinity* for subsequent binding of a second or third ligand is altered by the binding of the first ligand.[94] This is the case in protein, DNA or RNA biopolymer folding processes[95] or for example in oxygen binding to haemoglobin[96], where the first oxygen molecule facilitates the binding of subsequent molecules. Depending on whether one interaction favours or disfavours another, the effect is referred to as positive or negative cooperativity.[93]

Cooperativity should not be mistaken for **allostery**, which was first introduced in 1961 by Jacques Monod and François Jacob[97]. When the binding of a ligand leads to a *conformational* change in a protein, thus changing the availability of a distant site for another substrate, the term allostery is used. Through the utilization of regulatory molecules such as activators or inhibitors, which allostericly change the accessibility of a binding site for a different ligand, enzymes are able to modulate chemical reactions.[94]

While it is rather used as a term when the bonding of ions and molecules to *metal ions* is presented, **chelation** can also be used for the description of biochemical binding events and it refers to the binding of multiple ligands to an equal number of binding sites. This typically increases strength and stability of the binding event.[40]

Chapter 2.1.2.2 *The Purpose and Design of Multivalencies*

According to Lee and Lee, "the recognition and binding of carbohydrate is important in many biomedical topics, e.g., the initial recognition and the binding of invading microorganisms and their toxins. Inhibitors for the binding step may be potentially important therapeutic agents."[86] However,

affinities of single interactions with low selectivity, such as hydrogen bonds and hydrophobic as well as electrostatic interactions between monomeric ligands and receptors in biological systems, e.g. for the interaction of single saccharides with peptides, are often quite weak, with K_D values ranging in the millimolar scale, which is usually not sufficient enough to effectively mediate biological processes *in vivo*.[31]

Multivalent interactions on the other hand make up for those small monomeric affinity values. The bindings, which are still reversible, differentiate multivalency from covalent interactions.[98] Yet, multiple interactions between numerous binding sites for several ligands strengthen the binding and therefore enable K_D values in the order of micromolar.[90, 99] For glycosides, this is known as the 'cluster glycoside effect'[99-101] and it plays an important role in a vast array of biological and pathological process, such as cell signalling, cell growth and differentiation events, apoptosis, as well as the treatment of cancer and microbial infections.[40, 102-103]

Therefore, the demand for synthetic polymers with multiple side chain groups acting as multivalent ligands which increase avidity[33], is high.[37] By attaching carbohydrates, proteins and dyes to polymer scaffolds, multivalent conjugates can not only be used to exhibit targeting properties, but also to improve aqueous solubility and provide labelling features.[39] Such multivalent ligand carriers are emerging as molecular imaging probes and diagnostic tools as well as therapeutic delivery vehicles in the field of autoimmune diseases, infectious diseases, cancer and inflammation[40] and are for example applied as alternatives in pharmaceutical and biomedical uses in drug delivery[41] and in filtration of bacteria from water[42-43].[44] Multivalency can be used as a means to counterbalance ligand affinity loss. For example, Kanazaki et al.[104] discussed the binding affinity to serum albuminum, where a dye is multivalently coupled to POx, and Takasu et al. suggested that multivalent attachment of galactosides to POx polymers induced a clustering effect on the inhibition of the lac-suppressor.[105]

a. Multivalent Binding Modes

It is necessary to distinguish between the various forms of multivalent binding that can occur between multivalent ligands and the respective binding sites or receptors.

In his work[106], Robert Luxenhofer precisely and thoroughly describes the different multivalent binding modes (see **figure 2**). The most straightforward amplification of recognition events is explained by a statistical effect, where the binding moieties are arranged in close proximity to each other due to the connecting polymer backbone, therefore enhancing a rapid follow-up binding of neighbouring ligands (**figure 2 a**). Simultaneous binding of a number of ligands that are bound to the same scaffold (**figure 2 b**) decreases the rate of dissociation of each individual ligand, thus increasing the overall affinity of the substrate compared to monomeric ligands. Subsite binding, as it is depicted in **figure 2 c**, describes a chelation effect of multiple interconnected ligands interacting with different binding sites of the

receptor. In some biological systems, the attachment of one ligand can induce a signal that leads to receptor clustering, which in term enhances the chances of multivalent binding (**figure 2 d**). If the polymer backbone bears different ligands that pair with various receptors, the simultaneous binding of those to different receptors can induce cooperativity or allostery effects (**figure 2 e**). Finally, competitive binding of (monomeric) ligands can be impeded, if the multivalent system is sterically demanding and shields the receptor from other binding partners (**figure 2 f**).[106]

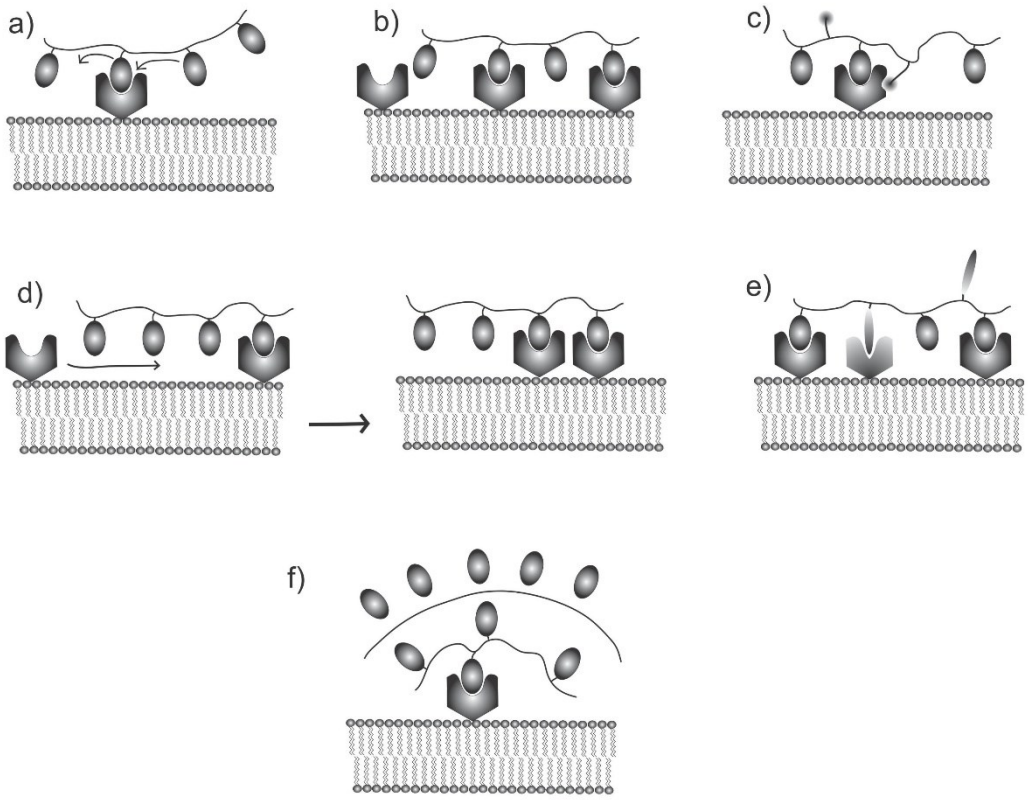

Figure 2: Simple illustration of various bindings modes of poly- and multivalent ligands: a) statistical effect, b) chelation of receptors, c) subsite binding, d) receptor clustering, e) simultaneous binding of different receptors and f) steric shielding. Reprinted with permission from [106].

Those different binding modes allow for a broad scope of multivalent polymer designs. The most relevant parameters that need to be considered are depicted hereafter.

b. Design

Concerning the design of multivalent polymers, there are several structural aspects to be considered: The length of the polymer, the polymer composition and functionality, the density of the ligands, the flexibility of the polymer backbone, and obviously the overall structure.[31, 107] For the latter factor, there are various architectures possible – linear, brush-like, branched, star-shaped, mesh and vesicle topologies (see **figure 3**).[107-108]

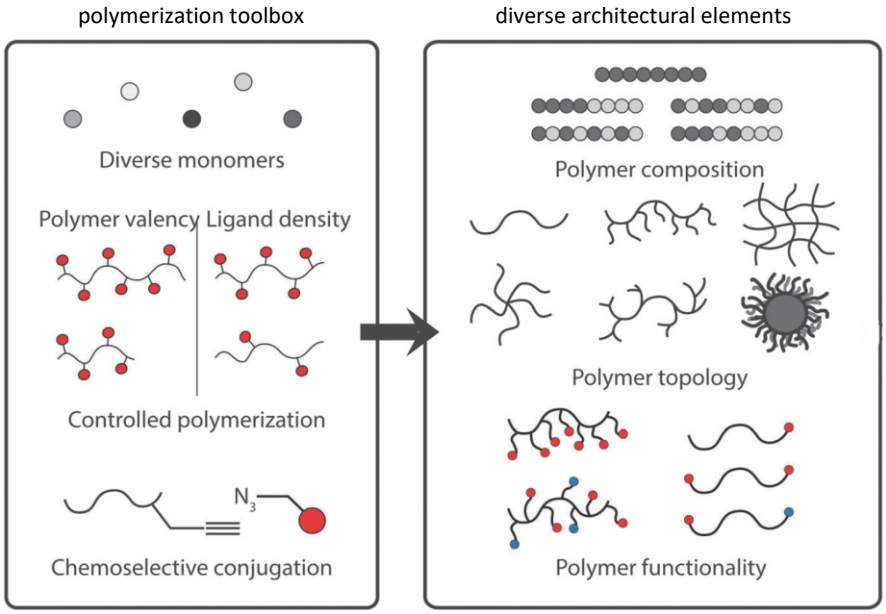

Figure 3: Diverse architectural elements for the design of multivalent polymers. Adapted from [107] with permission from The Royal Society of Chemistry.

Length and Functional Affinity

With regard to the length of polymers, using transmission electron microscopy, it could be shown for glycopolymers, that the number of bound receptors grows with increasing length and valency of the scaffold.[109-110] Polymers with a defined length can be used to measure the distance between binding sites, as it was used in the case of Concanavalin A (ConA), where studies found that the most active glycopolymers were able to at least bind to two different binding sites of the tetramer (see **figure 4**)[111] or in the case of peanut agglutinin (PNA), where the binding to the lectin was decreased for shorter spacer lengths, which made the sugar ligand less accessible to the binding sites[112].[44]

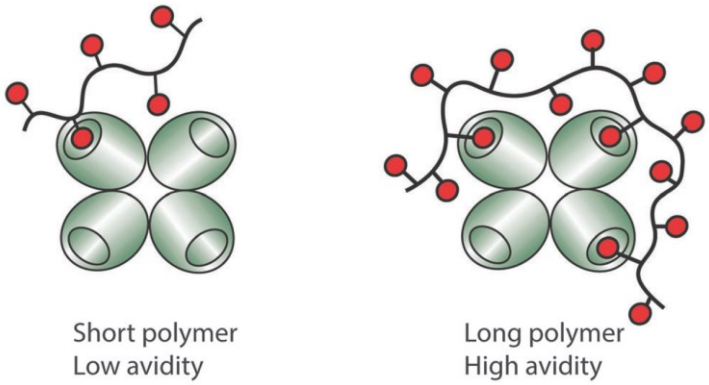

Figure 4: Increasing polymer length (and valency) allows polymers to span multiple binding sites in oligomeric proteins, thereby increasing their functional affinity (avidity). When all accessible binding sites are occupied, further increases in polymer length will not yield enhancements in functional affinity. Reprinted from [107] with permission from The Royal Society of Chemistry.

Density and Spacing of the Ligands

Appropriate spacing between different ligands, in other words, density of the ligands, can have a crucial influence on avidity.[107] In a study where the ratio of mannose units per polymer chain was varied[110], the authors found that an increase in density increased the avidity and ability of the glycopolymer to bind to ConA.

However, an increased density not necessarily leads to an increase in avidity, as research of Kiick and coworkers on the inhibition of glycopolymers to cholera toxin[113-114] displays. They argue that the interaction of the polymer with the receptor decreases with increasing density of the ligand due to non-optimal spacing between the different binding sites.

Therefore, control over the exact spacing between ligands seems to be more important than length of the polymer and density of the ligands in general.[34] These findings are backed by similar experiments, for example when spacing between ligands is matched to fit distances between binding sites in ConA[115] or when the distance of ligands is approached to the distance between dimeric 2Gl2 antibody binding sites[116].[107]

Flexibility of the Polymer Backbone

The Flexibility of the polymer backbone can have an additional influence on binding affinity.[85] For instance, Kobayashi et al. showed that the binding of glycopolymers to lectins is often weak for stiff ligands[117] and Stenzel et al. also showed that flexible PEG linker systems were more effective inhibitors than rigid poly 2-hydroxyethyl methacrylate (pHEMA) linker systems[118].[107]

Chapter 2.1.2.3 *Lectins and Carbohydrates*

Lectins count to one of the most extensively studied receptors of multivalent binding. There is a number of reviews to those cell surface receptor proteins[32, 86, 101-102, 119-120] as well as other protein-carbohydrate interactions[87-88]. Since 1960, a vast array of lectins has been isolated from plants, animals and micro-organisms together with the corresponding saccharides as specific binding partners.[32, 121] The legume family is the largest family among the simple plant lectins[32] and many of them have been isolated and structurally characterized[122]. Their molecular weight is usually around 40 kDa, with typically 2-4 binding sites[32] and prominent representatives are lectins such as ConA, RCA and PNA. They play a pivotal role in cell adhesion, immune defence as well as glycoprotein trafficking and clearance events, which have been extensively studied by methods such as ITC and SPR[90, 123].[44]

The binding sites of lectins called CRD, carbohydrate recognition domains, are often shallow depressions on the surface of the protein and usually correspond to about 120-160 amino acids, which are preformed, as only few conformational changes occur upon binding[124].[101, 125] However, as mentioned before, most saccharides only bind weakly to their lectin counterparts, with effective

mediation of biological processes only made possible by a multivalency effect, which in terms depends on the density of the recognition domains, cluster structure or design of the glycoconjugate.[125] Furthermore, although the CDR involves similar key amino acids being involved in carbohydrate binding, different lectins show unique specificity. For instance, while ConA is specific to glucose and mannose, PNA mainly binds galactose.[101]

a. Concanavalin A

ConA, a lectin extracted from jack beans, has been studied intensively since the 1970s[126-128] and is the most prominent lectin of the legume family. It has a tetramer structure (see **figure 5**) with four saccharide binding sites and its facile isolation, its interaction with a broad range of sugars[101, 129] as well as characterization by X-ray crystallography[127-128, 130-131] lay ground for extensive studies of sugar-protein interactions[132-134].[31] While it displays a strong affinity to mannose, ConA also binds glucose.[32]

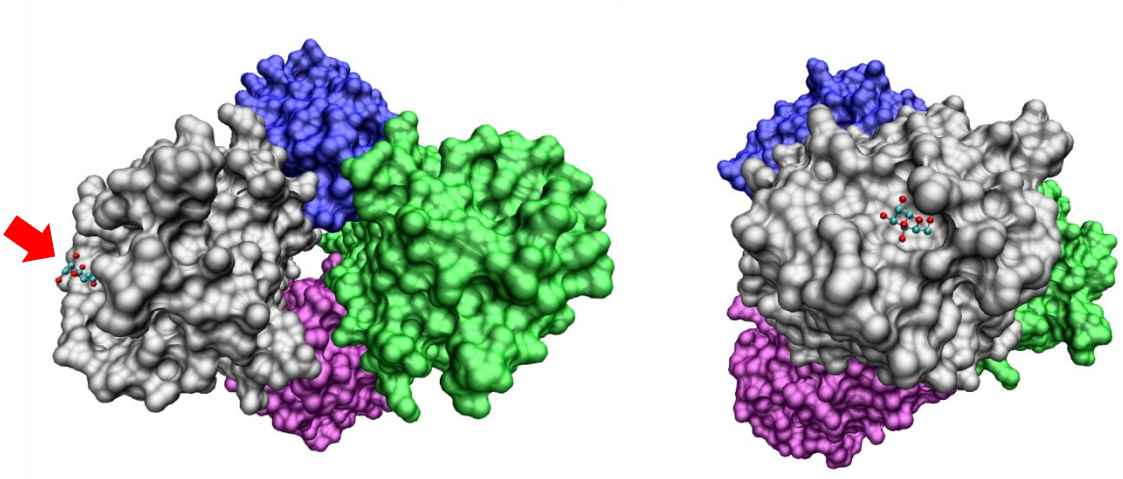

Figure 5: Tetramer structure of ConA with mannose (highlighted with red arrow) located in one of its four binding pockets. Pictures based on the crystal structure 5z5n from RCSB database[135] and created with VMD Molecular Graphics Viewer[136]. Left: Front view with the four tetrameric subunits. Right: Side view with focus on the saccharide binding pocket.

Apart from a vast array of studies with glycopolymers[89, 100, 110], the affinity of ConA to synthetic polymers such as POx glycoconjugates and the resulting formation of aggregates and clusters has been examined for example by Kempe et al.[37] and Hoogenboom et al.[137]. In their work, they used turbidity assays or light scattering to investigate different solution behaviour of the conjugates dependent on the conjugated compounds.[138]

b. Galectin

Galectins are a family of proteins based on their galactoside binding ability. Although to date, there are only 15 mammalian galectins identified as members of this family, they are involved in a wide range of physiological functions like cell migration, immune responses, inflammation, signalling and autophagy, associated with various heart diseases and cancer.[119] The architecture of galectins is manifold and they exist as monomers (galectin-5, -7, -10), homodimers (galectin-1, -2, -11, -13, -14, -15) or multimers (galectin-3, -4, -6, -8, -9, -12).[120] Focus in this work lies on the Recombinant Human

Galectin (Gal1), which is biologically active as a dimer in solution[139]. It is differentially expressed by various normal and pathological tissues and its expression, respective overexpression in tumors and tumor-surrounding tissue, which is often associated with dissemination of tumor cells and tumor immune-escape[140] makes the lectin an interesting target for up to date research[141-143].

The CRD of galectins, which contains about 130 amino acids[144] usually interacts with lactose or *N*-acetyl-lactosamine[86, 137] in relatively low levels of affinity (K_D ~50 µM)[145-146].

However, some galectins are able to recognize modifications of these saccharide ligands, which allows for the design of even more specific sugar derivates, as it was done for instance from Seibel et al.[147]. Beyond that, according to Johannes et al.[119], some galectins even interact with several non-galactose-containing binding partners, and their respective CRD and other areas of the protein exhibit non-carbohydrate binding sites as well[148-149]. Gal1 in particular is engaged in a great number of protein-protein interactions[140], which, for instance, are highlighted in the work of André et al., who identified a specific interaction between the galectin and a WYKYW peptide sequence.[150]

Chapter 2.1.2.4 *Challenges with Multivalency*

The construction and examination of multivalent compounds faces several difficulties, most of which are comprisingly addressed in a thorough review by van Dongen et al.[39] "*Multivalent Polymers for Drug Delivery and Imaging: The Challenges of Conjugation*", which therefore was utilized to serve as a basis to this subchapter.

a. Statistical Parameters

First, one must consider the extensive impact product distributions and conjugation statistics have on the analysis of multivalent conjugates. As an example, imagine a multivalent polymer scaffold with a large excess of binding sites that in theory is conjugated with 4 ligands, 5 drug molecules and 3 dye residues, as depicted in the review by van Dongen et al.[39]. A statistically controlled attachment reaction of each ligand leads to a Poisson distribution of products, with the theoretically intended 4-5-3-distribution of ligands in an ideal product making up only 1 out of every 250 (0.8 %) particles present[39], not to mention the dispersity in length of the polymer itself. A variety of influences such as solubility, mass transport, auto catalysis, binding cooperativity and steric hindrances may further promote non-statistical product formation.[151-152]

This can have a crucial impact in terms of biological behaviour such as targeting, imaging or therapeutic effects, since there might be a lot of products conjugate compounds lacking one or multiple of the attached ligands, therefore missing the respective function and property. In literature, mean conjugation numbers are often predicted from the initial stoichiometry of all educts and investigations of multivalent materials, where stoichiometry or the distribution of products were characterized, are very rare. Or, as van Dongen[39] puts it in his review: "Heterogeneity in theranostics resulting from

polymer conjugation is often overlooked, underestimated, or simply not addressed due to the difficulty in assessing it with available characterization tools."[39] Nevertheless, it is crucial to address this matter in the best possible way.

a. Measuring Techniques

Hest et al. state that "many of the methods most commonly employed to characterize synthetic polymers are difficult to extend to biological macromolecules".[22] This is easily understandable, as those molecules bear a vast array of functional groups and have a complex tertiary or quaternary architecture. Correspondingly, a lot of analytical methods are difficult to employ for polymer conjugates, due to the broad molecular weight distribution (dispersity) and an ambiguity concerning the binding site of the conjugated moiety.[22] Regardless of whether spacing and distribution of ligands along a polymer matrix, the influences of distance between ligand functionalities or other local resolution effects are in the focus of investigation, such material properties are extremely difficult to determine and rely on sophisticated analytical strategies. Although there is a range of measuring techniques to investigate conjugate samples, for example nuclear magnetic resonance, infrared and RAMAN spectroscopy, optical absorption (UV-Vis), or elemental analysis, none of these methods delivers any information about the ligand distribution of the final product species.

Following an argumentation of van Dongen et al., "even for physical techniques capable of measuring the distribution of products, such as chromatography[153-154], photobleaching[155], and mass spectrometry[152], characterization of conjugation distribution remains challenging in the presence of scaffold mass and structural dispersity."[39] Those methods are generally incapable of differentiating between individual species contributing to the distribution[151, 153] and in case of mass spectrometry in particular, all analytes need to bear the same ionization probability in order for a quantitative analysis to be successful.[39]

Synthetic strategies to overcome these challenges include the use of high density (excessive) ligand systems[156-158], the optimization and exploration of cluster and local concentration effects[159-160] and bio-inspired synthesis methodologies[161-165].

This work's approach in addressing some of these challenges in precisely determining aspects of polymer conjugation will be to gradually increase the complexity of the investigated systems in order to transfer parameters and analytical output from the most basic to progressively more complex compounds. Therefore, discoveries and conclusions from simple investigated structures and basic experiment setups can easily be transferred to increasingly intricate systems. Further elements of this approach will be illustrated in detail in Chapter 3 - The Approach of This Thesis.

Chapter 2.1.3 Chemical Coupling Strategies

This work is focused on the *grafting to* technique for the formation of polymer-peptide and polymer-peptide-glyco conjugates (see **figure 1**). In their review article, Gauthier and Klok[8] comprehensively summarize the various possibilities to prepare peptide-polymer conjugates, which will be recapitulated in this chapter by giving an overview over the strategies that can be employed to synthesize peptides, sugars and polymers with functionalities needed for *grafting to* conjugation and presenting several different conjugation methods of the respective components.

Chapter 2.1.3.1 *Preparation of Polymer-Reactive Peptides*

In this subchapter, multiple ways to introduce chemoselective handles onto natural or synthetic peptides/proteins are presented.

One of the basic requirements is the presence of specific amino acid residues that can be chemoselectively modified without influencing the side chains of other amino acids. This is especially challenging when site-specific modification is needed, but multiple copies of the respective amino acids are present. Three strategies can be chosen to tackle this issue: Either by selecting amino acids that are naturally less abundant in peptides or proteins such as tryptophan or cysteine. Another possibility is to select amino acids that are over-or underrepresented in their location in the peptide, which is for example the case for *C*- or *N*-terminal regions. Finally, it is possible to select amino acids by their surface exposure, which means to choose amino acids that are more easily accessible on the surface of proteins than in the core of the protein. At the same time, accessibility of amino acids on the surface of large proteins is an important factor for the success of functionalization reactions.[8] Another requirement for protein functionalization is that the protein conformation or function cannot be affected by polymer conjugation. This has to be taken into account when amino acids are targeted that can have a structure-forming impact on the protein such as cysteine by undergoing disulfide bridge formation.[8]

Peptide amino acids can be modified either at their side group or at the *N*- or *C*-terminal groups. Modification at the side group is different for each individual amino acid. Some examples for the most common amino acids are targeting the lysine side chain amino group with electrophilic reagents such as activated carboxylic acids[166], aldehydes or ketones[167], isocyanates/isothiocyanates[168], imidoesters and Traut's reagent[169] or thioesters and dithioesters[170]. For cysteine moieties, that only have a natural abundance of 1.5 %, the mildly nucleophilic thiol group is often selectively targeted by alkylation and disulfide formation reactions[61], either by using α-halocarbonyl compounds, maleimides or vinyl sulfones[171-172] or otherwise use orthopyridyl disulfides methanethiosulfonates[173] and bis(thiol) specific reagents[174].[8, 62] In the exceptional case that cysteine is located at the *N*-terminus of the peptide, native chemical ligation (NCL) can be performed for conjugation reactions[175-177], which

will be discussed in detail in chapter 2.1.4. The carboxylic acid groups of aspartic acid, glutamic acid and the *C*-terminus of a peptide can be easily modified by methods that are widely used for solid-phase peptide synthesis [178-179], can be converted into thioesters that can then be used for the Staudinger ligation[180] or NCL[176].[8]

Furthermore, instead of modifying amino acids in existing proteins, peptides can be directly synthesized via various chemical and biological pathways such as non-ribosomal peptide synthesis[61], tRNA engineering methods[76, 181] and solid phase peptide synthesis[182], which is a routine technique nowadays, to include *N*-, *C*- and site-specific functionality via choice of the resin, linker, orthogonal protecting groups or non-canonical amino acids.[8] The use of non-canonical amino acids or amino acids with non-natural residues allows for the introduction of functionalities that range from alkenyl, alkynyl or azide[183-184] to boronic esters[185] and aryl halide[186] side groups. As an example, this allows that a *N*-terminal phenylalanine residue is able to undergo NCL by the introduction of β-mercaptophenylalanine derivatives[187].[8]

Chapter 2.1.3.2 *Preparation of Peptide-Reactive Polymers*

In this subchapter, multiple ways to introduce chemoselective handles onto polymers are presented. Generally speaking, this is possible either through the use of functional monomers, initiators or terminators, or through quantitative post-polymerization modification. There is also a distinction between (multiple) functionalization at the side chain of the polymer and functionalization at the α or ω end terminus.

Terminal Functionalization

Usually, functionality at the end group of polymers is introduced by using suitable functional initiators (α functionalization) or terminating agents (ω functionalization) for the respective polymerization reactions. For example, in RAFT polymerization, this can be achieved by introducing the functionality in the free radical leaving group of the RAFT agent or by performing a post-polymerization modification reaction on the RAFT end-group[188]. ω functionalization of polymers by anionic polymerization can be accomplished by the introduction of terminating agents that bear masked functional groups[189] and using suitably functionalized nucleophilic reagents as terminating agents in the living cationic ring-opening polymerization (LCROP) reaction leads to functional ω end polyoxazolines[190], just to mention a few examples.

Side Chain Functionalization

There are several different polymerization methods such as radical polymerization, ring-opening polymerization, anionic polymerization and living cationic ring opening polymerization that also allow for the introduction of side chain functionalities.

With radical polymerization, monomers with functionalities such as protected maleimides[191], active esters[192-194], protected alkynes[195], azides[196-197], and p-aryl halides[198], protected or free aldehydes and ketones[194, 199-201], or even monomers containing amino acid derivatives[202-205] can be used for polymer synthesis. According to Gauthier and Klok[8], "Living ring-opening metathesis polymerization (ROMP), Ring-opening polymerization (ROP) of cyclic esters and acyclic diene metathesis (ADMET) polymerization are also of interest for developing side-chain functional polymers due to their tolerance to many functional groups such as acids, alcohols, aldehydes, ketones, esters, amides as well as to aqueous reaction media.[206-207]" Due to appropriate protecting techniques, the introduction of hydroxyl, carboxylic acid, amino, thiol, alkenyl, alkynyl, ketone and aldehyde groups into polystyrenes was made possible through anionic polymerization as another potent polymerization methodology.[208]

Finally, the cationic ring-opening polymerization (CROP) of functional 2-oxazolines has emerged as a strategy to synthesize polyoxazolines bearing alkenyl and alkynyl[209], amino[210], aldehyde[211], and azido[212], groups which make the polymers available for a variety of different ligation strategies or postpolymerization modification (PPM). The explicit functionalization reactions for polyoxazolines will be discussed in detail in chapter 2.2.3.

Chapter 2.1.3.3 *Preparation of Polymer-Carbohydrate Conjugates*

Carbohydrates play an important role in signalling and recognition events and it has been argued that carbohydrates are able to encode a higher information density in comparison to proteins and nucleic acids.[138, 213]

In order to create polymer and/or peptide carbohydrate conjugates, the most common methods are either the *grafting-through* technique, where glycopolymers are synthesized from sugar-containing monomers[137, 214-218] or carbohydrate initiators[219-220]. For example, Takasu et al.[221] and Schubert et al.[37] copolymerized galactosyl, respective glycosyl modified 2-oxazoline monomers to yield poly(2-oxazoline)s with pendant carbohydrates. Interference of the sugar hydroxyl groups with the CROP, however, is one of the main disadvantages of this method, requiring sophisticated protection and deprotection techniques.

Another strategy is postpolymerization modification of polymers with a functional sugar. For this approach, saccharides with a ligated azide[215, 222] or allyl[223-224] group are simply clicked onto the polymer, respective peptide[224-227].[137] For example, Schlaad et al.[228-230] and Kempe et al.[231] described the functionalization of side chain allyl functionalized POx with sugar moieties via thiol-ene chemistry. However, synthesis and polymerization of an allyl functional 2-oxazoline monomer is necessary for the subsequent thiol-ene reaction with those carbohydrates.[137] Furthermore, reductive amination has been employed to link saccharides to amine-containing polymers.[232-233]

In order to use carbohydrates for postpolymerization modification of polymers, the respective sugars need to bear appropriate functional groups. Modification of saccharides is either possible by installing a functionalizable handle at the anomeric position or at the remaining residue sites of the sugar ring.

In the first case, a protected starting saccharide, which is either derived from chemical synthesis or else isolated from natural sources by digestion of glycoproteins or glycolipids[234], is reacted with a functional linker molecule at the anomeric position, leading to a modified sugar molecule with the respective linker functionality. The reader is directed to a review by Park et al.[234], which extensively addresses commonly employed strategies for the introduction of two linker functionalities, alkenes and azides, that are the most common functionalities implemented in this step. It also focuses on methods to subsequently modify those functionalities in order to expand the available range of differently functionalized sugars.

A second review by Dimakos and Taylor[235] that is recommended to the reader gives a detailed overview of site-selective transformations of sugar hydroxy groups, which is possible by "esterification, thiocarbonylation, alkylation, glycosylation, arylation, silylation, phosphorylation, sulfonylation, sulfation, and oxidation. Emphasis is placed on recently developed methods that employ reagent or catalyst control to achieve otherwise challenging transformations or site-selectivities."[235] Focusing on the modification of saccharides however would exceed the scope of this thesis, therefore those methods will not be described in detail at this point. Allyl functionalized sugars that were used in this work were synthesized by a cooperation partner from the group of Prof. Seibel (Julius-Maximilians-Universität Würzburg) and used as received.

Chapter 2.1.3.4 *Conjugation Techniques*

There is a long list of reactions that can be used to couple polymers to biomacromolecules such as peptides or sugars. To present the variety of possible strategies, different conjugation techniques addressing the *convergent* approach (see **figure 1**), where both reaction partners have been synthesized and functionalized separately prior to conjugation will be presented in this subchapter, together with literature examples, where conjugations with macromolecules have been performed. However, those methods will only be listed, but not be discussed in detail, as this would exceed the scope of this work. For more detailed insight, the reader is directed to the review of Gauthier and Klok[8]**.** *Divergent* coupling strategies[26, 172, 236-238] such as a *grafting-from* or *grafting-through* techniques, that also lead to polymer-peptide hybrid materials, but do not have the need for conjugation reactions will - for similar reasons - not be discussed here as well.

Strategies to conjugate macromolecules range from classical peptide coupling chemistry that includes well-established protocols for coupling carboxylic acids and amines[239-240] to Pd^0 catalysed coupling reactions such as the Heck[241], Sonogashira[242] and Suzuki[243] coupling. There are ligation techniques like the Staudinger ligation[244], where azides and phosphines are reacted with each other as well as

cycloaddition reactions such as the Diels-Alder[245] or the Huisgen azid-alkin-click reaction[246]. Other methodologies used for macromolecular conjugation are the reductive alkylation[247], oxidative coupling[248] as well as oxime[78] and hydrazone[249] formation reactions. Most interestingly, there are thiol addition reactions like the Michael addition[250] or thiol-ene[251] reaction, which received particular attention for the modification of side-chain functional polymers due to its compatibility with functional groups such as amines, alcohols or carboxylic acids[252-253]. Finally, there is the native chemical ligation technique, that conjugates thioester and cysteine components and is of particular interest, as it forms a free thiol group at the conjugation site and therefore allows for post-conjugation modification by a third component via the former mentioned thiol-ene reaction[225].

In the approach of this work, three different components will be conjugated at one binding site. There are some advances in literature to create multicomponent conjugates, which will be discussed in the next paragraph.

Multicomponent Reactions

Multicomponent reactions (MCR) have emerged as a method to ligate multiple low molecular reaction partners in usually one-pot syntheses. Those techniques make use of an eligible combination of classical click reactions such as Huisgen cycloaddition, Diels–Alder as well as thiol-ene or -yne and most recently have also been used for polymer synthesis[54, 254-257] and the conjugation of macromolecules.[46-48] The methods are usually differentiated in three main types (see **scheme 1**), namely the Ugi, Passerini and Biginelli reaction.[51, 258] These double click reactions have been proven useful due to their high efficiency under moderate reaction conditions (e.g., non-inert atmosphere and room temperature).[51]

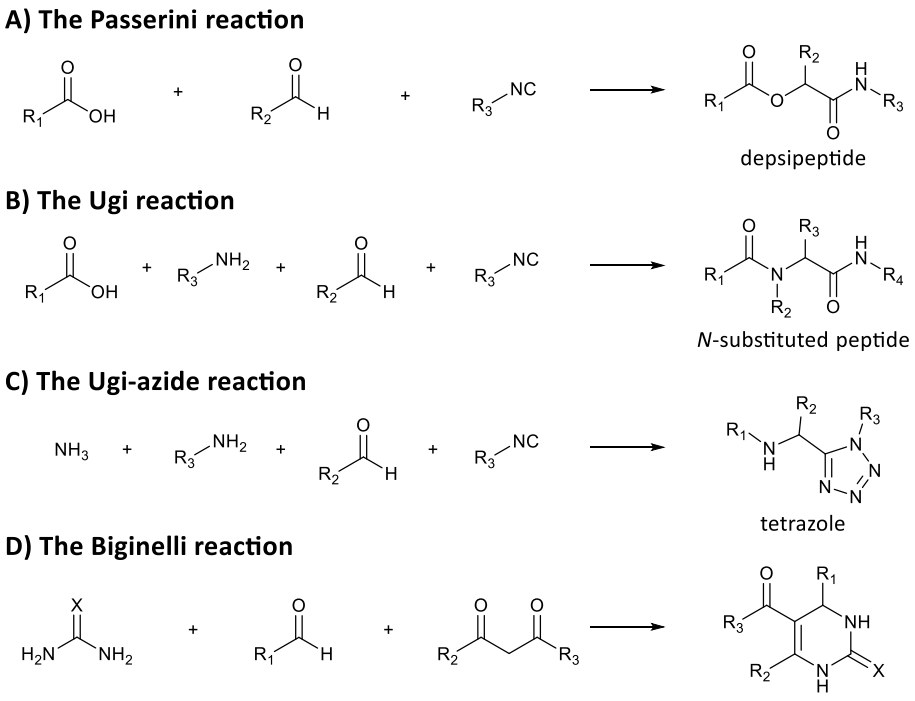

Scheme 1: Main types of multicomponent reactions. Adapted with permission from [51]. Copyright 2018 American Chemical Society.

However, although there are some examples of multicomponent reactions used for peptide conjugation in areas such as protein PEGylation, protein labelling and the synthesis of drug conjugates[50-51], only few polymers have since been used for MCR, with the main focus lying on (poly)saccharides[50, 52-53].[54]

Another approach is the successive conjugation of multiple reaction partners to polymers at the same site, which, following the statement from Driessen et al.[45], were mainly developed by the groups of Tozzi, Theato, and Espeel. They conclusively substantiate that so far, "in literature, very few examples have been reported that provide the possibility of introducing more than one functionality at the same site."[45]

While Tozzi et al. employed nucleophilic ring-opening of epoxides[259], Kakuchi and Theato utilized copper as a catalyst for three-component reactions between sulfonyl azides, terminal alkynes and secondary amines[260]. Most interesting, Espeel et al. used thiolactone handles that were introduced to poly(*N*-isopropylacrylamide), which allowed for the ring-opening by primary amines and subsequent modification of the residual thiol group, yielding tailor-made thermoresponsive polymers.[261] The thiolactone group was introduced by two different strategies, either through the radical polymerization itself[262] or through post-polymerization modification of polymers with a pendant hydroxyl and isocyanate functionalized thiolactone linkers.[45]

Similar to the thiolactone approach, this work will also make use of a cascade of two consecutive reactions, which both will be presented in detail in the following chapters - one being the NCL and the other being the thiol-ene reaction. Unlike the thiolactone approach however, this work will focus on peptides and saccharides as macromolecular reaction partners, contrary to the aforementioned examples, where the conjugated reaction partners were mostly low molecular substances.

Chapter 2.1.4 Native Chemical Ligation

In biochemistry, there is a wide variety of amide bond forming reactions, one of them being the very chemoselective and reliable *Native Chemical Ligation* (NCL). Melnyk et al.[263] recently published a comprehensive and thorough review on this reaction. The NCL is one of the major strategies to chemoselectively couple two components, where one of them, compound A is bearing a thioester group and the other one, compound B, bears a cysteine moiety.

Chapter 2.1.4.1 *History of the NCL*

First discoveries towards the NCL were made by Wieland[264] and Brenner[265-266] in 1955 to 1958, who discovered the formation of peptide bonds involving a highly reactive thioester residue. Further advances that brought forward the establishment of peptide ligation methods based on a capture-rearrangement mechanism were the ground-breaking works of Kemp[267-269], Kent[270-271] and Tam[272-273].

Since then, the NCL has gained importance for biochemical reactions and rose to become one of the major ligation techniques for peptides[274]. The reaction plays a pivotal and reliable role in enabling total and semisynthesis of increasingly complex peptide and protein targets[106].

Today, NCL not only plays an important role in peptide and protein synthesis, but also made its way into material science. For instance, Merkx and Meijer were pioneers in using the NCL for attaching oligopeptides and to dendrimers via bioconjugation[275-276].[62] Other works, for example, describe the NCL as a method to link RAFT polymers with thioester peptides[277].

Chapter 2.1.4.2 *Educts of the NCL: Thioester and Cysteine Residues*

a. Cysteine Residues

The first of the two compounds needed for NCL is one that bears an amino group in close proximity to a thiol group, in most cases an 1,2-aminothiol group. In peptide chemistry, the amino acid cysteine is the most prominent representative with such a functionality, therefore compounds bearing a free 1,2-aminothiol functionality will be referred to as *cysteine functionalized* in this work (see **figure 6**).

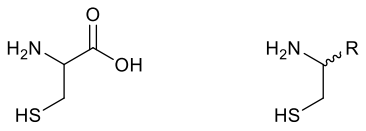

Figure 6: Cysteine (left), 1,2-aminothiol functionality (right).

When it comes to reactivity properties of the cysteine functionality, one has to consider that the nucleophilicity of thiolates is significantly higher th an that of thiols[278-279], but also more susceptible to oxidation by molecular oxygen into disulfides.[263]

For this specific redox process, the pH plays an important role. With a pK_a of around 7 for the cysteine thiol[280-281], oxidation processes are remarkably fast at neutral pH[263], especially in the presence of trace metal ions such as Fe(II) or Fe(III)[282-283]. For example, thiols such as the in biochemistry commonly used 2-mercaptoethanol or 3-mercaptopropionic acid have a half-life of only a few hours at neutral pH[284], if no measures to eliminate oxygen are taken.

Most of the time, adequately adjusting the pH to control the cysteine thiol reactivity is sufficient enough for the basic ligation of two peptide segments by NCL.[263] However, there are some reactants that can be added to the reaction in order to maintain the reduced state of thiols. Either by the excess use of thiol additives[285-286], that prevent disulfide formation by thiol-disulfide exchange, reducing agents such as dithiothreitol (DTT)[287] and tris(2-carboxyethyl)phosphine (TCEP)[288-289] that reduce freshly formed disulfides, or oxidation inhibitors such as ascorbic acid (vitamin C)[290].

When it comes to TCEP, caution is advised with sulfoxides that might be reduced to sulfides through heating in aqueous solvents.[291] Nevertheless, it was shown that dimethyl sulfoxide (DMSO) can still easily be used together with TCEP to perform NCL reactions with hydrophobic compounds.[292]

b. Thioesters

Properties

The other of the two compounds needed for NCL is one that bears a thioester functionality. As a functional group that partakes in a variety of bioprocesses apart from the NCL, such as lipid biosynthesis[293] or protein splicing[294], the thioester group has been thoroughly studied for its capability as a reaction partner in nucleophilic additions[295-301].[263]

Although the chemical structure of thioesters resembles those of amides and oxoesters, the different heteroatoms in these functional groups have a great impact on bond lengths[302-303], electron delocalization as well as resonance stabilization effects[304] and the electrophilic character of the carbonyl carbon[305]. Thioesters are therefore significantly stronger electrophiles than amides and oxoesters, but still less reactive than activated carboxylic acid anhydrides or acyl chlorides, which allows for relatively mild reaction conditions on a nonetheless acceptable reaction time scale.[263]

While thioesters show a significantly higher reactivity towards amines and thiolates than oxoesters[296, 298, 306], at neutral or acidic pH they remain as resistant to hydrolysis as their ester counterparts[295-296, 298, 301]. This makes thioesters ideal candidates for NCL reactions in acidic aqueous conditions. For basic conditions, those hydrolysis rates are significantly higher and it was further shown that aryl thioesters have larger hydrolysis rates than alkyl thioesters[299].

Synthesis

There are several reviews concerning the synthesis of thioesters.[263, 307-312] Most of those reviews concentrate on the generation of peptide thioesters, however, this can be easily transferred to other compounds as well, for example to create thioester functionalized PEG[313-314]. For peptide thioesters, Melnyk et al.[263] describe two basic strategy categories: One, where the thioester functionality is generated either via the coupling of a linker molecule in either solid-phase synthesis or solution *after* peptide elongation. The second category addresses ways to functionalize the peptide *before* elongation, where protecting steps or particular reaction conditions are needed. Both methods however rely on the activation of a carboxylic acid group either via alkylation, acylation, oxidation or condensation.

For alkylation and acylation, a sulphonamide group is activated using trimethylsilyldiazomethane[315], iodoacetonitrile[316] or *p*-nitrophenylchloroformate[317-318]. The thioester is then produced by thiolysis.[318-319] For oxidation or condensation, hydrazide groups are either oxidated with sodium nitrite in hydrochloride to form azides[320-322], or alternatively converted into *N*-acyl pyrazoles through a condensation reaction with acetyl acetone[323]. The thioesters are then produced by thiolysis in both cases.

There is a range of other methods to activate carboxylic acids. For example, Markey et al.[225] and Ryan et al.[324] describe a method of activating the carboxylic acid with isobutyl chloroformate under the presence of *N*-methylmorpholine and subsequent thiolysis with thiophenol. Another group uses DCC/DMAP-systems to activate the carboxylic acid for esterification[325].

Apart from activating carboxylic acids, there are several other methods of chemically creating thioester groups, such as synthesizing thioesters with the use of transition metal catalysts[326-327], phase-transfer reagents[328] as well as nitrogen, phoshor or sulfur reagents[329-332]. However, each of those methods has certain drawbacks or limitations concerning the use for peptides compared to the former described methods of carboxylic acid activation.

Alternatives to direct thioesters are systems that can create an 'in-situ' thioester group through a preceding acid activated *N,S*-acyl shift[334-336] (see **scheme 2**) which accounts for derivatives of *N*-(2-sulfanethyl)amide scaffolds. However, those reactions display slower reaction rates[337] and there is a high risk of competitive reactions with peptide chain cysteine.

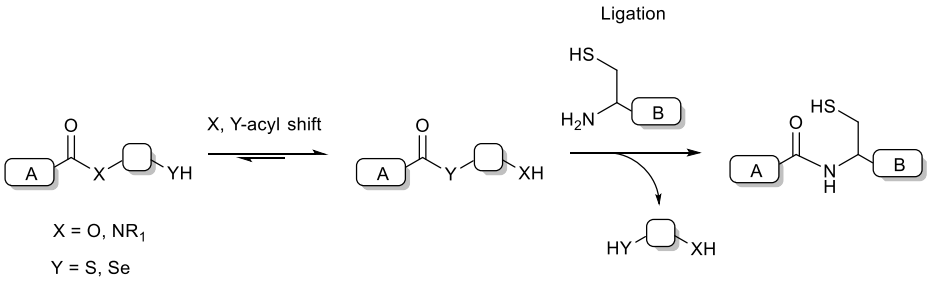

Scheme 2: *N,S*- and *O,S*-acyl shift to create 'in-situ' thioester groups for ligation. Adapted with permission from [263]. Copyright 2019 American Chemical Society.

Chapter 2.1.4.3 *Mechanism*

The basic mechanism of the NCL consists of three steps (see **scheme 3**): Starting, a thioester A or activated thioester A' through thiol-thioester exchange (step 1, catalysis) reacts with cysteine functionalized agent B to form a thioester-linked intermediate C (step 2, capture), which then rearranges to the final ligation product D (step 3, rearrangement).

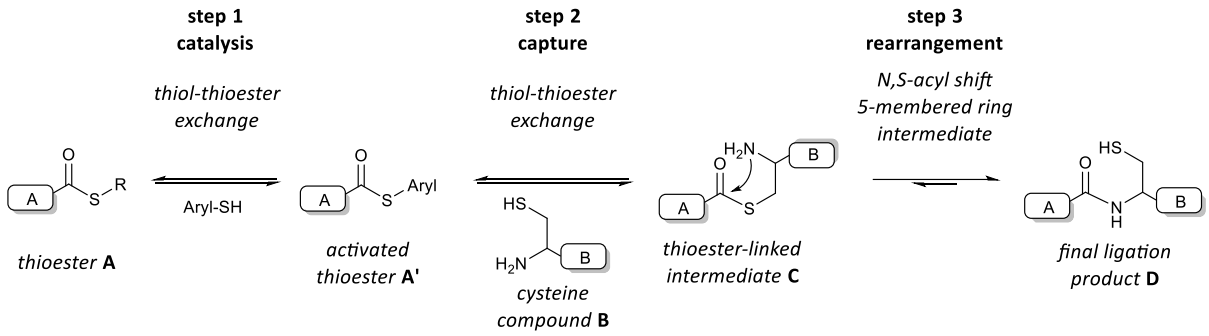

Scheme 3: Mechanism of the NCL. Adapted with permission from [263]. Copyright 2019 American Chemical Society.

a. Thiol-Thioester Exchange Reaction

Both the catalysis step as well as the capture step are basically thiol-thioester exchange reactions, namely *S,S*-acyl transfer reactions.

According to Agouridas et al.[263], the most widely accepted mechanism for this reaction is a stepwise process, in which a tetrahedral intermediate is formed after the attack from thiolate nucleophiles[298, 338] (see **scheme 4**).

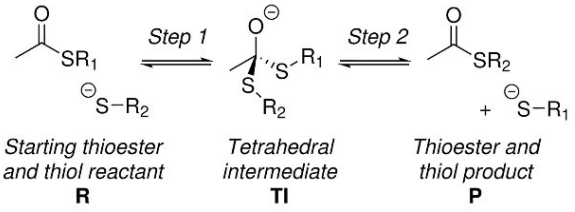

Scheme 4: The thiol–thioester exchange reaction is reversible and probably proceeds through a tetrahedral intermediate. Reprinted with permission from [263]. Copyright 2019 American Chemical Society.

It is mainly driven by the difference in thiol pK_a values of the nucleophile and leaving group and independent of the thiol's alkyl or aryl nature.[263] Because of the reversibility of the reaction, the addition of more reactive thiols or thiolates to a less reactive thioester provides a method to easily activate those thioesters for a subsequent NCL reaction *in situ*.

b. Capture-Rearrangement Reaction

The Rate-Limiting Capture Step

The close proximity of the two functional groups, the thiol and amino group, allows for a certain two-step mechanism that is determining for the NCL reaction, whereas the first step, where the thiol group plays a crucial role is accountable for the rapidness of the reaction, and the second step, where the adjacent amino functionality can undergo an intramolecular reaction, is responsible for the chemoselectivity of the reaction. The detailed mechanism is described in **scheme 3** on page 28.

Initially, the thiol group of compound B attacks the thioester group of compound A or A' in a nucleophilic attack. This step is rate-limiting for the NCL and is significantly faster with an aryl thioester than with an alkyl thioester, since aryl thiols are better leaving groups than alkyl thiols.[263] As discussed before, this step is a thiol-thioester exchange reaction and is therefore reversible. Studies[298, 338] showed, that in mixtures of different thioesters and thiols, an equilibrium between the thiol residues occurs (see **scheme 4**).

In peptides, there are a lot of other nucleophilic groups such as the phenol group of tyrosine, the imidazole group of histidine, the residue amino group of lysine, the *C*-terminal carboxylic acid group as well as the side chain carboxylic acid groups of aspartic acid and glutamic acid, the thiol group of internal cysteines and the thiol and amino groups of the *N*-terminal cysteine residue that can interact with thioesters. According to Melnyk et al.[263], each thioester species "can in principle react with those above-mentioned nucleophilic groups. However, side chain alcohol groups of serine or threonine, the phenol group of tyrosine and carboxylate groups of aspartic and glutamic residues are poor nucleophiles and do not interfere with the NCL reaction. The imidazole group of histidine probably reacts with the thioester functionality. However, the formation of *N*-acyl imidazole intermediates is thermodynamically unfavorable and reversible so that here again no interference is expected from histidine residues in the NCL reaction. Apart from thiolates, the other potent nucleophiles present on peptides are α- and ε-amino groups, which can irreversibly react with the thioester either inter- or intramolecularly to produce amide bonds."[263] However, for low peptide concentrations and a neutral pH, where amino groups are mostly protonated and not nucleophilic, this reaction is unfavourable compared to a kinetically favoured 5-membered ring intermediate and therefore, intermolecular thioester aminolysis reactions are unlikely to occur to a significant extent.[263]

Accelerating the NCL means accelerating the capture step, which can be accomplished by adding alkyl thiols such as 4-mercapto phenylacetic acid (MPAA)[286] or 3-mercapto benzyl sulfonate (MBSA)[339] as well as aryl thiols such as thiophenol[176], acting as nucleophilic catalysts.[263] In comparison between aryl and alkyl thiols, the reaction rate of aryl thiols can be as much as 70-fold higher than that of alkyl thiols[299], which is because the pK_a of the aryl thiol nucleophile is well below the pK_a of the leaving alkyl

thiol group.[263] Alkyl thiols are nonetheless able to catalyze the NCL reaction if they are less basic than the alkyl thiols that formed the original thioester.[263] Other methods to accelerate the reaction are using non-thiol-based catalysts such as nitrogen-based heterocycles (e.g. imidazoles)[340-341] or phosphorous-based nucleophiles (e.g. phosphines)[342-343] but will not be discussed here in detail.

The rate of the capture step also depends on the concentrations of the thioester and cysteine functionalities. Apart from increasing the concentrations of the reactants, specific conformational or self-assembly properties of the ligated compounds can be utilized to push the reaction partners into close proximity. Such reactions are called template- or folding-directed ligations[263] and can happen when the ligating segments have the capacity to interact with each other, such as in coiled-coil-templating[344-345] or natural peptide-peptide interaction[346-347].

The Irreversible Rearrangement-Step

The second step of the NCL mechanism makes the reaction irreversible, although it is not rate-limiting for the reaction since it proceeds significantly faster than the preceding thiol-thioester exchanges of the capture step.[348-349] The close proximity of an amino group in α position allows for an intramolecular nucleophilic attack of the amino group to the thioester group, which continues through a kinetically favoured 5-membered ring intermediate C to the final amide product D. The effect of an intramolecular attack having a much lower activation barrier[337] makes the reaction so effective.[263] As discussed earlier, the newly formed peptide bond is much more stable and less reactive as than the thioester bond, and is significantly less likely to be attacked by thiols in the reaction mixture. The reaction is therefore irreversible and the equilibrium is shifted to the peptide product.

The cysteine thiol group that initially attacked the thioester is recovered in this step. After the NCL, it is now available for subsequent reactions, such as the thiol-ene reaction.

c. Reaction Parameters

As discussed earlier, pH value has a great impact on the reaction, since it affects the nucleophilicity of the thiol and the amino group as well as hydrolysis of the thioester. Therefore, NCL reactions are performed best under neutral or slightly acidic conditions.

Other factors that affect the reaction outcome are the choice of solvents. In particular, a number of organic cosolvents are possible, for example DMSO[292] of trifluoroethanol[350].[263] The NCL reaction can even be conducted under anhydrous conditions in dimethylformamide (DMF) in the presence of an organic base like triethylamine[351-352], though thiol−thioester exchanges and thioester aminolysis are decelerated in the absence of water.[263] In case of phosphate buffer solutions, one has to be aware of the fact that phosphate ions can promote the hydrolysis of thioesters and can therefore diminish conversion rates for the NCL.[353-354]

The reaction can benefit from several additives as well. A competition reaction for the NCL is the dimerization of two thiol groups to form a disulfide bond, which occurs under oxidative conditions and can therefore be prevented by the addition of a reducing agent such as $NaBH_4$ or TCEP. Plus, although most NCL reactions can be performed in the absence of thiol additives, the presence of the latter has numerous advantages[263], as discussed earlier. Since some thioester derivatives achieved through thiol-thioester exchange are more powerful than the starting peptide thioesters, the excess of thiol additives can accelerate the process of driving 'unproductive' thioesters into an active form and excess thiols can avoid the creation of disulfides by retaining the number of thiyl radicals.[263]

Chapter 2.1.4.4 *Alternative Ligation Techniques*

Since cysteine is not always available as a reaction partner in biochemistry, a number of alternative ligation techniques has emerged in the field. One of them is the auxiliary-mediated NCL, where removable, thiol-based auxiliaries such as mercaptoethyl or mercaptobenzyl moieties are attached to the amino group of a peptide to imitate a cysteine residue.[355-356] The effectiveness of this method is however limited to the decreased nucleophilicity of the newly formed secondary amine.[357] Other ligation techniques use a brominated alkyl group or other nucleophilic amino acids like histidine or selenocysteine instead of a cysteine functionality.[358]

Moreover, further reactions that are used for amide forming ligations are the Staudinger ligation[359], where an azide is reduced to an amine under mild conditions as well as the imine ligation and the reductive amination (also known as reductive alkylation), that involves the conversion of a carbonyl group to an amine via an intermediate imine[360].[274]

Chapter 2.1.5 Thiol-Ene Reaction

The discovery by Charles Goodyear of vulcanization of natural rubber (poly(cis-isoprene)) by sulfur[361] marks the birth of the classical thiol-ene chemistry, where a thiol is added to a carbon double bond to form a thioether. In case of compounds that bear a terminal double bond with another alkyl carbon atom next to it, this $H_2C{=}CH{-}CH_2{-}R$ functionality is referred to as an *allyl* group in this work.

First reported in 1905 by Posner et al.[361], the thiol-ene reaction gained prominence in the late 1990s and early 2000s for its practicability and wide scope of applications.[362-363]

Chapter 2.1.5.1 *Applications*

There is a wide range of applications that take advantage of the versatility of thiol-ene chemistry. Selected examples will be presented to demonstrate the variety of areas where the reaction is used in literature.

Polymer Functionalization

By using thiol-ene reaction, Schlaad et al.[230, 364] were able to conjugate a variety to thiols to a polyoxazoline backbone, David and Kornfield[365] synthesized functionalized polybutadienes and Campos et al.[366-368] developed styrenic, methacrylic, and caprolactone monomers with alkene functionalities that could then also be modified by thiol-ene additions after polymerization.[369] The wide scope of reported thiol-ene conjugations that is supplemented by the work of further groups[253, 370-371], is a clear demonstration that a broad range of thiols is tolerated by the thiol-ene reaction.[362] One of the practical uses of the preparation of those functional copolymers was to tune the lower critical solution temperature of the materials, spanning lower critical solution temperature (LCST) ranges from 5-90 °C.[228]

Crosslinked Network Formation and Dendrimer Synthesis

Other groups used the technique to create crosslinked network formations such as hydrogels, thin films, and lithographic applications[369] with improved physical and mechanical properties. They targeted the kinetics[372] and energetics[373] of crosslinking reactions as well as the impact of alkene[372, 374], thiol[375] and photoinitiator structure[375-376] on the mechanical properties of the formed networks.[369]

The high yields and simple purification requirements allowed Killops et al.[377] for the synthesis of high purity dendrimers. With dendrimer synthesis being a field where highly selective reactions are crucial, further work by Rissing and Son[378] in developing carbosilane–thioether dendrimers is another example of the versatile applicability of the reaction.

Moreover, the mild reaction conditions of the thiol-ene reaction and its compatibility with sensitive biological processes could be proven in several works that focused on the design of biodegradable PEG-based gels that were used to encapsulate cells[379-381].

Bioorganic Chemistry

In bioorganic chemistry, Triola et al.[382] were able to prepare *S*-alkylated cysteines via a radical thiol-ene reaction without racemisation of the educts. Starting with the reduction of protected cysteine disulfides by DTT, they coupled hexadecane to the product with the aid of AIBN in dichloroethane. After a consecutive hydrolysis step, they obtained the final thioether product in yields of 42 % with 99 % ee. Further interesting is the general applicability of this approach, which was proven in reactions on hydrolysed trityl protected cysteine with 1-octene, 2-methyl-1-hexene, trans-2-octene, an ene-bearing fluorescent dansyl derivate as well as an ene-biotin at 90 °C, obtaining the respective thioethers in yields ranging from 28 to 91 %.[362]

Wittrock et al.[383] emphasized the efficiency of the radical thiol-ene reaction even for large macromolecules in conjugating proteins to create immune-compatible antitumor vaccines by synthesizing thiolated glycopeptides and reacting with allyl-functionalized bovine serum albumin (BSA). The approach could also be used for the introduction of fluorescent labels, biotin markers and spacer molecules.[362]

Chapter 2.1.5.2 *Click Chemistry*

The term *click* reactions was first introduced by Sharpless et al.[384] for reactions that are "*modular, wide in scope*, give *very high yields*, generate only *inoffensive byproducts* that can be removed by nonchromatographic methods, and are *stereospecific* (but not necessarily enantioselective). The required process characteristics include *simple reaction conditions* (ideally, the process should be insensitive to oxygen and water), *readily available starting materials and reagents*, the use of *no solvent or a solvent that is benign* (such as water) *or easily removed*, and *simple product isolation.* Purification—if required—must be by nonchromatographic methods, such as crystallization or distillation, and the product must be stable under physiological conditions."[384]

Classic representatives of this kind of reactions are the Cu(I)-mediated Huisgen reaction between an alkyne and an azide[385-388], the sharpless epoxidation of allylic alcohols[389-390] or the Diels–Alder reaction between a conjugated diene and a substituted alkene[391-392].

However, attention has also been paid to a number of thiol based reactions such as the thiol-ene[361, 369, 393], thiol-yne[394-396], thiol-isocyanate[397] and thiol-bromo[398] reaction.[362]

The thiol-ene reaction complies with the requirements of a typical *click* reaction: It is fast, offers simple synthetic strategies from a number of easily obtained starting materials, has a defined reaction

pathway that leads to exact products and complies with many different reaction conditions and solvents.[369, 393]

Chapter 2.1.5.3 *Mechanism*

Several reviews have been published on the thiol-ene reaction[223, 362, 369, 393, 399-404] and there is a basic distinction between two different mechanisms: One, where the reaction is accomplished via base catalysis or a nucleophilic attack.[405-406] This Michael-like mechanism occurs for strong nucleophilic thiols, respective thiolates and electron deficient double bonds with an electron withdrawing group next to it. In this case, the reaction is referred to as a thiol-michael reaction.

However, this work will focus on the second case, where the thiol-ene reaction follows a typical chain process with initiation, propagation and termination and is radically initiated, which can happen either thermally or UV light mediated. In the first-mentioned way, thermal lysis of the S-H bond, for example with AIBN, generates a thiyl radical.[407] For an UV light induced reaction, a range of photoinitiators such as 2,2-dimethoxy-2-phenylacetophenone (DMPA) and (2,4,6-trimethylbenzoyl) diphenylphosphine oxide (TMDPO)[408] are employed.[393, 409-410]

Those photoinitiators generate a thiyl radical from a free thiol group, which can then add to a C=C double or C≡C triple bond in the propagation step (see **scheme 5**) to yield an intermediate carbon-centred radical. A chain transfer step removing a hydrogen radical from a second thiol molecule and therefore generating a new thiyl radical gives the thiol-ene addition product with anti-Markovnikov orientation. Usual termination reactions involve typical radical–radical coupling processes.[362]

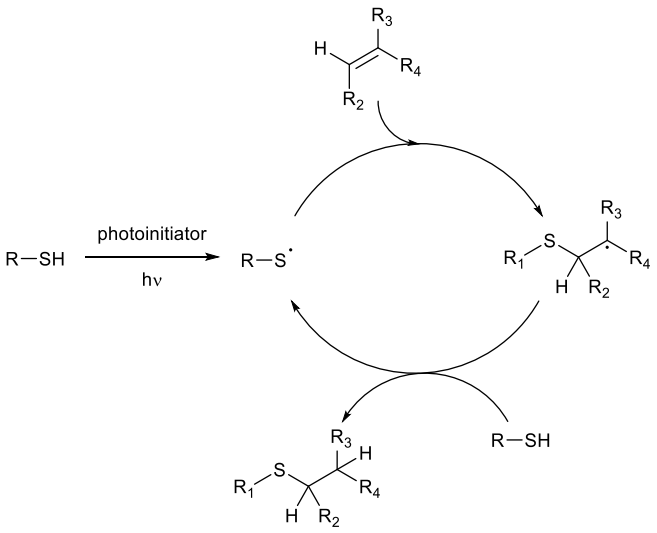

Scheme 5: Mechanism of a photoinitiated thiol-ene reaction. Adapted from [362] with permission from The Royal Society of Chemistry.

Chapter 2.1.5.4 *Educt Reactivities*

The reaction is known for its high reaction rates, which is dependent on the electronic properties of the thiol as well as the alkene compound.

a. Alkenes

Intensive investigations on the influence of thiol and ene structures on the thiol-ene reaction rate have been conducted by Morgan et al.[409]. In their work, they found out that the main influence on thiol-ene reactions depends on the electron density of the ene. It was shown that electron-rich enes have a higher conversion than electron-poor enes, except for highly conjugated double bonds.[409] Those structures copolymerize very slowly due to a high stability of the carbon-centered allylic radical that forms when the thiyl radical adds to the double bond.[393]

They also formulated a reactivity order, which is as follows: Norbornene > vinylether > propenyl > alkene ≈ vinylester > *N*-vinyl amide > allylether ≈ allyltriazine ≈ allylisocyanurate > acrylate > *N*-substituted maleimide > acrylonitrile ≈ methacrylate > styrene > conjugated diene.[393, 399] The reactivity decreases with a declining electron density of the double bond, except for norbonenes, whose high reactivity is connected to a loss of ring strain upon reaction with a thiyl radical, and methacrylates, styrenes and conjugated dienes, whose relatively stable intermediate carbon radicals lead to low hydrogen abstraction rates from thiols in the propagation reaction.[362, 393]

The reactivity of enes further depends on the degree of substitution[411], with less substituted alkenes being far more reactive than highly substituted enes.[393] This is especially true if terminal enes are compared to internal enes, where the latter ones are significantly less reactive towards hydrothiolation.[362] According to Claudino et al.[412], this effect is partly based on a thiyl radical mediated, competing cis-trans isomerisation process.[401]

b. Thiols

Concerning the thiol reactivity, very little research has been conducted on its effect on radical thiol-ene reactions.[362] This might be due to the fact that of the two propagation steps, the proton abstraction step is in most cases not rate-determining and therefore conversions are independent from the thiol structure.[393]

However, looking at the most general and widely used types of thiols, namely alkylthiols, alkyl thioglycolates and alkyl 3-mercaptopropionates, there is a descending order of conversion rates for propionates, glycolates and simple alkyl thiols.[409] It is assumed that this is due to polar effects that enhance deprotonation and therefore increase reactivity of the thiol.[230, 413]

The thiyl radical has only a short half-life and gets quenched quite easily, therefore reaction partners need to be readily available in close proximity, which means that high concentrations of educts and an excess of thiol-containing species[383] are beneficial to yield optimal conversion.[401, 412]

Although the thiol-ene reaction is reportedly insensitive to water and air[62, 362, 369], and can be performed in highly polar solvents such as water, alcohol or DMF[383, 414], a common concurrence reaction is still the formation of disufides between two thiol groups under oxidative conditions, therefore it is advised to perform the reaction under exclusion of oxygen or under the presence of reducing agents such as DTT, TCEP or *tris*(hydroxypropyl)phosphine (THPP).[368, 415] Another approach by the working group of Espeel et al. observed that standard oxygen-free procedures and acidic work-up did not prevent disulfide formation and therefore they used ethanethiol, not only as a reducing agent, but also as a solvent for their functionalization reaction with RAFT polymers.[262]

Chapter 2.1.5.5 *Alternative Coupling Reactions*

A great advantage of the thiol-ene reaction is that it can be used in orthogonality with copper catalyzed azide-alkyne cycloadditions[369, 416-418], which gives an interesting field of chemoselective targeting applications. This is also the case for the Michael-type of the thiol ene reaction, which can be used to selectively target acrylate moieties in the presence of alkenes as well as alkynes and allowing for multifold conjugations at the very same molecule.[369]

Another alternative to the radical thiol ene reaction is the michael reaction with maleimide groups. Those functional groups deserve a special comment, since the C=C bond of maleimides is particularly reactive and therefore, those thiol-ene reactions are remarkably fast and effective. This makes the reaction an interesting alternative as a bioconjugation tool[419-421].[362] There are multiple ways to introduce a maleimide group, for example by reacting amines with maleic anhydrides[422] and an advantage of the reaction is that it can be performed in slightly acidic conditions (pH 6–7). However, one of the drawbacks is that the resulting product is less stable in water.[62]

The closely related thiol-yne chemistry allows for the double attachment of two different thiols, which, in comparison to standard thiol-ene systems, can yield even more densely crosslinked networks in materials[423-424].

Chapter 2.2 Hydrophilic Polymers

Hydrophilic polymers nowadays have a number of applications in drug delivery[425], self-assembly[426-429] or catalysis[430]. Significant features of this type of polymer is the ability to interact with biomacromolecules like DNA or proteins[431-432] as well as their capacity to form hydrogels[433-436], nanoparticles[437-438] or biointerfaces by surface grafting[439-440].[10]

„Gold Standard" PEG

Apart from natural hydrophilic polymers such as proteins or cellulose, polyethylene glycol (PEG) still is the most prominent artificial polymer candidate in this field, next to polyvinyl alcohol (PVA) and polyvinylpyrrolidone (PVP).

PEG, which is also known as poly(oxyethylene) or poly(ethylene oxide) (PEO), is a synthetic polyether which is commercially accessible in a range of molecular weights. The polymers are amphiphilic and soluble in water as well as in a wide number of organic solvents. PEG has been stated to be nontoxic and is approved by the U.S. Food and Drug Administration (FDA) for use as a carrier in various cosmetics, foods, and pharmaceutical formulations.[441] Most PEGs with a molecular weight lower than 1,000 $g \cdot mol^{-1}$ are quickly removed from the body unaltered, exhibiting clearance rates that are inversely proportional to polymer molecular weight.[442] These qualities, together with the availability of a broad variety of PEGs with different end-functionalizations, contributes to a wide use of these polymers in biomedical research: Drug delivery, surface functionalization or tissue engineering scaffolds.[443]

Coupling a PEG polymer chain to molecules and macrostructures, such as a drug, therapeutic protein or vesicle, either covalently or non-covalently, is called PEGylation.[425] The attachment of PEG to a drug or therapeutic protein can reduce the immunogenicity and antigenicity of the target by masking it from the body's immune system and it can increase its hydrodynamic size, which prolongs its circulatory time in the organism.[444-446] PEGylation can also provide water solubility to otherwise hydrophobic drugs and proteins.[447]

Polyoxazolines as PEG Alternatives

However, it is important to notice that PEG has shown severe drawbacks like "hypersensitivity, unexpected changes in pharmacokinetic behavior, toxic side products, and an antagonism arising from the easy degradation of the polymer under mechanical stress as a result of its ether structure and its non-biodegradability, as well as the resulting possible accumulation in the body"[425].[11-12, 448]

Therefore, a lot of research has been done to find potential alternatives to PEG, some of which are biodegradable polymers like poly(amino acid)s as well as polyglycerols, polyacrylamides and last but not least, polyoxazolines, which will be in focus of this work.[11, 425, 449] Although some of the drawbacks

already known for PEG might also – at least in part – associated with those materials[138], they display a high potential being established as promising biomaterials.[13] One advantage of POx in contrast to PEG is that means for functionalization are not only available at the telechelic end, but also at the side chain of the polymer by the use of functional monomers, which drastically increases its potentials as a versatile material for polymeric constructs such as hydrogels or bioconjugates.[436, 450]

Other closely related polymer families like the higher homologues of POx, the poly(2-oxazine)s (POzi)[451] recently have also gained some attention for the design of biomaterials[138], but will not be covered in this work.

Chapter 2.2.1 (Poly)Oxazolines as Hydrophilic Polymers

There is a large number of books and review articles to polyoxazolines, covering the topic in general[452-454], comparing POx to other polymers[11, 455], tackling POx functionalization[449, 456], synthesis[457-459], monomer synthesis[460-461] or properties[462-463], reporting from biological or biomedical applications[138, 464-466] or addressing specific subjects like POx for drug delivery[467-468], POx hydrogels[435-436, 450], nanoparticles[469] as well as surface coating[439-440]. This chapter will concentrate on the most important characteristics of this kind of polymer.

Chapter 2.2.1.1 *History of POx*

In 1966, Polyoxazolines were discovered independently by four different research groups[470-473], which means they have been known for a little over 50 years now.[474] Although there is a large number of 2-oxazoline monomers, both the amphiphilic poly(2-ethyl-2-oxazoline) (PEtOx) as well as poly(2-methyl-2-oxazoline) (PMeOx), which is even more hydrophilic, are still the most investigated candidates out of a pool of various commonly used POx.[138] This might be due to the excellent water- and organosolubility and their FDA approval.[456]

Chapter 2.2.1.2 *Properties*

Polyoxazolines are considered bioinspired polymers, being structural isomers of both polyacrylamides and polypeptides due to their amide group.[449, 453]

Just as it is done for the PEG gold standard counterpart, the assessment of degradability, immunogenicity, toxicity and biodistribution aspects of POx based biomaterials is still under investigation. Recent research showed that PEtOx and PMeOx exhibit high cyto- and hemocompatibilities similar to PEG[475-477], which also accounts for immunomodulatory properties[478] and biodistribution[479-481]. There is a number of studies showing a low toxicity of POx derivates and concerning the degradability of POx materials, although they are amendable to basic and acidic hydrolysis, the effect is not significant under physiological conditions[482-483].

According to Lorson et al.[138], "a major breakthrough for the community was indubitably the first-in-human study of a POx-rotigotine conjugate initiated in 2015[484]. Even though this study is ongoing and final results have not been published, it appears that preliminary results are promising[485]."

Concerning physical properties, the side chain group of POx has several effects on the mechanical[486-487] and thermal[488-491] properties of the polymer, such as solubility in common solvents and/or water, which goes hand in hand with the polymer's hydrophilicity.

PMeOx and PEtOx are hydrophilic[489] whereas longer alkyl side chain groups or aromatic groups lead to a hydrophobic character[492]. Also, their glass-transition temperatures are dependent on the length of the side chain, ranging from 15 to 105 °C[488-490, 493]. Still, POx with alkyl side chains are stable in temperatures up to 300 °C and more[494-495].[463]

A key property of POx is their tuneable thermoresponsive behaviour[496-497] which is often used to build drug carriers[498]. The polymers can be designed to have a lower critical solution temperature (LCST)[228], which can be modified from 5 to 90 °C depending on the residual side chain group[488, 493, 499].[449]

Concerning the mechanical stability, Schubert et al. prepared a library of alkyl side chain POx, consisting of PMeOx, PEtOx, P*n*PrOx, P*n*BuOx, P*n*PeOx, P*n*HxOx, P*n*HpOx, and P*n*NonOx[487]. With an increasing length of the side chain, the Young's modulus of amorphous polymers decreased linearly.[456]

Chapter 2.2.2 Synthesis of POx

Chapter 2.2.2.1 *Synthesis of Oxazolines*

Most oxazoline derivatives that are needed for the synthesis of polyoxazolines are not commercially available yet and therefore need to be synthesized prior to polymerization.

Rossegger et al.[456] and Glassner et al.[463] precisely describe the different synthesis routes to those monomers (see **scheme 6**): One option is the three-step synthesis from non-activated carboxylic acids, involving activation by *N*-hydroxysuccinimide[230, 500], another route is the Wenker method[501], which is a two-step synthesis via cyclization of β-halo amides, as well as the Henkel patent from carboxylic acids and esters[456] and the Witte–Seeliger synthesis from nitriles[502-503]. Other less common synthesis routes towards more complex 2-oxazolines are for example the α-deprotonation of 2-methyl-2-oxazoline followed by alkylation.[211, 504] Additionally, by using chiral α-amino acids for the synthesis, chirality can be introduced at the 4 and 5 position.[106]

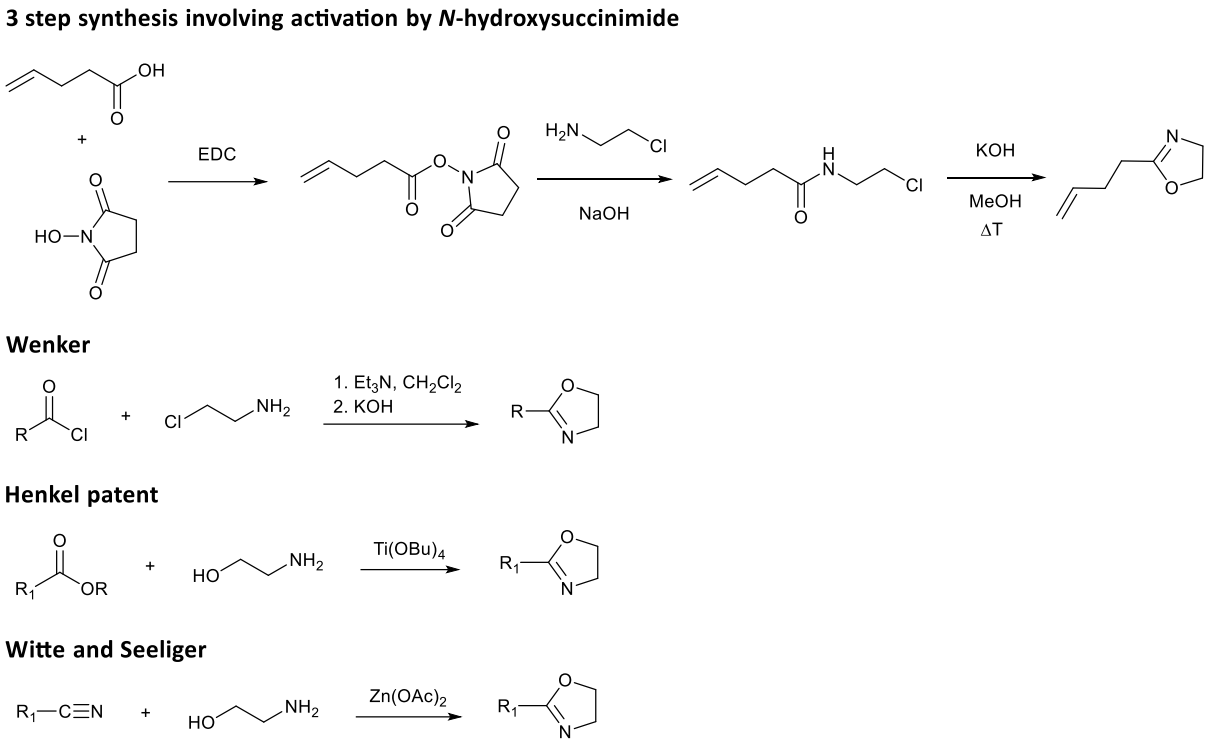

Scheme 6: Common strategies for the synthesis of 2-oxazoline monomers.

The 2-oxazoline monomers are then available for a living cationic ring opening polymerization (LCROP), described in the next chapter), to yield the desired polyoxazolines.

Chapter 2.2.2.2 *The Living Cationic Ring Opening Polymerization (LCROP)*

a. Definition of a Living Polymerization

The "living" character of a polymerization describes that the end of a growing polymer chain is active for propagation until a terminating agent is added to the reaction. It allows for the synthesis of very well defined polymers with a low molar mass distribution and of polymers with unusual architecture such as star polymers and block copolymers.[505] Usually, in living polymerizations, chain initiation is much faster than propagation. Therefore, the polymer chains grow at a more constant rate with similar lengths and their polydispersity index stays low.[506]

Cationic Ring Opening means that the living polymerization reaction is initiated by a cationic species[505] and the monomer is a heterocycle such as an epoxide, an oxazoline or an aziridine. Here, focus will lie on the LCROP of 2-oxazolines.

b. Mechanism

The LCROP consists of three steps, the initiation, propagation and termination (see **scheme 7**). Glassner et al.[463] describe the mechanism as follows: In the initiation step, the nitrogen lone pair of a 2-oxazoline monomer attacks an electrophilic initiator and forms an oxazolinium cation. This attack is highly regioselective and can only occur with the nitrogen atom of a 2-oxazoline monomer, but not

with the oxygen.[507] In another nucleophilic attack, a second 2-oxazoline monomer initiates the ring opening and formation of an amide. This propagation step creates a reactive oxazolinium chain end that can undergo the mechanism again. In an ideal living polymerization, the absence of chain coupling, transfer or termination reactions and the fast and quantitative conversion guarantees polymer products with a narrow molar mass distribution, which is described by a low dispersity Đ < 1.2. This is the case if the reaction constant of the initiation is much greater than the reaction constant of the chain growth ($k_{ini} > k_{growth}$). Adding a nucleophilic reagent to the reaction terminates the process by attacking the living cationic chain end.

The polymerization reaction displays different propagation rates depending on the electron donating character of the 2-substituent at the alky-oxazoline monomer. Comparing alkyl and aryl substituents, the CROP is faster for alkyl-oxazolines[463] and it is highest for 2-methyl-2-oxazoline (MeOx) and lesser for EtOx and 2-isopropyl-2-oxazoline (*i*PrOx).[508] However, longer chain lengths up to *n*-nonyl chains have only little influence on the propagation rate.[508] Comparing 2-oxazolines with a propyl side-chain, the propagation rate increases for *i*PrOx < *n*PrOx < *c*PrOx.[509]

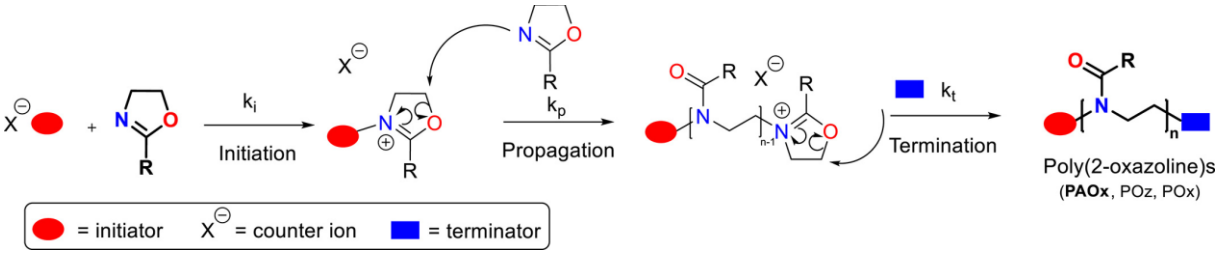

Scheme 7: Three-step mechanism of the cationic ring-opening polymerization of 2-oxazolines with initiation, propagation and termination. Reprinted with permission from [463]. Copyright (2017) John Wiley and Sons.

The polymerization rate R_P is defined by the propagation rate and follows first-order kinetics[510]:

$$R_P = -\frac{d[M]}{dt} = k_P[P^*][M] \qquad \textbf{Eq. 1}$$

with [P*] being the concentration of the active propagating species, [M] the monomer concentration, and k_P the polymerization constant of the respective monomer.

Under ideal living conditions, the concentration of living chain ends is presumed to always be equal to the initial initiator concentration $[I]_0$. Eq. 1 is therefore reformulated and integrated into:

$$ln\left(\frac{[M]_0}{[M]_t}\right) = k_P[I]_0 t \qquad \textbf{Eq. 2}$$

with $[M]_0$ for the initial monomer concentration and $[M]_t$ for the monomer concentration at any time point throughout the polymerization. The slope of a first order kinetic plot, from which k_P can be derived, is linear in an ideal living polymerization.[510]

c. Side Reactions

During propagation, chain transfer reactions like β-elimination, repolymerization and other coupling reactions can decrease the homogeneity of the polymer product.[511-515] This has to be taken into account especially when high molar mass POx are synthesized.

Since any kind of nucleophile is prone to act as a terminating agent and can therefore influence the dispersity of the polymer, LCROP solvents and reagents have to be free of impurities like water, initiator by-products or other competing nucleophilic sites that induce chain transfer and termination reactions.[449] In order to synthesize POx with a narrow molar mass distribution, thorough purification is therefore crucial for the reaction and a recent patent by Hoogenboom and Monnery that uses specialized vacuum techniques and low temperature polymerization shows that it is possible to synthesize high molar mass POx by excluding these side reactions.[516]

d. Block, Gradient and Random Copolymers

With LCROP, the possibilities in combining multiple monomers allows for the creation of different structured copolymers. Apart from extraordinary variants like alternating copolymers, graft copolymers, and stereoblock copolymers, three main types of copolymers are distinguished[517]: *Random*[504], *Gradient*[518] and *Block*[519] copolymers, which can be seen in **figure 7**.

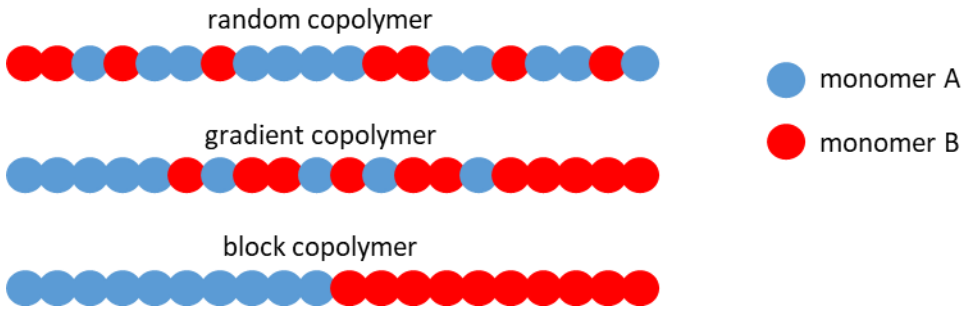

Figure 7: Different types of copolymers: Random, gradient and block copolymer.

For random copolymers, two monomers with a similar propagation rate are polymerized together[455]. The kinetics of the propagation step have a great impact on the product copolymer formation.[520] If there is a difference in propagation speed, gradient copolymers will form, with the more reactive monomer species being integrated into the growing chain with a higher probability first. The greater the difference between propagation rates, the less random is the monomer distribution in the final polymer. This effect can be as determining as to be responsible for the formation of block copolymers.

Based on the fact that the polymerization of oxazolines is that of a LCROP type, another possibility to synthesize block copolymers is by adding another monomer B to the reaction mixture, *after* monomer

A is already used up completely by the propagation reaction.[519, 521] Due to the living chain end[458, 468], this process can be repeated multiple times to create multiblock copolymers (A-B-C-D or A-B-A-B).

e. Microwave-Assisted Polymerizations

It has been reported multiple times that the use of microwave reactors has beneficial impacts on the polymerization reaction of polyoxazolines.[456, 494, 520, 522-524] Mainly, this is based on the significant reduction of the long reaction times of the polymerization of oxazolines by using microwave irradiation and therefore heating reaction mixtures very fast and under pressure even above the boiling points of the solvent. Microwave-assisted polymerizations of homopolymers as well as di-, tri- and tetrablock copolymers from monomers such as MeOx, EtOx, PhOx and *n*NonOx have been described by multiple working groups[456, 494, 520, 522-524] without any negative impact of microwave irradiation, except for influences through higher reaction temperatures[525].

Chapter 2.2.3 Functionalization of Polyoxazolines

There are multiple sites on a polyoxazoline molecule that allow for functionalization of the polymer (see **scheme 8**). Functionalization at the α-end is achieved via the use of functional initiators[526] and functionalization at the ω chain end is obtained by functional terminating agents[527]. Finally, polyoxazolines offer the possibility for functionalization at the side chain. This can be achieved by using functional monomers[212], that bear a functional pendant group at the 2-position of the oxazoline ring. Depending on the type of functionalization that is aimed for, there is a need for appropriate protecting groups.[449]

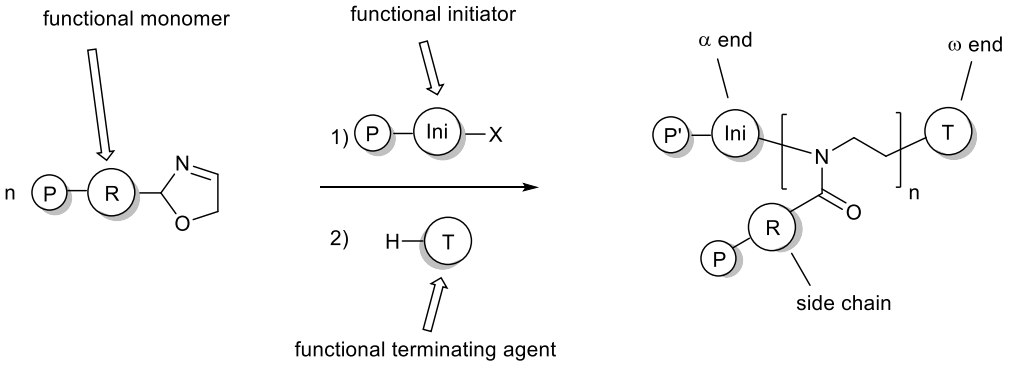

Scheme 8: Synthesis of functional polyoxazolines. Adapted with permission from [449]. Copyright (2012) John Wiley and Sons (Ini = initiator, T = terminating agent, P and P' = protecting groups).

Chapter 2.2.3.1 *Initiators*

When functionalizing POx via the initiator, the functional group must not interfere with the LCROP[528]. Otherwise, initiators that bear groups such as thiols, alcohol or amines need to be converted into thioethers, acetate groups[220] or urethanes[190]. If there are no impurities and the initiation is faster than the propagation, an advantage of the initiation route compared to the termination route is that it is easier to ensure quantitative functionalization.[138]

The most commonly used initiators are reagents that are strongly electrophilic and almost carbocationic.[456] For example, alkyl ester initiators such as tosylates and triflates are initiators that deliver methyl cations, with polymerization rates declining in the order of methyl triflate > methyl tosylate > methyl iodide.[529]

Some unconventional initiators are metal cations such as zirconium, metallocenes and bismuth salts[530-531], alkyl halide initiators that are iodine-based initiators, such as methyl, benzyl or acetyl iodine[532], chloride-based[533-534], bromide based[535-536], as well as molecular iodine[537] or Lewis acids such as boron trifluoride[538].

Initiators that bear alkyl chains or perfluorinated chains of various lengths have been studied extensively[493, 520, 527, 529, 539-541], revealing that unsaturated initiators bearing double bonds[542-544] or triple bonds[533, 545-546] do not interfere with the LCROP mechanism. This opens up the wide field of well-known *click* reactions, such as the thiol-ene reaction or the Huisgen cycloaddition that allow for post-polymerizatic functionalization with further functional groups that are incompatible with the LCROP[453]. Moreover, cyclic compounds[547], acetals, oxiranes[548], esters[536, 549] and silanes[550-551] can also be used without complications.[449]

Concerning the synthesis of large macromolecules, it is noteworthy that macroinitiators can also be utilized to initiate the polymerization of polyoxazolines. Examples for such macroinitiators are α-methoxy-ω-4-toluene-sulfonate poly(ethylene oxide)[552], diacylglycerol[548], 1,2-*o*-diooctadecyl-*sn*-glyceryl[540] as well as macroinitiators deriving from vegetable oils[549] or cholesteryl[548].[449]

Chapter 2.2.3.2 *Terminating Agents*

Functionalization of polyoxazolines via a suitable terminating agent has the advantage that functional groups can be chosen, which, in other ways, would interfere with the LCROP. The most widely used terminating agent is water[529, 553-554], leading to an OH terminus of the polymer. However, although most nucleophiles attack at the 5-position of the oxazoline ring, reactions with weaker nucleophiles like water may lead to an unwanted attack at the C2 atom, which is followed by a ring-opening and the formation of a secondary amine and an ester (see **scheme 9**).[553-554]

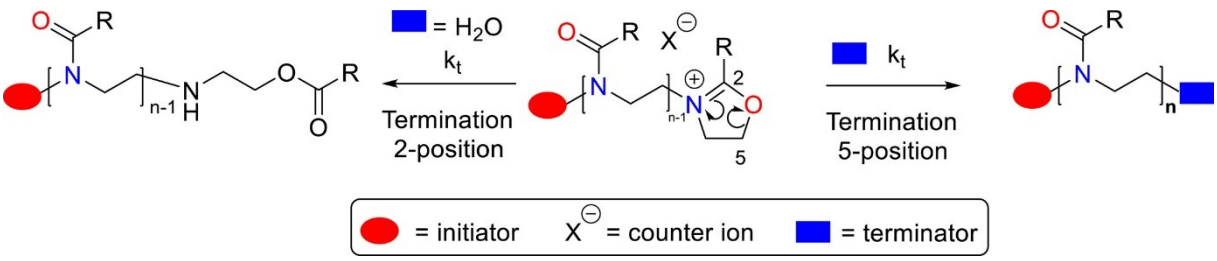

Scheme 9: Termination reaction of polyoxazolines in 2- and 5-position. Reprinted with permission from [463]. Copyright (2017) John Wiley and Sons.

Guillerm et al.[449] give a thorough list of the most prominent amine types of terminating agents, each having the adequate nucleophilic character (pKa > 10) to be able to react with oxazolinium species, that will be presented as is: "The basic nitrogen derivative, ammonia, has been used successfully as a terminating agent[555], while primary amines are the most-important group, ranging from aliphatic compounds with long chains to obtain amphiphilic copolymers[556], to aniline[557], to various functional primary amines.[558-559] Secondary cyclic amines as terminating agents are represented by piperidine[560], piperazine derivatives[209, 534], or morpholine[561], and by bis-functional acyclic amines.[562-563] Even if tertiary amines such as pyridine[548] and pyrrole[535] and linear amines with long alkyl chains are less reactive than those less substituted, they react as terminating agents for biocide applications.[190] An interesting nitrogen terminating agent is sodium azide (NaN_3) which further leads to Huisgen's cycloaddition to generate amphiphilic copolymers by the click reaction.[564-565]"[449] In any case, termination with amine agents may lead to termination with water, if the reagents are not complete dry.[553]

Sulfur derivatives like sodium thiolates[468, 566-567] have also been used to terminate the LCROP, as well as several carboxylic acids or corresponding carboxylate salts such as glutaric acid[568], acrylic acid[468, 569], methacrylic acid[220, 570-571], cinnamic acid[572], maleic acid[573] and terephthalic acid[570].[449]

Chapter 2.2.3.3 *Monomers*

The possibility to introduce functionality at the side chain of polyoxazolines is one of the big advantages that POx have compared to PEG.[502] The most straightforward kind of functionalization is polymerization of 2-oxazolines with linear alkyl chains of various lengths, ranging from methyl to undecyl groups[464, 511-512, 554-555, 574-577] or branched alkyl chains like *iso*propyl[555], *iso*butyl[502] or *tert*butyl[578] groups. It has already been discussed in chapter 2.2.1.2 how these residues influence the mechanical and thermal characteristics of the polymer.

Similar to the functionalization of the initiator, there exists a range of alkene[502, 576] and alkyne 2-oxazoline monomers such as 2-butenyl-2-oxazoline (ButEnOx)[230], 2-decenyl-2-oxazoline (DecEnOx)[456] or 2-(Penty-4-nyl)-2-oxazoline[209], that allow for the introduction of a double or triple bond used for further *click* reactions like thiol-ene[362], thiol-yne[579] or Huisgen[580] reactions.

Furthermore, 2-oxazolines with aromatic side groups[511] and a variety of substituents[212, 502, 577], including perfluoro groups[576, 581], have been reported in literature.

The choice of monomers is only limited by the incompatibility of nucleophilic reactive groups with the CROP process, therefore other functionalities like amines, alcohols, thiols or carboxylic acids rely on the use of protection techniques.[463] Alcohols, aldehydes[211] and carboxylic acids[512, 582-583] are usually protected by esters[512] or acetal groups[502, 584], whereas amines and thiols are protected with *Boc*-groups[210, 585], respective thioethers[586]. An overview of protected functional groups is listed in **scheme 10**.

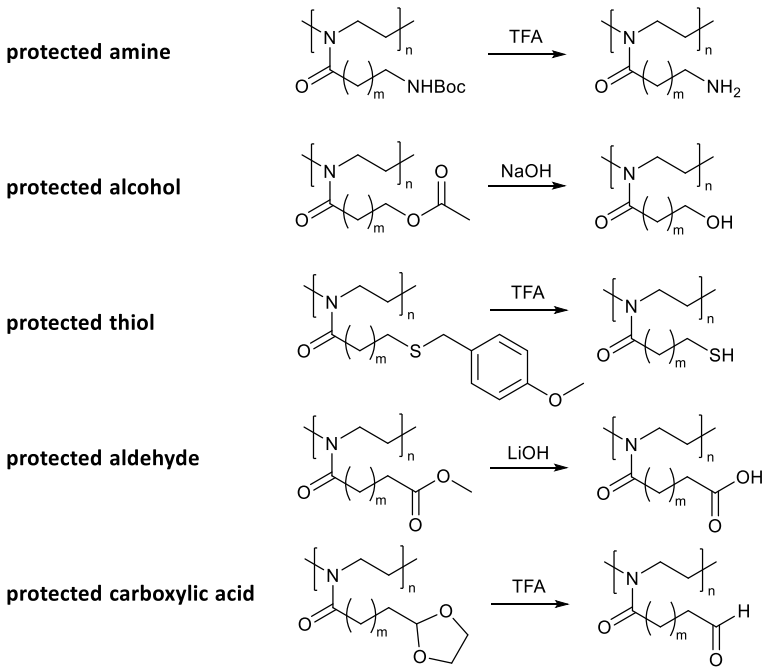

Scheme 10: Synthesis of side chain amine, alcohol, thiol, aldehyde and carboxylic acid functionalized POx by post-polymerization deprotection of POx with respective protecting groups. Adapted with permission from [463]. Copyright (2017) John Wiley and Sons.

An alternative way to functionalize polyoxazolines that utilizes coupling to ethylene imine units in partially hydrolyzed POx has also been exploited recently[138, 557], but will not be in focus of this work.

Chapter 2.2.3.4 *Conjugates with POx*

The differently functionalized POx have been used to conjugate a number of biomolecules such as glycans, peptides or proteins to the polymer in order to create biohybrid polymers. The following passages will present some brief examples for POx conjugates of each type. Other POx conjugates that have been reported in literature are POx-lipid[568, 587-588] and POx-drug conjugates[484, 589-590].

a. POx-Glyco Conjugates

Several research groups used different functionalization techniques to create a variety of POx glycopolymers. For example, Weber et al.[220] synthesized linear α-glyco-OEtOx-MA and oligomerized

them to yield small polymer brushes. Tauhardt et al.[591] modified EtOx/ButEnOx-copolymers with thioglucose and thiogalactose for potentially enhanced endocytosis in tumor cells and Katagiri et al.[105] even conjugated peptides plus glycols to a polyoxazoline polymer to enhance cell-penetration and induce protein expression in E.coli.[138]

Hoogenboom et al.[137] examined the reductive amination of partially hydrolyzed POx with glucose and maltose and observed a different solution behaviour of the glycopolymers depending on the attached carbohydrate. They further showed that the two different carbohydrates exhibit distinct interactions with the glucose binding protein concanavalin A.[138]

b. POx-Peptide/Protein Conjugates

Next to polymer glycol conjugates, the field of polymer peptide conjugates is extensively studied in literature. For example, Trzebicka et al.[592] reviewed thermoresponsive polymer-protein conjugates, which included multiple examples of POx protein conjugates and a number of reviews focuses on POx bioconjugates in particular[138, 464-465].

Typically, peptide-polymer conjugates are either utilized to enable interactions of the polymers with cells via protein interactions or to enhance the properties of peptides by means similar to PEGylation. According to Luxenhofer et al.[138], "POx homopolymers and block copolymers have been used to modify proteins, in particular, enzymes to improve their catalytic activity, stability, and solubility as well as cellular uptake and biodistribution." Specifically, POxylation[593] of enzymes for instance can be seen as a tool to increase their solubility in organic solvents in order to perform enzymatic reactions that would not be possible otherwise due to inactivation and/or insolubility[594].

There is a variety of synthetic strategies to obtain such compounds, for example click chemistry, aldehyde/aminooxy coupling or native chemical ligation.[106]

Groll et al.[55] reported a synthesis, were a protected cysteine reagent was conjugated to allyl functionalized POx via a thiol-ene reaction. After deprotection, NCL was performed with a peptide bearing a *C*-terminal thioester. Luxenhofer et al.[106] synthesized a peptide-POx conjugate in the orthogonal way by coupling *N*-terminal cysteine bearing peptides to POx with thioester side chains.

Furthermore, there is the work of Lühmann et al.[595], who introduced non-natural amino acids into the protein backbone of interleukin 4 to use those protein handles for the attachment of POx via copper catalysed azide alkyne cycloaddition and then compared POx conjugation to PEG conjugation. They also observed an improved thermal stability of the conjugates and confirmed that activity *in vitro* was still comparable to wild type interleukin 4.

Chapter 3

The Approach of This Thesis

Chapter 3 The Approach of This Thesis

In this work, three macromolecules were coupled chemoselectively and vicinally at one binding site: a thioester functionalized polymer, a cysteine functionalized peptide and an allyl functionalized sugar. The aim was to create telechelic polymer conjugates that prove their specificity and selectivity in biomacromolecular recognition experiments and transfer those reactions to side chain functionalized polymers. The feasibility of this strategy will be displayed by examining each step of the reaction cascade with an array of various analytical tools, ranging from infrared (IR) and nuclear magnetic resonance (NMR) spectroscopy to SAW and SPR measurements.

However, analytics on a polymer, respectively macromolecular level, are facing several difficulties, based on one major problem: the molecules are too big and vary too much in length (dispersity) to deliver distinct and definite results with most of the analytical methods established for small molecules. The intensity of signals coming from single characteristic functionalities or relevant building blocks is weak in comparison to the rest of the macromolecule that remains unchanged by the respective functionalization reaction. Therefore, chemical modifications at a sole end group or a small number of side chain groups are hard to detect, which makes it difficult to obtain reliable verification of ongoing reaction processes in polymers.

To approach this challenge, a variety of analytical methods, such as NMR, IR, RAMAN and UV-VIS spectroscopy, titration studies, matrix-assisted laser desorption ionization – time of flight (MALDI-TOF) mass spectroscopy, size exclusion chromatography (SEC), dialysis techniques, investigation of material properties (e.g. gel formation, solubility) as well as SAW and SPR spectroscopy were applied in order to analyse the intermediates and products from as many different angles as possible. For each method, qualitative as well as quantitative evaluation of the experimental and analytical results was considered. When it comes to conversion rates, structural information, purity and yields of large macromolecules, it is particularly demanding to acquire *quantitative* statements, as it has aleady been addressed in chapter 2.1.2.4 to multivalency. The individual following chapters elucidate the level of accuracy that could be achieved by the respective analytical methods.

Nevertheless, analytical challenges are far easier to tackle, if the investigated system is small and overseeable, as it is the case for low molecular substances. Therefore, this work's approach was to eliminate as many influencing factors as possible while reducing the investigated system to its most basic form. Starting from there, the complexity of the investigated systems could be increased with each consecutive step, while know-how from each preceding stage was transferred to the increasingly complex structures (see **figure 8**).

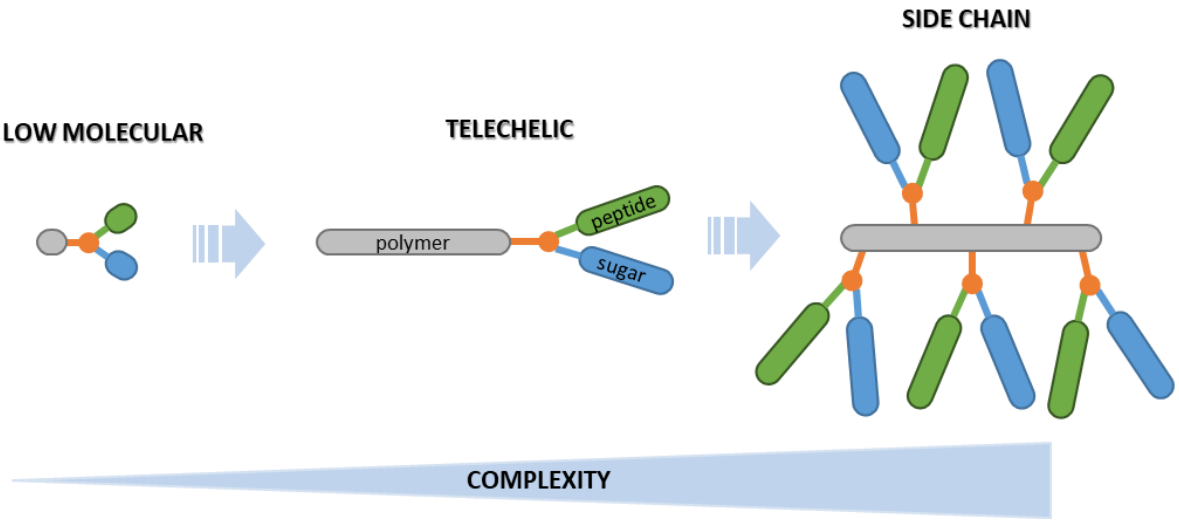

Figure 8: Complexity of the investigated systems increases from low molecular to telechelic polymers to side chain functionalized conjugates. Expertise and know-how from basic experiments can therefore be transferred with each step to the increasingly complex systems. Chapter 4.1 focuses on the low molecular model reactions, chapter 4.2 on the synthesis of telechelic polymers and chapter 4.3 on the display of multivalent side chain functionalized conjugates.

Thus, as a proof of principle, all reactions that were going to be subject to polymer modification later on, were initially performed on a **low molecular level.** This provided A) the right reaction parameters, B) experience and knowledge concerning the reactions and C) concise information about the analytical details and subtleties. The results of those studies will be subject in **chapter 4.1 - Low Molecular Model Reaction**.

Afterwards, those reactions were transferred to a macromolecular level with polyoxazolines as a polymer matrix and peptides as well as sugars as biomacromolecules. In doing so, the initial stage of complexity was to functionalize the macromolecular building blocks only *once* at the chain end, which is called **telechelic** functionalization. With a single functional group per polymer, control over binding site and degree of functionalization as a means of reducing complexity was maintained. Most of the research was performed on this level, therefore **chapter 4.2 - Telechelic Functionalization** is the main section of this work.

Finally, this work proceeds to lay foundations in creating three-fold conjugates with *multiple* functionalization sites at the **side chain** of the polymer. Brush-like constructs were the result of those reactions and the insights from this topic are displayed in **chapter 4.3 - Side Chain Functionalization.**

On each level of complexity (*low molecular*, *telechelic* and *side chain*), a cascade of three subsequent reaction stages will be displayed: I) A thioester synthesis, II) a native chemical ligation and III) a thiol-ene reaction (see **figure 9**). Starting with the synthesis of a thioester from its carboxylic acid analogon, including polymerization of a precursor allyl functionalized polymer, the product was coupled to a cysteine-functionalized reactant via NCL. Since the resulting free thiols from this NCL reaction tend to form dimers through oxidation, a way of reducing those disulfides is presented. This allowed to use

them for an ensuing thiol-ene-reaction with allyl-functionalized substrates. Telechelic conjugates created in this way, with multiple biomaterials attached, can have a high relevance in drug delivery systems or intervene in biological processes such as protein adsorption or cell binding. Therefore, a basis for applications with biological systems was created. This was achieved through the subsequent investigation concerning the affinity of those conjugates to lectins in biomacromolecular recognition experiments.

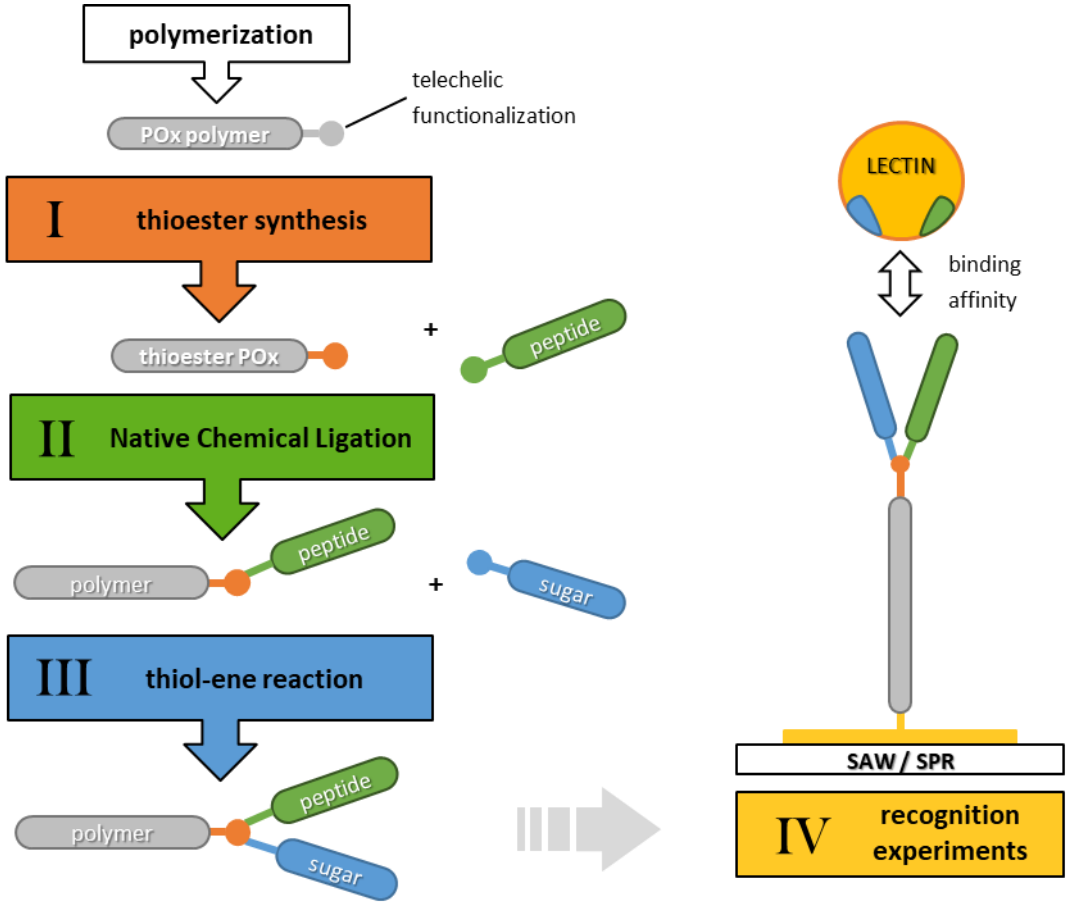

Figure 9: Schematic overview of the main steps of the reaction cascade with telechelic polymers. Steps I-III will be examined in each of the following chapters (low molecular, telechelic and side chain), which will be structured accordingly. In addition, chapter 4.1 will also include a section on means of disulfide reduction, chapter 4.1 and chapter 4.2 will present complementary thiol-ene pilot studies and chapter 4.2 as well as chapter 4.3 will furthermore deal with the polymerization of the precursor polymers. Moreover, chapter 4.2 as the main section will also focus on IV, the macromolecular recognition experiments with lectins.

A large part of this work focused on the synthesis, purification and analysis of intermediate products. In low molecular reactions, by-products and excess educts can be removed by a variety of purification methods. Regarding large macromolecules, this aspect requires a distinct look: Polymers other than natural proteins usually have a certain dispersity and there are little possibilities for the isolation of single polymer derivates from a large batch of macromolecules with a similar composition.[596-598] The larger a polymer (the longer its chain length or molecular weight), the lower is the impact of (telechelic or side chain) functionalization changes of discrete functional groups on the overall material properties

(solubility, polarity, charge, etc.) of the macromolecule. Consider a polymer chain with a length of 50 or more repeating units: For the most part, its properties are predominantly defined by the first 49 chain units with the same architecture. A conformational change of the last, telechelic building block has very little impact on those overall attributes. Nonetheless, changes in material properties are usually the basis for purification steps such as extraction or column chromatography, which explains the increasing difficulty one must face for polymers with increasing sizes.

In this work, a lot of effort was put into finding the right reaction parameters to maximize conversion rates and minimize by-product formation. Additionally, dialysis and SEC offers means of purification and separating conjugates of significantly different size. Apart from that, each polymer batch was used from start to end, which means that in each stage of the cascade, one has to consider that polymer fractions which have not reacted in the desired manner were dragged along, and the proportion of polymer fractions with the adequate functionalization was diminished by a certain extent on each stage of the reaction cascade. It was always checked whether by-products or remaining unreacted educt polymers influenced subsequent reaction steps and since a lot of effort was put into minimizing side reactions, the impact was considered to be rather low. Nevertheless, it was difficult to quantify and therefore, the theoretically expected value always served as a basis for stochiometric calculations, discounting the repercussions of erroneous conversion rates.

In order to attain insights into the processes of each individual reaction step as most detailed and thorough as possible, this work utilized a variety of analytical methods that assisted in comprehensively determining the success of each stage of the cascade. This consequently yielded an encompassing understanding of the whole procedure described.

Chapter 4

Results and Discussion

Chapter 4 Results and Discussion

This work is the continuation of the author's master thesis. Therefore, some of the results were already presented[599] and will be described for the sake of completeness. More precisely, this accounts for chapter 4.1.1, chapter 4.1.2 and chapter 4.1.3 of the Low Molecular Model Reaction, chapter 4.2.1 of the Polymer Synthesis (except for chapter 4.2.1.1b) and the respective chapters in the Experimental Section.

Research done in this work also served as a basis for the master thesis of Bettina Böhm[600], which was published in May 2019. In her work, she transferred the established reaction cascade described in chapter 4.2.1 to α-terminus functionalized telechelic polymers. The synthesis of such polymers is described in chapter 4.2.1.1b.

Comparing to the work of Markey et al.[225], who describe a similar reaction cascade for the conjugation of *peptides*, this work focuses on the conjugation of *polymers* as starting materials.

Parts of this work are also intended to be published as a research article in the future.

Chapter 4.1 Low Molecular Model Reaction

In order to create a basis for the reactions that should later be transferred to a macromolecular level, the complete reaction cascade will be realised on a low molecular level first. This allows for the establishment and examination of suitable reaction parameters as well as gaining analytical experience that would not be possible in on a macromolecular level. The complete cascade is described in **scheme 11**.

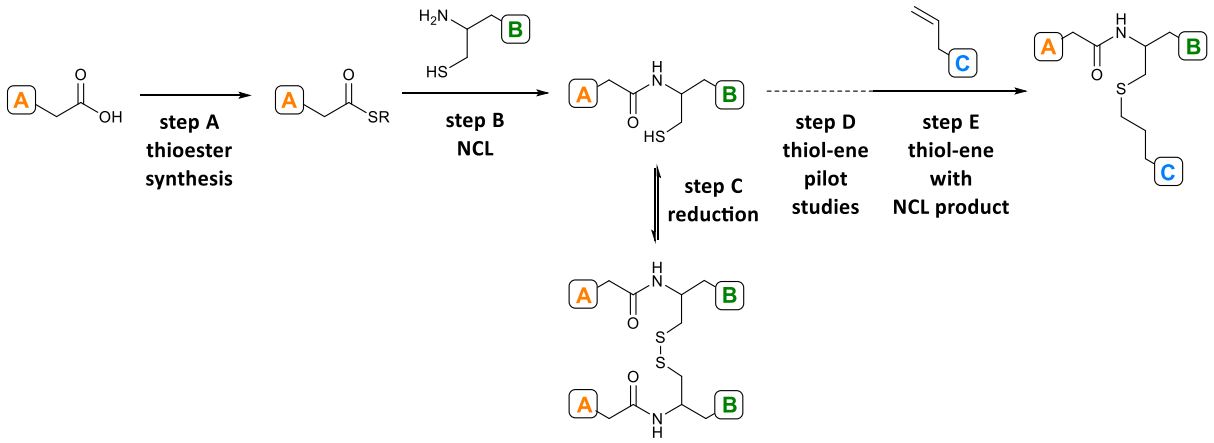

Scheme 11: Overview of the low molecular model reaction cascade.

The cascade begins with the creation of a thioester functionality from a carboxylic acid moiety (**step A**), which will be described in chapter 4.1.1. **Step B** is the conjugation of the thioester component with a cysteine functionalized moiety via NCL, as portrayed in chapter 4.1.2. The subsequent reduction of a dimer-forming NCL product species (**step C**) will be discussed in chapter 4.1.3. Chapter 4.1.4.1 addresses pilot studies that were conducted in order to find an optimal set of reaction parameters for the thiol-ene reaction (**step D**) and finally, **step E**, the attachment of an allyl functionalized molecule to the product of the NCL reaction via thiol-ene reaction is described in chapter 4.1.4.2.

Chapter 4.1.1 Thioester Synthesis (Low Molecular)

Modifying a described procedure of Markey et al. [225], two different thioester, thioester **A** (2-[(*tert*-Butyloxycarbonyl)amino]thiopropionic acid *S*-phenyl ester) and thioester **B** (*p*-toluic acid *S*-phenyl ester) were synthesized from their carboxylic acid analogues (see **scheme 12**). This procedure on a low molecular level was used as a model reaction describing the transformation of a carboxylic acid group into a thioester group.

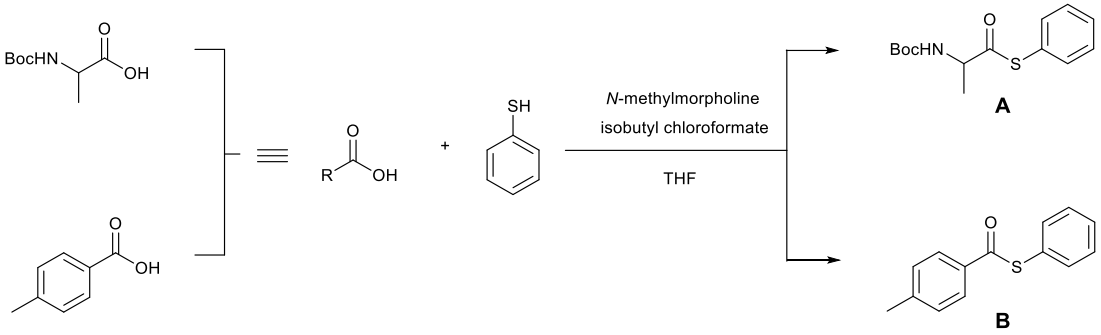

Scheme 12: Synthesis of thioester **A** (top; 2-[(*tert*-Butyloxycarbonyl)amino]thiopropionic acid *S*-phenyl ester) and thioester **B** (bottom; *p*-toluic acid *S*-phenyl ester) from thiophenol as well as *Boc* protected alanine and *p*-toluic acid.

In brief, the commercially available carboxylic acid starting material was treated with *N*-methylmorpholine, isobutyl chloroformate and thiophenol in tetrahydrofuran (THF) for 24 h at room temperature.

In the previous work[599], two different carboxylic acid compounds were used. *Boc* protected alanine, which led to the formation of thioester **A** and *p*-toluic acid, which led to the formation of thioester **B** (see **scheme 12**). It was found that the purification of thioester **B** could be accomplished by simply washing the raw product with cyclohexane. This is less time-consuming and leads to higher yields compared to the purification via multiple use of column chromatography, as it was performed in the case of thioester **A**. Because this made thioester **B** readily available, this thioester was used for further experiments in this work. Further improvement of the procedure, such as multiple washing steps of the raw product, led to an increased yield of 76 %, compared to the previous work[599], where a yield of 38 % was achieved.

Chapter 4.1.2 Native Chemical Ligation (Low Molecular)

The subsequent low molecular native chemical ligation was also described in the author's previous work[599]. For the NCL model reaction, thioester **B** was reacted with two different cysteine functionalized compounds: Cysteamine hydrochloride and cysteine hydrochloride monohydrate (see **figure 10**).

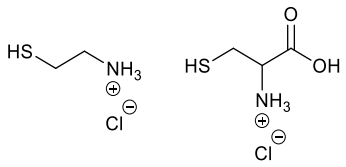

Figure 10: Cysteine-functionalized reactants cysteamine hydrochloride and cysteine hydrochloride.

The cysteine functionalized reactant was reacted with thioester **B** according to a method that is described in literature[225] (see **scheme 13**). The cysteine functionalized compound is dissolved in methanol. Sodium borohydride and the thioester were then added and the reaction was stirred overnight at room temperature. A strong, characteristic odour of thiophenol can be perceived as an indication for a successful reaction.

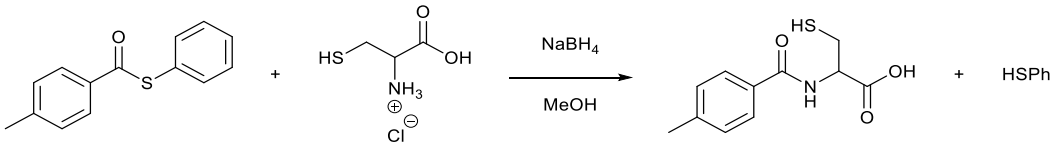

Scheme 13: NCL of thioester **B** and cysteine hydrochloride.

NCL of thioester **B** with cysteine hydrochloride monohydrate as well as with cysteamine was successful, although multiple sets of signals in the ^{1}H-NMR spectrum (see **figure 12**) suggest that the product forms a dimer by establishing a disulfide bond between two free thiol groups (see **figure 11**).

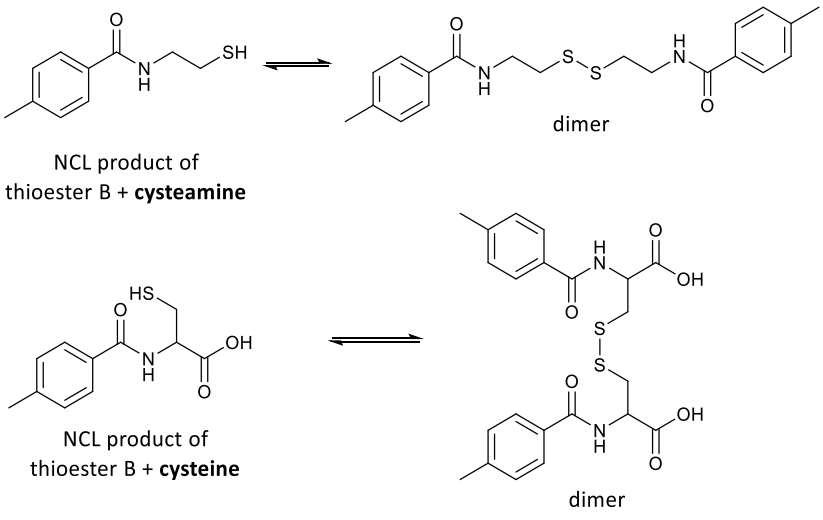

Figure 11: Products of the low molecular NCL. Top: Cysteamine hydrochloride + thioester **B**, Bottom: Cysteine hydrochloride monohydrate + thioester **B**; Right side: Monomer, Left: The product forms a dimer through a disulfide bond formation.

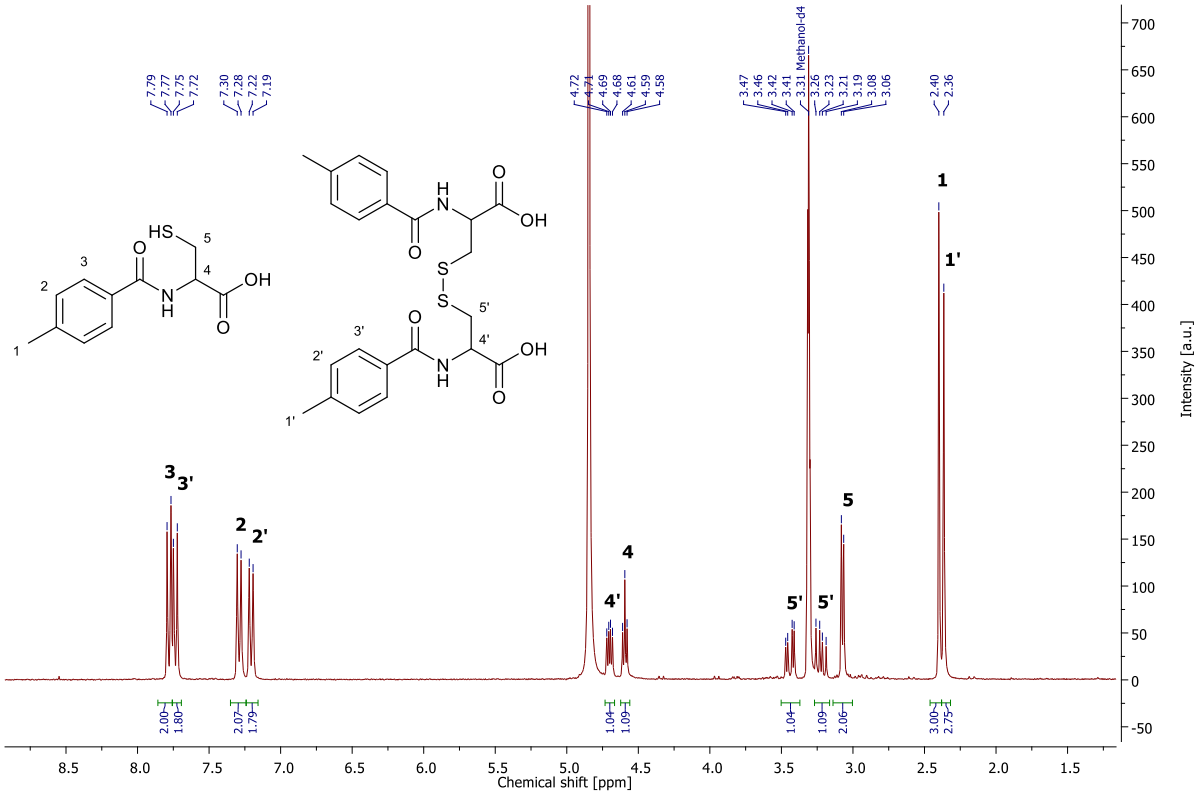

Figure 12: ^{1}H-NMR spectrum of NCL with cysteine hydrochloride monohydrate and thioester **B** in MeOD with two sets of signals for monomer and dimer product.[599]

A strong signal for disulfides in the RAMAN spectrum at 500 cm^{-1} (see **figure 13**) confirms that the thiol functionalities of the NCL product get oxidized to form disulfides immediately after the reaction. The same effect occurs for both the cysteamine NCL product as well as the cysteine NCL product, but for reasons of clarity, only data of the latter one is being shown here.

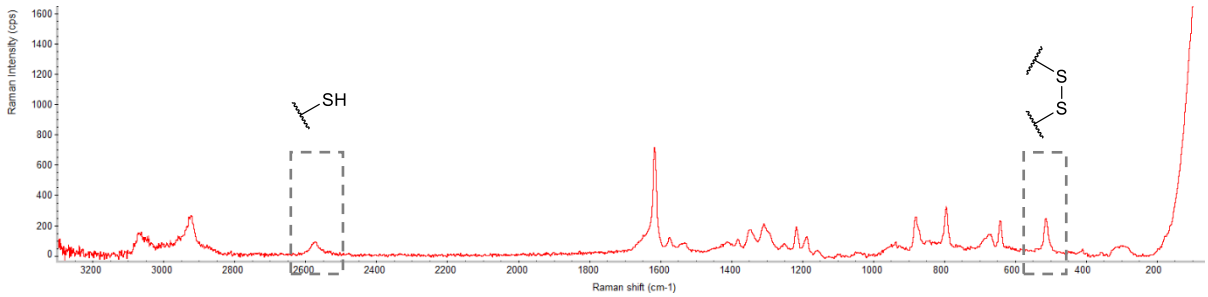

Figure 13: RAMAN spectrum of NCL with cysteine hydrochloride monohydrate and thioester **B** with a strong disulfide signal.[599]

Oriented towards literature[262, 601], numerous experiments were conducted in order to investigate the formation of disulfides and to identify approaches in counteracting this phenomenon. Those experiments included carrying out the reaction under great dilution of the educts as well as the exclusion of oxygen by degassing all solvents prior to the experiment.[368, 601] However, signals in the ^{1}H-NMR spectrum show the same pattern as in former experiments, indicating that each product is still forming a dimer. Since neither of the applied measures prevented the product from dimerization, a way was found to reduce those dimers after the reaction, which will be presented in the following section.

Chapter 4.1.3 Reduction of Disulfide-Dimers (Low Molecular)

The monomer products from the NCL reaction are going to be used in a subsequent thiol-ene reaction. Since this reaction requires the presence of a free thiol functionality, the NCL product dimers need to be reduced in an intermediate step.

It was observed that the dimers could be reduced using either TCEP or THPP as a reducing agent. Small amounts of TCEP, respectively THPP are added to an aqueous or methanolic solution of NCL product and stirred for 30 min. After removal of solvent, RAMAN spectroscopy shows the disappearance of disulfide signals (see **figure 14**).

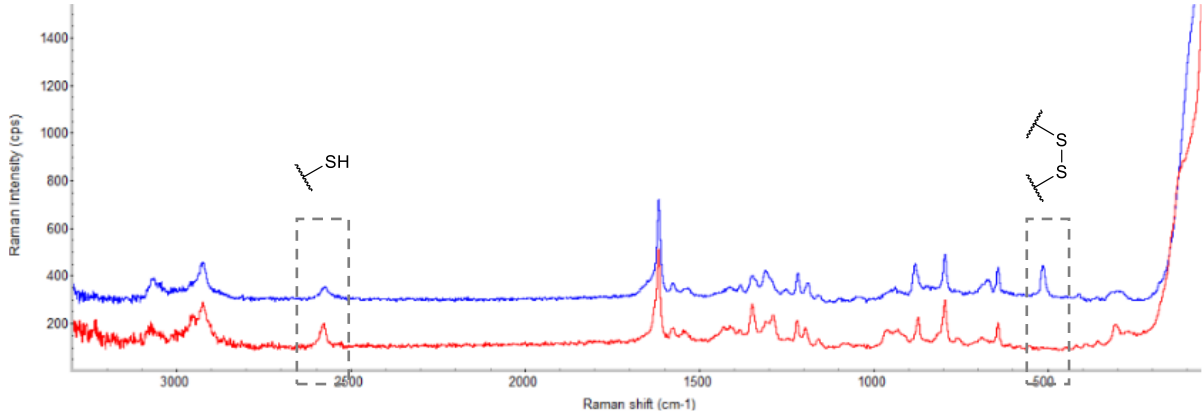

Figure 14: RAMAN spectra of NCL product before (blue) and after (red) reduction with TCEP.[599]

^{1}H-NMR spectroscopy also shows only one set of monomer signals after addition of reducing agent (see **figure 15**). Nevertheless, there are still residue signals from the reducing agent (TCEP) visible in the spectrum at 2.43-1.74 ppm.

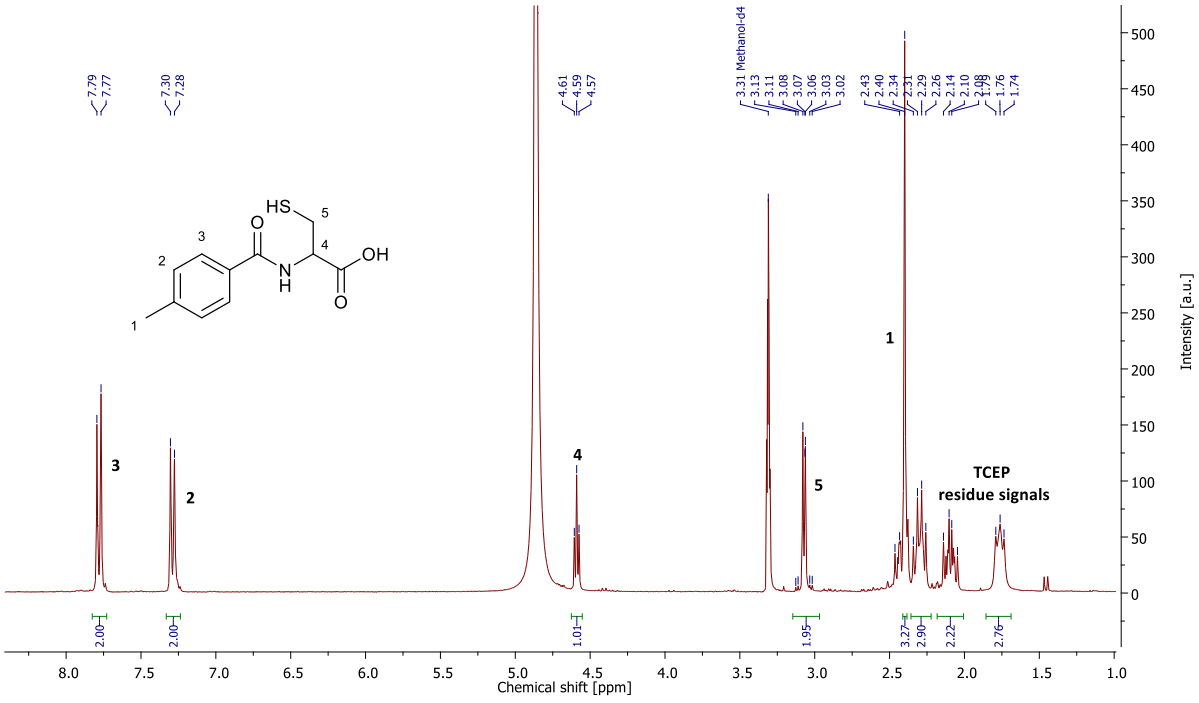

Figure 15: ^{1}H-NMR spectrum of the reduced NCL product in MeOD with TCEP residue signals.

It was possible to remove the reducing agent residues from the reaction mixture via column chromatography. However, without the presence of reducing agent, the product directly starts to form dimers once again. In order to circumvent this constraint, it was elucidated whether the reducing agents can be present while still performing the next reaction step.

As elucidated in chapter 2.1.5.4, it has been shown in literature, that the thiol-ene reaction is relatively insensitive to a wide number of solvents and chemicals.[62, 262, 362, 369, 383, 414] The thiol-ene model reaction experiments presented in the following chapter 4.1.4 confirm that this also accounts for reducing agents such as TCEP and THPP, which have no impact on the subsequent reaction. Therefore, it is possible to use the raw product in further thiol-ene reactions by *in situ* reduction through adding reducing agent to the thiol-ene reaction mixture.

Chapter 4.1.4 Thiol-Ene Reaction (Low Molecular)

Products from the NCL exhibit a free thiol group and can therefore be used in a subsequent thiol-ene reaction. However, the NCL products obtained from the reaction described in chapter 4.1.2 and chapter 4.1.3 easily form dimers and are therefore delicate to handle. For this reason, pilot experiments to determine the appropriate reaction parameters were initially performed with commercially available thiol compounds as described in the following chapter 4.1.4.1 and then transferred to thiol-ene reactions with NCL products, which will be described in chapter 4.1.4.2.

Chapter 4.1.4.1 *Thiol-Ene Pilot Studies (Low Molecular)*

Prior to using NCL products in a thiol-ene reaction, model experiments with different commercially available educts were conducted. The different reaction conditions of these experiments, such as the reaction time, choice and amount of photoinitiator, stoichiometry of educts, choice and amount of solvent as well as the presence of reducing agents were varied in order to determine the optimal reaction parameters. In each experiment, the allyl and thiol compound were either mixed or dissolved in solvent and a photoinitiator was added. The reaction mixture was then stirred under UV light irradiation.

As reactants, thiophenol was chosen as a highly reactive thiol component and allylpentafluorobenzene was chosen as a suitable allyl component, as it can be used as a fluoric marker to easily determine the success of the coupling reaction via ^{19}F-NMR spectroscopy.

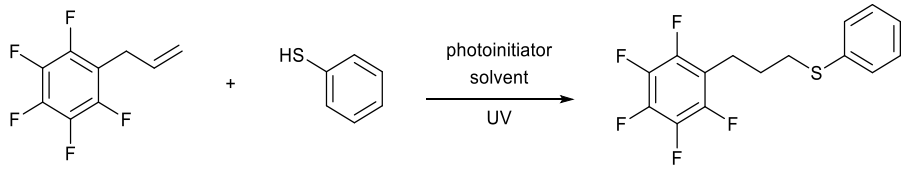

Scheme 14: Thiol-ene model reaction between commercially available allylpentafluorobenzene and thiophenol.

Other compounds that were evaluated as reactants in the model reaction were allylamine as allyl compound and cysteamine as thiol compound. Nevertheless, these reactions were not examined thoroughly, since the compounds bear amino groups that strongly interfere with column material and make it difficult to purify the thiol-ene product via column chromatography.

A complete purification and characterization of the reaction product, was performed for the thiol-ene reaction between the first-mentioned compounds, allylpentafluorobenzene and thiophenol (see **scheme 14**). The ^{1}H-NMR spectrum of the thiol-ene product (see **figure 16**) shows two signals at 7.35-7.26 and 7.21-7.16 ppm for the aromatic ring from thiophenol as well as three signals at 2.97, 2.88 and 1.88 ppm for the alkyl chain of the attached allylpentafluorobenzene with no impurities. In the

^{19}F-NMR spectrum (see **figure 17**), the expected appearance of three signals for the three different fluorine atoms at -146.36, -161.09 and -165.94 ppm confirms the successful formation of the product.

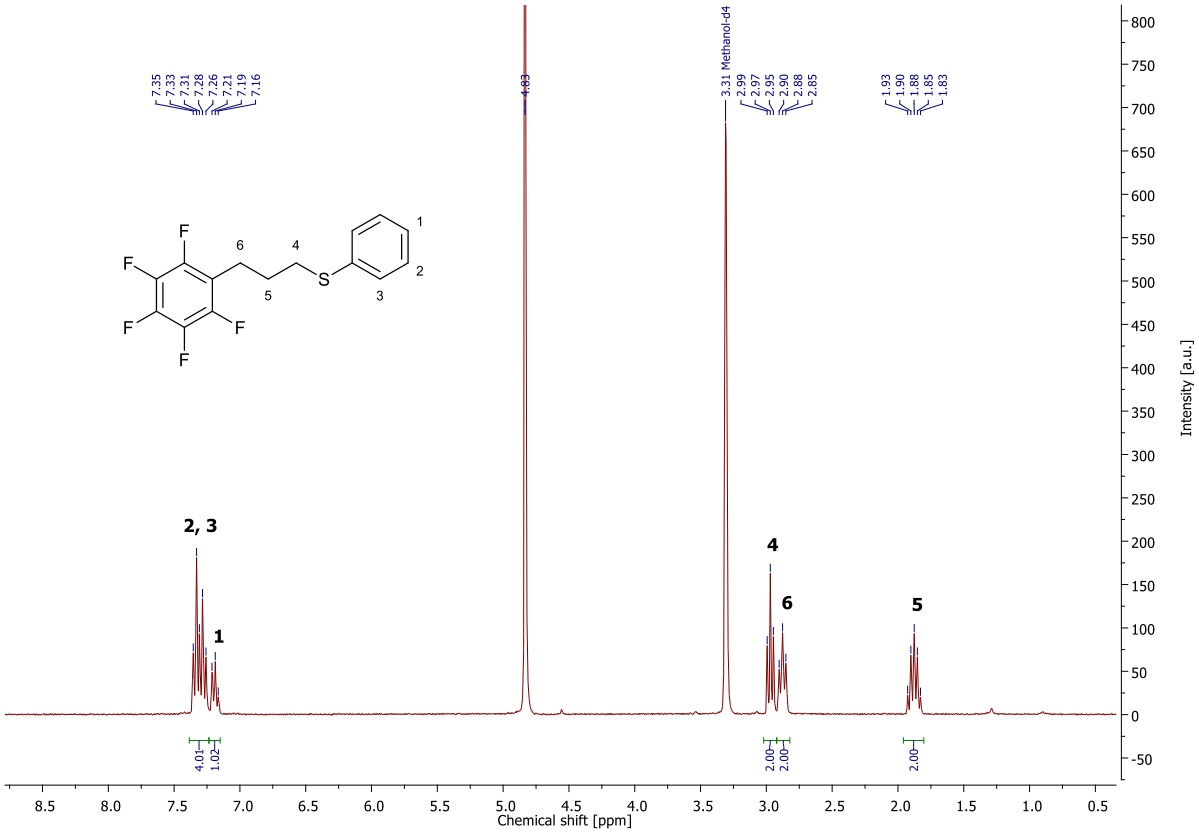

Figure 16: ^{1}H-NMR spectrum of product from thiol-ene reaction between allylpentafluorobenzene and thiophenol in MeOD.

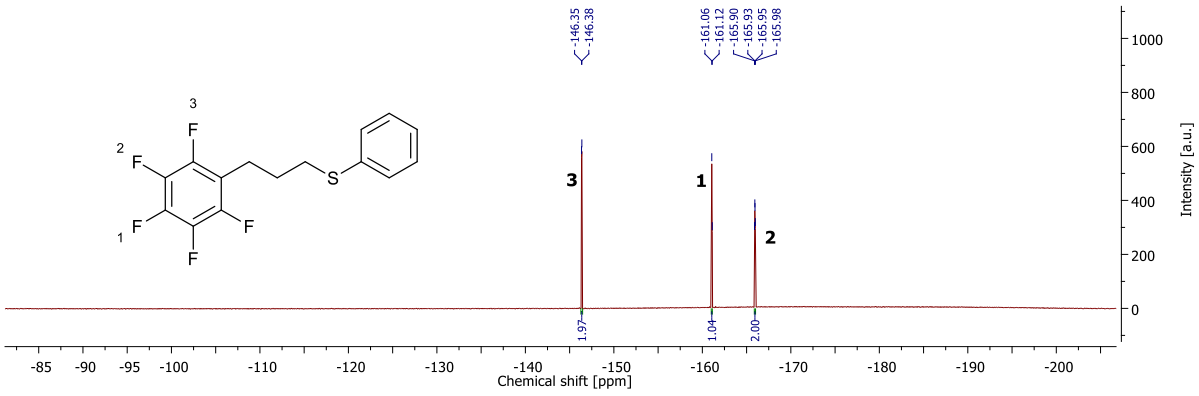

Figure 17: ^{19}F-NMR spectrum of product from thiol-ene reaction between allylpentafluorobenzene and thiophenol in MeOD.

The experiment was repeated under different conditions by changing one of the following parameters each: Reaction time (20-100 min), choice of solvent (no solvent, $CHCl_3$, MeOH, DMSO), concentration of educts (solvent-free, 0.24-2.40 mmol·mL^{-1}), stoichiometry of educts (1:1-1:6 eq.), choice of photoinitiator (DMPA, Irgacure 2959), amount of photoinitiator (0.05-0.5 eq.), presence of reducing agents (TCEP, THPP) and presence of water.

The success of each experiment was determined by the disappearance of allyl signals and appearance of alkyl product signals in the ^{1}H-NMR spectrum of the raw product. Especially the allyl signals of the educt allylpentafluorobenzene act as good markers for the reaction, since they are clearly visible in ^{1}H-NMR spectra and appear in a range where no overlap with other functional groups occurs. The degree of conversion was determined by the integral ratios of allyl educt signals and alkyl product signals in the ^{1}H-NMR spectrum.

Although the thiol-ene reaction yielded in a formation of the desired product in every experiment, the degree of conversion varied strongly, depending on the different parameters:

- **Reaction times** are not a restricting factor since the thiol-ene reaction is based on a rapid radical mediated mechanism. However, to ensure complete conversion, reaction times of at least 30-40 min should be chosen.
- The reaction runs smoothly with a *minimum amount* of 0.05 equivalents of **photoinitiator**.
- The **choice of photoinitiator** should be made depending on the solubility of the educts. 2-hydroxy-4'-(2-hydroxyethoxy)-2-methylpropiophenone (Irgacure 2959) was successfully tested as an alternative to DMPA.
- Although the reaction also works reliably for a 1:1 **stoichiometric ratio of educts**, maximum conversions are obtained for an excess of thiol component with a minimum amount of 2-3 equivalents. Above this, the **stoichiometry of educts** has little effect on the reaction.
- The **choice of solvent** has a strong effect on the reaction. The use of $CHCl_3$ and MeOH leads to a complete conversion, although $CHCl_3$ seems to be more suitable than MeOH for this model reaction. In contrast, the use of DMSO, leads to only 50 % conversion. Due to insolubilities of the educt allylpentafluorobenzene, water could not be tested as solvent in this model reaction.
- A high **concentration of educts** plays an **important role** for the reaction and a minimum of solvent or solvent-free conditions (if possible) should be chosen.
- The **presence of reducing agents** (such as THPP and TCEP) as well as the presence of water has **no effect** on the outcome of the reaction.

Those findings are in good accordance with low molecular thiol-ene literature.[366, 383, 393, 402, 409] However, it is conceivable that the best parameters found for this specific model reaction still need adjustment when different compounds or macromolecular educts are used. For polymers, literature usually reports an either equimolar[363] or excess amount of thiol compound, ranging from 1.2 eq.[230], to 1.5-3.0 eq.[601], 5.0 eq.[366] or even 10-fold[362] excess of thiol. The reaction is usually performed at room temperature[230, 601], with some exceptions that use temperatures of up to 70 °C[362]. The choice of solvent is pointed out to be important, with best results received for water or methanol and low conversion rates for reactions with DMSO.[601] Some works even performed the reaction under bulk conditions.[377] The use of either DMPA or Irgacure as initiators in amounts of approximately 1 % of

total sample weight is reported[363, 366, 601] and it has been described that the presence of mild reducing agents such as sodium borohydride or performing the reaction in thoroughly degassed solution leads to clean conjugation reactions without the formation of disulfide bridges.[368]

With literature and the low molecular model reactions serving as a guideline, further thiol-ene experiments were conducted as far as practicable with the least possible amount of solvent (preferably MeOH, $CHCl_3$ or solvent-free), 0.2-0.5 eq. DMPA or Irgacure 2959 as photoinitiator, 40-60 min reaction time and an excess of 2-6 equivalents thiol component. In case when the thiol component easily forms dimers, TCEP or THPP were added as reducing agent.

Chapter 4.1.4.2 *Thiol-Ene Reaction with NCL Product (Low Molecular)*

After having found suitable reaction parameters in the foregoing pilot studies, the last step of the model reaction cascade now uses the *products from the NCL* described in chapter 4.1.2 and chapter 4.1.3 in a thiol-ene reaction.

As shown in chapter 4.1.4.1, the presence of reducing agents does not affect the outcome of the reaction. Therefore, raw product from the NCL, a mixture between monomer and dimer of (4-methylbenzoyl)cysteine was used as a thiol component, together with TCEP as a reducing agent for *in situ* reduction of the disulfide bonds.

In first experiments allylpentafluorobenzene from the thiol-ene model reaction described in chapter 4.1.4.1 was used as an allyl component. The appearance of alkyl product signals in the respective ^{1}H-NMR spectrum suggests that the thiol-ene reaction was successful, however, there are still allyl signals present, which is a sign for an incomplete conversion. Since the fluorinated aromatic ring of allylpentafluorobenzene has a strong electron withdrawing effect and it was shown that electron-rich enes have a higher conversion than electron-poor enes[409], this compound is deemed to be a poor reaction partner for thiol-ene reactions.

Therefore, a different, more potent allyl compound was chosen and experiments using allyl functionalized acetylated mannose, which was provided by the working group of cooperation partner Prof. Seibel (Julius-Maximilians-Universität Würzburg), were conducted (see **scheme 15**).

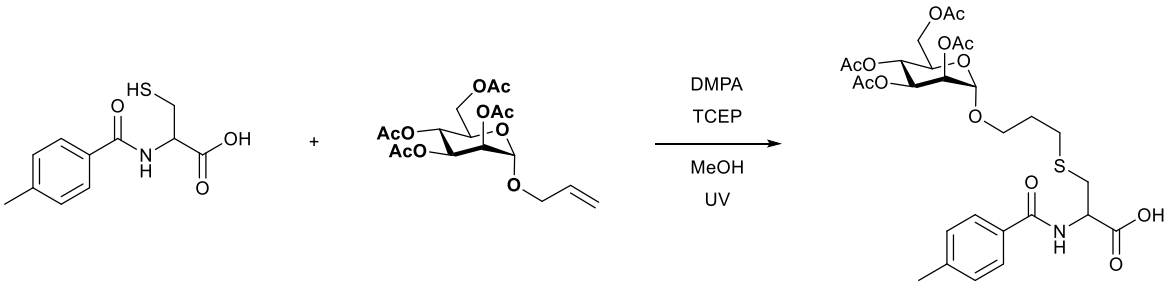

Scheme 15: Thiol-ene reaction between (4-methylbenzoyl)cysteine and acetylated allyl mannose under the presence of TCEP.

Acetylated allyl mannose and the raw NCL product were dissolved in MeOD under the presence of TCEP. DMPA was added and the reaction mixture was stirred under UV light irradiation. The raw product was then purified by column chromatography. Although column chromatography led to high losses in yield, the reaction was still successful and led to the formation of the final low molecular model reaction product, *N*-(4-methylbenzoyl)-*S*-(3-(perfluorophenyl)propyl)cysteine, which could be characterized via ^{1}H-NMR, ^{13}C-NMR, IR and MS.

The ^{1}H-NMR spectrum of the product (see **figure 18**) shows all expected signals. Next to a signal at 1.94-1.80 ppm, which belongs to the alkyl chain, four strong signals at 2.16-2.02 ppm from the sugar acetyl protecting groups are present. Also clearly visible is the singlet signal at 2.40 ppm from the methyl group at the aromatic ring, that originally belonged to thioester B. The signals at 2.80-2.59, 3.29-3.14, 3.80-3.45 and 5.04-5.02 ppm can be assigned to the alkyl chain of the newly formed thioether bond, whereas the signals at 4.01-3.95, 4.30-4.11, 4.81 and 5.38-5.24 ppm stem from the mannose ring. The broad signal of the N-H group is visible at 7.17-7.13 ppm. The aromatic ring of the former thioester provides two characteristic signals at 7.26-7.24 and 7.76-7.73 ppm. All signals of the corresponding carbon atoms can be found in the respective ^{13}C-NMR spectrum.

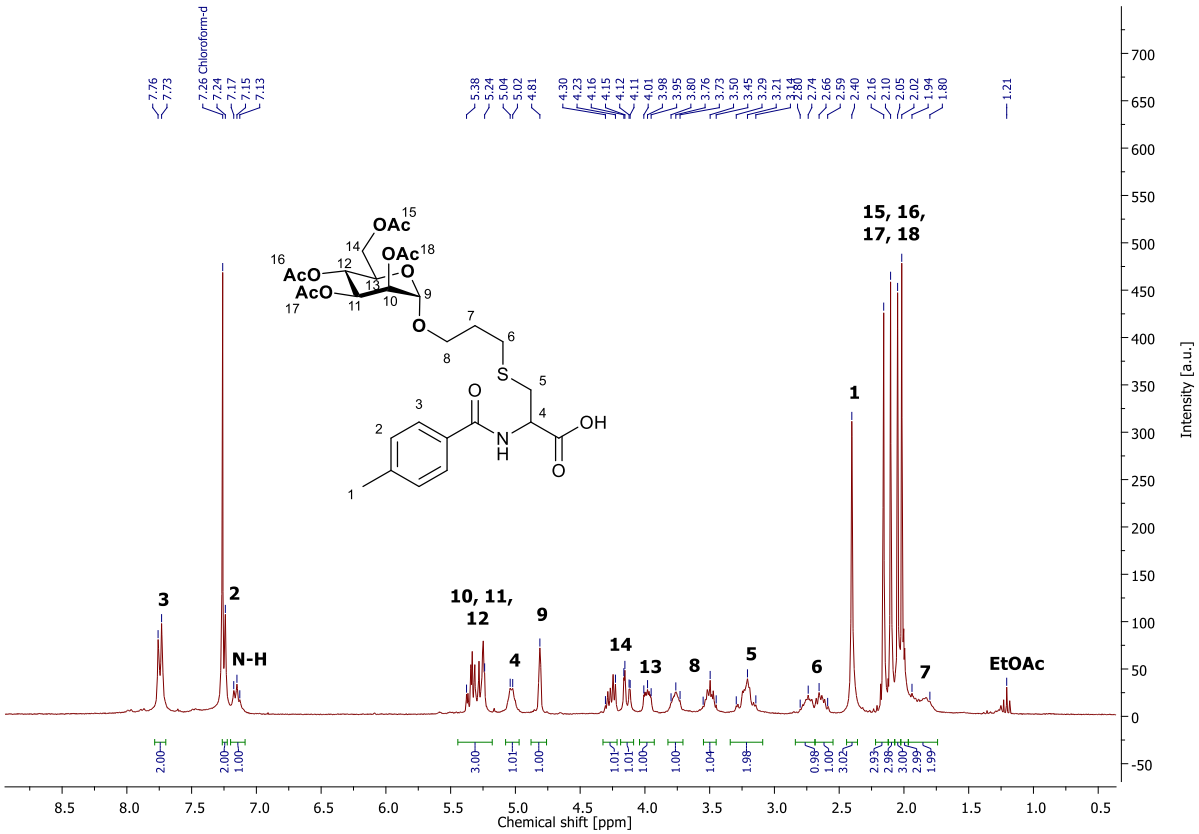

Figure 18: ^{1}H-NMR spectrum of low molecular thiol-ene product in $CDCl_3$.

FT-IR spectroscopy provides further proof for a successful reaction. The product from the NCL reaction served as an educt in the thiol-ene reaction. Its FT-IR spectrum was compared with the spectrum of the second educt, acetylated allyl mannose and the spectrum of the thiol-ene reaction product (see **figure 19**). In the spectrum of the thiol-ene reaction product, a strong signal appears at 1742 cm^{-1}. This signal is characteristic for the C=O stretching vibration of the acetyl groups of pure acetylated allyl mannose and cannot be found in the spectrum of the former NCL product. The appearance of this signal in the thiol-ene product spectrum is therefore a strong indicator that the mannose sugar has been attached to the NCL product via thiol-ene reaction. This becomes clearly visible when both educt and product spectra are overlaid, as shown in **figure 19**. When acetylated allyl mannose is conjugated to polymers in later chapters, similar findings can be observed.

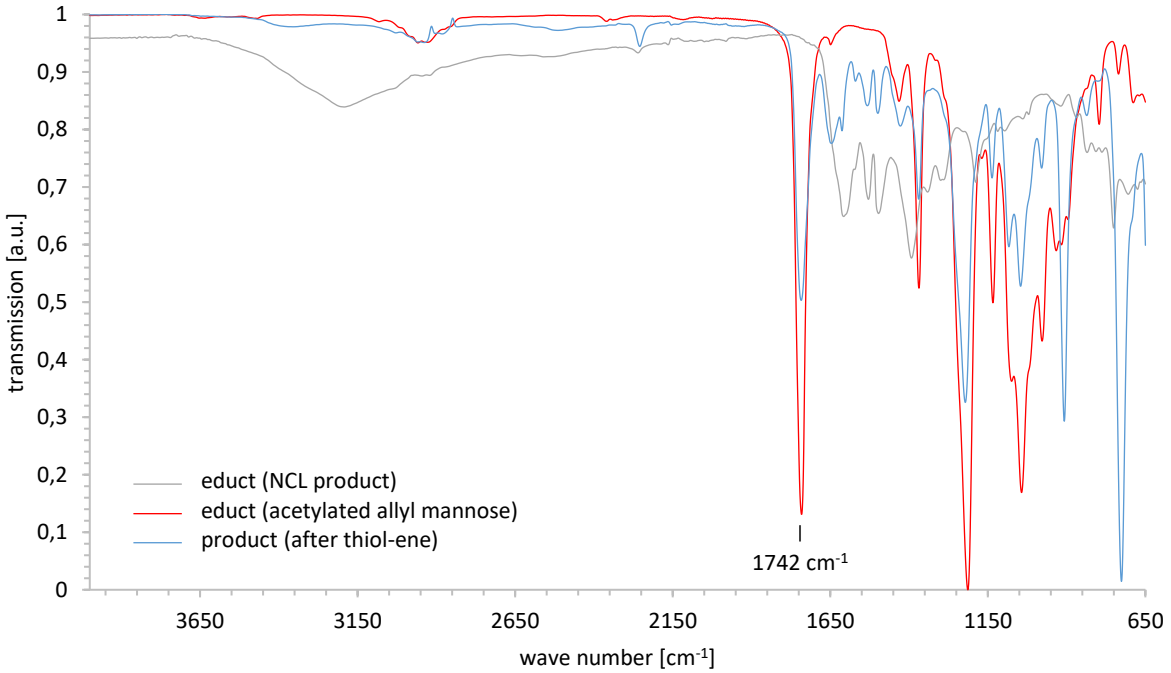

Figure 19: Superimposed IR spectra of acetylated allyl mannose (red), NCL product (grey) and thiol-ene reaction product (blue) with characteristic C=O stretching vibration of the sugar acetyl groups at 1742 cm^{-1}.

Having established the reaction cascade on a low molecular level by synthesizing a fully characterized three-part conjugate as a final product, it was now possible to transfer the set of reactions onto the stage of telechelic polymers.

Chapter 4.2 Telechelic Functionalization

As described in chapter 2.2.3, polyoxazolines can either be functionalized at the end of a polymer chain (telechelic) or at the side chain. While there is only one functional group introduced in telechelic functionalized polymers, with side chain functionalized polymers, it is possible to introduce multiple functional groups per polymer chain and thus, the complexity of the system increases.

This chapter focuses on performing the complete reaction cascade with single functionalized telechelic polymers, while chapter 4.3.1 will address the reaction cascade with multiple side chain functionalized polyoxazolines.

As further described in chapter 2.2.3, there are two different ways to functionalize polyoxazolines at one of their end termini: Functionalizing at the "starting point" of the polymer chain (α telechelic) via the use of a suitable initiator and functionalizing at the "rear end" of the polymer chain (ω telechelic) via the use of a suitable terminating reagent. Both ways will be addressed in the following chapters.

Chapter 4.2.1 Polymer Functionalization

The desired functionality of polyoxazolines after polymerization that will be of further use in this work is an allyl functionality. For ω telechelic polymers, this allyl functionality will be introduced by using allylamine as a terminating reagent for the polymerization (see chapter 4.2.1.1a). In case of α telechelic polymers, the allyl functionality will be introduced by allyl *p*-toluenesulfonate as an initiator (see chapter 4.2.1.1b).

After polymerization, there is little difference in reactivity between α and ω allyl functionalized polymers with the same chain length. Therefore, all subsequent reaction steps can be performed equally for both α and ω telechelic polymers and will be discussed only for ω allyl functionalized polymers. The necessary steps to thioester functionalized polymers (see **scheme 16**) are the attachment of a carboxylic acid unit via a thiol-ene reaction (see chapter 4.2.1.2) that can successively be converted into a thioester group via a thioesterification reaction (see chapter 4.2.1.3).

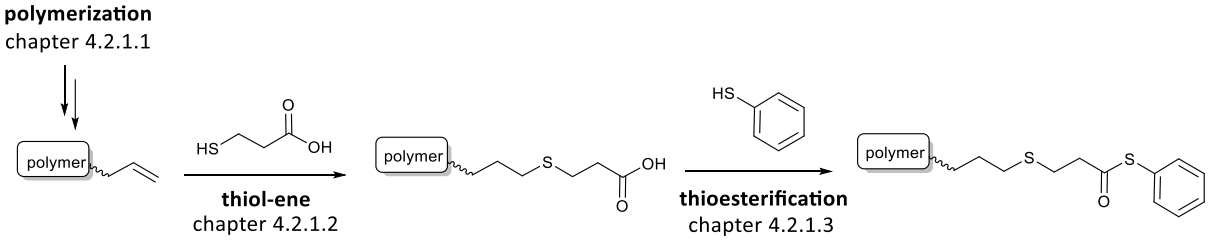

Scheme 16: Functionalization of α and ω telechelic polymers.

Concerning the chain length of a polymer, literature[602-605] and also a variety of experiments in this work showed that due to solvation or steric effects, short oligomers with less than 20 repeating units are more reactive than polymers with longer chains. Also, functionalization of short polymers delivers signals in ^{1}H-NMR spectroscopy with a good signal-to-noise ratio that are still clearly visible compared to the ever-present, strong backbone signals. Hence, short oligomers are more feasible to be used in *proof of principle* experiments. However, polymers with a longer chain are easier to purify via dialysis and are far more promising to be used in biomedical applications, since the retention time in organisms is prolonged with a growing mass of the polymer[444-446]. Therefore, POx with different chain lengths will be investigated in this work. Since the polymerization mechanism of polyoxazolines is a living polymerization (LCROP), the chain length of the resulting polymer can be controlled by the stochiometric use of monomers by using different stochiometric ratios of monomer to initiator during the polymerization reaction.

In this work, telechelic allyl functionalized PMeOx with chain lengths of 15, 20, 25, 30, 50, 60, 100 and 150 repeating units were synthesized. The synthesis and functionalization of telechelic, respectively side chain functionalized polyoxazolines is similar for different chain lengths and will be explained in detail by always taking the example of polymers with 50 repeating units.

Chapter 4.2.1.1 *Synthesis of Telechelic Allyl Functionalized Poly(2-Oxazoline)s*

a. Polymerization with Functionalization at the ω-end

To synthesize telechelic allyl functionalized PMeOx (see **scheme 17**), the initiator methyl *p*-toluenesulfonate and MeOx as monomer were first dissolved in dry acetonitrile. The stochiometric ratio of monomer to initiator determines the chain length of the polymer. In this case, 50 equivalents of MeOx and 1 equivalent of initiator were used to achieve a chain length of 50 repeating units. Before use, all educts were dried over CaH_2 and distilled. The polymerization was then carried out as a microwave reaction at 100 °C for 90 min under inert gas atmosphere. The detailed mechanism of the polymerization (LCROP) is described in chapter 2.2.2.2. In order to introduce the allyl functionality, allylamine was used as a nucleophilic terminating agent. It was added to the polymer solution after the microwave reaction and then stirred for two days at 45 °C. The polyoxazoline product was purified by precipitating from cold diethyl ether.

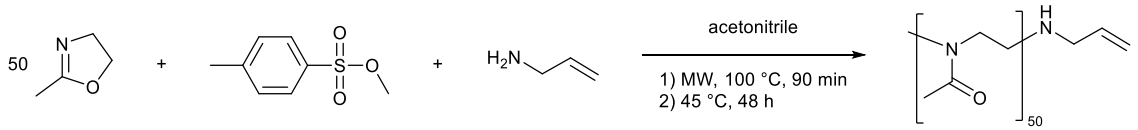

Scheme 17: Synthesis of ω telechelic allyl functionalized $PMeOx_{50}$.

The resulting polymer was analysed by ^{1}H-NMR spectroscopy (see **figure 20**). The signal at 3.04-2.93 ppm originates from the methyl group of the initiator and serves as intern reference in order to calculate the degree of polymerization. The appearance of this signal as a doublet structure is due to a possible rotation of the methyl group around the amide function, which leads to either a *syn*- or *anti*-conformation, as it was already investigated by Nuyken et al. in 1996.[553] Clearly recognizable are the strong signals at 3.46-3.43 and 2.12-2.05 ppm, which stem from the polymer *backbone*. The integral value of these signals delivers a chain length of 49-50 repeating units, which is in good accordance with the amount of 50 equivalents of monomer that were used in the polymerization reaction. Well distinguishable by their high chemical shift are the signals at 5.84-5.75 and 5.22 ppm, which, together with a signal at 3.02 ppm, originate from the terminating allyl group. Further signals that can be recognized in the spectrum at 7.68, 7.13, 2.32 and 1.18 ppm stem from the tosylate counterion and diethyl ether residues.

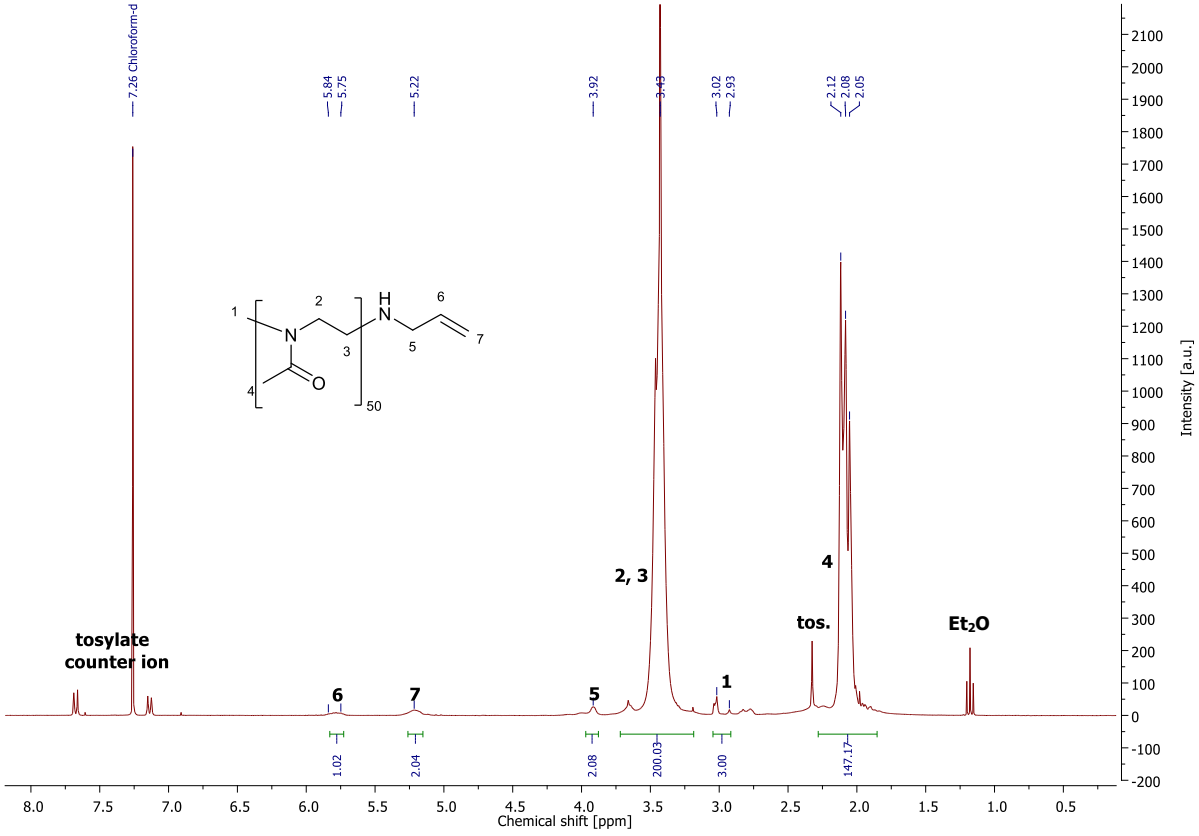

Figure 20: ^{1}H-NMR spectrum of telechelic allyl functionalized $PMeOx_{50}$ in $CDCl_3$.

SEC Measurements

SEC measurements in DMF show a narrow molecular weight distribution with a symmetric elugram (see **figure 21**), but a small shoulder towards high molecular weights yielding a dispersity of $Đ = 1.05$.

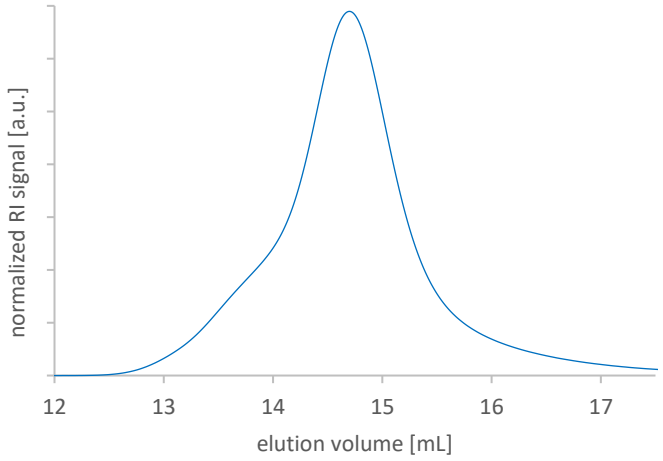

Figure 21: SEC elugram of telechelic allyl functionalized $PMeOx_{50}$ in DMF.

The molecular weight determined by SEC ($M_n = 4196$ g·mol^{-1}, $M_w = 4413$ g·mol^{-1}) corresponds to the molecular weight calculated from ^{1}H-NMR spectroscopy ($M_n = 4284$ g·mol^{-1}) and is in good accordance with the expected theoretical molecular weight ($M_n = 4326$ g·mol^{-1}). Since SEC is a relative measuring method, deviations in molecular weight values can be attributed to the use of commercially available PEG standards for calibration, which can show a different hydrodynamic radius and coiling behaviour compared to the respective POx derivates in different solvents.

In this work, dispersities between $Đ = 1.04$ and $Đ = 1.07$ have been achieved for telechelic allyl functionalized polymers up to 60 repetition units in size (see **table 5** of chapter 6.2.6 in the Experimental Section).

It is shown in Literature[511-512, 601, 606], that the reaction temperature, as well as the choice of initiator (and its corresponding salts) have a high impact on the probability of side reactions, which, in turn, can negatively affect a polymer's dispersity. With increasing temperatures up to 140 °C, as it is often used in microwave reactions, dispersity values can rise up to values of $Đ = 1.3$ and higher.[601] Compared to this, reaction temperatures of 100 °C, as they were applied in the aforementioned experiments, are considered to be moderate for this reaction and little probability for side reactions therefore leads to small dispersity values in this work.

Another factor that influences the dispersity is the impact from the length of the polymer. The longer a polymer is, the higher are the chances of chain-transfer reactions that lead to the initiation of new

chains while the active species of the old polymer chain is deactivated, as it has been proposed by Monnery et al. in 2018.[606]

For telechelic polymers with increasing chain lengths, the dispersity has slightly increased values of $Đ$ = 1.08 for polymers with 100 repetition units (9 kDa) and $Đ$ = 1.11 for polymers with 150 repetition units (13 kDa), which is still within the expected range of dispersity for polymers acquired by LCROP.

In other works[606], low temperatures of 40 °C and strict measures such as performing the polymerization by static distillation under high vacuum led to dispersity values of $Đ$ = 1.1-1.2 even for polymers with up to 300 kDa, but such drastic measures (with long reaction times up to 20-28 days) would have been uneconomic and not necessary in this case. Furthermore, those measures only account for poly(2-ethyl-2-oxazoline)s. In the case of poly(2-methyl-2-oxazoline)s, Sedlacek et al.[607] reported that a transfer of those reaction parameters can only be applied to polymers with molecular masses below 15 kDa, leading to dispersities below $Đ$ = 1.3. They postulate that lower steric hindrances of the α-proton of MeOx are responsible for higher chain-transfer rates.

As it is frequently depicted in Literature[55, 106, 511, 516, 601, 606, 608-609], it is not unusual for SEC spectra of polymers to exhibit one or multiple of the following characteristics: A shoulder towards high molecular weights, broadening of the signal or tailing towards low molecular weights. These effects will be considered in detail hereafter.

A *shoulder towards high molecular weights* can have its cause in side reactions such as chain transfer, described in the works of Monnery et at.[606] and Hoogenboom et al.[608], nucleophilic impurities, that lead to an E2 β-elimination reaction competing with the propagation reaction, as postulated by Litt et al.[511-512], as well as the formation of temporary adducts or aggregation effects, as discussed in the works of Paulus[610] and Luxenhofer[106]. Other influences of different initiators, solvents, temperatures, heating options and dialysis are thoroughly reviewed in a work of Liebscher[601], but reasons for resulting high molecular weight shoulder phenomena could not be clarified conclusively. However, sometimes those effects can get so strong, that even under high vacuum conditions (< 10^{-5} torr)[606], the occurrence of branching points and the risk of chain coupling, responsible for the formation of high molecular weight species, is high enough to yield bimodal elution curves.[458, 600-601]

In case of the spectrum depicted in **figure 21**, the shoulder is very weak in comparison to SEC spectra that are described elsewhere.[600-601, 609] It is assumed that the formation of temporary adducts is responsible for its formation. Because the effect is diminished with enhanced solubility of the substrate, the shoulder is not existent for short polymers with 15 repetition units (see **figure 90** of chapter 6.2.6 in the Experimental Section) and increases in intensity for longer polymers.

Tailing or *broadening* of the signal, as described extensively by Held et al.[611-612], is usually caused by a high salt content or interaction of functional groups of the substrate with column material, resulting in (ionic) adsorption or inclusion effects.[613] Furthermore, since tailing and broadening also affect the parameters that are used for the determination of dispersity values, those effects can distort otherwise representative measuring results and lead to artificially higher dispersity values. In some cases, interaction between substrate and column material is so strong, that no signal of the substrate can be detected.[613]

In the present work, tailing particularly occurs for carboxylic acid polymers (as described in chapter 4.2.1.2 as well as in chapter 4.3.1.3) and for long polymers (see the respective figures in the Experimental Section). It is assumed that any (carboxylic acid) functionality leads to strong interactions with column material, regardless of the different solvents and columns with different materials that were used in the experiments. The effect is significantly stronger for side chain functionalized polymers, presumably due to the attachment of multiple functional groups per polymer chain. Interaction between substrate and column material is especially the case for peptides, where those effects are so strong that the peptide is retained in the chromatography column, which therefore leads to a complete failure of the measurement. Aggregation of peptides with polymer peptide conjugates is for example also described in the work of Line et al.[614], where SEC measurements of polymer peptide conjugates delivered molecular mass values that differed from the expected values by a factor of 10.

SEC was performed for *all* polymers and polymer conjugates throughout this work. Since the choice of solvent has a great impact on the coiling behaviour of polymers[615], SEC measurements were performed with various column sizes and in different solvents: Water, chloroform and DMF. However, for polymer peptide conjugates, the measurements did not yield unambiguous results. If no SEC is mentioned in later chapters, the measurements did not deliver any convincing data.

MALDI-TOF Mass Spectroscopy Measurements

MALDI-TOF mass spectroscopy was used as another supplementary analytical method with the allyl functionalized polymer $PMeOx_{25}$. MALDI-TOF is an ionization technique, where a pulsed laser is used to desorb fragments of the target substance that has been embedded in a matrix. With this, it is possible to create ions from large molecules such as polymers and biomolecules with minimal fragmentation. The mass of the fragments is then determined by time of flight spectroscopy towards an ion detector. **Figure 22** shows the MALDI TOF mass spectrum of the polymer. It shows the mass distribution of the individual polymer chains, and the most intensive signal can be assigned to a polymer chain with 25 repeating units, which is in good accordance with the theoretically expected

values. The mass difference between two signals is 85.1 g·mol^{-1} each, which corresponds to one repeating unit of the polymer.

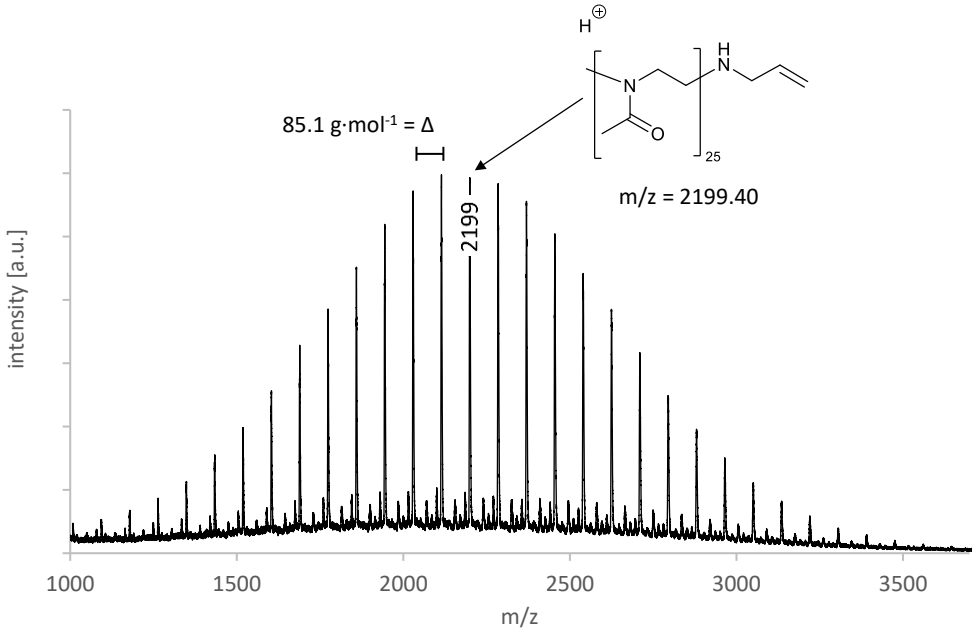

Figure 22: MALDI-TOF mass spectrum of telechelic allyl functionalized PMeOx$_{25}$.

b. Polymerization with Functionalization at the α-end

A different approach to synthesize telechelic allyl functionalized PMeOx is to use an allyl functionalized initiator such as allyl *p*-toluenesulfonate in the polymerization reaction. In this case, the allyl functionality will not be introduced at the ω-, but at the α-end of the polymer. This method is also described in greater detail in the master thesis of Bettina Böhm[600].

Functionalizing the polymer with an allyl group at the α end allows for the introduction of a second functional group at the ω end group by using a specific termination agent. In this work, a short polymer with 20 repeating units that bears an α-end allyl group and an ω-end thioether group will be synthesized (see **scheme 18**) and referred to as allyl-PMeOx$_{20}$-SEt. The thioether ω-end group will be introduced by using ethanethiol as a terminating agent of the reaction. The reason to introduce two different telechelic functionalities is to allow the polymer and its conjugates to be used for SAW and SPR affinity measurements, which will be described in detail in chapter 4.2.5.

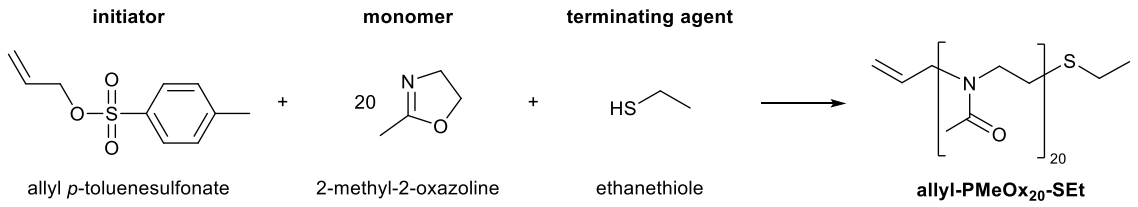

Scheme 18: Synthesis of telechelic α allyl and ω thioether functionalized allyl-PMeOx$_{50}$-SEt.

Initiator Synthesis

First, the initiator allyl *p*-toluenesulfonate was synthesized from allyl alcohol and tosyl chloride under the presence of benzyltrimethylammonium chloride as stabilizing agent (see **scheme 19**). The reaction was performed as described in literature[600, 616-618] for 90 min at 0 °C in a solution of THF with 2.5 M NaOH as a base. After washing the organic phase with water and removal of solvent, the final product could be obtained in yields of 67 %, which is in good accordance with literature.[600, 616-618]

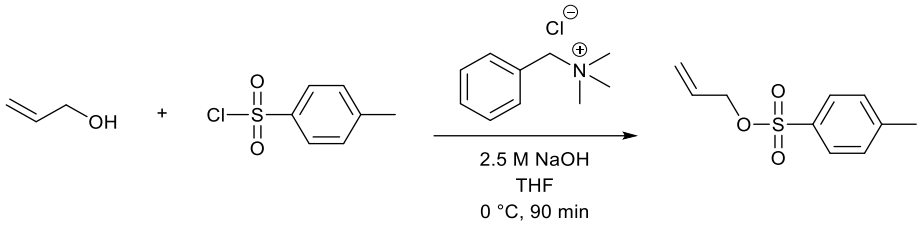

Scheme 19: Synthesis of allyl *p*-toluenesulfonate.

The ^{1}H-NMR spectrum of allyl *p*-toluenesulfonate (see **figure 23**) shows two dublets at 7.78 and 7.33 ppm from the signals 4 and 5 of the aromatic ring, two characteristic signals at 5.87-5.74 ppm and 5.34-5.21 ppm, corresponding to the signals 2 and 1 from the allyl functionality, a doublet at 4.52 ppm from the alkyl CH_2 group and a strong singlet at 2.43 ppm that can be assigned to the three methyl group protons. The spectrum shows no impurities.

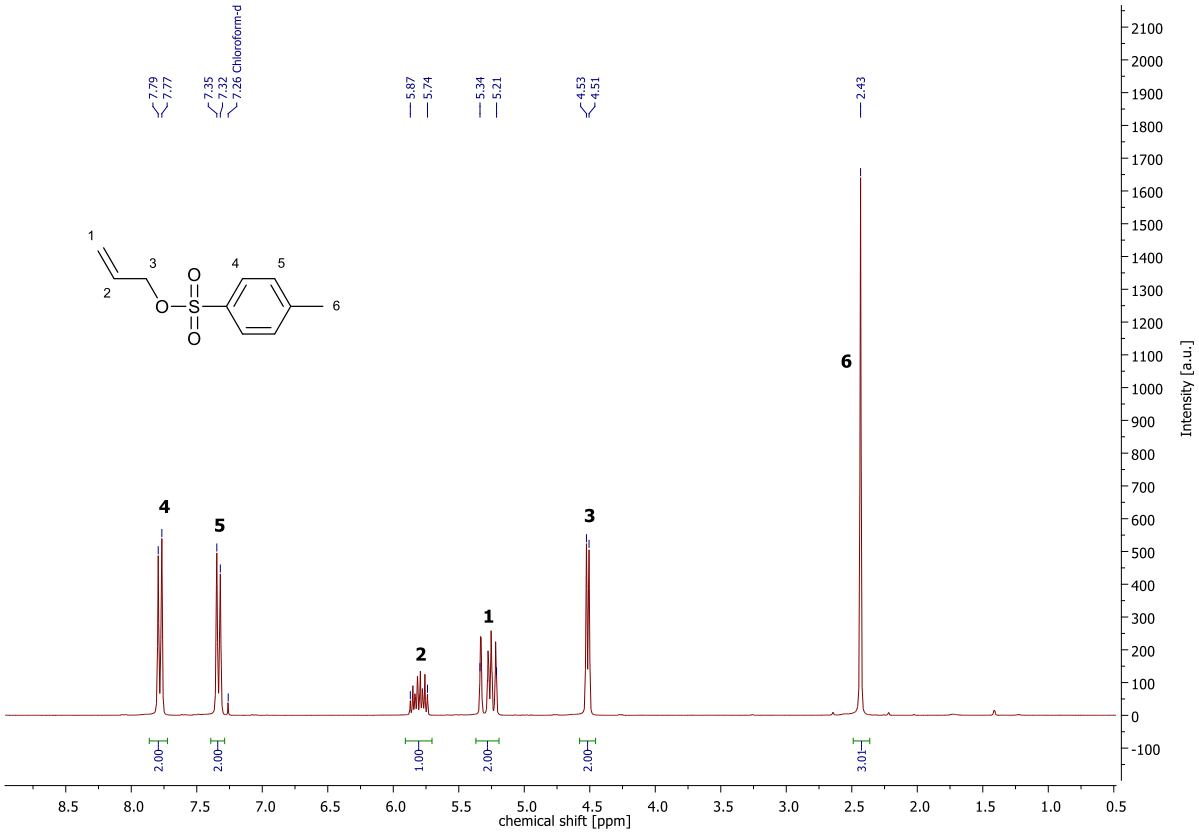

Figure 23: ^{1}H-NMR spectrum of allyl *p*-toluenesulfonate in $CDCl_3$.

Polymerization and Termination

The polymerization and termination of telechelic α-end allyl functionalized polymer was performed in analogy to the ω-end allyl functionalized polymer (see **scheme 20**). The initiator allyl *p*-toluenesulfonate and MeOx as monomer were first dissolved in dry acetonitrile. In this case, 20 equivalents of MeOx and 1 equivalent of initiator were used to achieve a chain length of 20 repeating units. Before use, solvent and monomer were dried over CaH_2 and distilled. The polymerization was then carried out as a microwave reaction at 100 °C for 60 min under inert gas atmosphere. In order to introduce the thioether functionality, ethanethiol was used as a nucleophilic terminating agent. It was added to the polymer solution after the microwave reaction and then stirred for 24 h at 40 °C. The polyoxazoline product was purified by precipitating from cold diethyl ether. It will be referred to as allyl-$PMeOx_{20}$-SEt.

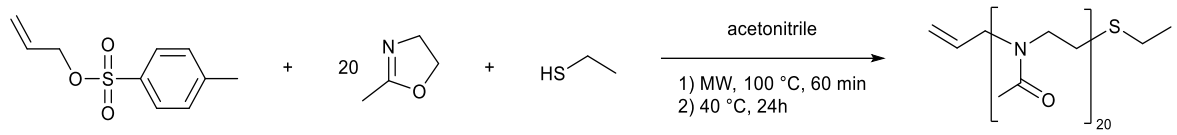

Scheme 20: Synthesis of telechelic α-end allyl and ω-end thioether functionalized allyl-$PMeOx_{20}$-SEt.

The resulting polymer was analysed by ^{1}H-NMR spectroscopy (see **figure 24**).

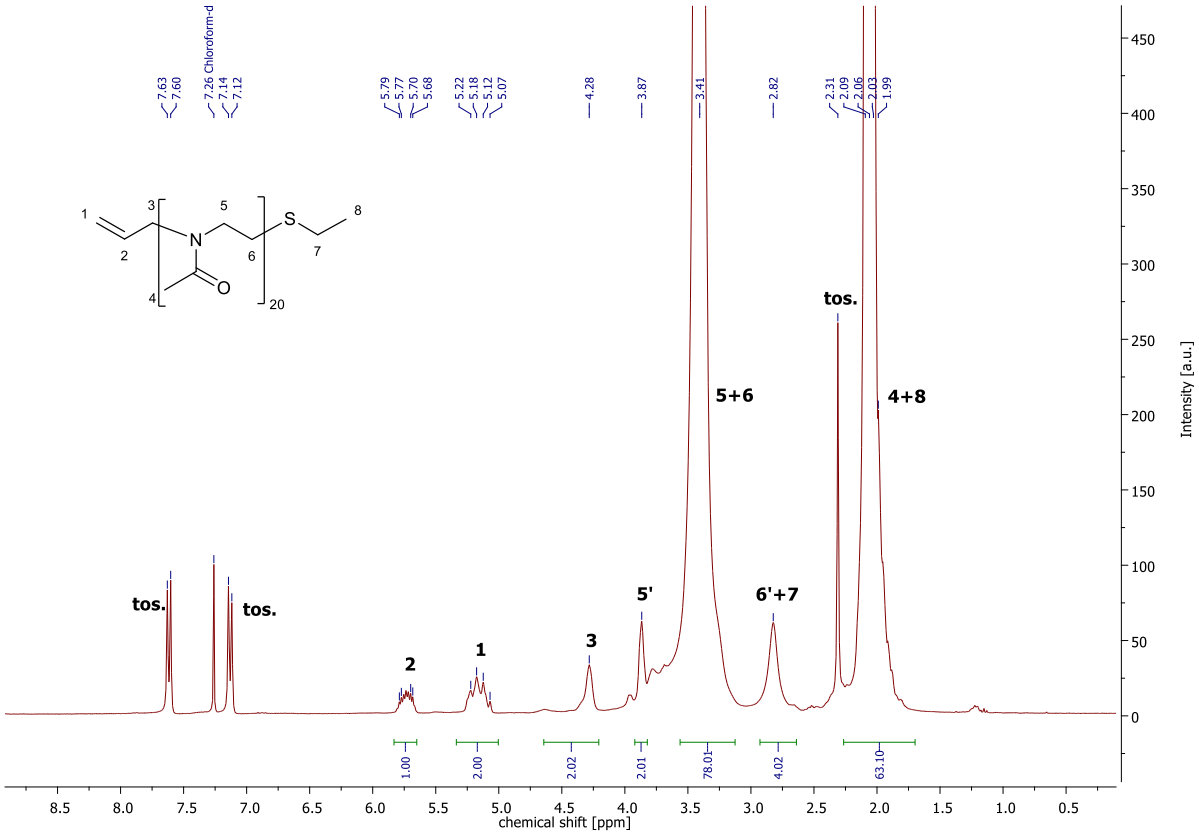

Figure 24: ^{1}H-NMR spectrum of telechelic α-end allyl and ω-end thioether functionalized allyl-$PMeOx_{20}$-SEt in $CDCl_3$.

The characteristic signals at 5.79-5.68 ppm and 5.22-5.07 ppm originate from the allyl group of the initiator and serve as intern reference in order to calculate the degree of polymerization. The signal at 4.28 ppm stems from the alkyl chain CH_2 group of the initiator. Clearly recognizable are the strong signals at 3.41 and 2.09-1.99 ppm, which stem from the polymer *backbone* and side chain methyl groups. Integration of these signals delivers a chain length of 20 repeating units, which is in good accordance with the amount of 20 equivalents of monomer that were used in the polymerization reaction. It is notable that the last repeating unit of the polymer chain displays slightly shifted signals 5' and 6' due to the attached thioether group, which in turn delivers a signal at 2.82 ppm and another signal that is overlaid by the methyl side group signal, hence the higher integral value. Further signals that can be recognized in the spectrum at 7.62, 7.13 and 2.31 ppm stem from the tosylate counterion.

SEC measurements in DMF show a narrow molecular weight distribution with a symmetric elugram (see **figure 25**) and a dispersity of $Đ = 1.05$. The molecular weight determined by SEC ($M_n = 1759\ g{\cdot}mol^{-1}$, $M_w = 1854\ g{\cdot}mol^{-1}$) corresponds to the molecular weight calculated from ^{1}H-NMR spectroscopy ($M_n = 1847\ g{\cdot}mol^{-1}$) and is in good accordance with the expected theoretical molecular weight ($M_n = 1804\ g{\cdot}mol^{-1}$). The spectrum exhibits a minimal shoulder towards high molecular weights, which also has its cause in the formation of temporary adducts and its form is even smaller compared to the spectrum of the ω functionalized polymer from the preceding chapter. In this case, the polymer has 20 repetition units and as mentioned before, the results substantiate the observation that aggregation effects are diminished because of the increased solubility of shorter chain length polymers.

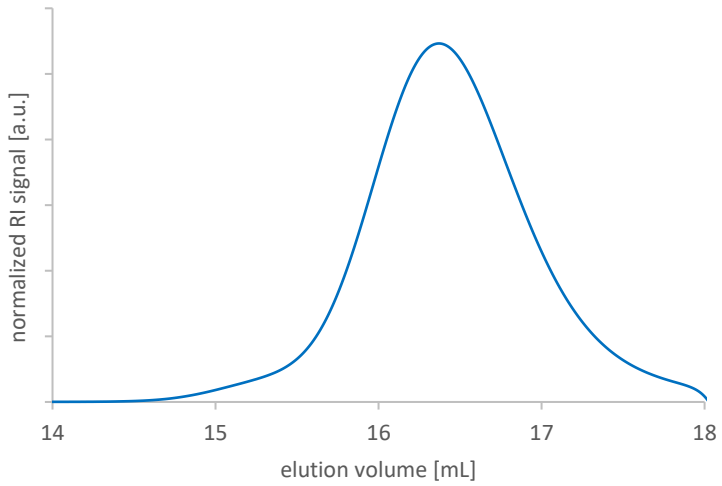

Figure 25: SEC elugram of telechelic allyl functionalized allyl-PMeOx$_{20}$-SEt in DMF.

Chapter 4.2.1.2 *Synthesis of Telechelic Carboxylic Acid Functionalized Poly(2-Oxazoline)s*

In order to introduce a carboxylic acid functionalization into the polymer, the allyl end group can be reacted with 3-mercaptopropionic acid in a thiol-ene reaction (see **scheme 21**). For this, both the allyl functionalized polymer and 3-mercaptopropionic acid were dissolved in dry methanol, DMPA was added as a photoinitiator and the reaction was stirred under UV light irradiation for 60 min. The detailed mechanism of the thiol-ene reaction is described in chapter 2.1.5. The resulting carboxylic acid functionalized polymer will be referred to as $PMeOx_{50}$-COOH.

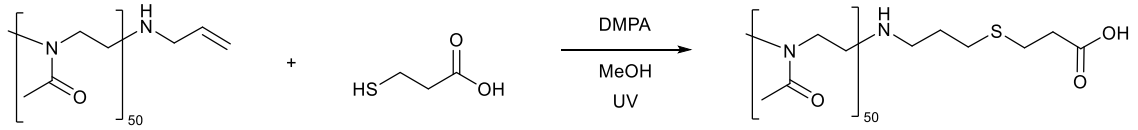

Scheme 21: Synthesis of telechelic carboxylic acid functionalized $PMeOx_{50}$-COOH.

The resulting polymer was analysed by ^{1}H-NMR spectroscopy (see **figure 26**). Most remarkably, the characteristic allyl signals from the educt polymer at 5.84-5.75 and 5.22 ppm have disappeared, which is a good indicator for a successful thiol-ene reaction, as shown in the low molecular model reaction (see chapter 4.1.4). Instead, new signals from the formed alkyl chain as well as alkyl signals from the attached mercaptopropionic acid appear at 2.94-2.90, 2.78-2.69 and 2.65-2.57 ppm.

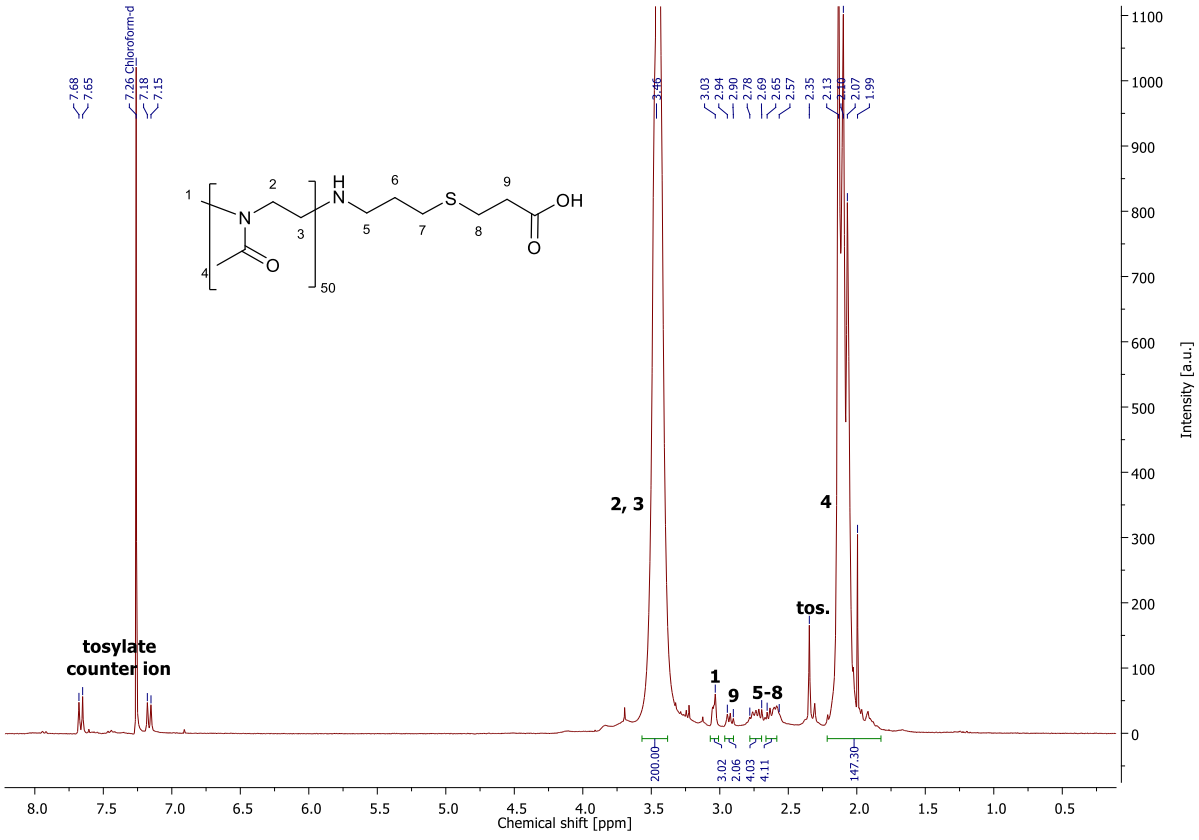

Figure 26: ^{1}H-NMR spectrum of telechelic carboxylic acid functionalized $PMeOx_{50}$-COOH in $CDCl_3$.

The signal from the initiator methyl group can still be found at 3.03 ppm, as well as the broad signal at 3.46 ppm from the polymer *backbone,* which was used as intern reference, and the broad side chain methyl group signal at 2.13-1.99 ppm. Further signals at 7.67, 7.17 and 2.35 ppm stem from the tosylate counter ion.

IR spectroscopy is another method that can be used to monitor the reaction cascade pathway. The stretching vibration of C=O from the attached carboxylic acid group delivers a characteristic signal in the IR spectrum at 1721 cm^{-1} (see **figure 27**), which is not present in the IR spectrum of the precursor allyl functionalized polymer. While the signal is still weak for a single telechelic functionalization, its intensity increases for multiple side chain functionalized polymers, which will be discussed in more detail in chapter 4.3.1.3.

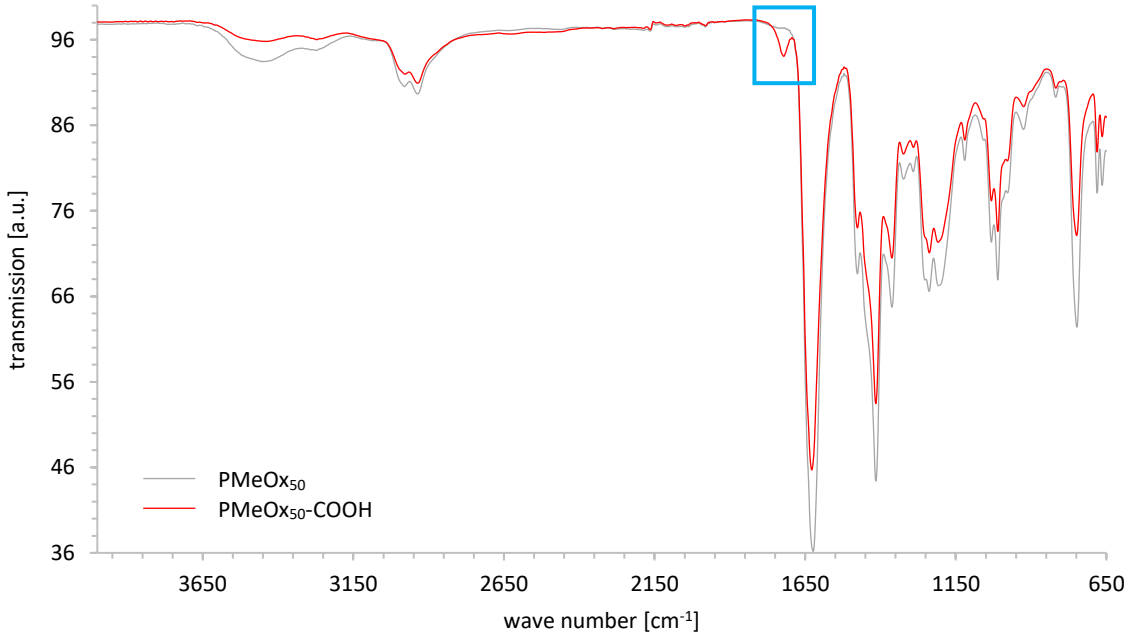

Figure 27: Superimposed IR spectra of educt allyl functionalized polymer $PMeOx_{50}$ (grey) and product carboxylic acid functionalized polymer $PMeOx_{50}$-COOH (red) with characteristic C=O stretching vibration of the carboxylic acid group at 1721 cm^{-1} (highlighted with blue box).

Although no major changes in the molecular mass of the polymer are expected from functionalization, SEC measurements were performed on this stage of the reaction cascade as well. With M_n = 4353 g·mol^{-1} and M_w = 4793 g·mol^{-1}, the results correspond to the theoretically expected value of M_n = 4433 g·mol^{-1}. Due to the attached carboxylic acid group however, high interactions with column material occur and lead to a long tailing of the elution signal (see **figure 28**), which has already been discussed extensively in the preceding chapter 4.2.1.1. This tailing effect is also associated with a higher dispersity of $Đ$ = 1.10, compared to the precursor polymer that shows a dispersity of $Đ$ = 1.05.

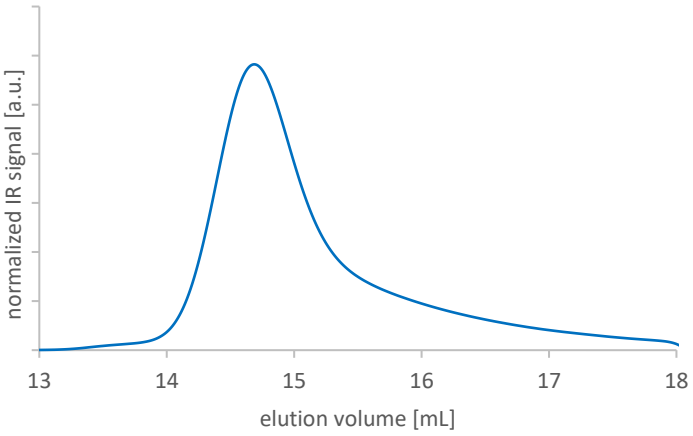

Figure 28: SEC elugram of telechelic carboxylic acid functionalized $PMeOx_{50}$-COOH in DMF.

As an additional analytical method, MALDI-TOF mass spectroscopy was performed with the carboxylic acid functionalized polymer $PMeOx_{25}$-COOH, which is shown in **figure 29**. Compared to the precursor polymer (see chapter 4.2.1.1), the increase in mass through the attachment of 3-mercaptopropionic acid can be observed. With a measured molecular mass of 2305 g·mol^{-1}, the most intensive signal of the spectrum corresponds to the theoretically expected value of the polymer with 2304 g·mol^{-1} plus an adjacent proton. The mass difference between two signals is still 85.1 g·mol^{-1} each, which corresponds to one repeating unit of the polymer.

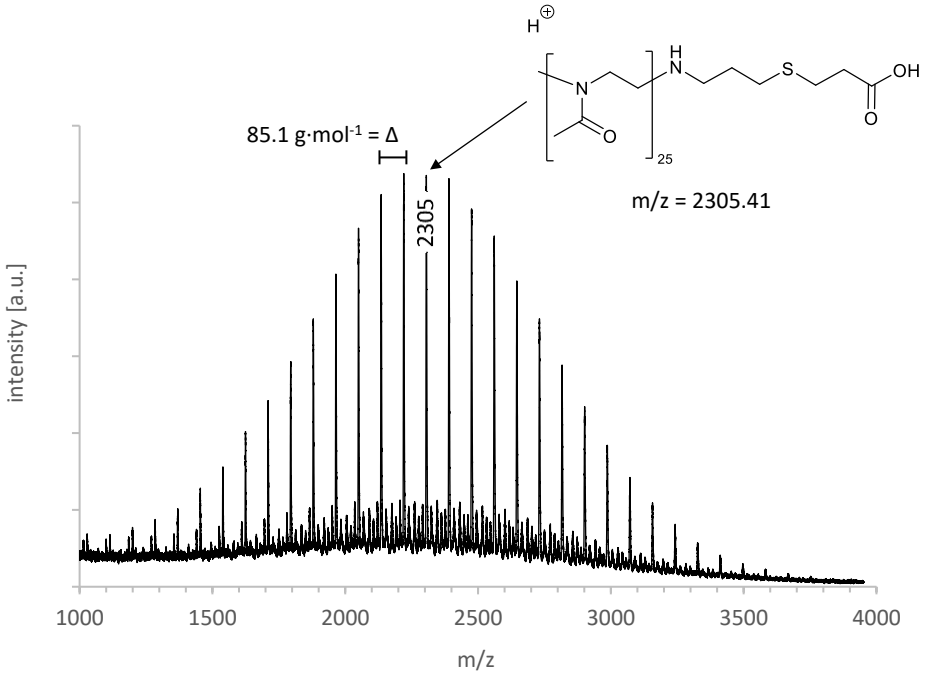

Figure 29: MALDI-TOF mass spectrum of telechelic carboxylic acid functionalized $PMeOx_{25}$-COOH.

Titration is a further supplementary method that was performed in order to yield information on the functionalization of the polymer with carboxylic acid groups. The results of the titration of telechelic carboxylic acid functionalized polymers are in good accordance with the theoretically expected values and will be discussed together with the results from side chain functionalized polymers in chapter 4.3.1.3.

Chapter 4.2.1.3 *Synthesis of Telechelic Thioester Functionalized Poly(2-Oxazoline)s*

The carboxylic acid group of telechelic functionalized PMeOx$_{50}$-COOH can be converted into a thioester functionality via thioesterification (see **scheme 22**), analogous to the low molecular model reaction (see chapter 4.1.1). For this, PMeOx$_{50}$-COOH, together with *N*-methylmorpholine as a base, is dissolved in a mixture of chloroform and THF. After 90 min, isobutyl chloroformate as an activating agent for the carboxylic acid and thiophenol are added and the reaction is stirred overnight. In order to absorb water that is formed during the reaction, dry 4 Å molecular sieve is put into the reaction flask. The resulting thioester functionalized copolymer will be referred to as PMeOx$_{50}$-COSPh and is obtained and purified via filtration and precipitation from cold diethyl ether.

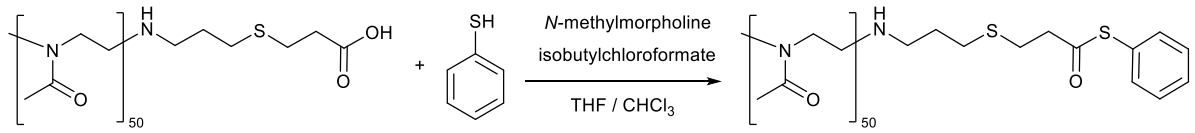

Scheme 22: Synthesis of telechelic carboxylic acid functionalized PMeOx$_{50}$-COSPh.

The resulting polymer was analysed by ^{1}H-NMR spectroscopy (see **figure 30**). The most relevant signal can be found at 7.41 ppm and stems from the attached thiophenol. Interestingly, the aromatic ring does not yield multiple signals in the aromatic range as one would expect, but only one singlet signal with an integral of 5 for the five phenyl ring protons. This effect is already known, as it is also observed in the low molecular model reaction (see chapter 4.1.1) and in analogous reactions of peptides that are described in literature[225].

The ^{1}H-NMR spectrum also exhibits three signals at 4.25-4.16, 4.00-3.96 and 2.83-2.81 ppm that do not belong to the copolymer, but stem from a by-product (bp) that was formed from an isobutyl chloroformate side reaction. This by-product shows similar solubility as the desired polymer and can therefore not be removed by precipitation from cold diethyl ether. Certain control experiments, where each educt was reacted with one another were conducted in order to investigate the origin and behaviour of this by-product as well as its influence on further reaction steps. Those experiments revealed that formation of the side-product is independent from the thioester formation, since it occurs when only *N*-methylmorpholine, carboxylic acid and isobutyl chloroformate, but no thiol compound is present. The experiments also prove that it is possible to remove the by-product via dialysis against water. However, this technique was not utilised to purify the product at this stage of the reaction cascade as it affects the water-sensitive thioester group of the functionalized polymer. Nevertheless, the by-product does not affect the NCL reaction, therefore the raw copolymer could be used in subsequent reactions without further purification.

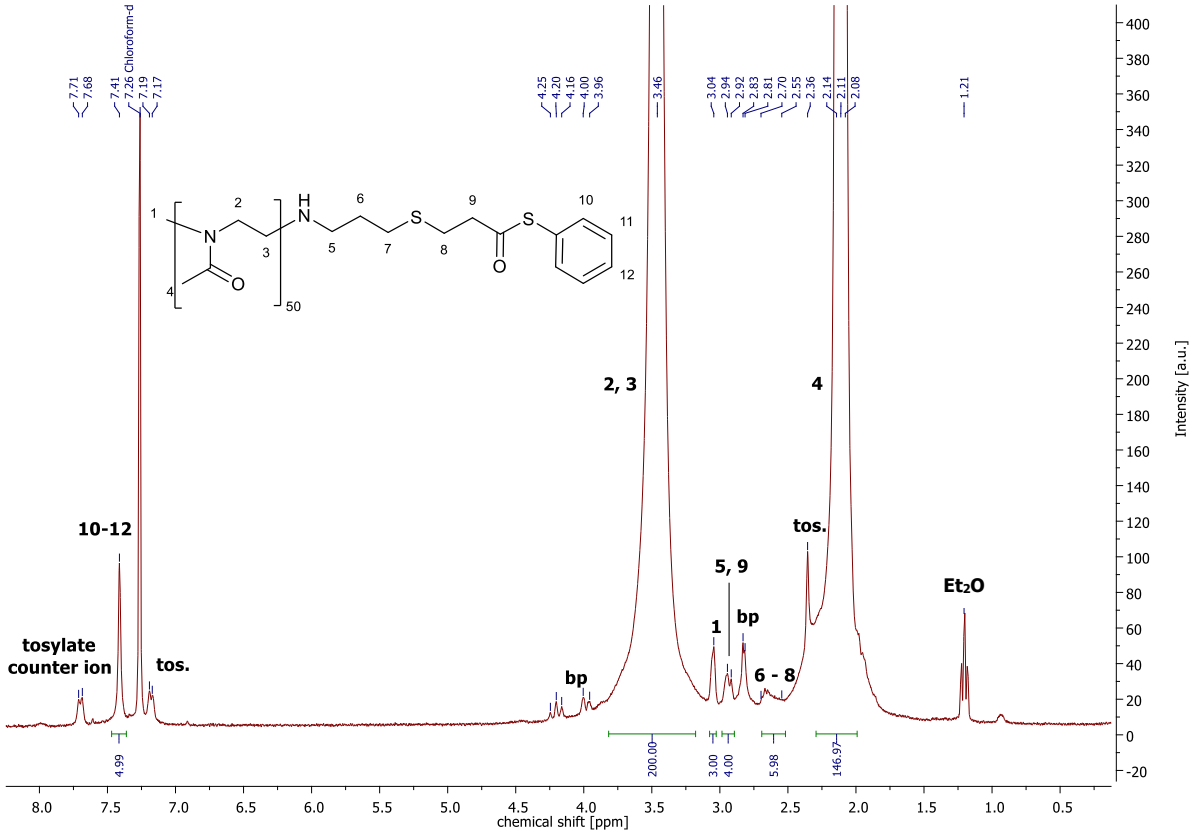

Figure 30: ^{1}H-NMR spectrum of telechelic thioester functionalized $PMeOx_{50}$-COSPh in $CDCl_3$ with additional signals from an isobutyl chloroformate by-product (bp).

In analogy to the precursor carboxylic acid functionalized polymer, the remaining signals can easily be assigned to the rest of the polymer: Strongly present is the broad *backbone* signal at 3.46 ppm which was again used as an internal reference. Also visible is the signal from the methyl initiator group at 3.04 ppm. The signals at 2.94-2.92 and 2.70-2.55 ppm stem from the ω-terminal alkyl chain of the polymer, whereas the broad signal at 2.14-2.08 ppm stems from the side chain methyl groups. Further visible are tosylate counter ion and diethyl ether residue signals at 7.69, 7.18, 2.36 and 1.21 ppm.

With increasing polymer chain lengths of 100 and 150 repetition units, the side reaction diminishes and the spectra of those polymers no longer show any signals of by-products, while the rest of the signals such as initiator signals and thioester group signals are still present (see **figure 31**). It is assumed that the side reaction is insignificant for large macromolecules and occurs only for short oligomers due to reactivity differences between short and long polymers. It is conceivable that short polymers have a higher susceptibility to side reactions because of their higher reactivity in solution.

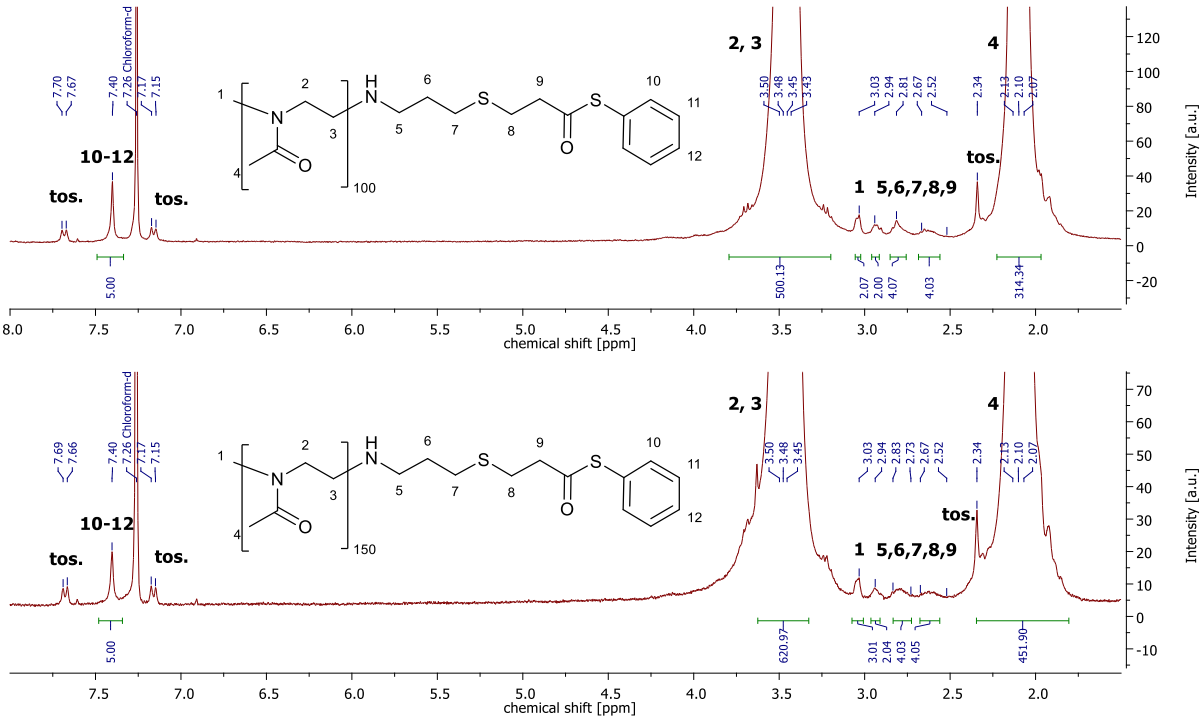

Figure 31: ^{1}H-NMR spectra of long chain telechelic thioester functionalized $PMeOx_{100}$-COSPh (top) and $PMeOx_{150}$-COSPh (bottom) in $CDCl_3$ without any by-product signals.

SEC measurements were performed on this stage of the reaction cascade as well. Although there is a weak high molecular shoulder as well as a low molecular plateau in the elugram, it displays one distinct and symmetrical main signal (see **figure 32**). Again, the shoulder is assumed to have its cause in aggregation effects, as discussed previously. With M_n = 4427 g·mol^{-1}, M_w = 4672 g·mol^{-1}, the results correspond to the theoretically expected value of M_n = 4525 g·mol^{-1}. It appears that the thioester group interferes less with the column material than the precursor carboxylic acid functional group, which leads to significantly less tailing effects. Contrary to the carboxylic acid functionalized derivate, where tailing effects led to an increased dispersity of $Đ$ = 1.10, the measured dispersity of $Đ$ = 1.06 now again complies with dispersity of the allyl functionalized base polymer ($Đ$ = 1.05).

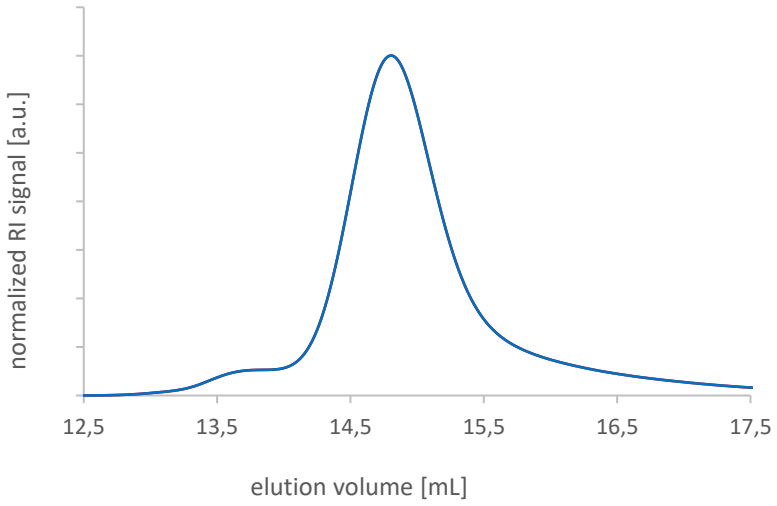

Figure 32: SEC elugram of telechelic thioester functionalized $PMeOx_{50}$-COSPh in DMF.

IR spectroscopy measurements were also performed with the thioester functionalized polymer and confirm a successful conversion of the carboxylic acid group into a thioester group, which is observable through a wavelength shift from 1721 cm^{-1} to 1703 cm^{-1} of the respective C=O stretching vibration signal. Because the thioester functionality only delivers a weak band in the spectrum, those signals are easier to recognize for the reader, when they can be compared to relatively stronger signals from multiple side chain functionalized polymers. Therefore, the spectra of those measurements will be depicted in chapter 4.3.1.4 together with the spectra from the side chain functionalized polymers.

Exactly like the precursor steps, this stage of the reaction cascade was as well examined by MALDI-TOF mass spectroscopy as a supplementary analytical method. With a molecular mass of 2397 $g \cdot mol^{-1}$, the mass value of the most intensive signal of the spectrum is in good accordance with the theoretically expected value of 2397 $g \cdot mol^{-1}$ and confirms the attachment of the aromatic thiol in the thioesterification reaction (see **figure 33**). The mass difference between two signals is still 85.1 $g \cdot mol^{-1}$ each, corresponding to one repeating unit of the polymer.

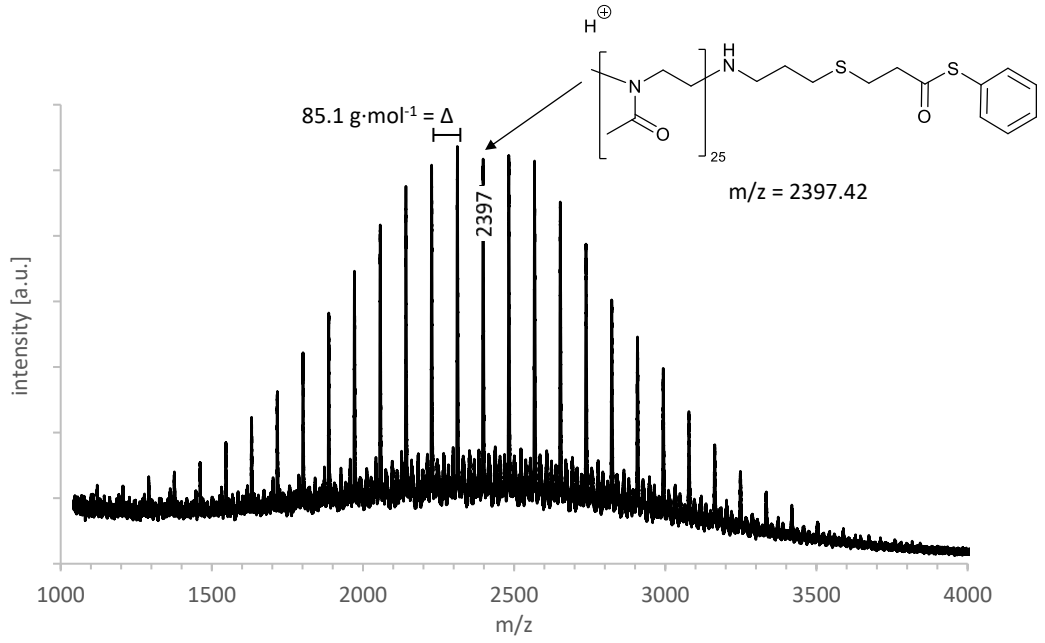

Figure 33: MALDI-TOF mass spectrum of telechelic thioester functionalized $PMeOx_{25}$-COSPh.

Chapter 4.2.2 NCL with Different Peptides

The telechelic and later on also the side chain functionalized thioester polymers (see chapter 4.3.2) were conjugated with a number of peptides in an NCL. The detailed mechanism of this reaction is described in chapter 2.1.4. All peptides and polymers used for conjugation are presented in **figure 34** on page 86. For reasons of clarity and comprehensibility, the used polymers and peptides will furthermore not be depicted with their whole molecular structure or peptide sequence, but in a simplified way. This depiction, as well as a definite term to which each (co)polymer and (co)polymer-peptide conjugate will be referred to in the text, is also shown in **figure 34**.

The used peptides are CGGGF, CKFKFQF and CGGWYKYW. A cysteine functionality is necessary for the NCL, therefore each of the three peptides bears an *N*-terminal cysteine. The peptides were chosen based on criteria concerning their structural properties:

CGGGF and CKFKFQF act as model peptides for the reaction, with CGGGF being a short peptide with little side chain functionality and good solubility in water and organic solvents. CKFKFQF is a longer peptide with side chain functionalities that decrease its solubility and allow the peptide to form gels and fibrils in water.[619-620] Both peptides bear a phenylalanine amino acid, whose aromatic phenyl side chain group allows for a straightforward recognition in NMR spectroscopy.

According to literature[150], the amino acid sequence WYKYW exhibits an affinity to galectins. Binding such a peptide to polymers would yield the possibility to measure biomacromolecular polymer-peptide-conjugate affinities to lectins, in this case, galectins. To enable binding of the peptide sequence with a polymer, the chain was prolonged by addition of two glycine units as spacers and a terminating NCL-reactive cysteine unit, which resulted in a peptide sequence of CGGWYKYW. This peptide was then ordered and synthesized from *GeneCust*.

Each peptide was conjugated with both telechelic and side chain functionalized (co)polymers, with the reaction parameters being oriented to the low molecular model reaction. This chapter focuses on the conjugation to telechelic polymers, with a subchapter for each peptide. Later on, chapter 4.3.2 will then present the conjugation to side chain functionalized polymers.

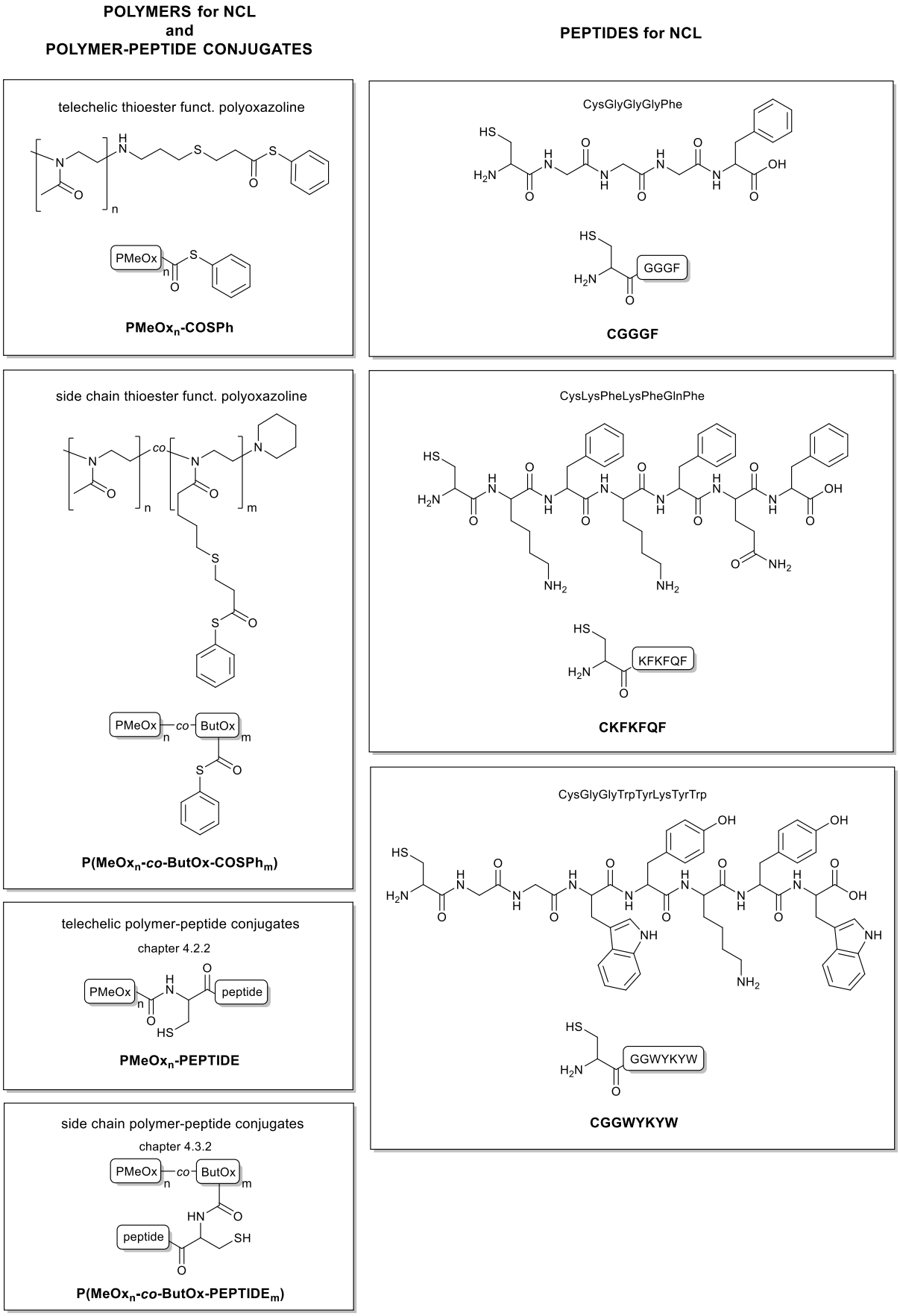

Figure 34: Polymers (left) and peptides (right) used in the NCL to form polymer-peptide conjugates (bottom left).

Chapter 4.2.2.1 *NCL with Telechelic Functionalized Polymers and CGGGF*

The telechelic thioester functionalized PMeOx$_{50}$-COSPh can be conjugated with the peptide CGGGF in a NCL (see **scheme 23**) analogous to the low molecular model reaction (see chapter 4.1.2). For this, CGGGF was dissolved in methanol and sodium borohydride was added. PMeOx$_{50}$-COSPh was added and the reaction was stirred for 4 days at room temperature. The resulting peptide functionalized polymer will be referred to as PMeOx$_{50}$-CGGGF and was obtained and purified via precipitation from cold diethyl ether.

Scheme 23: Synthesis of telechelic peptide functionalized PMeOx$_{50}$-CGGGF.

The resulting polymer was analysed by ^{1}H-NMR spectroscopy (see **figure 35**). The signal from the former thioester group at 7.39 ppm is no longer present, which is a first indicator for a successful reaction. The most relevant signal however can be found at 7.21 ppm and stems from the aromatic ring of phenylalanine, which is one of the amino acids of the attached CGGGF peptide.

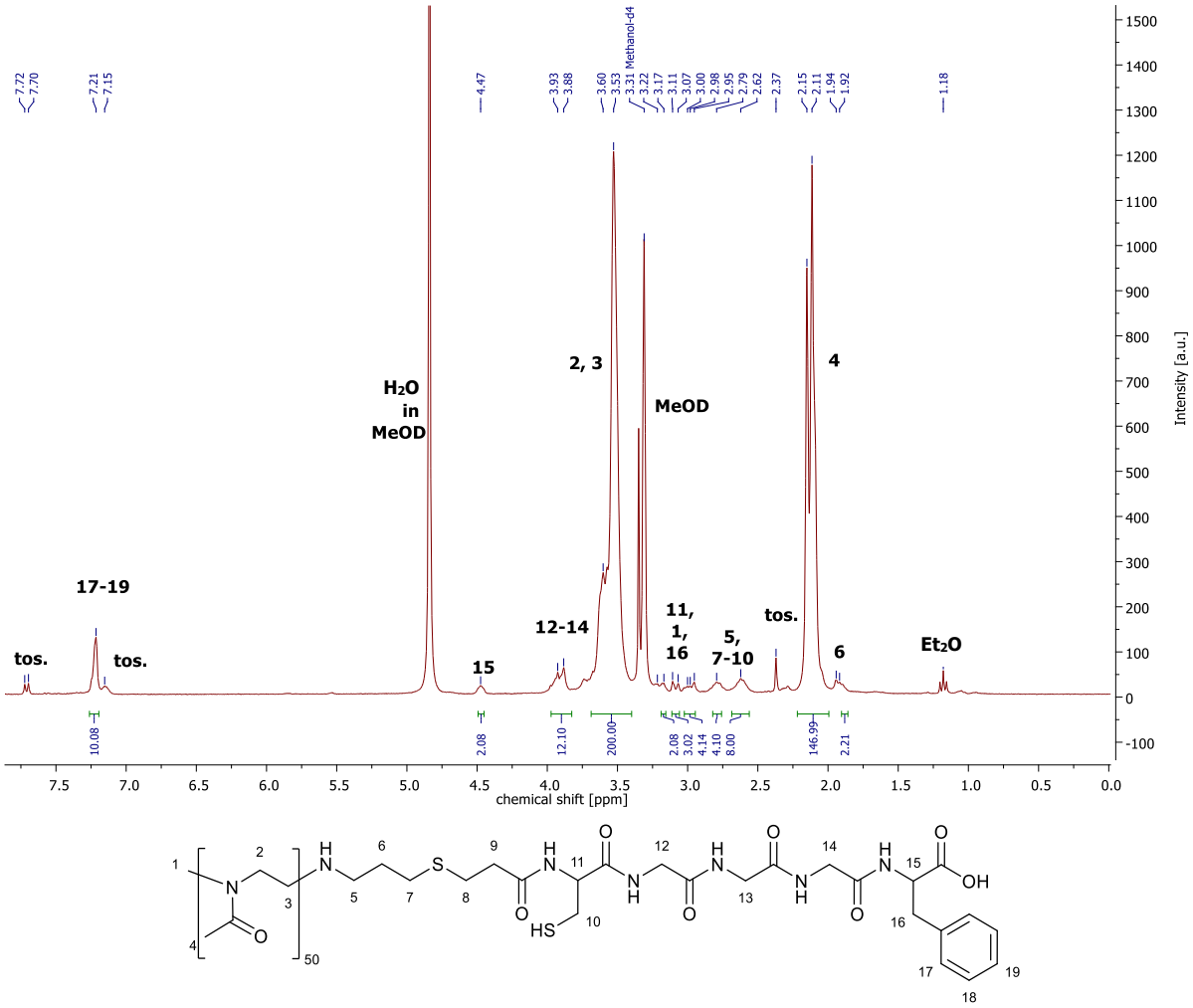

Figure 35: ^{1}H-NMR spectrum of telechelic peptide functionalized PMeOx$_{50}$-CGGGF in MeOD.

The ^{1}H-NMR spectrum also exhibits a characteristic signal at 4.47 ppm that stems from the single phenylalanine proton right next to the carboxylic acid end group of the peptide. The remaining signals can either be assigned to the polymer or peptide part of the molecule. Strongly present is the broad *backbone* signal at 3.53 ppm which was again used as an internal reference and the broad signal at 2.15-2.11 ppm from the side chain methyl groups. Also visible are signals from the methyl initiator group, the former ω-terminal alkyl chain of the polymer and the peptide backbone. However, those signals overlap each other, which does not allow for specific assignment of each proton. Further visible are tosylate counter ion and diethyl ether residue signals at 7.71, 7.15, 2.37 and 1.18 ppm. Also, the integral values of the peptide signals are higher than expected. This might be due to interactions of polymer-bound peptide with excess peptide in solution. By-products of the reaction and excess peptide could be removed via dialysis as shown in chapter 4.2.3.2a and chapter 4.2.4. However, this leads to high losses in yield, especially for telechelic polymers. Therefore, in this case, the raw product was first used in a subsequent thiol-ene reaction before dialysis of the final product. The polymer-bound peptide signals are still present after dialysis, which can be seen in **figure 50** of chapter 4.2.3.2a.

IR spectroscopy measurements were also performed with the conjugate and confirm a successful conjugation with the peptide. The product exhibits a characteristic amide bond signal at 1531 cm^{-1}, which has also been used in other works to identify CGGGF peptide conjugation to Pox polymers.[601] Since the attached peptide only delivers a weak shoulder in the spectrum, those signals are easier to recognize for the reader, when they can be compared to relatively stronger signals from multiple side chain functionalized polymers. Therefore, the results of those measurements will be discussed in detail in chapter 4.3.2.1 together with the results from the side chain functionalized polymers.

SEC measurements were performed for $PMeOx_{50}$-CGGGF and all other peptide polymer conjugates in water as well as in DMF as solvent, but did not yield any reliable results due to either insolubilities of the conjugates in the SEC solvents or otherwise very strong interactions with column material. Reasons for this behaviour were already extensively discussed in chapter 4.2.1.1.

MALDI-TOF Mass Spectrometry Measurements

MADI-TOF mass spectrometry is a method which, despite certain limitations by molecular weight and functionalization, enables the measurement of large molecules such as polymers without fragmentation.[621-626] This is achieved by embedding the analyte in a matrix that co-crystallizes with the substrate and allows for a ‘soft’ ionization by a pulsed laser, ablating small parts of the analyte-matrix matter and accelerating them towards a Time-Of-Flight mass spectrometer. MALDI-TOF can yield information concerning the chain length, functionalization and also distribution of polymers with a different multiplicity of conjugation, as it was done for example in a work of Schmitz et. al[55].

However, the feasibility of the method strongly relies on the success of the ionization step, which, in turn, is strongly influenced by the molar mass, structure, complexity and functionalization of the analyte and analyte-matrix sample. Because miscibility of the analyte with the matrix is essential for a successful co-crystallization, sample preparation therefore plays an crucial role, whereby the choice of matrices as well as the concentration of analyte in the respective matrix are two of the main factors influencing the experiment.[625]

Literature depicts a general way to approach MALDI-TOF for polymers: In a first step, a suitable matrix is identified.[625, 627] With the aid of tabulation search[628] for a preselection, this is basically still performed by trial-and-error, since the exact role of the matrix is still not fully understood.[624-625] Next, the concentration and target preparation procedures are varied to obtain optimal measuring results.

In this work, MALDI-TOF measurements of the synthesized polymer derivates have been extensively investigated. As matrices, two different substances, sinapic acid and α-cyano-4-hydroxy cinnamic acid have been selected and in most cases, the best concentration of analyte in matrix has been found to be a mixture of 1:10 (analyte:matrix).

A range of polymers, with I) different chain lengths (25 rep. units, 50 rep. units), II) different rates of functionalization (10 %, 20 %, 40 %) and III) different functionality or conjugation (allyl, carboxylic acid and thioester functionality, as well as peptide and peptide-sugar conjugation) have been examined in a setup where both A) the embedding matrix (sinapic acid and α-cyano-4-hydroxy cinnamic acid) and B) the ratio (1:1, 1:2, 1:5 and 1:10 mixtures) of analyte to matrix have been varied, resulting in a multitude of measuring experiments. Concerning these measurements, two general trends could be observed: The larger and more branched a molecule is, the poorer it gets ablated from the target, and the less functionalized or complex a polymer is, the better it “flies”, always in strong dependence on the used matrix. These findings are in accordance with literature[623, 625] and moreover, all of the successful measurements delivered results that are in accordance with theoretical expected masses and preceding analytic methods (NMR, SEC).

Yet, little of the multitude of measurements yielded informative success. From more than 30 polymer derivates measured, only four delivered satisfying spectra. Whereas short telechelic polymers of 20 repetition units could be measured easily (see the respective chapter 4.2.1.1, chapter 4.2.1.2 and chapter 4.2.1.3), the spectra for longer telechelic polymers with 50 repetition units were indistinguishable from background noise, even if the number of laser pulses was increased by a factor of 100 from 800 to 80,000. It is conceivable that an improvement in vacuum could lead to better results, however access to a device capable of these requirements was not available. Side chain polymers and *a fortiori,* peptide and/or sugar functionalized polymers did not yield any signal at all,

although different matrices and concentrations of analyte were tested. These findings are supported by a work of Schmitz et. al, who see little difference in the MALDI-TOF spectra of POx polymer before and after functionalization with peptides.[609] It is hypothesized that polymer and peptide have such a different structure and ionization capability that either one or the conjugate as a whole is only poorly miscible with the matrix material and therefore no desorption of the material can be triggered. In some cases, low molecular weight fragments are detectable in the spectra that can be assigned to molecular masses of peptide or sugar fragments and can indicate the existence of the respective moieties. However, no additional polymer signals were visible in those cases and it is assumed that matrix signals were mistaken for these signals.

Literature suggests, that in case of MALDI measurements where the polymer cannot be characterized, it might be possible to chemically modify the polymer and then record the spectrum of the altered substrate.[625] In this work, MALDI-TOF measurements were performed for all conjugate derivates in order to screen for potential successful combinations of polymer (conjugate) and matrices, but if not mentioned in the respective chapters, the measurements did not deliver any convincing data.

Chapter 4.2.2.2 *NCL with Telechelic Functionalized Polymers and CKFKFQF*

a. Educt Peptide Characteristics

The peptide CKFKFQF is an interesting reaction partner in the NCL with polymers for two reasons: First, it contains multiple phenylalanine units, whose aromatic rings allow an easy identification in ^{1}H-NMR spectroscopy. Second, it exhibits interesting solubility properties, such as fibril formation[619-620] and gelation in water. The gel formation behaviour of CKFKFQF in mixtures with different ratios of water and DMSO was investigated and it was observed that in water, the peptide forms gels at concentrations higher than 25 mg·mL^{-1}. In DMSO, the peptide is infinitely soluble and no gel formation was observed at all. Therefore, DMSO is suitable as a solvent to dissolve even high amounts of peptide.

b. NCL Reaction

For the NCL of peptide CKFKFQF with telechelic thioester functionalized PMeOx$_{50}$-COSPh (see **scheme 24**), the peptide is dissolved in DMSO and sodium borohydride is added. A solution of PMeOx$_{50}$-COSPh in DMSO is added and the reaction mixture is stirred for 24 h at room temperature. The reaction was performed in analogy to the NCL with peptide CGGGF (see chapter 4.2.2.1), except DMSO was used as a solvent instead of MeOH.

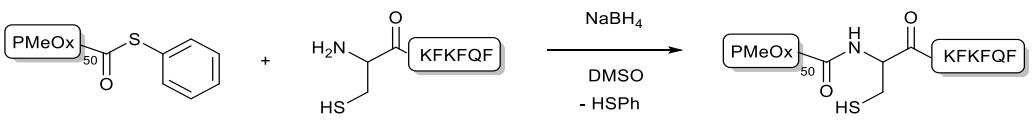

Scheme 24: Synthesis of telechelic peptide functionalized PMeOx$_{50}$-CKFKFQF.

The resulting telechelic peptide functionalized polymer will be referred to as PMeOx$_{50}$-CKFKFQF and was obtained and purified via dialysis against water (cut-off: 1000 g·mol^{-1}).

The conjugate was analysed by ^{1}H-NMR spectroscopy (see **figure 36**). Because of the poor solubility of the conjugate in common solvents such as MeOH or water, the spectrum was taken in deuterated DMSO. The signal from the former thioester group at 7.39 ppm is no longer present, which is a strong indicator for a successful reaction. The most remarkable signal can be found at 7.20 ppm. It stems from the aromatic rings of the three phenylalanine units of the attached peptide. However, the integral value of the signal is higher than expected, since it is overlaid with signals from NH and NH$_2$ groups, which are also visible in DMSO spectra and deliver broad signals in the aromatic range. The same effect accounts for the peptide backbone signals at 5.07-4.07 ppm.

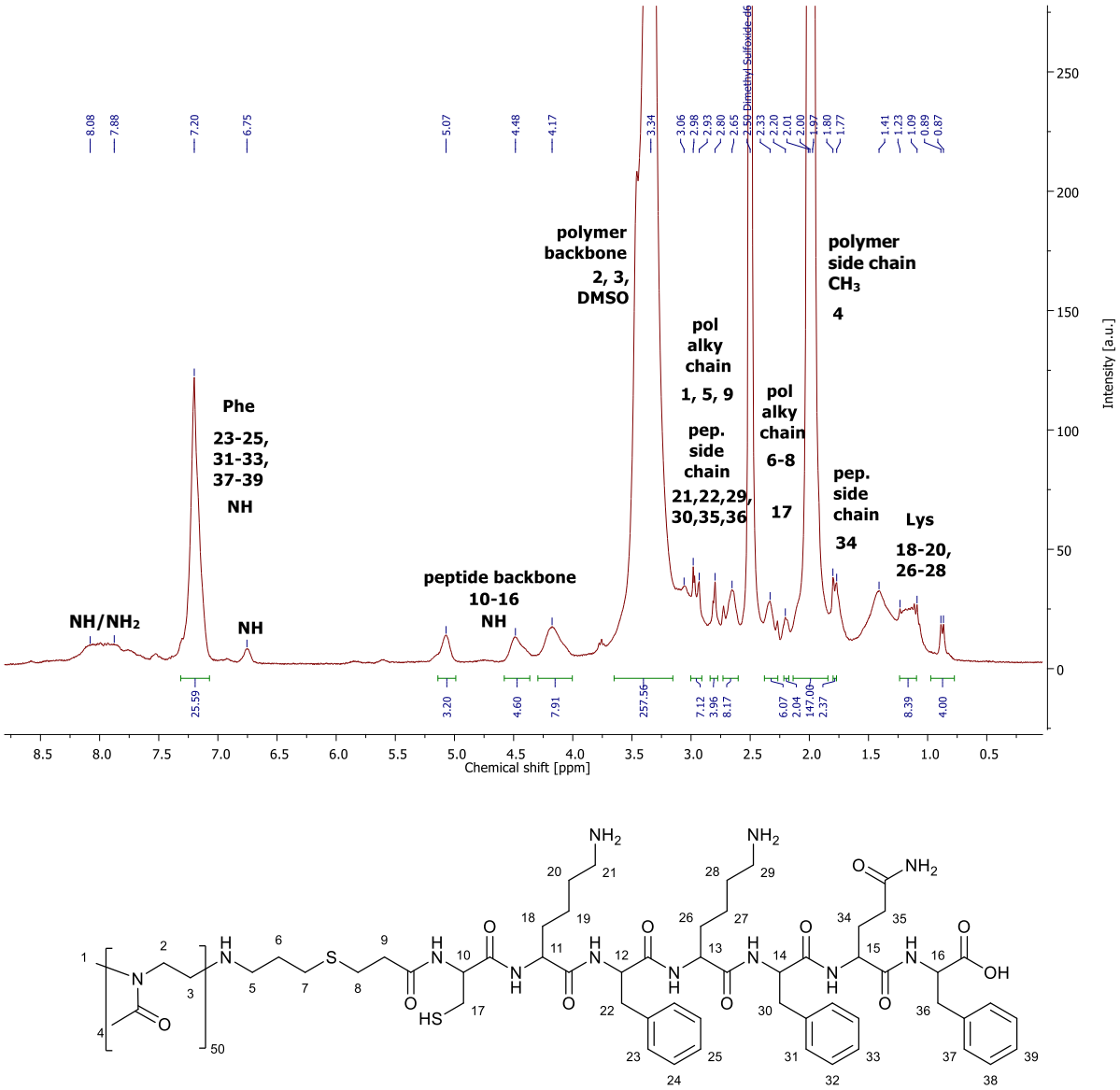

Figure 36: ^{1}H-NMR spectrum of telechelic peptide functionalized PMeOx$_{50}$-CKFKFQF in deuterated DMSO.

The remaining signals can either be assigned to the polymer or peptide part of the molecule. Strongly present is the broad *backbone* signal at 3.34 ppm and the broad signal at 2.01-1.97 ppm from the side chain methyl groups. The latter one was used as internal reference, as the first one is overlaid by the DMSO solvent signal. Also visible are signals from the methyl initiator group, the former ω-terminal alkyl chain of the polymer and the peptide side chains. However, those signals overlap each other, which does not allow for specific assignment of each proton. Further visible is an artefact signal from labile carboxylic acid or thiol group protons, which occurs after dialysis at 1.41 ppm, whereas diethyl ether residue signals and signals from the tosylate counter ion are not visible anymore, since those residues are removed by dialysis.

IR spectroscopy was performed in order to confirm the results from NMR spectroscopy. Compared to the educt polymer spectrum, a characteristic peptide signal from the N-H amide bond bending vibration of the peptide is visible in the product spectrum after conjugation (see **figure 37**). This signal is present at 1545 cm^{-1} and is one of the strongest signals in the raw CKFKFQF peptide spectrum. While the mere educt polymer spectrum shows no signal at this position, the polymer-peptide conjugate displays an apparent peak. A similar characteristic peptide signal was also observed with the conjugation of CKFKFQF to side chain polymers (see chapter 4.3.2.2). Since the spectrum was taken after dialysis of the product, the findings affirm a qualitative conjugation of peptide to the polymer.

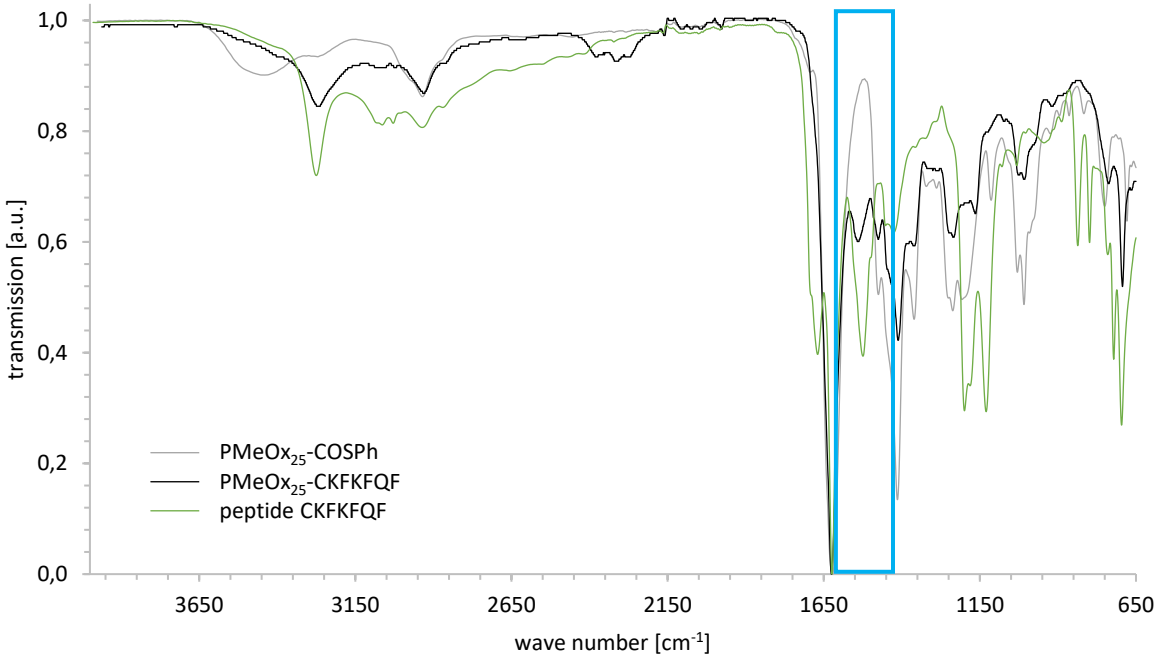

Figure 37: Superimposed IR spectra of educt polymer $PMeOx_{25}$-COSPh (grey), product polymer peptide conjugate $PMeOx_{25}$-CKFKFQF (black) and peptide CKFKFQF (green) with characteristic C=O stretching vibration of CKFKFQF at 1545 cm^{-1} (highlighted with blue box).

Quantitative Statements from IR Spectroscopy

IR spectroscopy excels in the identification and assignment of characteristic functional groups. Due to the inherent measuring method however, no absolute statements concerning the *rate or amount* of conjugation can be made from IR spectroscopy in this setup. Unlike NMR spectroscopy, absorptivities and signal intensities in IR spectroscopy usually follow non-linear relationships and it is not possible to yield quantitative statements on the number or ratio of functional groups from simple signal integration.[629] Depending on the slit width of used infrared cell, stray radiation might affect the absorbance and even slight deviations in wavelength can give rise to large variations in absorbance.[630] Another challenge lies in maintaining constant sample layer thicknesses and wavelengths in consecutive experiments.[629]

In practice, these challenges are resolved through calibration.[629, 631-633] In order to achieve precise quantitative statements from IR spectroscopy, the spectra need to exhibit an isolated reference signal that is not influenced or overlapped by other absorption bands and the measurements need to be referenced to an internal or external standard.[629, 631-633] These two basic criteria are partly realizable in this work's setup as a result of the inherent structural properties of the investigated polymer systems. In the present case, the signal from the C=O stretching vibration of the polymer *backbone* at 1630 cm^{-1} is easily recognized, mostly isolated and also the strongest signal present. It was taken as an internal reference signal whenever IR spectra were normalized throughout this work, since the length of the polymer *backbone* and thus the number of C=O groups attributing to the final signal are not influenced by functionalization or conjugation reactions. This band is also commonly used as a reference standard in literature.[634-636]

However, one must consider that the signal is partly overlapped by other neighbouring C=O stretching vibration signals that can influence its intensity. Throughout this work, a number of polymer derivates is described, where the C=O stretching vibration of a specific functional group is used to identify the respective functional moiety: Polymers with carboxylic acid or thioester functionalization, polymer peptide conjugates with amide bonds and conjugates with acetylated allyl mannose bearing ester groups. In each of those components, the signal of the C=O stretching vibration is shifted to different wavenumbers that are characteristic for its respective structural element, since each C=O group is situated in a distinct chemical environment. While those C=O stretching vibration signals are used as characteristic reaction markers, the signals merge to some extent, which rules out using one of them for an exact quantification of the respective other. Since all signals in the fingerprint region overlap each other, this accounts for all of the other signals in the polymer spectra as well.

Although it is therefore not feasible to determine concrete numbers, it is possible to obtain a qualitative statement on the order of magnitude for certain functionalization or conjugation ratios, especially when polymer derivates with similar structural properties are compared to each other. In this case, depending on the size of the polymer chain, the characteristic peptide signal is relatively stronger, the shorter the chain length of the polymer is, which again substantiates the feasibility of this method to evaluate the success of the conjugation reaction. While the signal is comparably weak for a conjugate with a polymer chain length of 50 repeating units, in case of a conjugate with a polymer chain length of 25 repeating units, the signal is clearly visible (see **figure 38**).

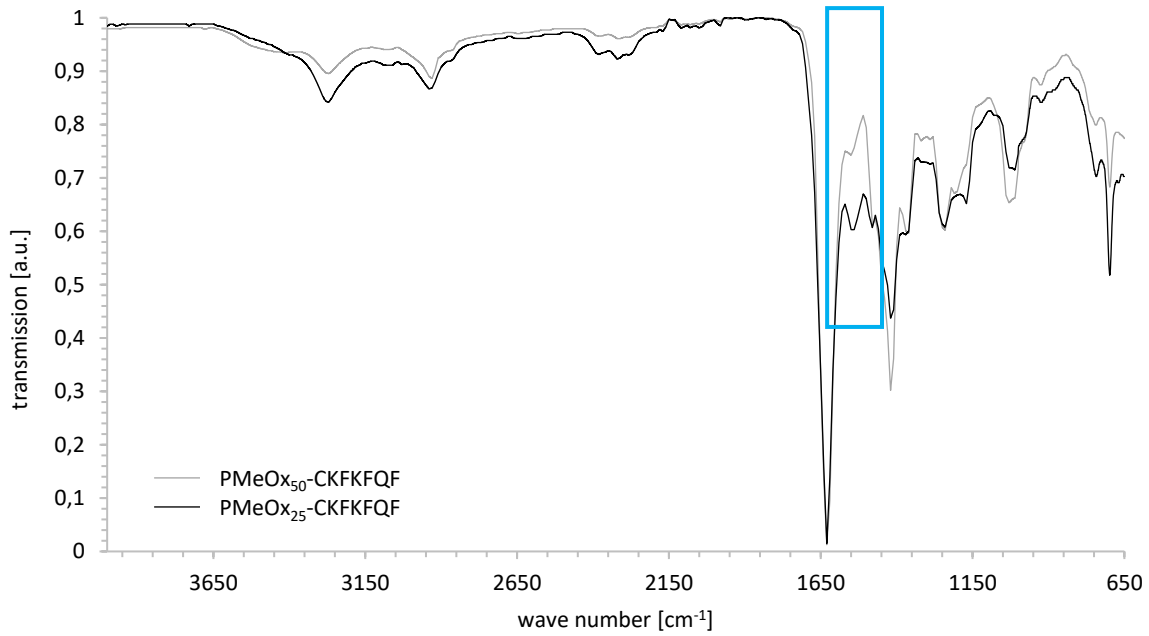

Figure 38: Superimposed IR spectra of long polymer conjugate $PMeOx_{50}$-CKFKFQF (grey) and short polymer conjugate $PMeOx_{25}$-CKFKFQF (black) with characteristic N-H amide bond bending vibration of CKFKFQF at 1545 cm^{-1} (highlighted with blue box). The characteristic peptide signal is relatively stronger with shorter chain lengths of the polymer. The strongest signal in each spectrum, the C=O stretching vibration of the polymer backbone at 1630 cm^{-1}, was taken as a reference.

Chapter 4.2.2.3 *NCL with Telechelic Functionalized Polymers and CGGWYKYW*

a. Educt Peptide Characteristics

As shown in the previous section, the poor solubility of CKFKFQF conjugates makes them an unsuitable candidate for the next reaction cascade step, the thiol-ene reaction, where high concentrations of educts are needed. Therefore, a third peptide, CGGWYKYW, was used for conjugation with polymers. Despite at high concentrations, it also forms gel-like mixtures with water, it shows better solubility properties than CKFKFQF, and it still has some aromatic side chain units (tyrosine, Y and tryptophan, W) that allow for straightforward recognition in ^{1}H-NMR spectroscopy. Hence, it combines the advantages of CGGGF and CKFKFQF.

Furthermore, with 8 amino acid units, it is longer than the previous used peptides and according to literature[150], the sequence WYKYW shows a high affinity to galectins. This makes CGGWYKYW and its polymer conjugates an interesting target to be used in affinity studies with galectin (see chapter 4.2.5.2). The peptide was ordered and synthesized from *GeneCust* and used as received.

In order to be able to have an appropriate insight into NMR spectroscopy of polymer-peptide conjugates, it is crucial to look at the raw peptide spectra first. ^{1}H-NMR spectroscopy of CGGWYKYW was done in D_2O, MeOD and deuterated DMSO.

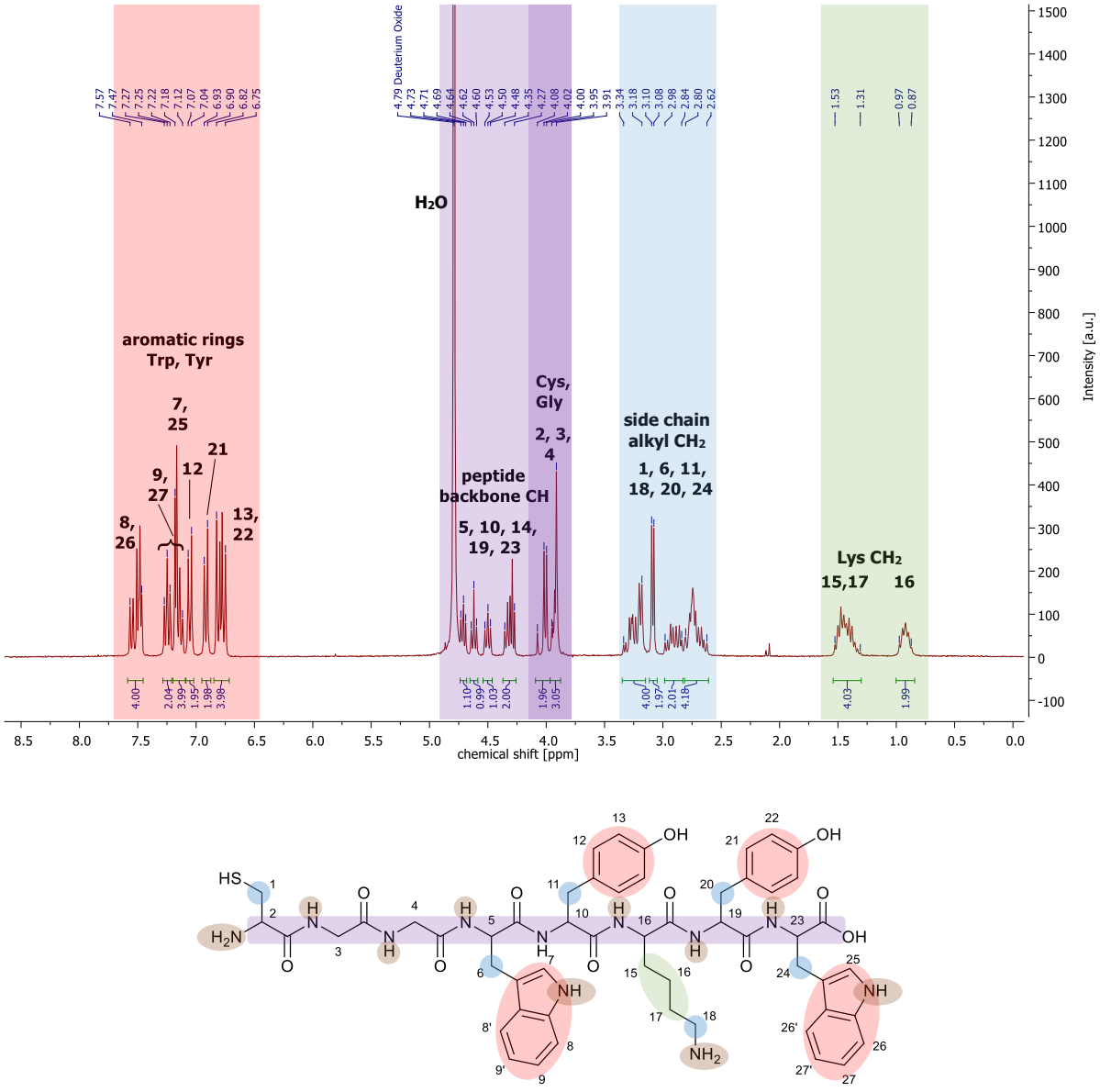

Figure 39: ^{1}H-NMR spectrum of peptide CGGWYKYW in D_2O with the 'aromatic region' (red), 'peptide backbone region' (purple), 'side chain alkyl region' (blue) and 'lysine region' (green).

The spectra in D_2O and MeOD exhibit similar signals, therefore only the spectrum in D_2O is discussed (see **figure 39**). All signals can be assigned to the corresponding protons of the peptide. In this regard, four main regions of the spectrum with protons of similar substructures can be defined: There is an

'aromatic region' between 7.57 and 6.75 ppm, where signals from the aromatic rings of tyrosine and tryptophan can be found. Each nodal point in a peptide chain, which is to say the point where the amino acid residues are attached to the peptide backbone, exhibits a CH group, whose signals are visible in the 'peptide backbone region' between 4.73 and 3.91 ppm. More specifically, the signals from the cysteine and glycine units can be found between 4.08 and 3.91 ppm. Next, there is a 'side chain alkyl region' between 3.34 and 2.62 ppm, where signals from alkylic CH_2 groups of the amino acid residues are present. And finally, there is a 'lysine region' between 1.53 and 0.87 ppm, where signals from the long lysine CH_2 chain can be found.

The spectrum in deuterated DMSO (see **figure 40**) can be subdivided into the same regions and the signals can be assigned in analogy to the spectrum in D_2O and MeOD. However, some of the signals in the peptide backbone region are overlaid by residue water signals of DMSO, therefore the integral values of those signals are higher than expected. Furthermore, NH and NH_2 groups also deliver signals in DMSO, which appear in an additional 'NH and NH_2 region' between 10.83 and 7.50 ppm. The integral values of those signals only partially match the actual number of protons bound to nitrogen atoms and because the NH and NH_2 region overlaps the aromatic region, the specific assignment of each proton is not feasible. Nevertheless, there is one characteristic doublet signal of the tryptophan indole NH proton at 10.79 ppm that can easily be identified and can be used as a distinct 'peptide marker' in the future peptide polymer conjugate.

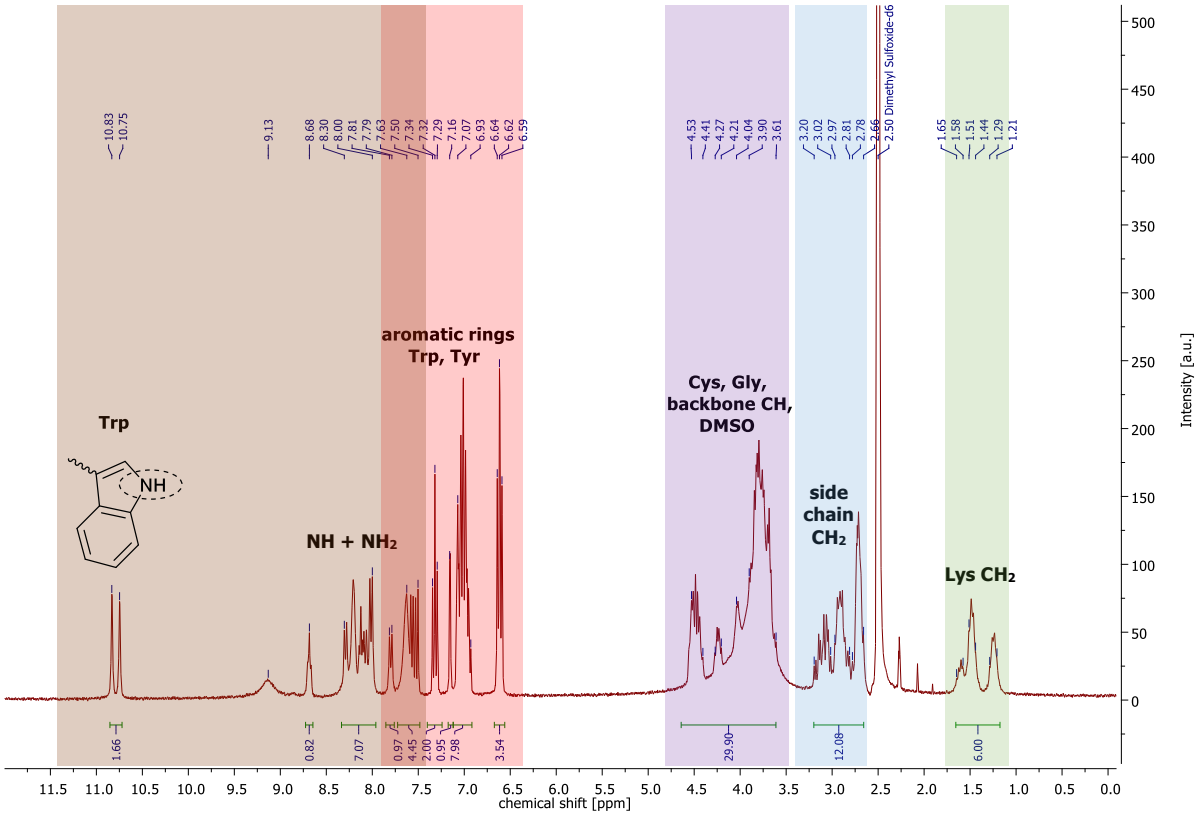

Figure 40: ^{1}H-NMR spectrum of peptide CGGWYKYW in deuterated DMSO with the 'NH and NH_2 region' (brown), 'aromatic region' (red), 'peptide backbone region' (purple), 'side chain alkyl region' (blue) and 'lysine region' (green).

b. NCL Reaction

For the telechelic functionalization of polymers with the peptide CGGWYKYW, both a short α telechelic polymer as well as a long ω telechelic polymer were used. Since the α telechelic conjugate was afterwards used for affinity measurements (see chapter 4.2.5), its synthesis will be described here. For the ω telechelic polymer, all reaction parameters and analytics however are similar.

The short α telechelic polymer allyl-PMeOx$_{20}$-SEt (see chapter 4.2.1.1b) was functionalized in analogy to ω telechelic PMeOx$_{50}$ with a carboxylic acid group (referred to as COOH-PMeOx$_{20}$-SEt) and afterwards a thioester group (referred to as COSPh-PMeOx$_{20}$-SEt). In analogy to the preceding NCL reactions, the latter polymer was then used in a reaction with CGGWYKYW (see **scheme 25**), where the peptide was dissolved in MeOH and a solution of COSPh-PMeOx$_{20}$-SEt in MeOH was added. The reaction mixture was then stirred for 24 h at 65 °C and the product was purified by dialysis against water.

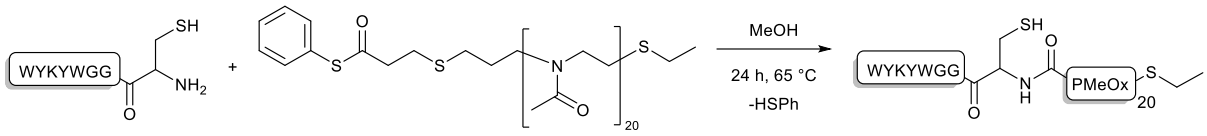

Scheme 25: Synthesis of side chain peptide functionalized CGGWYKYW-PMeOx$_{20}$-SEt.

The resulting polymer-peptide conjugate will be referred to as CGGWYKYW-PMeOx$_{20}$-SEt and was analysed by ^{1}H-NMR spectroscopy (see **figure 41**). Because of a mediocre solubility of the conjugate in water and MeOH, the spectrum was taken in deuterated DMSO.

The NMR spectrum displays both characteristic signals from the peptide as well as the polymer. Clearly recognizable are some individual signals such as the tryptophan indole NH at 10.72 ppm, the aromatic ring signals of tyrosine and tryptophan at 7.56-6.56 ppm from the peptide part of the conjugate or the methyl side chain group at 1.99-1.97 ppm from the polymer part of the conjugate. Those signals are suitable for referencing. With so many protons contributing to the final spectrum and superimposing each other, it is not feasible to assign the rest of the signals individually. Instead of assigning and integrating single proton signals, the spectrum can be subdivided into different regions exactly like it was done for the educt peptide spectrum (see **figure 39**). The total integral values that where determined for each region match the expected number of protons of each part of the conjugate.

There is the 'NH and NH$_2$ region' and 'aromatic region' between 10.74 and 6.56 ppm, where signals from the amino groups of the conjugate as well as the aromatic rings of tyrosine and tryptophan can be found. The CH groups from each nodal point of the attached peptide are visible in the 'peptide backbone region' between 4.48 and 3.60 ppm. More specifically, the signals from the cysteine and glycine units can be found between 3.69 and 3.60 ppm, but are partly overlaid by the broad polymer

backbone signal at 3.34 ppm, which in turn contains the DMSO water residue signal. Next, there is a 'side chain alkyl region' between 3.07 and 2.66 ppm, where signals from alkylic CH_2 groups of the amino acid residues, signals from the ω-terminal alkyl chain of the polymer as well as the initiator CH_3 group of the polymer are present. At 1.99-1.97 ppm, the methyl side chain groups plus the thioether CH_3 end group of the polymer deliver a broad signal which was used as internal reference. This signal is next to a broad singlet artefact signal from dialysis at 1.77 ppm. Finally, there is a 'lysine region' between 1.41 and 0.87 ppm, where signals from the lysine side chain CH_2 groups can be found.

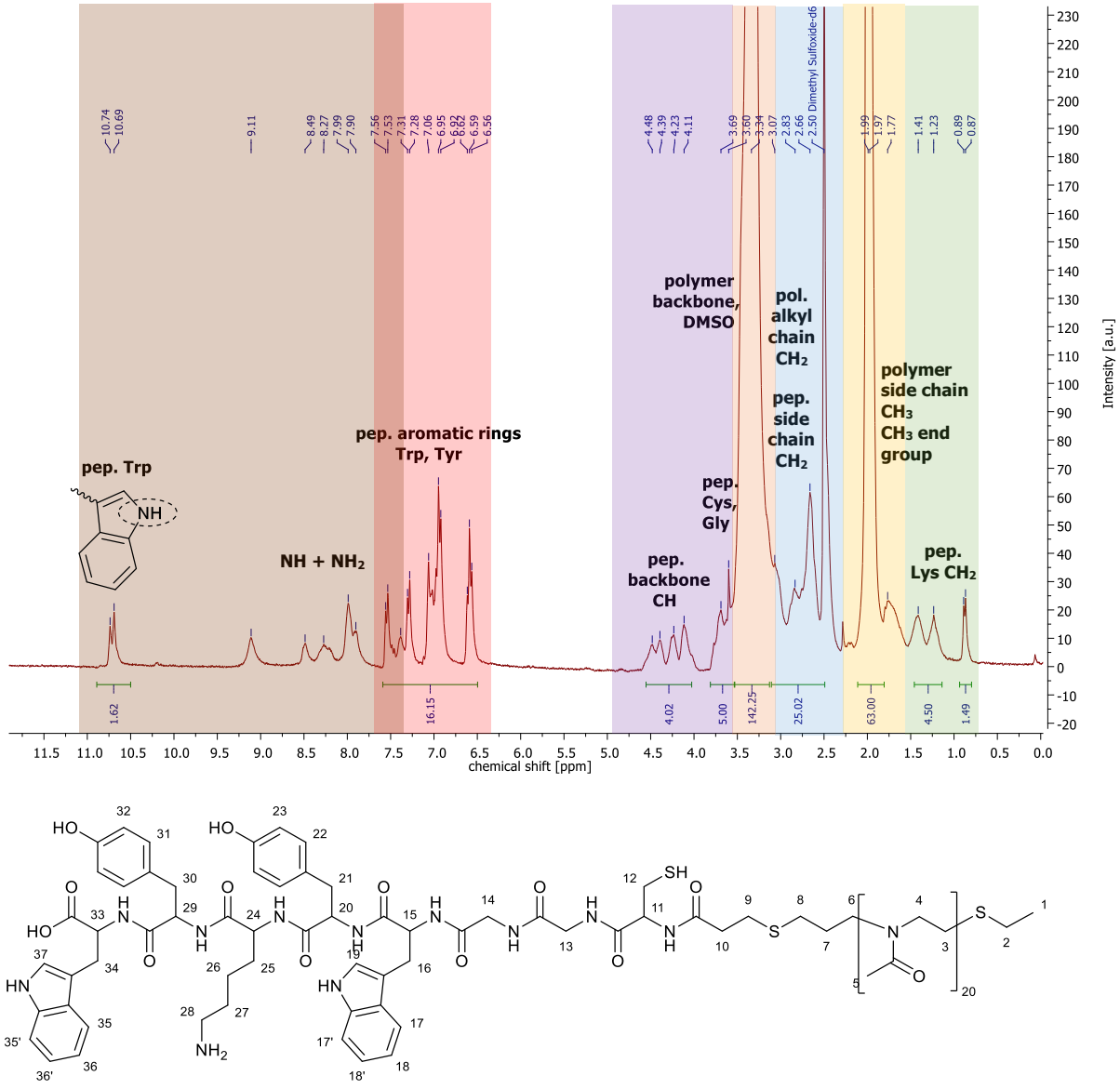

Figure 41: ^{1}H-NMR spectrum of telechelic peptide functionalized CGGWYKYW-PMeOx$_{20}$-SEt in deuterated DMSO with "pep" for signals that belong to the peptide part of the conjugate and "pol" for signals that belong to the polymer part. The spectrum is subdivided into different regions: 'NH and NH_2 region' (brown), 'aromatic region' (red), 'peptide backbone region' (purple), polymer backbone (orange), 'side chain alkyl region' (blue), 'polymer side chain region' (yellow) and 'lysine region' (green).

IR spectroscopy measurements were also performed with the conjugate. Compared to the educt polymer spectrum, a characteristic signal from the N-H amide bond bending vibration of the peptide is visible in the product spectrum after conjugation (see **figure 42**). This signal is present at 1515 cm^{-1} and is one of the strongest signals in the raw CGGWYKYW peptide spectrum. While the mere educt polymer spectrum of COSPh-PMeOx$_{20}$-SEt shows no signal at this position, the polymer-peptide conjugate CGGWYKYW-PMeOx$_{20}$-SEt displays an apparent peak. The same accounts for the N-H stretching vibration at 3282 cm^{-1}. Since the spectrum was taken after dialysis of the product, the findings affirm conjugation of peptide to the polymer.

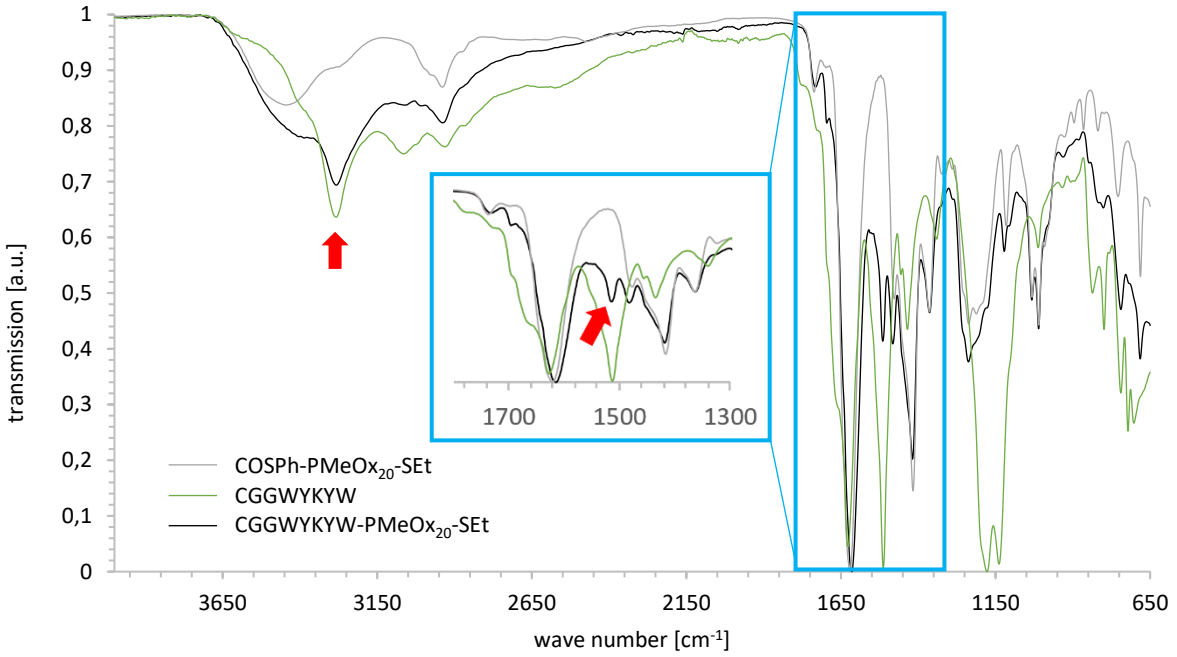

Figure 42: Superimposed IR spectra of educt polymer COSPh-PMeOx$_{20}$-SEt (grey), product polymer peptide conjugate CGGWYKYW-PMeOx$_{20}$-SEt (black) and peptide CGGWYKYW (green) with characteristic N-H stretching vibration and amide bond bending vibration of CGGWYKYW at 3282 and 1515 cm^{-1} (highlighted with red arrows). The relevant part of the spectrum is enlarged.

Chapter 4.2.3 Thiol-Ene Reaction

There is a basic idea behind the strategy to comprehensively approach the thiol-ene reaction on a macromolecular polymer level: Increasing the complexity of the macromolecular reaction partners (*P*olymers) step by step, while retaining the same set of allyl components that were also used in the low molecular model reaction (see chapter 4.1.4).

Namely, those allyl components are allylpentafluorobenzene, acetylated allyl mannose and, in a logical manner, allyl mannose (see **figure 43**). Allylpentafluorobenzene is commercially available, so it was used as received whereas the sugars were provided by the working group of Prof. Seibel (Julius-Maximilians-Universität Würzburg) and were also used as received.

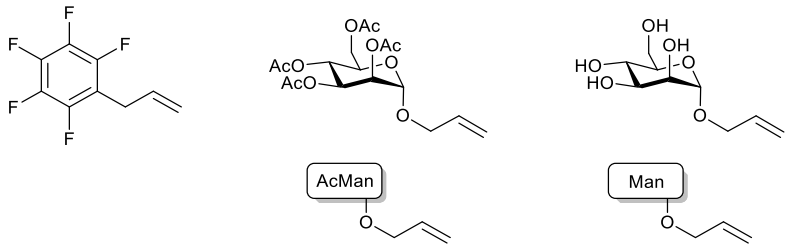

Figure 43: Allyl compounds that were used for the thiol-ene reactions: allylpentafluorobenzene (left), acetylated allyl mannose (mid) and allyl mannose (right).

As thiol components, different polymers with increasing complexity were used (see **figure 44**). This chapter for telechelic polym ers and chapter 4.3.3 for side chain functionalized polymers are structured according to the increasing complexity of the thiol functionalized polymer reaction partners.

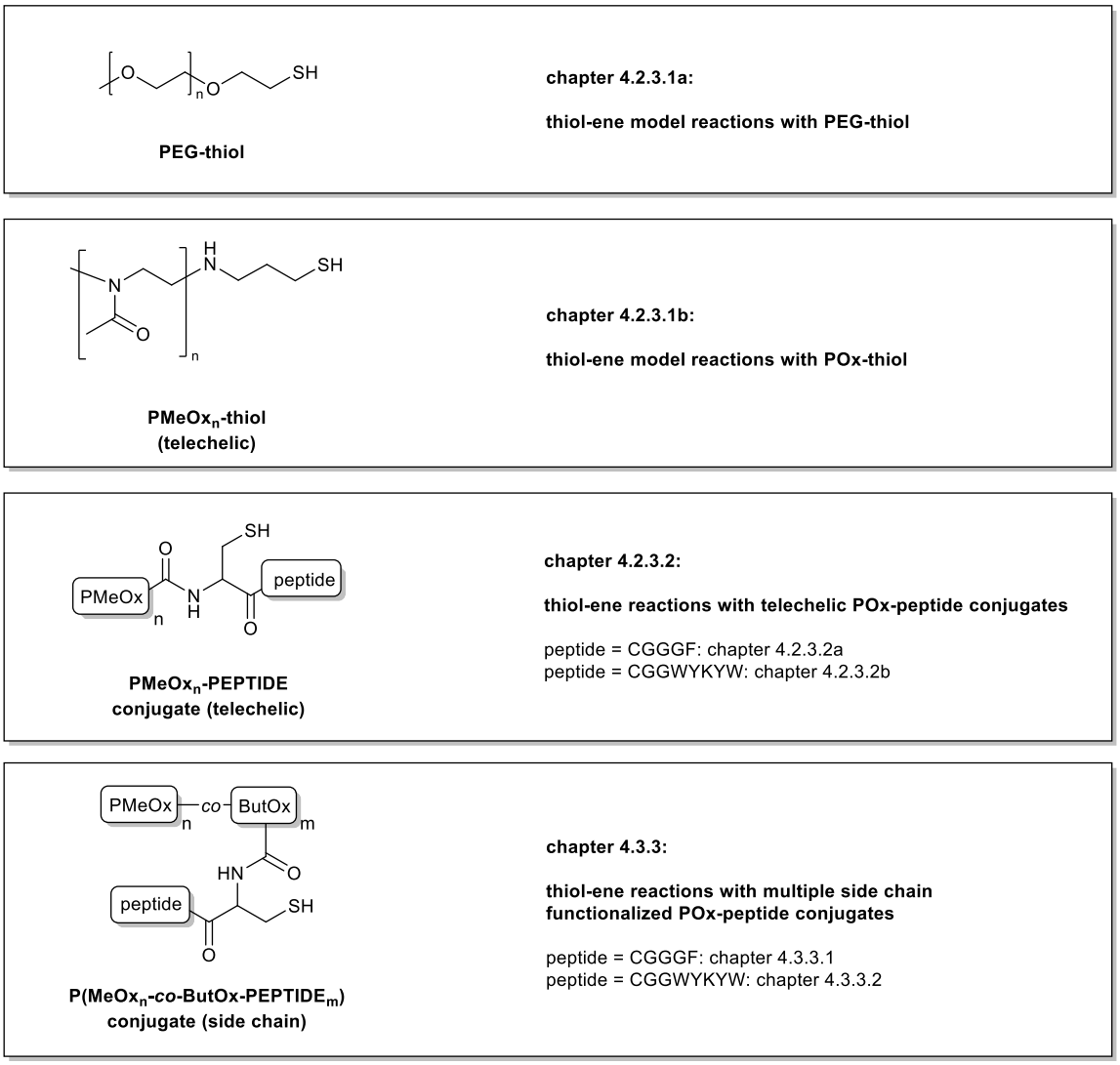

Figure 44: Thiol polymer compounds with increasing complexity that were used for the thiol-ene reactions: PEG-thiol, POx-thiol and POx-peptide conjugates (telechelic and side chain).

First model reactions were performed with well researched and commercially available thiol functionalized PEG (PEG-SH). The next step was to proceed to POx, but still use only simple thiol functionalized polyoxazolines and not yet conjugates. Model reactions on this level cover telechelic as well as side chain functionalized polymers and required the synthesis of suitable precursor polymers.

Finally, after obtaining insight into reaction conditions and gain experience with the process, the most complex POx-peptide conjugate products from the NCL reactions, whose synthesis was described in detail in the previous chapter 4.2.2, were used for thiol-ene reactions.

The main focus was to display the *feasibility* of the reaction by qualitatively examining indicators for a successful reaction in each case. On each level, the choice of reaction parameters for the macromolecular thiol-ene reaction was based on the findings from the low molecular model reactions (see chapter 4.1.4.1) and was further developed to match polymer requirements.

Chapter 4.2.3.1 *Thiol-Ene Polymer Model Reactions*

a. Thiol-Ene with Thiol Functionalized PEG

Commercially available PEG-SH with a molecular weight of 6000 g·mol^{-1} was reacted with two different allyl components, allylpentafluorobenzene and acetylated allyl mannose (see **scheme 26**). In both reactions, the polymer is dissolved in methanol - with volumes as small as possible, since it is known from the low molecular model reaction that the thiol-ene reaction works best with a minimal amount of solvent (see chapter 4.1.4.1). TCEP is added to prevent dimerization of the thiol group, which was investigated in detail in chapter 4.1.3. Findings from the low molecular model reaction proved that it does not interfere with the reaction and it can be removed via dialysis afterwards. It is also known that the reaction works best for an excess of thiol component. However, this could not be implemented with this reaction, as the applied purification methods do not allow for removal of excess polymer and therefore, educts were reacted in equimolar amounts. The allyl compound is added together with DMPA as a photoinitiator and the reaction mixture is stirred under UV irradiation for 60 minutes. The resulting conjugate was then purified via dialysis against water for 5 days (cut-off: 1000 g·mol^{-1}).

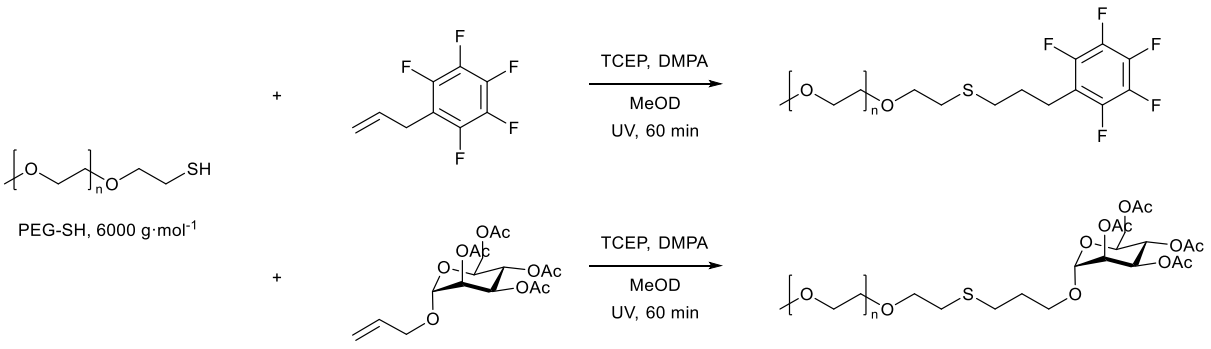

Scheme 26: Thiol-ene reaction of PEG-SH with allylpentafluorobenzene (top) and acetylated allyl mannose (bottom).

The ^{1}H-NMR spectrum of the allylpentafluorobenzene conjugate can be found in the appendix on page 247 and will not be shown here, since there is no noticeable change compared to the PEG-SH educt spectrum, except for an expected shift of the thiol adjacent alkyl signal. Other newly formed alkyl signals are either too weak or most likely overlaid by the polymer backbone signal.

The ^{19}F-NMR spectrum in contrast provides more detailed information (see **figure 45**). With its fully fluorinated benzene ring, allylpentafluorobenzene acts as a reliable marker for a successful reaction by displaying three characteristic signals in ^{19}F-NMR spectroscopy. The appearance of those signals in the product spectrum is a clear indicator that allylpentafluorobenzene was attached to the polymer - otherwise, the compound would have been removed in the dialysis purification step. However, this is only a qualitative statement and quantitative predictions concerning the conversion rate of the reaction are not possible with this setup.

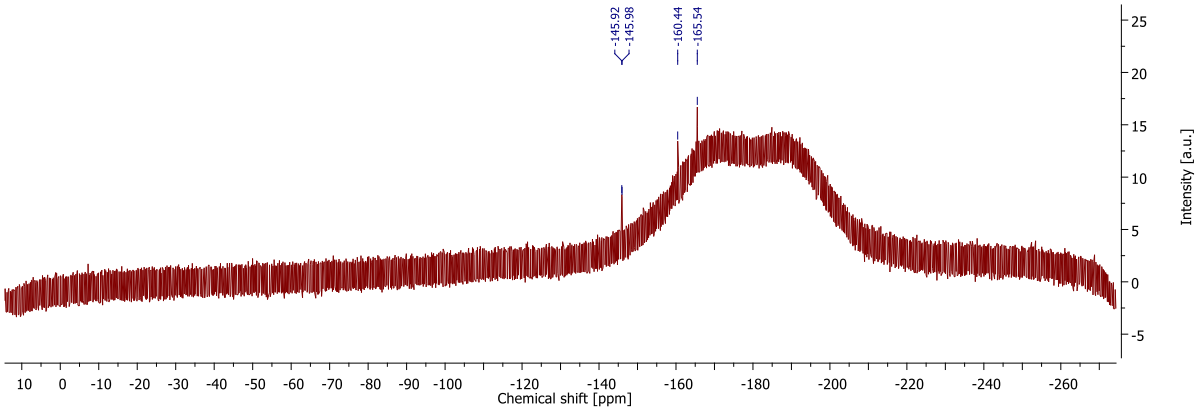

Figure 45: ^{19}F-NMR spectrum of the conjugate between PEG-SH and allylpentafluorobenzene in MeOD.

In contrast to that, quantitative statements are possible when it comes to the second conjugate of PEG-SH with acetylated allyl mannose. The acetyl groups make for excellent reaction markers, since they deliver characteristic signals at 2.24-2.07 ppm that can easily be identified in the ^{1}H-NMR spectrum (see **figure 46**). Integration of those signals in the product spectrum shows that on average, every third polymer chain was conjugated with a sugar unit.

It should be mentioned at this point that the C=O double bond of those sugar acetyl groups also delivers a characteristic signal at 1467 cm^{-1} in IR spectroscopy, which, in comparison with the educt and product spectra of the polymer and polymer sugar conjugate, underpins a successful reaction (see **figure 47**).

Other ^{1}H-NMR signals from the mannose sugar are visible at 5.38-5.26 ppm and 4.32-4.21 ppm. Clearly present is the strong signal at 3.74 from the polymer *backbone*, which also exhibits two satellite signals at 3.97 and 3.49 ppm and an alkyl chain signal at 3.87 ppm, which in turn stems from the last repeating unit in the polymer chain. Next to the characteristic singlet signal from the initiator group at 3.41 ppm is a newly formed triplet signal at 2.99 ppm from the attached alkyl chain. Another indicator for the

reaction turnover is the signal at 2.77 ppm, which belongs to the alkyl chain group next to the sulphur atom and experiences a shift to 2.83 ppm in case of sugar attachment. Integration of those two signals is in accordance with the ratio of 2:1 of unconjugated to conjugated polymer.

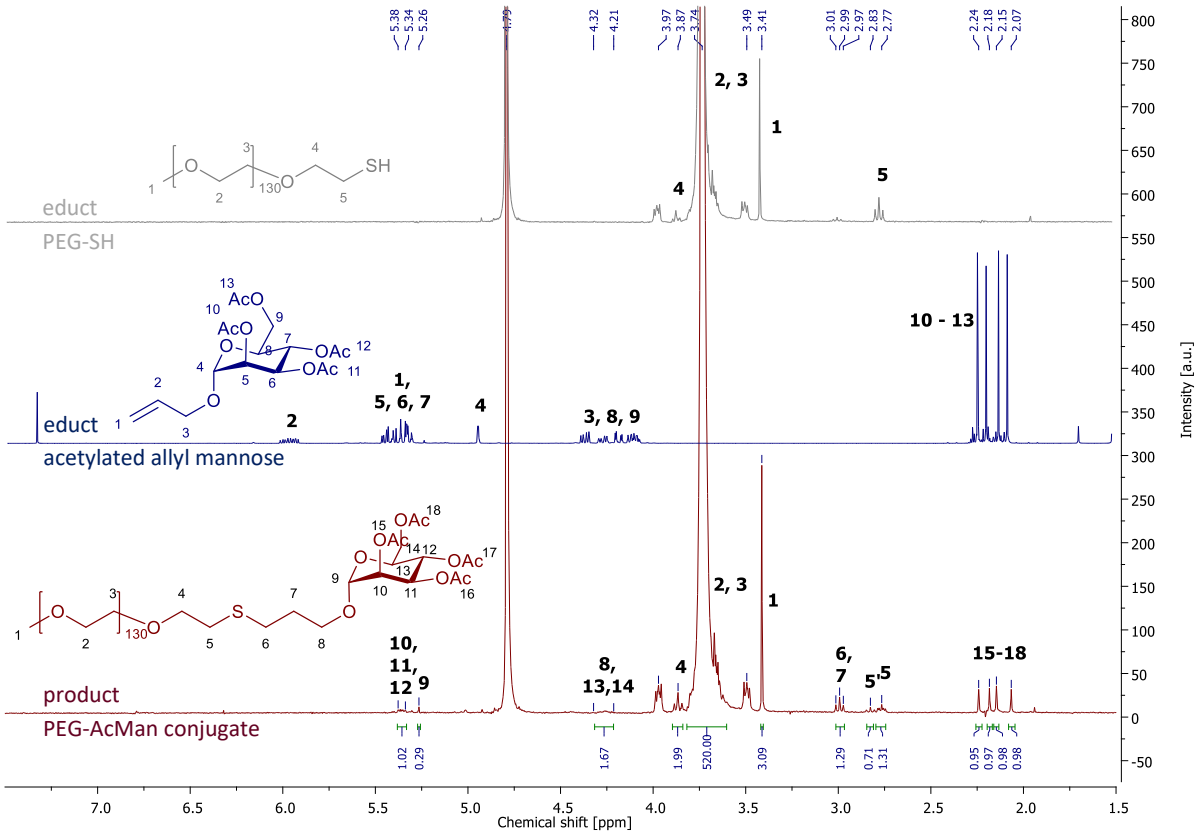

Figure 46: Stacked ^{1}H-NMR spectra of educt thiol functionalized PEG-SH (grey, top) in D_2O, educt acetylated ally mannose (blue, middle) in $CDCl_3$ and the product conjugate (red, bottom) in D_2O.

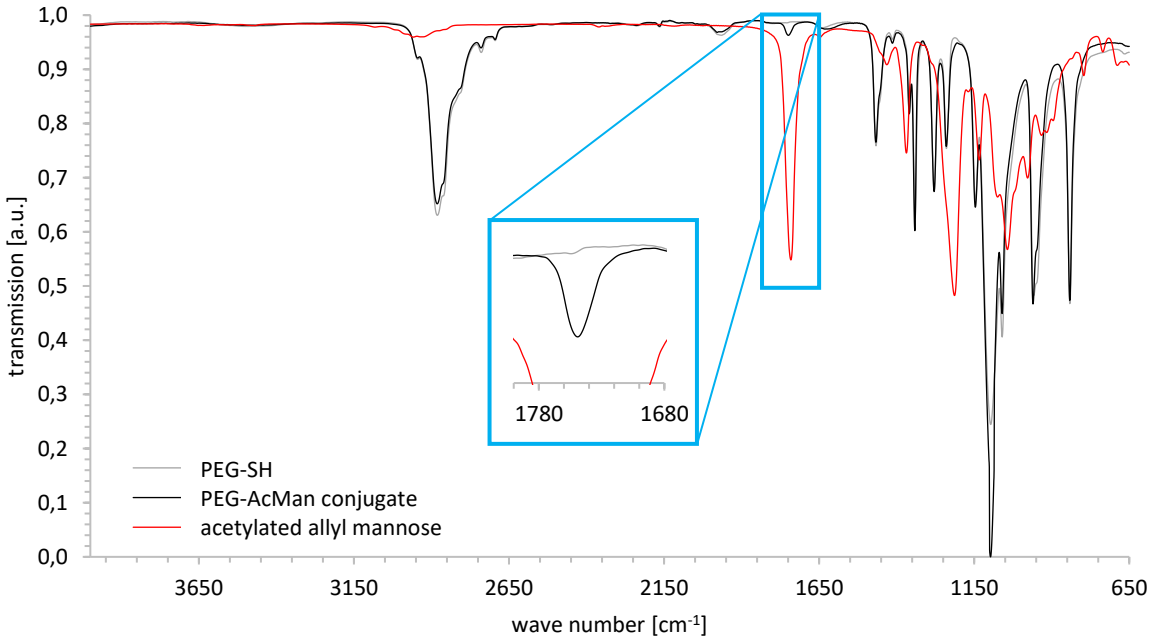

Figure 47: Superimposed IR spectra of educt polymer PEG-SH (grey), product polymer sugar conjugate PEG-AcMan (black) and educt acetylated allyl mannose sugar (red) with characteristic C=O stretching vibration of acetylated allyl mannose at 1467 cm^{-1} (enlarged and highlighted with blue box).

Based on the detailed observations from the low molecular model reaction, it was hereby possible to show a feasibility of the reaction on a macromolecular level. These findings will be utilized and transferred to the next step, thiol-ene reactions with polyoxazolines.

b. Thiol-Ene with Thiol-POx

Polyoxazolines with a thiol functionality were not commercially available. Therefore, for the thiol-ene reaction, thiol functionalized polyoxazolines needed to be synthesized first.

Precursor Polymer Synthesis

The synthesis of thiol functionalized polyoxazolines follows a two-step mechanism (see **scheme 27**), which has been described in literature for side chain functionalized polyoxazolines[601, 637]. First, allyl functionalized polyoxazoline is conjugated with thioacetic acid in a thiol-ene reaction. For this, polymer and excess thioacetic acid are dissolved in a small amount of methanol, DMPA is added as a photoinitiator and the reaction mixture is stirred under UV irradiation for 60 minutes. Similar to literature, the conversion of the reaction was monitored via the disappearance of the allyl signals in the ^{1}H-NMR spectrum.

Next, the product is reacted with cysteine in a NCL. For this, the product is dissolved in methanol together with cysteine and sodium borohydride. The reaction cleaves off the acetyl group to yield the the final PMeOx$_{38}$-SH polymer with the free thiol functionality as a product and acetylcysteine as a by-product. To prevent dimerization of the thiol group, purification was performed by dialysis against degassed water for 2.5 days (cut-off: 1000 g·mol^{-1}).

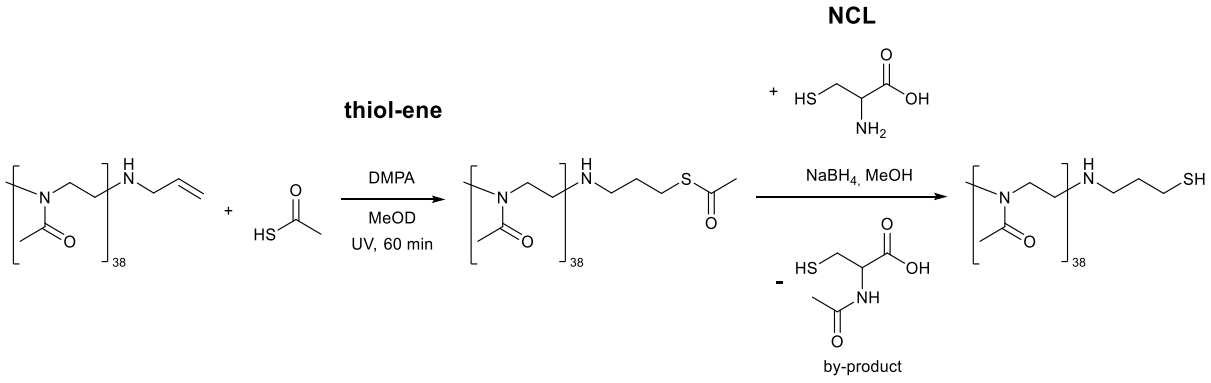

Scheme 27: Two-step mechanism to create thiol functionalized polyoxazolines. First step: Thiol-ene reaction of allyl functionalized PMeOx$_{38}$ with thioacetic acid. Second step: NCL reaction with cysteine to cleave off the acetyl group.

The free thiol group of PMeOx$_{38}$-SH delivers a signal in the NMR spectrum (see appendix, page 247), which is visible as a triplet at 1.18 ppm. The spectrum also contains some minor impurities at 3.10 and 1.29 ppm. However, the free thiol group is sensitive to dimerization during prolonged dialysis and therefore, purification was not intensified at this stage. Instead, a thorough purification was performed

after the following step, where the product is not as susceptible to oxidative side reactions and less delicate to handle.

Thiol-Ene Reaction

The thiol functionalized polyoxazoline was reacted with acetylated allyl mannose in a thiol-ene reaction. The polymer and the sugar were dissolved in water with Irgacure 2959 as photoinitiator, as these conditions showed a more successful reaction behaviour than a reaction with methanol and DMPA. Since the thiol functionalized educt polymer is susceptible to oxidation, degassed solvents were used and TCEP was added to obtain reductive conditions and prevent the polymer from dimerization. The reaction mixture was stirred under UV irradiation for 60 minutes (see **scheme 28**) and the product was purified by dialysis against water (cut-off: 1000 g·mol^{-1}).

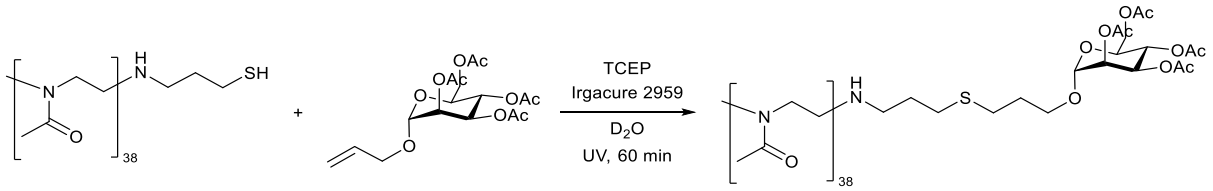

Scheme 28: Thiol-ene reaction between thiol functionalized PMeOx$_{38}$-SH and acetylated allyl mannose.

The conjugate was analysed by ^{1}H-NMR spectroscopy. Still clearly present are the strong signals from the polymer backbone at 3.45 and 2.10 ppm, as well as the signal from the initiator methyl group at 3.04-2.95 ppm. In addition to this, there is a set of signals at 5.26-5.20, 4.86-4.79, 4.30-4.26, 4.13-4.08 and 3.98 ppm that stands out from surrounding background noise. Those signals correspond to the signals of the attached sugar, which is especially prominent in comparison with the educt acetylated allyl mannose spectrum (see **figure 48**). Since those signals are very weak and barely protrude from background signals, no quantitative statements by integration can be made concerning the conjugation rate and unfortunately, the comparatively stronger signals from the acetyl groups which would be sharp enough for integration are overlaid by the polymer backbone signal. Nevertheless, the set of signals acts as a qualitative indicator that the polymer was being conjugated with the sugar.

In order to increase resolution, spectra were measured with an increased number of scans and on instruments with different measuring frequencies. **Figure 48** shows a comparison between the enlarged section of two spectra from the same sample that have both been measured with 128 scans on NMR machines with different measuring frequencies (MHz). Yet, there is little difference in resolution and the 600 MHz NMR spectrum (bottom) yields no additional information compared to the 300 MHz spectrum (middle).

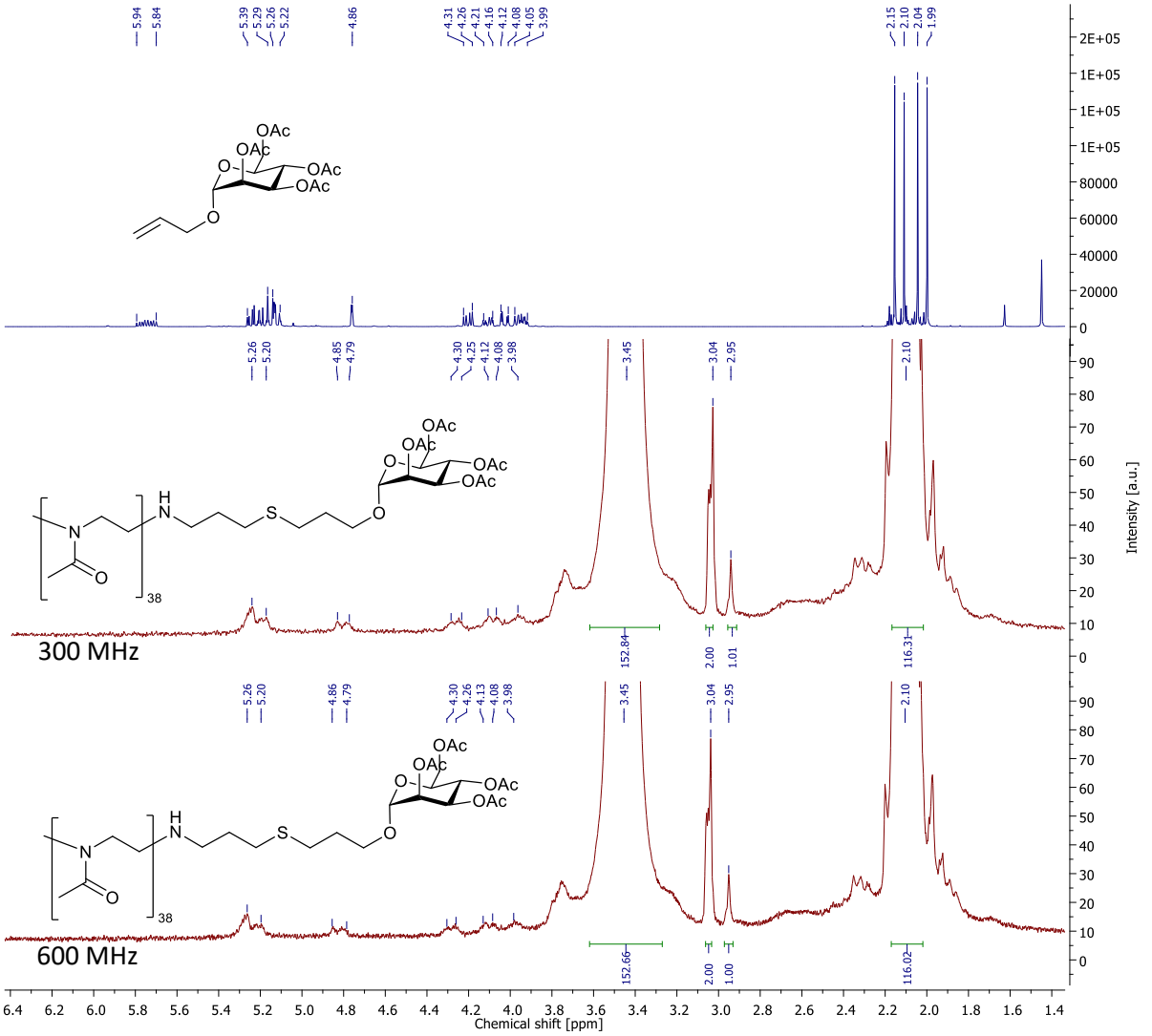

Figure 48: Stacked ^{1}H-NMR spectra of educt acetylated allyl mannose (blue) in $CDCl_3$ and the product conjugate (red) in $CDCl_3$. A comparison between the two red polymer spectra (mid: 300 MHz, bottom: 600 MHz) shows little difference between spectra that were measured on instruments with different frequencies.

The findings from NMR spectroscopy are supported by IR spectroscopy. Compared to the educt polymer IR spectrum, a characteristic sugar signal from the C=O stretching vibration of the acetyl groups is visible in the product spectrum after conjugation (see **figure 49**). This signal is present at 1745 cm^{-1} and is one of the strongest signals in the raw acetylated allyl mannose spectrum. While the mere educt $PMeOx_{38}$-SH polymer spectrum shows no signal at this position, the polymer-sugar conjugate $PMeOx_{38}$-AcMan displays an apparent peak. Since the spectrum was taken after dialysis of the product, the findings affirm a qualitative conjugation of sugar to the polymer.

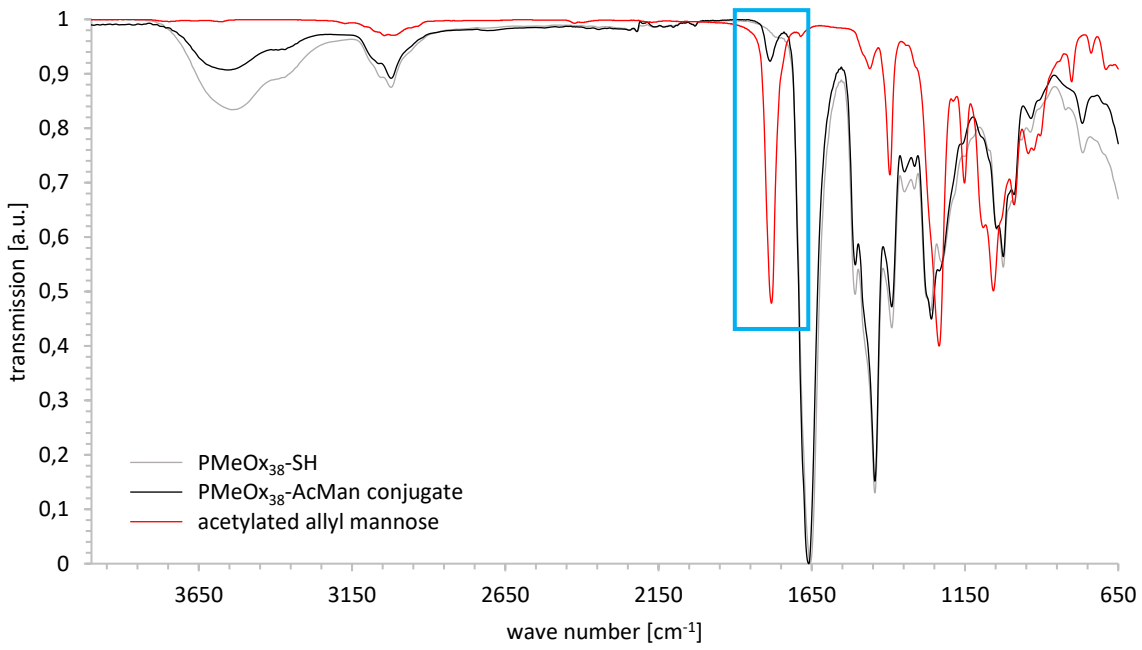

Figure 49: Superimposed IR spectra of educt polymer $PMeOx_{38}$-SH (grey), product polymer sugar conjugate $PMeOx_{38}$-AcMan (black) and educt acetylated allyl mannose sugar (red) with characteristic C=O stretching vibration of acetylated allyl mannose at 1745 cm^{-1} (highlighted with blue box).

With a qualitative attachment of sugars to polyoxazoline polymers was proven possible, the reaction is transferred to the products from the NCL reaction as the next step.

Chapter 4.2.3.2 *Thiol-Ene with Telechelic NCL Products*

In chapter 4.2.2, several two-part conjugates between polyoxazolines and peptides such as CGGGF and CGGWYKYW were prepared via a NCL reaction. In comparison to the thiol functionalized polymers from the previous chapter, the thiol group in those conjugates originally stems from peptidic cysteine residues and is formed anew during the NCL reaction. If those products of the NCL are then reacted with an allyl bearing compound in a thiol-ene-reaction, they form three-part conjugates with a polymer, a peptide and a sugar moiety. In this work, several different allyl compounds were used to synthesize three-part conjugates with the polymer-peptide conjugate products from the NCL in different lengths and functionalization degrees, which accumulates to a large array of product combinations. All different conjugates, including side chain polymer conjugates, are listed in **table 1**. For reasons of clarity and comprehensibility, all ensuing reactions will be explained by taking the example of proof-of-principle reactions with acetylated allyl mannose (AcMan) as allyl compound, with the two main conjugates that will be discussed in detail in this chapter being highlighted in bold. The first one, $PMeOx_{50}$-CGGGF-AcMan is based on an ω telechelic polymer, the second one, AcMan-CGGWYKYW-$PMeOx_{20}$-SEt on an α telechelic polymer.

Table 1: Overview of different polymer peptide sugar conjugates.

peptide moiety of the conjugate	telechelic functionalized conjugates	side chain functionalized conjugates (degree of funct., chain length)
CGGGF	**PMeOx$_{50}$-CGGGF-AcMan**	P(MeOx$_{45}$-*co*-ButOx-CGGGF$_5$-AcMan$_5$) (10 %, 50)
	Man-CGGGF-PMeOx$_{20}$-SEt	P(MeOx$_{40}$-*co*-ButOx-CGGGF$_{10}$-AcMan$_{10}$) (20 %, 50)
		P(MeOx$_{30}$-*co*-ButOx-CGGGF$_{20}$-AcMan$_{20}$) (40 %, 50)
		P(MeOx$_{16}$-*co*-ButOx-CGGGF$_4$-AcMan$_4$) (20 %, 20)
CGGWYKYW	PMeOx$_{50}$-CGGWYKYW-AcMan	P(MeOx$_{45}$-*co*-ButOx-CGGWYKYW$_5$-AcMan$_5$) (10 %, 50)
	AcMan-CGGWYKYW-PMeOx$_{20}$-SEt	P(MeOx$_{16}$-*co*-ButOx-CGGWYKYW$_4$-AcMan$_4$) (20 %, 20)
	Man-CGGWYKYK-PMeOx$_{20}$-SEt	

Synthesis of the conjugates was always similar, oriented at the preceding model reactions. All reactions were, if not stated otherwise, performed under reductive conditions to ensure that the thiol group needed for the reaction is constantly and readily available for the reaction.

a. CGGGF

The first polymer-peptide conjugate that was used for a thiol-ene reaction with acetylated allyl mannose was telechelic PMeOx$_{50}$-CGGGF (see **scheme 29**). Both educts were dissolved in water under the presence of TCEP to guarantee reductive conditions that prevent the free thiol group from dimerizing. It was already shown in the low molecular model reaction (see chapter 4.1.4) that the reducing agent does not interfere with the thiol-ene reaction. Irgacure 2959 was chosen as initiator because of its better water solubility compared to DMPA and the reaction mixture was stirred for 60 min under UV light irradiation. The resulting peptide and sugar functionalized polymer will be referred to as PMeOx$_{50}$-CGGGF-AcMan and was purified via dialysis against water.

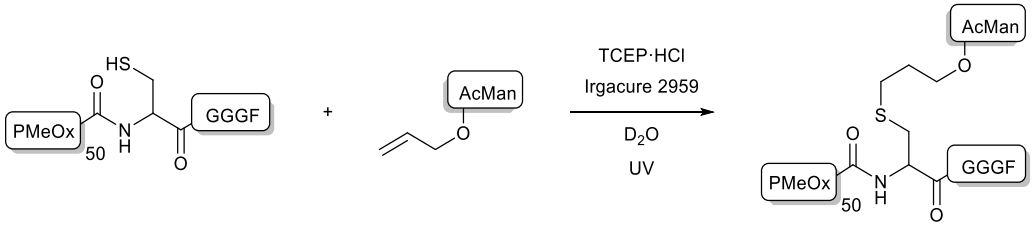

Scheme 29: Synthesis of telechelic peptide and sugar functionalized PMeOx$_{50}$-CGGGF-AcMan via thiol-ene reaction.

^{1}H-NMR spectroscopy of the product shows successful conjugation with the sugar (see **figure 50**). The disappearance of the characteristic allyl signal from the educt acetylated allyl mannose at 5.94-5.84 ppm is a first indicator for complete conversion. The most relevant signal can be found at 5.27-5.23 ppm. It belongs to three of the protons of the mannose ring and is easily identified by comparing the spectrum with a raw sugar spectrum. Other signals of the attached sugar ring can be found at 4.83 and 4.13-3.95 ppm, but are either overlaid by the MeOD solvent signal or not as distinctively isolated. The alkyl chain that connects the sugar to the polymer backbone delivers a signal at 4.26 ppm. The

other CH_2 groups are overlaid by polymer signals, which is also the case for the acetyl group signals that appear together with the broad CH_3 side chain signal of the polymer.

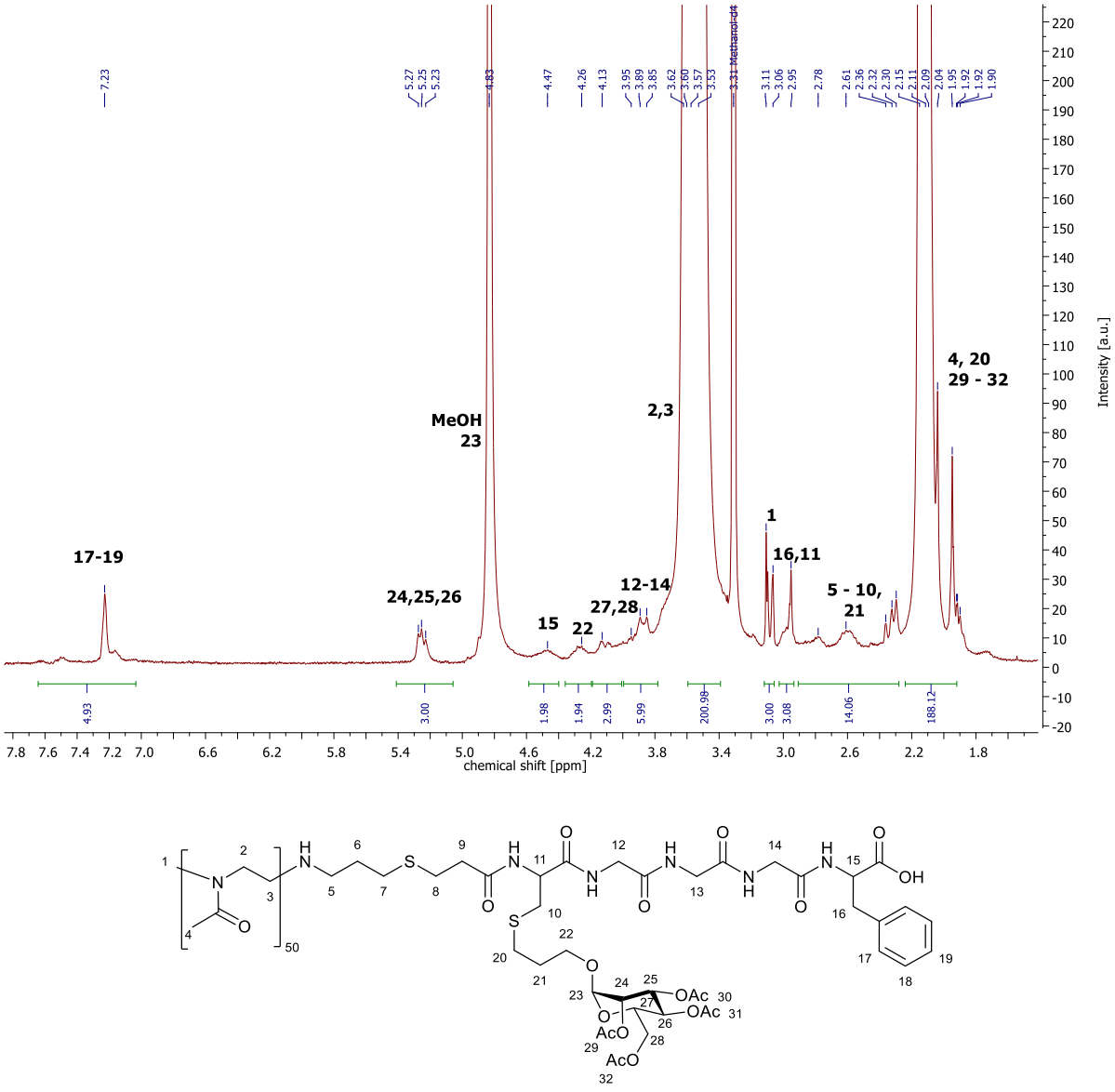

Figure 50: ^{1}H-NMR spectrum of telechelic peptide and sugar functionalized PMeOx$_{50}$-CGGGF-AcMan in MeOD.

Further interesting signals that are still present in the spectrum are the peptide signals at 7.23 ppm from the phenylalanine ring, at 4.47 and 3.89-3.85 ppm from the peptide backbone CH_2 groups and at 2.95 ppm for the peptide side chain CH_2 residue group. Dialysis as a purification step removes all peptide and sugar moieties that are not chemically, but only physically attached to the polymer, as explained in detail in chapter 4.2.4. Compared to the educt polymer peptide conjugate, where no dialysis was performed for purification, the fact that CGGGF peptide and mannose sugar signals are still present in the product spectrum, is not only a proof for a thorough conjugation, but also a confirmation that excess physically attached peptide that was still present in the raw educt (see chapter 4.2.2.1) has now been washed away by dialysis. Integral values of the peptide and sugar signals

reveal that each polymer chain is conjugated with one peptide and one sugar molecule, which indicates high rates of conversion for each conjugation step.

Other signals that are present are the broad polymer backbone signal at 3.62-3.53 ppm, the initiator methyl group signal at 3.11-3.06 ppm that was used as internal reference, as well as the telechelic alkyl chain signals at 2.95-2.30 ppm.

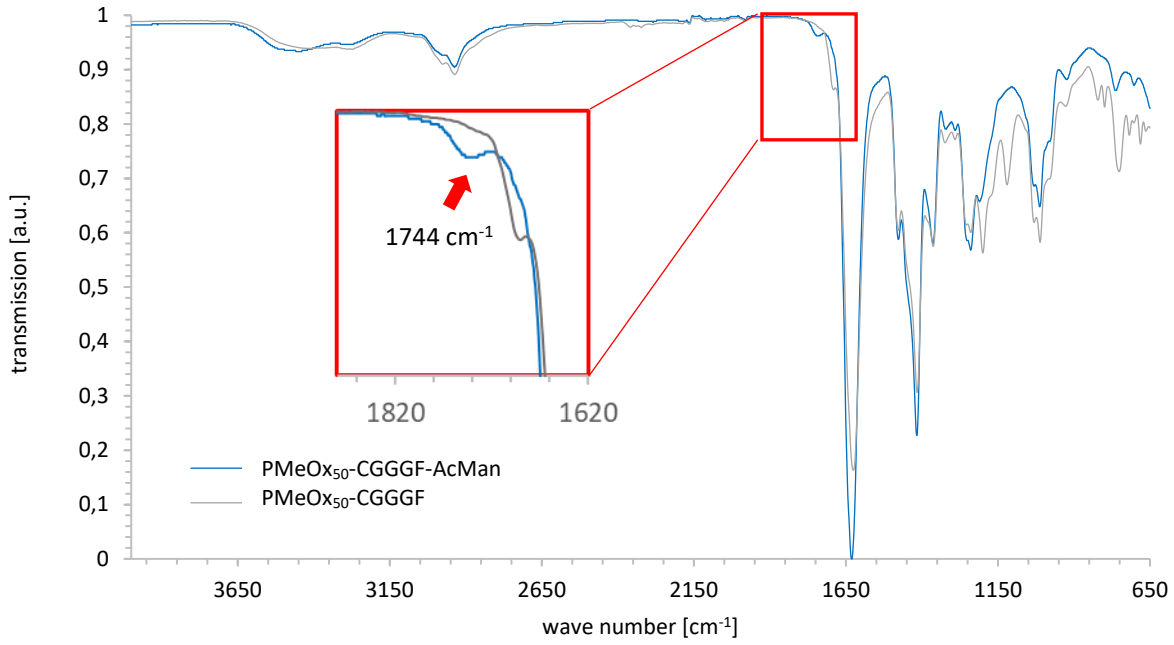

Figure 51: Superimposed IR spectra of educt polymer $PMeOx_{50}$-CGGGF (grey) and product polymer sugar conjugate $PMeOx_{50}$-CGGGF-AcMan (blue) with weak, but characteristic C=O stretching vibration of acetylated allyl mannose at 1744 cm^{-1}. The relevant part of the spectrum is enlarged.

IR spectroscopy was performed as an ancillary analytic method (see **figure 51**). It shows that a signal from the attached sugar, that was already identified as the characteristic acetylated mannose signal in the previous model reactions (see chapter 4.2.3.1), is visible in comparison to the precursor spectrum. Even though the signal is weak in relation to the strong polymer backbone signals, it still confirms that the reaction was successful. A thorough discussion concerning IR spectroscopy of the sugar conjugates is resumed in chapter 4.3.3.1, together with the side chain functionalized polymers.

b. CGGWYKYW

In analogy to the $PMeOx_{50}$-CGGGF conjugate, the same thiol-ene reaction was performed with the α telechelic CGGWYKYW-$PMeOx_{20}$-SEt peptide conjugate (see **scheme 30**) to examine if conjugation with the sugar is possible for both α and ω telechelic conjugates and with more sterically demanding peptide moieties. The reaction was performed similarly to the reaction described in the previous chapter, except that little amounts of DMSO were added to the reaction mixture to facilitate solubility. The resulting peptide and sugar functionalized polymer was also purified via dialysis against water and will be referred to as AcMan-CGGWYKYW-$PMeOx_{20}$-SEt.

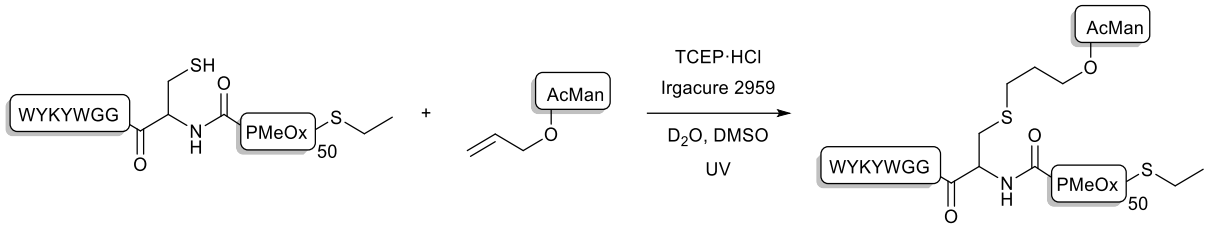

Scheme 30: Synthesis of telechelic peptide and sugar functionalized AcMan-CGGWYKYW-PMeOx$_{20}$-SEt via thiol-ene reaction.

The product conjugate was examined by ^{1}H-NMR spectroscopy (see **figure 52**).

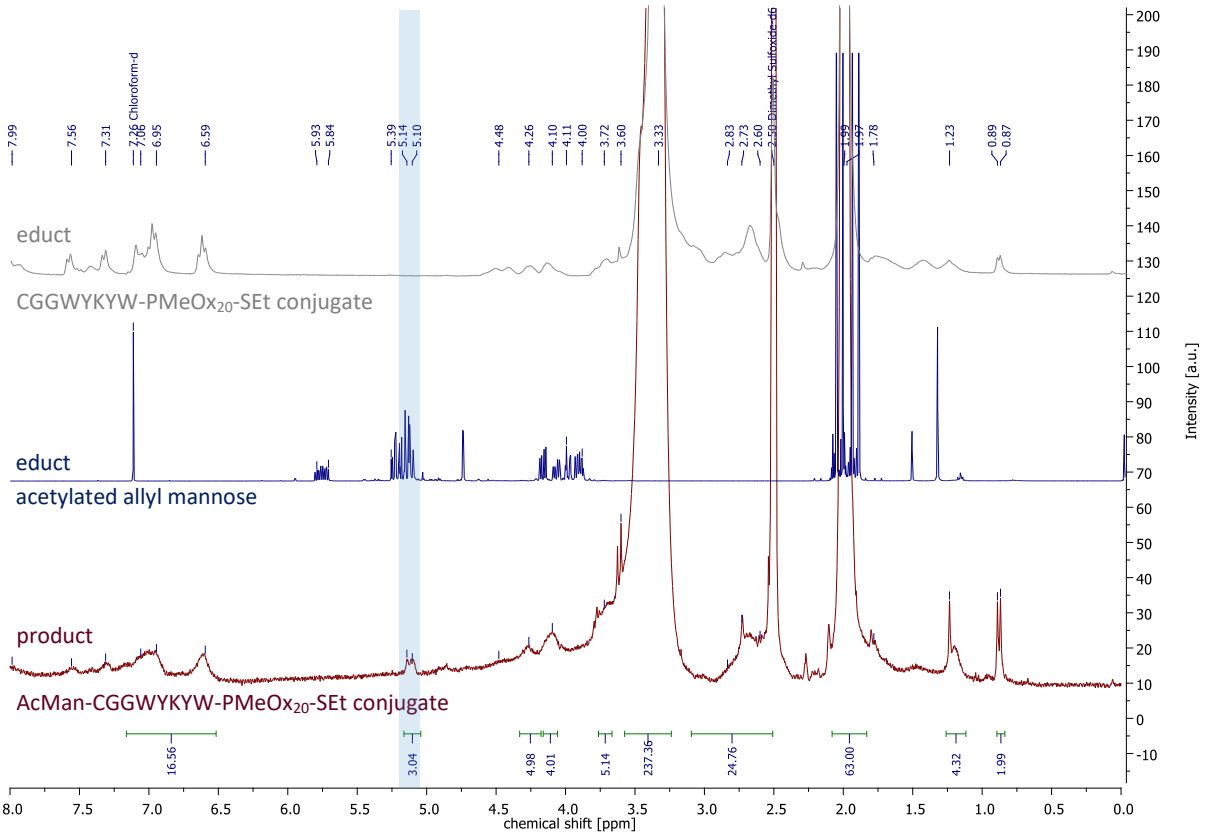

Figure 52: Stacked ^{1}H-NMR spectra of educt CGGWYKYW-PMeOx$_{20}$-SEt (grey, top) in deuterated DMSO, educt acetylated ally mannose (blue, middle) in $CDCl_3$ and the product AcMan-CGGWYKYW-PMeOx$_{20}$-SEt conjugate (red, bottom) in deuterated DMSO with the most relevant signal highlighted in blue.

^{1}H-NMR spectroscopy indicates that conjugation with the sugar was successful, since no more allyl signals are present in the product spectrum at 5.93 - 5.84 ppm and there is a newly formed characteristic signal at 5.10 ppm that corresponds to the attached mannose unit. It can be found in a region of the spectrum, where no other signals are present in the precursor conjugate spectrum. However, signal broadening due to the size of the conjugate does not allow for a precise assignment and integration of each individual signal and measuring the spectrum with more scans or higher frequencies did not improve signal resolution, as already shown in the previous chapter.

Therefore, IR spectroscopy was performed in order to adduce evidence for the accomplished conjugation. The IR spectrum (see **figure 53**) exhibits the weak, but nevertheless already well-known

characteristic signal for the sugar at 1736 cm^{-1} and therefore confirms findings from NMR spectroscopy. A thorough discussion concerning IR spectroscopy of the sugar conjugates is resumed in chapter 4.3.3.2, together with side chain functionalized polymer.

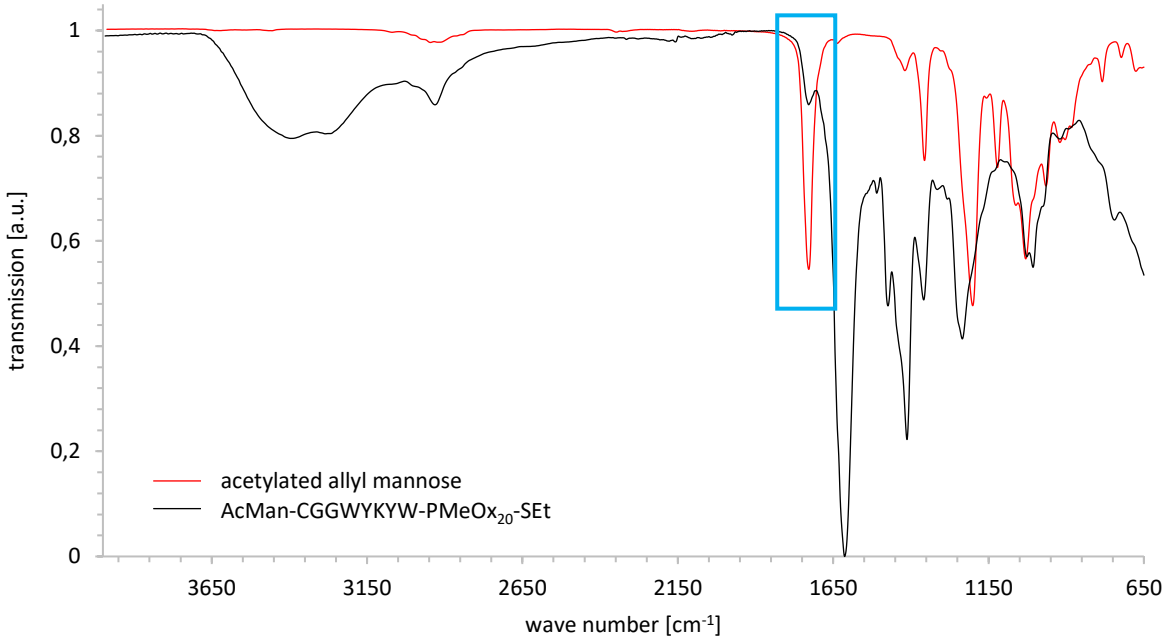

Figure 53: Superimposed IR spectra of acetylated allyl mannose (red) and product conjugate AcMan-CGGWYKYW-$PMeOx_{20}$-SEt (black) with weak, but characteristic C=O stretching vibration at 1736 cm^{-1} (highlighted with blue box).

At this stage of the reaction cascade, the challenge of demonstrating the unambiguousness of the results and verifying the conjugation of all three components, which is accompanied by analytical impediments, can be reliably addressed by focusing on material properties: Saccharides such as mannose exhibit a high affinity to lectins such as Concanavalin A and consequently, saccharides that are attached to a polymer conjugate will also show an affinity towards lectins. On the other hand, polymers that have not been conjugated with saccharides, will not show this affinity.

Hence, the last step of the cascade can be proven with a method that measures affinities to lectins. Chapter 4.2.5 will therefore focus on two analytical methods, SAW and SPR, to investigate affinity studies of the conjugates with lectins such as Concanavalin A as a concluding evidence for a successfully pursued reaction cascade.

Chapter 4.2.4 Dialysis as a Purification Method and Analysis Tool

In order to purify polymers by the removal of side products and excess precursor material, dialysis is a simple means to separate molecules of different sizes and remove small organic molecules and salts. It is therefore considered a standard procedure often used in polymer synthesis.[46] Moreover, it can also be implemented as an analytical tool, which will be highlighted in this chapter.

In almost each synthesis step of the aforementioned reaction cascade, dialysis was applied as a method to purify the desired products. In order to show the effectiveness of this powerful processing tool that is already in use for polymer purification since the 1960s[638-639], several control experiments were conducted and will be presented as follows:

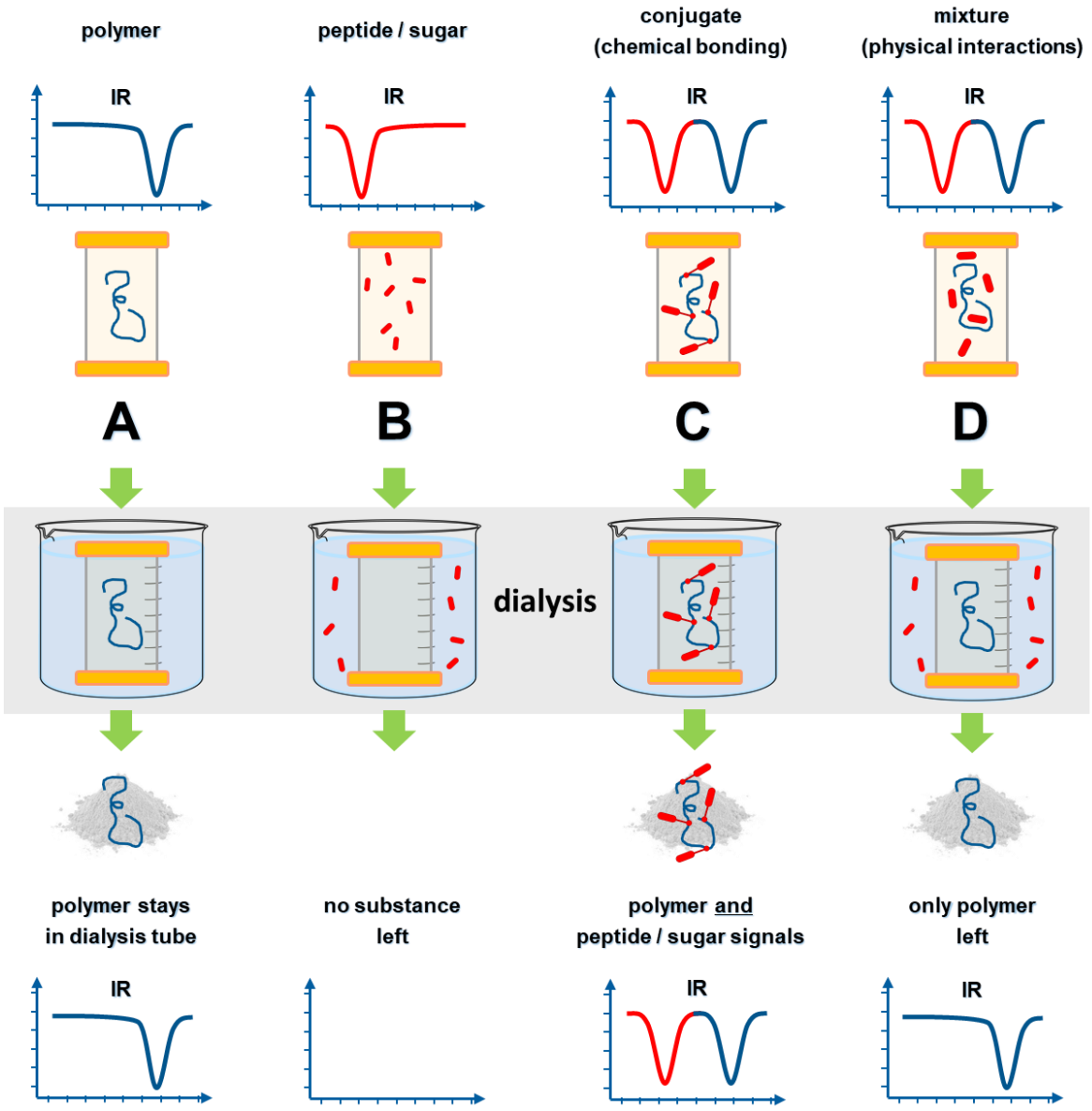

Figure 54: Set-up of dialysis experiments. A: Pure polymer; B: Pure peptide/sugar; C: Polymer-peptide/polymer-sugar conjugate; D: Polymer-peptide/polymer-sugar mixture.

In each experiment **A-D**, dialysis tubes with the same molecular weight cut-off (1000 g·mol^{-1}) were filled with solutions of equal amounts of products as well as educts from the former described NCL and thiol-ene conjugation reactions (see **figure 54**). Dialysis tube **A** contained a solution of raw polymer, dialysis tube **B** contained a solution of raw peptide (respectively sugar), dialysis tube **C** was filled with a solution of the polymer-peptide conjugate (respectively polymer-peptide-sugar conjugate) and dialysis tube **D** as a control tube contained a solution of a mixture of raw polymer and raw peptide (respectively sugar) that were not reacted with each other in a conjugation reaction. All tubes were then dialysed under the same conditions for several days and afterwards lyophilised. The remaining material was weighed and analysed by IR spectroscopy.

The experiments were conducted individually for *all* of the different telechelic and side chain polymers, peptides, sugars and polymer-peptide as well as polymer-peptide-sugar conjugates, which covers all of the reactions described in chapter 4.2.2, chapter 4.2.3, chapter 4.3.2 and chapter 4.3.3.

The results were similar for all experiments: As expected, in case of raw polymer (**A**), 50-80 % of the initial mass is retained after dialysis and in case of raw peptide or sugar (**B**), no substance was left over after dialysis. This is not surprising, as the polymers have a higher molecular mass than the used cut-off of 1000 g·mol^{-1} and mostly stay in the tube, as opposed to the peptides and sugars, which have masses lower than 1000 g·mol^{-1} and therefore get washed out of the dialysis tube completely.

In case of the chemically bound conjugates (**C**), which have an even higher molecular mass than the raw polymer, up to 80-90 % of the material can be retained after dialysis.

The control tube **D** provides information about the either physical or chemical character of the interaction between the conjugation partners. Especially peptides show strong physical interaction properties such as physical gel formation or entanglement and it is conceivable that those interactions, as well as entrapment or substance inclusion can also occur with the used polymers. If those physical interactions are strong enough, they could easily be mistaken as chemical bonding. Dialysis is thought to separate conjugates that are physically attached in contrary to conjugates that are chemically bound. However, this must be verified first. In order to examine the character of the interaction and to test the capability of dialysis for separating physically attached components, the conjugation partners were mixed in similar ratios as in the coupling reactions, although no catalyst or conjugation agent was added, so neither NCL nor thiol-ene reactions can take place. After dialysis, IR spectroscopy of the retained material showed the disappearance of characteristic signals from substances such as peptides and sugars, which proves that those substances have been washed out of the mixture completely, while most of the polymer is retained in the tube. Therefore, it was possible to show that

only components that are chemically bound to the polymer by NCL or thiol-ene reaction will not be washed out through dialysis and only physically attached substances will be removed.

With the dialysis of a conjugate between a fluorescent dye and polymer, the dialysis process is made visible to the bare eye, as depicted in **figure 55**. On day 1, most of the excess and non-covalently bound dye is washed out of the dialysis tube, which leads to a strong inking of the dialysis water. Over the course of the following days, the dialysis water, which is exchanged each day, is less and less dyed, while obviously, the polymer-dye conjugate with its strong orange-yellow colour is retained inside the dialysis tube.

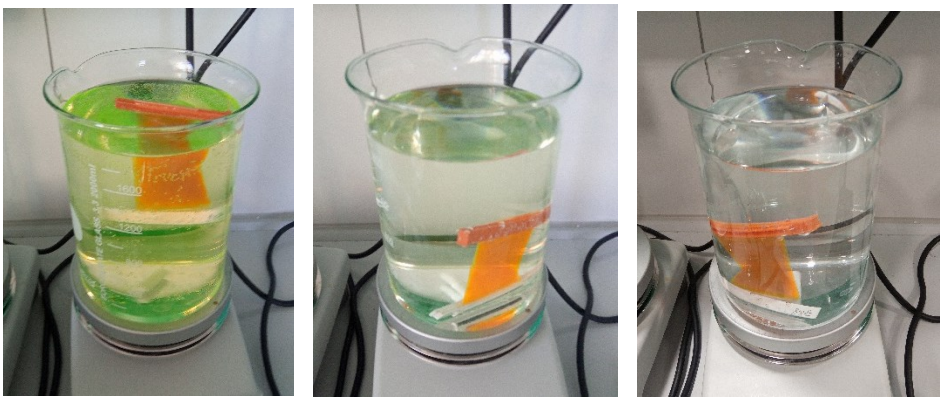

day 1 **day 2** **day 4**

Figure 55: Dialysis process with a fluorescent conjugate over the course of four days.

However, dialysis as a purification method has one major drawback, and that is a great loss in yield. The smaller and less branched a conjugate is and the longer the dialysis times are, the higher are losses, which can sum up to 60 % decrease in yield over the course of typically 3-5 days of dialysis. The effect of large macromolecules escaping a dialysis tube (even though their molecular mass is far above the molecular weight cut-off of the dialysis membrane[640]) can be compared with shaking a colander of spaghetti for a prolonged period of time – just as the noodles, whose diameter is smaller than the hole size of the sieve, the usually strongly entangled polymer chains can uncoil and “wind” their way out through the pores of the dialysis membrane. Therefore, it is advised to use dialysis only for the last step of a reaction cascade or if low molecular impurities in earlier stages hinder a subsequent reaction step.

Chapter 4.2.5 Biomacromolecular Recognition Experiments

Polymers that have been functionalized with peptides and sugars can be used in biomacromolecular recognition experiments. Measuring the affinity between the conjugates from the preceding chapters and biomacromolecules such as lectins is beneficial in two ways:

First, from an innovative perspective, new possibilities in the field of polymer design for bioactive conjugates are explored. It is conceivable, that by choosing the right binding pairs and the proper length of linker molecules, bivalent polymer conjugates can be created that take advantage of synergistic and cooperative binding effects and have therefore a manifold higher binding affinity than each single binding partner on its own.

Second, in a more straightforward and down-to-earth prospect, positive affinity measurements themselves can validate all the preceding steps that lead to the formation of the used conjugate or, in other words, they then act as an affirmation tool that the entire reaction cascade that was described in the previous chapters was successful.

For the conjugated compounds from the preceding chapters, specific binding pairs were identified: Sugars such as mannose and its derivates show a high affinity to sugar-binding lectins such as ConA[32, 101], and according to literature[150], the WYKYW amino acid sequence of the peptide CGGWYKYW exhibits an increased binding affinity to Galectin-1.

Grafting those peptide and mannose components to polymers as it was described in the previous chapters allows for affinity studies with the respective lectins. Two different methods for the analysis of substrate binding affinities were chosen to investigate the conjugates at hand: SAW and SPR measurements. In SAW measurements, binding affinities of substrates are measured via alteration of phase, amplitude and frequency of surface acoustic waves in case of a binding event. SPR spectroscopy is a standard method for measuring adsorption of material onto surfaces or nanoparticles and relies on the excitation of surface plasmons by polarized light, irradiated through a prism. Changes of the refractive index of a surface due to binding events are measured. Both methods however depend on the attachment of the substrate to a gold surface.

Therefore, a specific design of the polymer and its conjugates is needed for SAW as well as SPR measurements. The polymer needs to have an '*anchor*', that allows for fixation of the molecule at the target gold surface. Thiol and thioether groups fulfil that function, since those functional groups exhibit high affinities to gold[641-642]. Hence, a short polymer was designed, with a thioether group at the ω-terminus, that allows for binding to the SAW and SPR sensor chip gold surface and an allyl function at the α-terminus, that allows for further functionalization and conjugation with peptides and sugars (see **figure 56**).

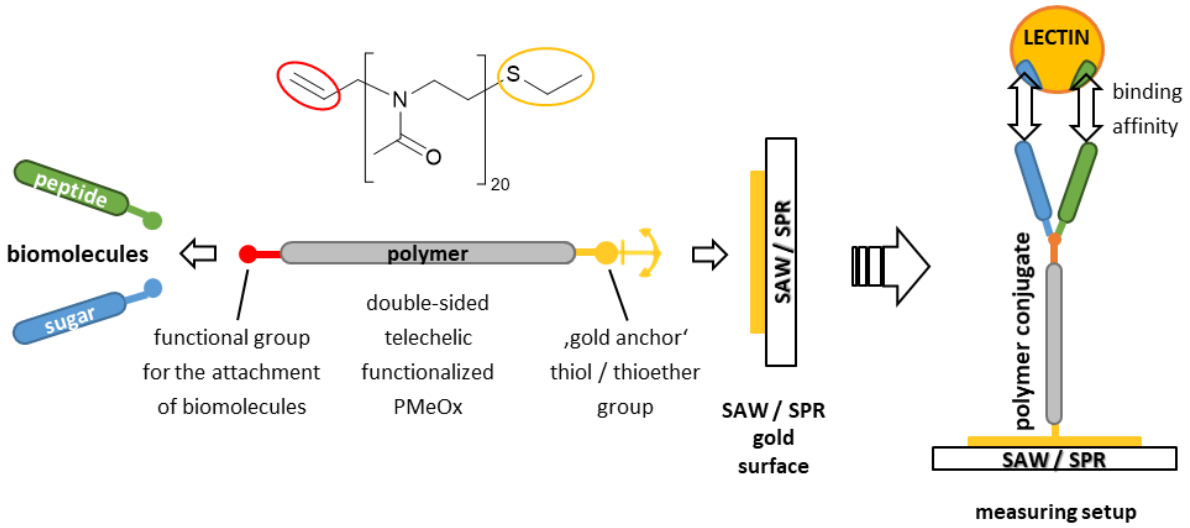

Figure 56: Simplified depiction of a polymer design for SAW and SPR measurements.

The synthesis of such a polymer and its conjugation with a CGGWYKYW peptide is described in chapter 4.2.1.1b and chapter 4.2.2.3. The attachment of a protected model sugar, acetylated mannose, to the polymer peptide conjugate is described in chapter 4.2.3.2. For SAW and SPR measurements with ConA, conjugation with a more specific sugar, namely mannose, is desired and described hereafter.

Chapter 4.2.5.1 *Synthesis of Specifically Designed Peptide/Sugar-Polymer Conjugates*

The same procedure from the preceding chapter 4.2.3 was used to synthesize conjugates with deprotected allyl mannose as a similar sugar derivate. The reaction will not be described in detail, as it is an exact repetition of the reactions described earlier. In analogy to the previously explained experiments, the sugar is reacted with the conjugate in a thiol-ene reaction under reductive conditions. Analogous conditions were also applied for purification via dialysis and analysis via NMR and IR.

However, in contrast to acetylated allyl mannose that was used in earlier experiments, deprotected allyl mannose has no distinctive, characteristic signals in IR and NMR spectroscopy. It only delivers signals in an area of the ^{1}H-NMR spectrum, where they are easily overlaid by a great number of CGGWYKYW peptide and polymer backbone signals. Consequently, the most important sign for a successful reaction is the disappearance of the allyl signals at 5.98-5.15 ppm, which was already proven to be a good indication for conversion in each of the previous model reactions (see chapter 4.1.4, chapter 4.2.3.1 and chapter 4.2.3.2). Yet additionally, some minor sugar signals at 3.97-3.84 ppm and an increase of integral values can be detected, as well as one small singlet signal at 4.65 ppm that is not present in the precursor spectrum and is assigned to the anomeric proton of the sugar ring (see **figure 57**).

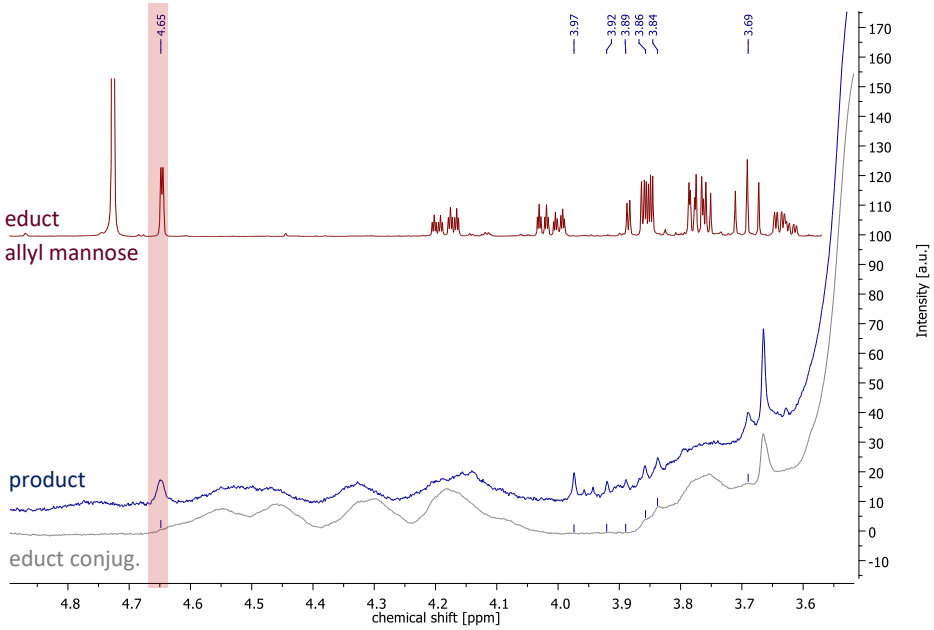

Figure 57: Section of the Man-CGGWYKYW-PMeOx$_{20}$-SEt product spectrum (blue) where sugar signals are visible. The anomeric proton is highlighted in red. The spectrum is stacked with the precursor spectrum (grey) and the educt allyl mannose spectrum (red). The complete Man-CGGWYKYW-PMeOx$_{20}$-SEt product spectrum can be found on page 248 in the appendix.

Even though the indication is challenging, nonetheless it is supported by the experience from preceding experiments and it is therefore assumed that the conjugation reaction with mannose was successful. This will be further validated by consecutive SAW and SPR measurements which are described in the next passage.

Following the above described procedure, another system specialized for affinity measurements was synthesized: **Man-CGGGF-PMEOx$_{20}$-SEt**, a conjugate with a mannose unit that has been attached to a polymer-CGGGF precursor. The respective NMR spectrum of the conjugate can be found in the appendix.

Chapter 4.2.5.2 *SAW Affinity Studies*

SAW measurements consist of three steps. At first, the polymer or polymer conjugate is attached to the gold surface by incubating three of the available five measuring lanes with polymer solution. The two remaining empty lanes serve as blind test lanes. Next, non-covered surface area is saturated with BSA. This step, the saturation with BSA, already yields a first information concerning the binding of polymer or polymer conjugate to the surface. For the blind lanes, a high phase change is measured, whereas for gold lanes that are covered with polymer, the binding of BSA is significantly lower (see **figure 58**).

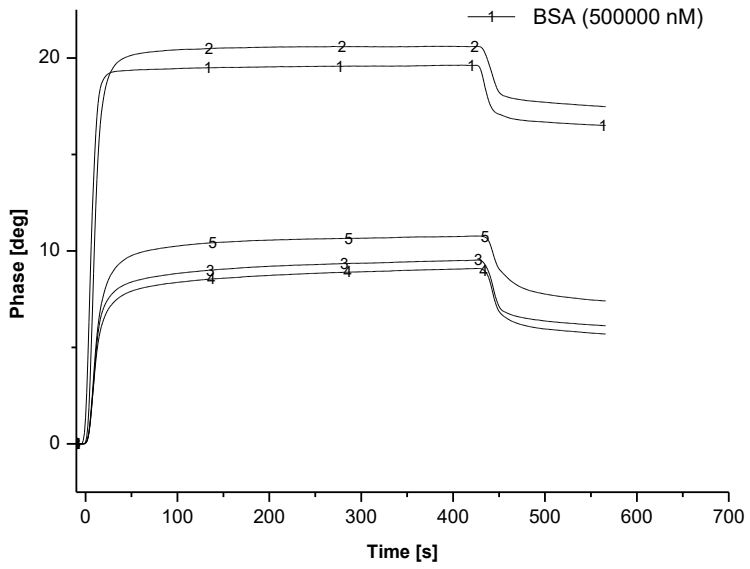

Figure 58: Saturation of the gold surface with BSA. The blind test lanes 1 and 2 (top curves) have not been coated with polymer and therefore allow for more binding of BSA.

Following the preparation of the gold surface with the polymer conjugates and saturation with BSA, the main measurement can be performed by analysing the binding affinity of the lectin to the functionalized surface. For this, a constant flow of a series of ConA dilutions with defined concentrations of ConA is injected on each channel and the phase change of surface acoustic waves, which is influenced by binding events, is monitored. If there is no binding event, no change in phase can be detected (see **figure 60**, top left). In case of a binding event, the phase curve rises as long as there is a constant flow of lectin solution over the measuring lanes until it reaches a saturation plateau after a few minutes (see **figure 60**, top right). Since ConA is not covalently bound to the conjugates, as soon as the flow of lectin stops, the curve declines as a result of a detachment event of ConA from the surface. Between the measurements with different concentrations of ConA, all lanes are regenerated with an acidic glycine solution to detach all remaining bound proteins. After measuring four different ConA concentrations, the binding and dissociation curves are fitted and the K_D value is then calculated.

As shown in **figure 59**, five different experimental settings for the interaction of polymer conjugates with ConA were investigated.

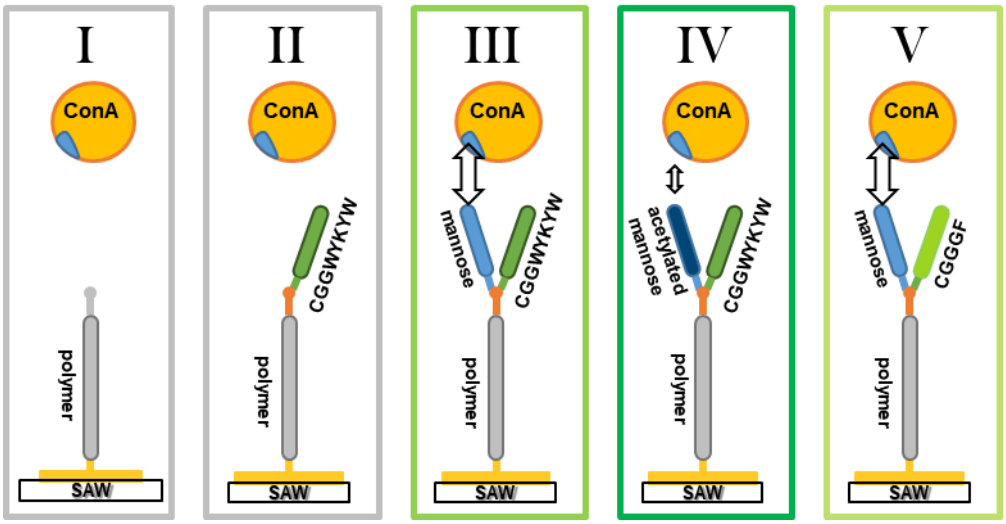

Figure 59: Experimental settings for SAW affinity studies (schematic). The polymer or polymer conjugate is attached to the SAW gold surface through the thioether group and affinities to ConA are measured. The conjugates used in experiment I-V are: I) allyl-PMeOx$_{20}$-SEt, II) CGGWYKYW-PMeOx$_{20}$-SEt, III) Man-CGGWYKYW-PMeOx$_{20}$-SEt, IV) AcMan-CGGWYKYW-PMeOx$_{20}$-SEt and V) Man-CGGGF-PMeOx$_{20}$-SEt.

In experiment I, unfunctionalized polymer was attached to the surface and served as a negative control. Affinity measurements show no binding event of ConA to the surface (see **figure 60**, top left), which is as expected.

There is no indication, neither in literature nor by preceding experiments, for a specific interaction of ConA to peptides with a CGGWYKYW sequence. Thus, the conjugate of polymer and CGGWYKYW is also not expected to show affinity to ConA, which could be proven in experiment setting № II. The measurement curves look similar to experiment I and no binding event was observed.

In contrast, mannose sugar derivates are expected to have a high affinity to ConA[32, 101]. Literature values for the K_D between a mannose substrate and ConA lie in the range of 200±50 µM[643] respective 189±2.5 µM[644]. However, affinity studies with monosaccharide units *in solution* remain a challenge due to the low molecular mass of the sugar substrates. In the respective cases, therefore either the lectin or the saccharide have been grafted to a surface prior to the measurement.

Mannose polymer conjugates that have been described in literature show K_D values between 0.25±0.06 µM[645], 42±5 µM[646] and 53 µM[647], although also displaying a strong dependency on the used methods (e.g. ITC, SPR or quartz crystal micro balance) as well as the structure and composition of the investigated mannose derivates. In each study, slightly modified mannose derivates were used. The different derivate substructures, respective their conjugation to the measuring surface in SPR studies, however, seem to have a noticeable influence on the steric properties of the substrate and

thus also on the affinity to the lectins. A comparison between the experiment setups is therefore only possible in terms of a similar order of magnitude of the received affinity values.

The polymer and mannose conjugates that were synthesized in this work should also show strong binding to ConA. This was examined in experiment III, where a conjugate between polymer, peptide CGGWYKYW and mannose sugar was attached to the gold surface. As shown in **figure 60** (top right), an affinity to the lectin with a K_D of 388 ± 57 nM could be measured, which is in the same order of magnitude as the respective literature values[645-647]. This experiment not only shows interaction between the polymer conjugate with ConA, but is furthermore a striking confirmation that the attachment of sugar to the polymer, which has been described in chapter 4.2.5.1, was successful. The experiment was repeated several times with different batches of polymer conjugate and each time yielded identical results with similar K_D values. In literature, only few other examples are present that investigate binding events between ConA and *polyoxazoline* conjugates. These works mainly focus on qualitative binding, using dynamic light scattering (DLS)[137] or turbidity assays[37] to monitor, whether the respective POx saccharide conjugate shows interaction with the lectin or not, and, unlike the setup presented in this work, no quantitative statements can be achieved with those methods.

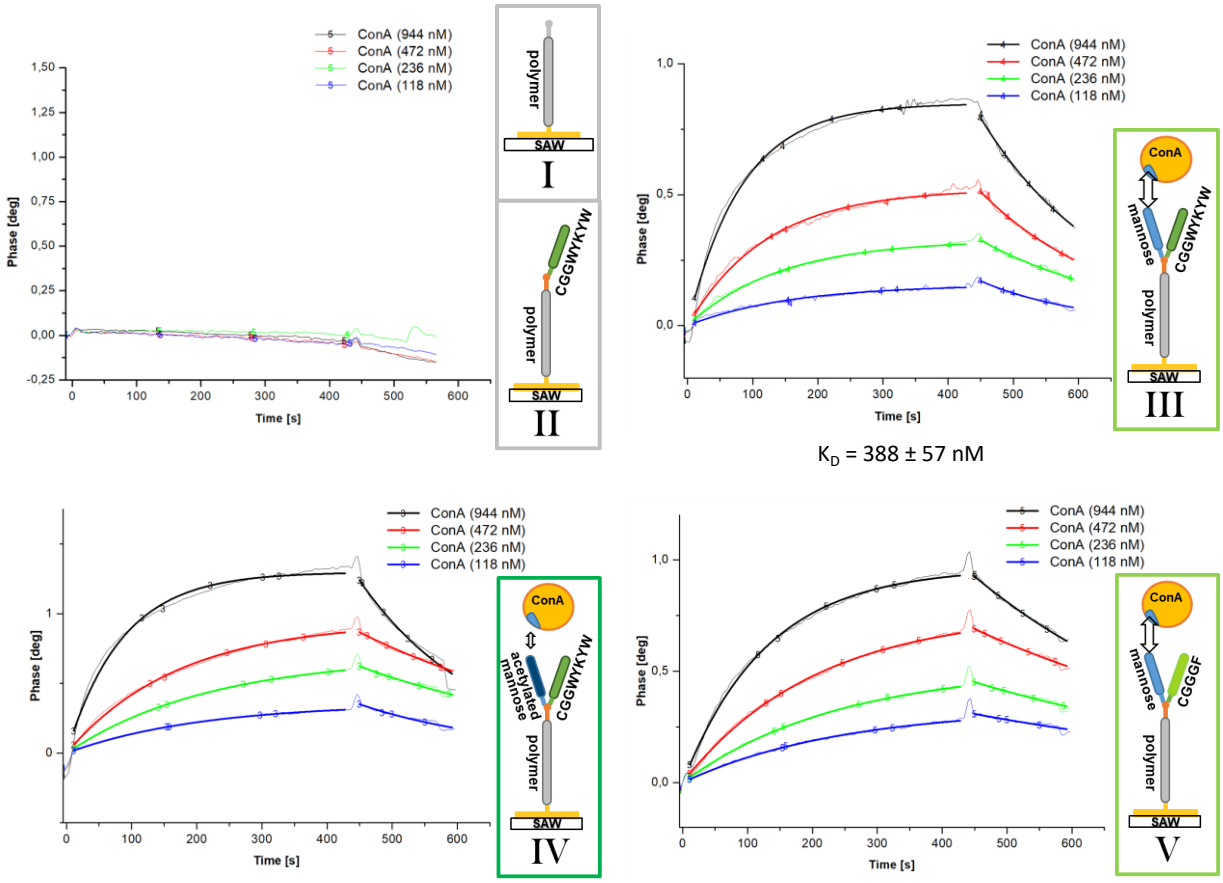

Figure 60: Exemplary SAW measurement curves for experiment I-V. For each experiment, four different lectin concentrations were measured. Experiment I and II (top left) did not show any binding event.

It was expected that modifying the sugar unit should have an influence on the binding affinity to the lectin. In experiment IV, a similar conjugate as in experiment III was examined, but the mannose unit attached to the polymer was still protected with acetyl groups. In this case, there is still an affinity to the lectin (see **figure 60**, bottom left). However, with a K_D value of 1316 ± 179 nM, the binding of ConA to the surface is significantly weaker than before. (Note that K_D is the equilibrium *dissociation* constant and therefore, the smaller its value, the greater the binding affinity of the ligand for its target). This is certainly not surprising, as the acetyl groups prevent an optimal fit of the mannose unit into the binding pocket of ConA.

For a complete set of experiments, in setting № V, the CGGWYKYW peptide was exchanged with a different peptide to show that the choice of peptide does not influence sugar binding affinity. CGGGF does not show specific interaction with ConA and the K_D value of 397 ± 97 nM for this experiment is comparable to experiments with CGGWYKYW (see **figure 60**, bottom right).

It would however be interesting to investigate if this effect is negligible when peptides are used that are known to explicitly *have* an affinity to certain biomacromolecules. Experiments that focus on this aspect will be discussed further below.

Avidity Studies

Additionally, some basic and straightforward avidity pilot studies were performed with the system. In literature, avidity experiments cover a wide range of different focuses and aims. Some experiment with the increase of substrate density attached to a polymer chain[107, 109], others regulate spacing between ligands[34, 115] or investigate the influence of substrate architecture[110] or concentration[113-114]. Here, mixtures of polymers from exp. I and III were grafted to the gold surface in different ratios of functionalized and unfunctionalized polymer. In doing so, the unfunctionalized polymer chains should act as spacing units between functionalized conjugates, thus varying the substrate density with varying polymer concentrations. In case of high dilutions and low densities, they thereby prevent avidity effects from taking effect in the ConA binding measurements (see **figure 62**).

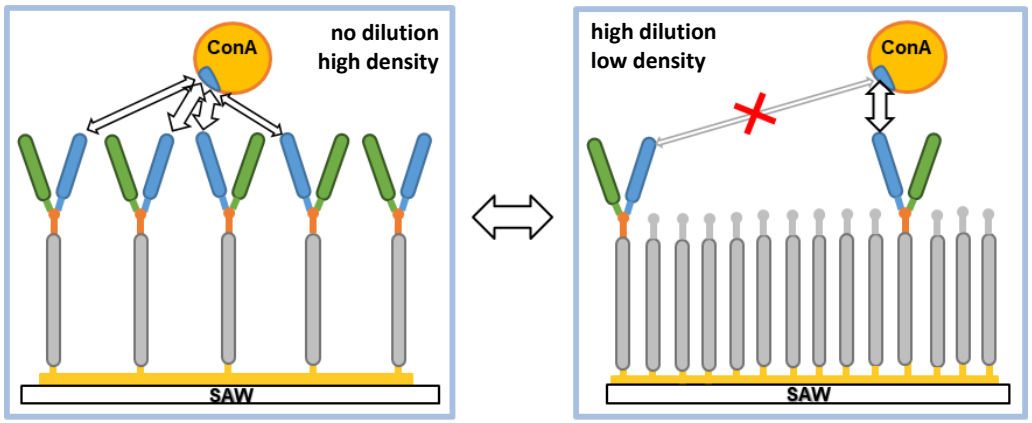

Figure 61: Simplified depiction of expected avidity differences between surfaces with a high density of functionalized conjugates (left) and surfaces with a low density of functionalized polymers (right).

However, expected differences between surfaces with a high and low density of functionalized polymers were not observed (see **figure 62**). None of the dilutions significantly diminished the affinity values. It is conceivable that either the magnitude of dilution was not sufficient enough to inhibit avidity effects, clustering effects on the surface took place or functionalized and unfunctionalized polymers show different gold binding properties. However, since the binding curves of coatings with the lowest ratio of functional conjugates were already barely measurable, which is an indication for a wide spread coating with functionalized polymer, it seems more plausible that even coatings out of pure functionalized conjugate do not display avidity effects with ConA at all.

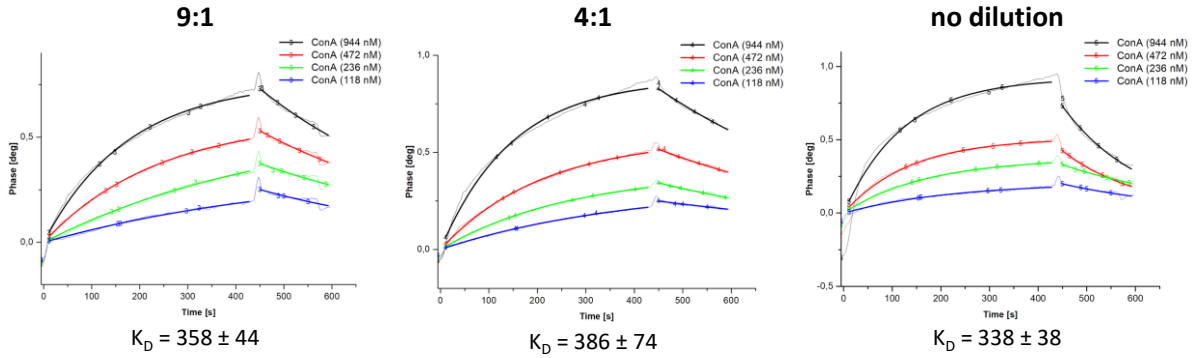

Figure 62: Avidity studies with different ratios of functionalized and unfunctionalized polymer. Ratio of unfunctionalized to functionalized conjugate: Left: 9:1; Middle: 4:1; Right: pure functionalized conjugate (no dilution).

Different Lectins

It would be interesting to create polymer conjugates that take advantage of synergistic and cooperative binding effects and have therefore a manifold higher binding affinity than each single binding partner on its own. For this case, a biomacromolecule with an affinity to *two* different targets would be in focus of investigation.

The first task prior to the respective binding experiments is to identify another potential binding partner for lectins. Instead of choosing another sugar moiety, the use of a peptide was preferred in this work. In practical terms, using both a sugar and a peptide moiety in proof of principle reactions would broaden the field of application for the resulting conjugate. With regard to this, the peptide CGGWYKYW, which is said to have an increased affinity to galectin[150] was chosen as a potential bioactive conjugation partner. Consequently, for the ensuing SAW measurements, ConA as a biomacromolecule was exchanged with a different lectin, human Galectin-1, and the measurements were repeated with conjugates I-III.

However, contrary to literature[150], neither one of the two conjugates that is bearing a CGGWYKYW peptide unit, CGGWYKYW-PMEOx_{20}-SEt and Man-CGGWYKYW-PMEOx_{20}-SEt, displayed any binding affinity with the lectin. Several explanations are conceivable, why findings from literature could not be reproduced and the CGGWYKYW peptide did not yield any measurable binding activity to Gal1. In the respective work by André et al.[150], a high affinity between the WYKYW sequence and Gal1 was

determined by phage-display, yet no strength of the binding event was evaluated. It could be possible that the binding affinity is simply too weak to be measured by means of SAW or SPR. The work also investigated only a 5-peptide sequence WYKYW. The attachment of a further CGG unit and the conjugation to a polymer backbone may have changed the affinity, increased rigidity or decreased substrate flexibility. It is further conceivable that the employed linker was too short and that steric hindrances could impede the peptide of the surface-anchored conjugate from reaching the relevant binding site of the protein. This has also been monitored in literature[44, 112], where binding of lectin was decreased for shorter spacer lengths, which made the sugar ligand less accessible to the binding sites. Increasing the length of the glycine linker chain between the cysteine and the specific WYKYW sequence could be an approach in tackling this challenge and might be subject to further investigations.

All results from the SAW measurements are listed in **table 2** on page 108 together with the results from SPR spectroscopy.

Chapter 4.2.5.3 *SPR Affinity Studies*

SPR spectroscopy was performed as an ancillary analysis that supports the findings from SAW measurements. Preparing the samples is identical to SAW measurements. The SPR measuring channels were coated with polymer solution and unoccupied gold surface was saturated with BSA. The main measuring curves of the binding event of ConA to the surface have a similar shape as those measured by SAW. As an example, one of them is depicted in **figure 63**. The attachment and detachment events for different concentrations of ConA are clearly visible.

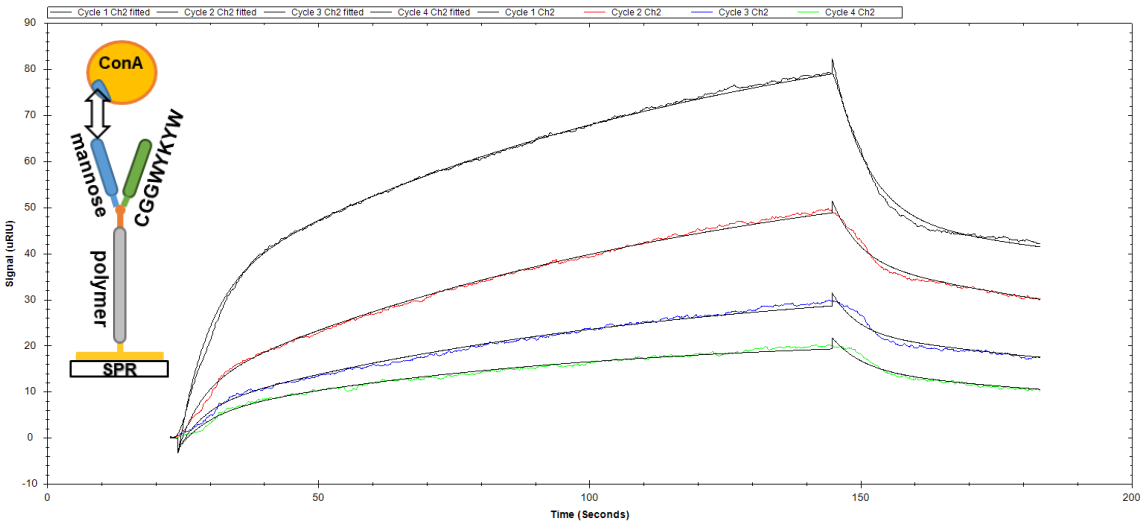

Figure 63: SPR measuring curve of the binding and detachment events of a series of ConA dilutions to a surface that has been covered with Man-CGGWYKYW-PMeOx$_{20}$-SEt.

All results from SPR spectroscopy are listed in the third column in **table 2**. The SPR measurements deliver K_D values that comply with the results obtained by SAW measurements. For unfunctionalized

allyl-PMeOx$_{20}$-SEt and peptide polymer conjugate CGGWYKYW-PMeOx$_{20}$-SEt, no binding event was monitored. For conjugates with mannose, there is no significant difference in K_D values between conjugates with different peptides. The conjugates exhibit K_D values of 250 ± 34 nM for Man-CGGWYKYW-PMeOx$_{20}$-SEt and 255 ± 40 nM for Man-CGGGF-PMeOx$_{20}$-SEt. With a K_D value of 1138 ± 193 nM, the conjugate of acetyl protected mannose displays a significantly lower binding to ConA than its deprotected derivate. Overall, the K_D values determined by SPR spectroscopy are in the same order of magnitude as the K_D values determined by SAW measurements.

Table 2: K_D values of SAW and SPR affinity measurements. Each experiment was conducted on three (SAW) resp. four (SPR) lanes with four different lectin concentrations being measured on each lane. The average K_D value resulting from all individual measurements combined is highlighted in bold (no aff. means no affinity of the conjugate to the lectin could be determined).

lectin (method) / conjugate (exp. №)		ConA (SAW) K_D [nM] lane 1	ConA (SAW) K_D [nM] lane 2	ConA (SAW) K_D [nM] lane 3	Gal1 (SAW) K_D [nM] lane 1-3	ConA (SPR) K_D [nM] lane 1	ConA (SPR) K_D [nM] lane 2	ConA (SPR) K_D [nM] lane 3	ConA (SPR) K_D [nM] lane 4
allyl-PMeOx$_{20}$-SEt (I)			**no aff.**		**no aff.**		**no aff.**		
CGGWYKYW-PMeOx$_{20}$-SEt (II)			**no aff.**		**no aff.**		**no aff.**		
Man-CGGWYKYW-PMeOx$_{20}$-SEt (III)			**351 ± 77**		**no aff.**		**250 ± 34**		
	(1)	257±60	388±92	383±46	no aff.	214±32	229±38	273±42	285±46
	(2)	N/A	329±42	430±34	-		-		
	(3)	278±44	432±71	467±62	no aff.		-		
	(4)	303±75	388±57	215±25	-		-		
AcMan-CGGWYKYW-PMeOx$_{20}$-SEt (IV)			**1325 ± 97**		**-**		**1138 ± 193**		
		1316±179	1426±293	1232±266		894±117	1081±83	1242±136	1336±126
Man-CGGGF-PMeOx$_{20}$-SEt (V)			**332 ± 63**		**-**		**255 ± 40**		
		272±21	328±55	397±97		234±41	204±22	281±49	293±53

The results from SPR spectroscopy therefore reinforce the findings from the preceding SAW measurements. On top of that, both series of affinity measurements serve as a ratification of the whole reaction cascade described in the preceding chapters. Demonstrating that the polymer conjugate bears a mannose unit that can interact with a biomacromolecule such as ConA, serves as a proof that each of the previous steps, which all build on one another, have also been successful in order to lead to the formation of the final conjugate.

Although a postulated interaction between the WYKYW sequence of a polymer peptide conjugate and galectin could not be certified, it was shown that the reaction cascade provides a versatile toolbox for the design of strategically selected, bioactive three-part conjugates. Further studies that can build upon this groundwork will be discussed in chapter 5.

Chapter 4.3 Side Chain Functionalization

Side chain functionalization adds another dimension to the structured functionalization of polymers. Multivalent pendant groups demand for even more sophisticated handling of practical methods and analytical tools. The synthesis of side chain functionalized polymer peptide sugar conjugates will be described in this chapter.

Chapter 4.3.1 Polymer Functionalization

In order to functionalize the polymer at the side chain, statistical, hydrophilic polyoxazolines were synthesized by copolymerization of ButenOx monomer and MeOx monomer. While MeOx is responsible for the hydrophilicity of the final polymer, the allyl bearing ButenOx creates a basis allyl functionality at the side chain of the polymer that can be used to attach a carboxylic acid group, which can successively be converted into a thioester group. The reaction steps for this are similar to those used for the telechelic polymers (see chapter 4.2.1) and are employed in analogy (see **scheme 31**).

The rate of functionality per polymer chain can be controlled by using stochiometric proportions of the two monomers. It is conceivable to add further functionality via the use of functionalized initiators respectively terminating agents, but in order to ensure a consistent functionalization only at the side chain, *p*-toluenesulfonate was used as an initiator to deliver a methyl group at the α-terminus of the polymer and piperidine was used as a terminating agent.

In telechelic functionalized polymers, each polymer chain has only one functional group available for substitution in the reaction cascade, whereas side chain functionalized polymers can bear multiple functional groups. It is a big advantage that the presence of multiple functional groups per polymer chain delivers proportionately stronger signals that are more visible and easier to recognize in polymer analytics than the single functional group signal of telechelic polymers. In many cases, experiments with side chain functionalized polymers therefore deliver results to *qualitatively* undergird analytics of telechelic functionalized polymers. Additionally, *quantitative* statements, such as the degree of substitution for each of the available side chain groups or predictions concerning the conversion rates will also be the focus of discussion later in this chapter.

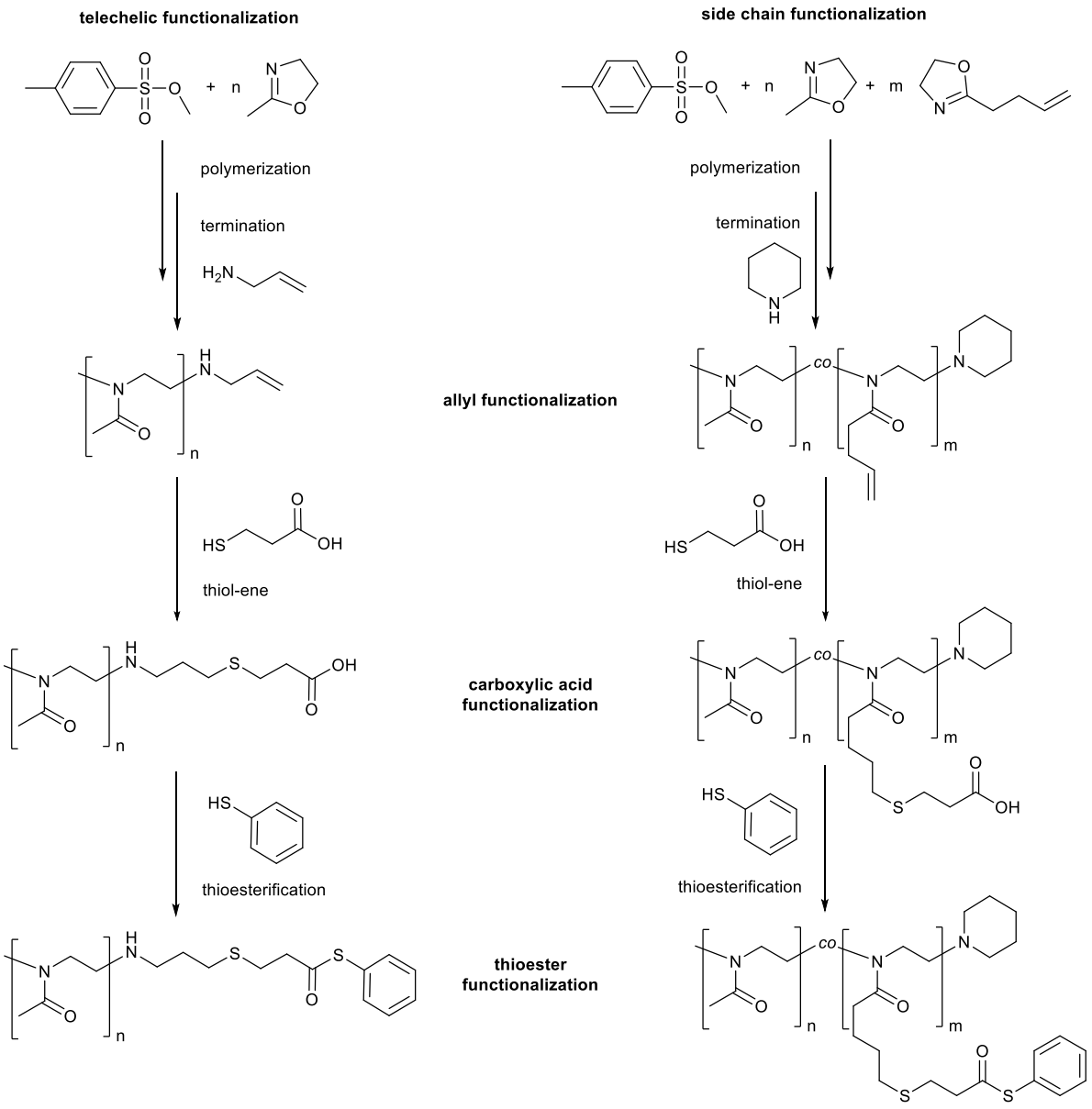

Scheme 31: Synthesis of telechelic (left) and side chain (right) functionalized polyoxazolines.

Apart from the total chain length of a side chain functionalized polymer, which is determined through the molar ratio between monomers and initiator, the degree of side chain functionalization, which is determined through the molar ratio between the different monomers themselves, affects the properties of the final polymer. In this work, side chain functionalized polyoxazoline copolymers with chain lengths of 20, 50, 100 and 500 repeating units were synthesized, while the degree of ButenOx functionalization was varied between 5 %, 10 %, 20 % and 40 %. Since synthesis and analytics are similar for different chain lengths and functionalization degrees, all reactions will be described, if not otherwise stated, by taking the example of polymers with 50 repeating units and a functionalization degree of 10 %.

Chapter 4.3.1.1 *Monomer Synthesis*

The monomer MeOx is commercially available and was purified by distillation before use. The allyl functionalized monomer ButenOx was synthesized according to literature in a three-step mechanism (see **scheme 32**).[230, 500]

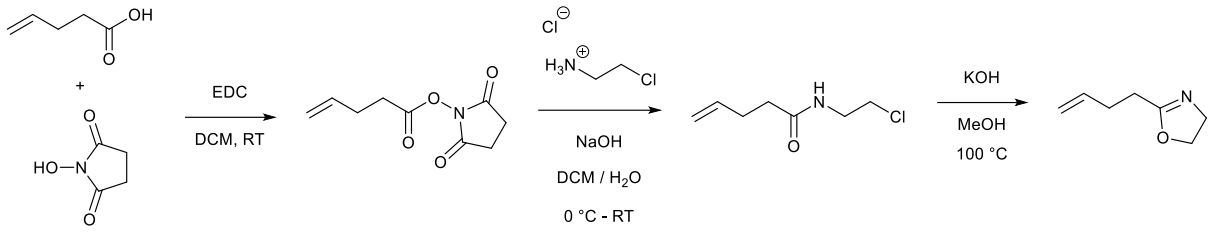

Scheme 32: Synthesis of ButenOx.

4-pentenoic acid and *N*-hydroxysuccinimide (NHS) were reacted under the presence of 1-ethyl-3-(3-dimethylaminopropyl)carbodiimide (EDC) as a carboxyl activating agent. The succinimidyl group was then exchanged with 2-chloroethyl ammonium chloride under alkaline conditions to form *N*-(2-chloroethyl)-4-pentenamide. The ring closing procedure was performed with the use of potassium hydroxide at 100 °C in methanol. After drying the raw product with CaH_2 and distillation under low pressure (1 mbar, 65 °C), the final product after all three steps could be obtained in yields of 69 % (relative to 4-pentenoic acid), which is in good accordance with literature.[230]

The NMR spectrum of ButenOx (see **figure 64**) shows two characteristic signals at 5.84-5.71 ppm and 5.03-4.91 ppm, corresponding to the signals 2 and 1 from the allyl functionality, two triplets at 4.15 and 3.72 ppm from the signals 4 and 3 of the alkyl chain and a strong singlet at 2.30 ppm that can be assigned to the ring protons 5 and 6. The spectrum shows no impurities.

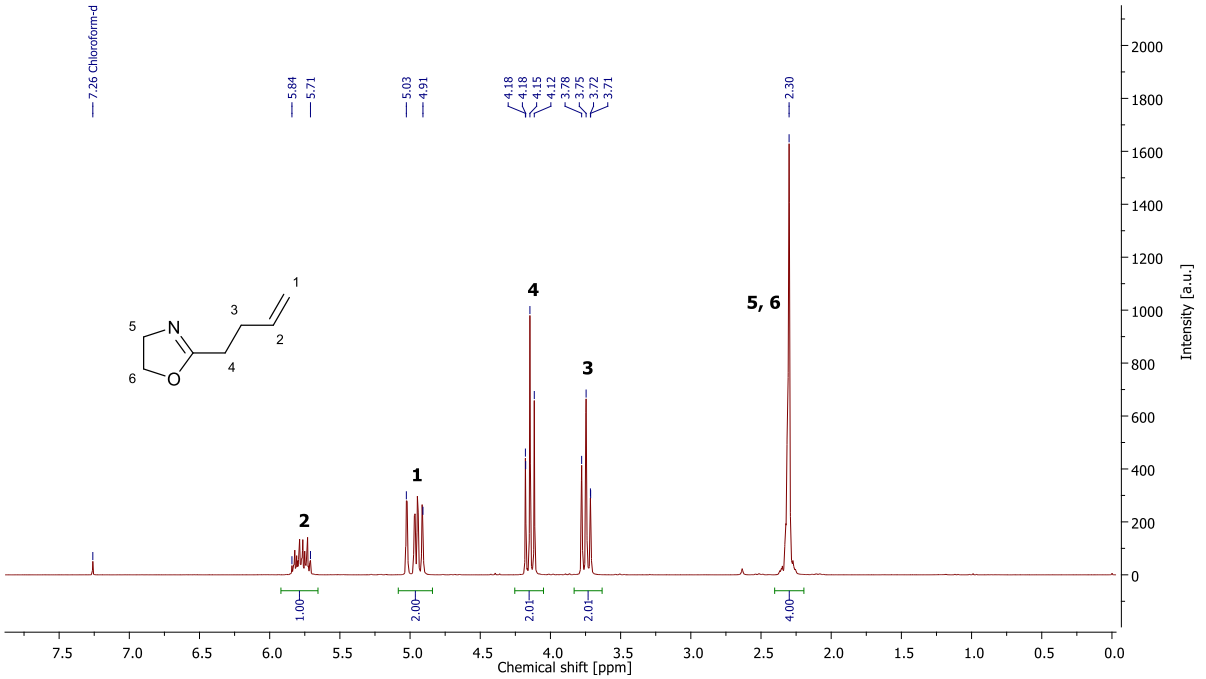

Figure 64: ^{1}H-NMR spectrum of ButenOx in $CDCl_3$.

Chapter 4.3.1.2 *Synthesis of Side Chain Allyl Functionalized Poly(2-Oxazoline)s*

The synthesis of side chain allyl functionalized poly(2-methyl-2-oxazoline-*co*-2-butenyl-2-oxazoline) P(MeOx-*co*-ButenOx) was performed according to literature[55]. The initiator methyl *p*-toluenesulfonate, as well as ButenOx and MeOx as monomers were dissolved in dry acetonitrile. The stochiometric ratio of monomers to initiator determines the chain length of the polymer, whereas the ratio of MeOx to ButenOx defines the rate of allyl functionalization of the final copolymer. The standard procedure will be demonstrated by the example of a polymerization with 1 equivalent initiator, 45 equivalents MeOx and 5 equivalents ButenOx. The resulting 10 % allyl functionalized copolymer with a chain length of 50 repeating units will be referred to as P($MeOx_{45}$-*co*-$ButenOx_5$). Other copolymers that were synthesized by using the method described below range from 20 to 500 repeating units in size and bear up to 40 % allyl functionalization.

Both monomers as well as the initiator and the solvent were dried over CaH_2 and distilled prior to using them for the polymerization reaction, as impurities could easily compromise the character of a living cationic ring opening mechanism.[511-512] The polymerization was then carried out as a microwave reaction at 100 °C for 60 min under inert gas atmosphere, terminated with piperidine overnight at RT and precipitated from cold diethyl ether to purify the product (see **scheme 33**). The detailed mechanism of the polymerization (LCROP) is described in chapter 2.2.2.2.

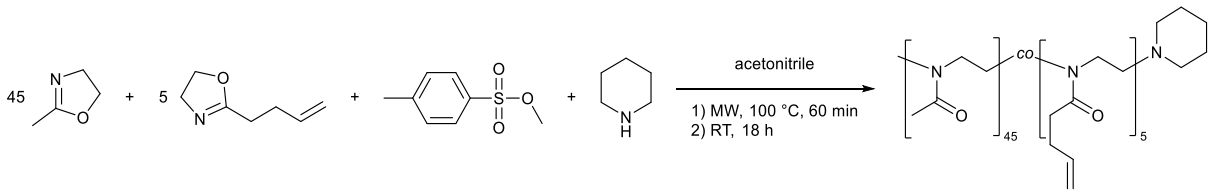

Scheme 33: Synthesis of side chain allyl functionalized P($MeOx_{45}$-*co*-$ButenOx_5$).

The resulting copolymer was analysed by ^{1}H-NMR spectroscopy (see **figure 66**). Clearly recognizable are two characteristic double bond signals at 5.81 and 5.07-5.01 ppm, which stem from the side chain allyl functionalization of the ButenOx units, as well as the broad signal at 3.44 ppm from the polymer *backbone*. The signal at 3.03-2.94 ppm originates from the methyl group of the initiator and serves as intern reference in order to calculate the degree of polymerization. Similar to the methyl group signal in the spectrum of telechelic polymers, this signal also appears with a doublet structure, due to a possible rotation of the methyl group around the amide function. By integrating the backbone signal, a total chain length of 49 repeating units could be calculated, which is in good accordance with the intended chain length of 50 units. The signal at 2.45-2.35 ppm can be assigned to the alkyl side chain of the ButenOx units and it partly overlaps the signal from the methyl group of the tosylate counter ion. Therefore, its integral is slightly higher as the expected amount of 18 protons. Another strong, broad signal that appears at 2.13-2.06 ppm stems from the methyl group of the MeOx units. The integration of the MeOx signals delivers a content of MeOx 44 units, while the integration of the allyl

signals delivers an allyl content of 4.5 ButenOx units. This is in good accordance with the intended chain length of 50 units and an MeOx to ButenOx ratio of 45 : 5. The termination with piperidine delivers three distinct signals at 1.78, 1.57 and 1.44 ppm for the piperidine ring. Two further signals that can be recognized in the spectrum are at 7.70 and 7.18 ppm, which stem from the tosylate counterion. Additionally, there is one prominent signal at 3.11 ppm in the raw product spectrum, which is similarly described in a work of Liebscher.[601] There, the author hypothesizes a side reaction between piperidine with the *p*-toluene sulfonate salt (see **figure 66**), which would result in the appearance of a triplet signal, emerging at higher ppm than the signal for piperidine alone. This shift would be in accordance with the ^{1}H-NMR signals of 1-tosylpiperidine found in literature[648]. The explanation of Liebscher seems legit, as the signal only appears for reactions where piperidine was used as a terminating reagent and not for reactions with allylamine or ethanethiol (as described in chapter 4.2.1.1). Moreover, the integral values of the respective protons (indicated with an *i* in **figure 66**) correspond well to the integral values of the aromatic tosylate signals. It is furthermore shown in the next chapter and also proven in the work of Liebscher[601], that the signal will not appear anymore after dialysis as a means of removing low molecular impurities.

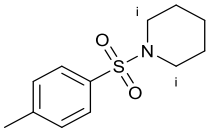

Figure 65: Side product from the reaction of *p*-toluene sulfonate with piperidine, as suggested in [601].

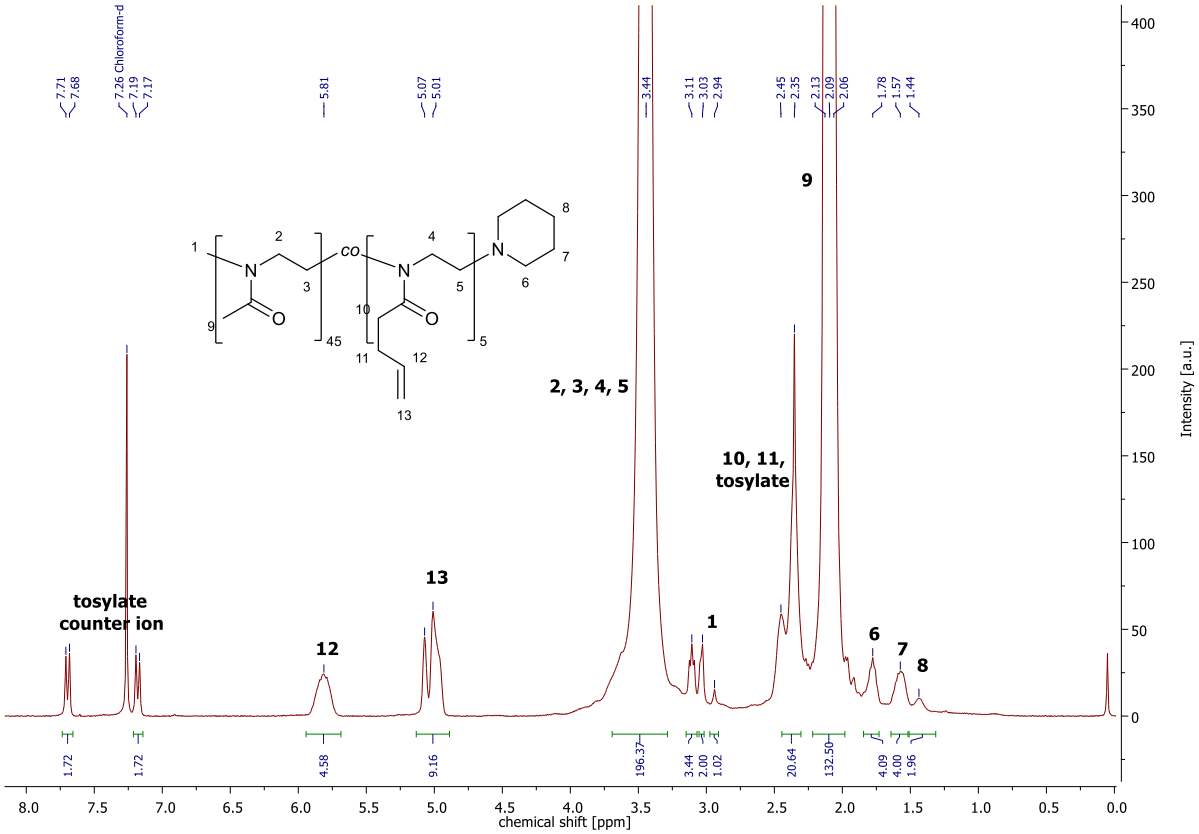

Figure 66: ^{1}H-NMR spectrum of side chain allyl functionalized P(MeOx$_{45}$-*co*-ButenOx$_{5}$) in $CDCl_3$.

SEC measurements in DMF show a narrow molecular weight distribution with a symmetric elugram (see **figure 67**), a small shoulder towards high molecular weights and a dispersity of $Đ = 1.03$. For side chain functionalized polyoxazolines, the effects that influence SEC data are similar to those described for telechelic polymers (a detailed discussion thereof can be found in chapter 4.2.1.1). With a dispersity of $Đ = 1.03$, the reaction matches well with the $Đ < 1.2$ criteria for a living polymerization. The molecular weight determined by SEC ($M_n = 4526\ g{\cdot}mol^{-1}$, $M_w = 4649\ g{\cdot}mol^{-1}$) corresponds to the molecular weight calculated from ^{1}H-NMR spectroscopy ($M_n = 4345\ g{\cdot}mol^{-1}$) and is in good accordance with the expected theoretical molecular weight ($M_n = 4555\ g{\cdot}mol^{-1}$). The small high molecular weight shoulder in the spectra is assigned to aggregation effects and is still weak in comparison to SEC spectra of similar copolymers that are described elsewhere and sometimes even exhibit bimodal distribution curves.[600-601, 609] Further SEC elugrams of derivates with variable chain lengths and degrees of functionalization can be found in the experimental section. For those with a higher percentage of ButenOx, the shoulder for higher molecular weights is slightly increased. It is susceptible that higher functionalization rates with up to 40 % ButenOx promote chain entanglement and therefore influence the coiling behaviour of those polymer fractions. For polymers with up to 500 repeating units in size, the SEC curves displays a marginal tailing effect, which, as discussed before, is accounted to increased interaction of long polymers with column material.

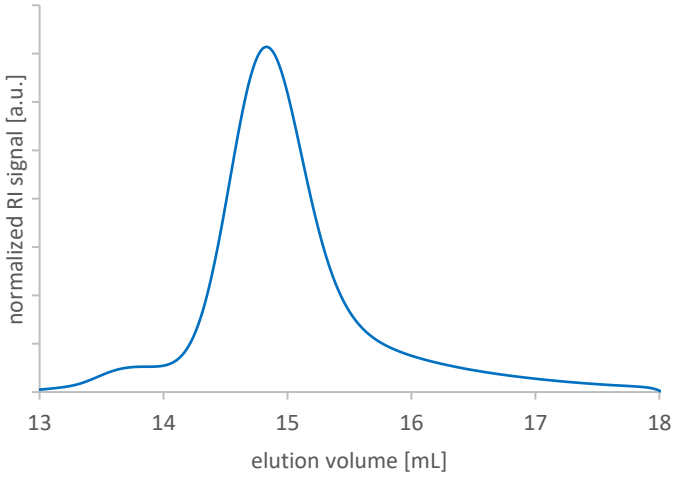

Figure 67: SEC elugram of side chain allyl functionalized P($MeOx_{45}$-*co*-$ButenOx_5$) in DMF.

Degree of Functionalization

Concerning side chain allyl functionalization, a variety of copolymers with different chain lengths and functionalization degrees was synthesized. Those polymers are listed in chapter 6.2.30 in the experimental section and were all synthesized with the same reaction procedure, except different ratios of monomer and initiator educts were used.

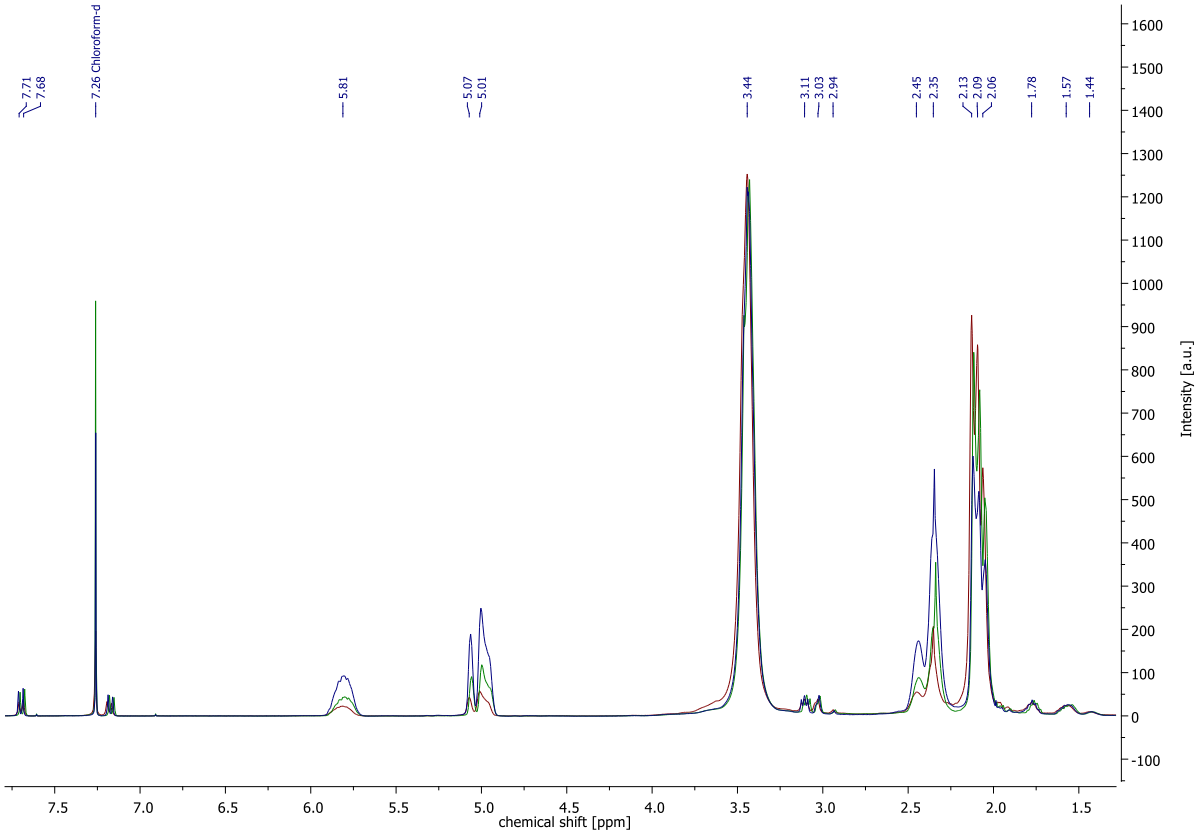

Figure 68: Superimposed ^{1}H-NMR spectra of side chain allyl functionalized copolymers P(MeOx$_{45}$-*co*-ButenOx$_{5}$) (red), P(MeOx$_{40}$-*co*-ButenOx$_{10}$) (green) and P(MeOx$_{30}$-*co*-ButenOx$_{20}$) (blue) in $CDCl_3$. The spectra were normalized to the initiator signal.

Apart from an increase in dispersity (which is accounted to higher interaction of functionalized polymers with SEC column material), with increasing degree of functionalization, no differences concerning side reactions, impurities or incomplete conversion were observed with NMR and IR spectroscopy. This is illustratively depicted in **figure 68**, which shows superimposed ^{1}H-NMR spectra of three copolymers with the same chain length of 50 repeating units, but a 10 %, 20 % and 40 % degree of functionalization. The spectra are almost identical, except for the proportionately different integral values of the allyl and side chain signals.

Chapter 4.3.1.3 *Synthesis of Side Chain Carboxylic Acid Functionalized Poly(2-Oxazoline)s*

In order to introduce a carboxylic acid functionalization into the copolymer, the allyl group can be reacted with 3-mercaptopropionic acid in a thiol-ene reaction (see **scheme 34**) analogous to the reaction with telechelic functionalized polymers (see chapter 4.2.1.2). For this, both the polymer and 3-mercaptopropionic acid were dissolved in dry methanol, DMPA was added as a photoinitiator and the reaction was stirred under UV light irradiation for 90 min. The detailed mechanism of the thiol-ene reaction is described in chapter 2.1.5.3. The resulting carboxylic acid functionalized copolymer was purified by precipitation from cold diethyl ether and will be referred to as P(MeOx$_{45}$-*co*-ButOx-COOH$_{5}$).

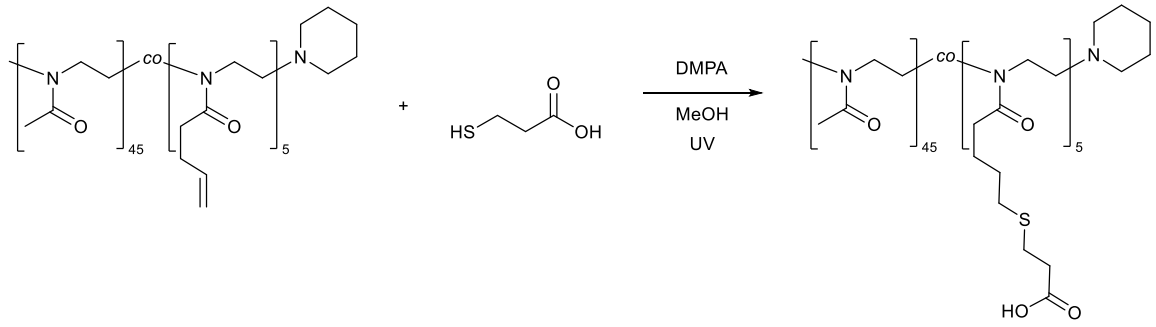

Scheme 34: Synthesis of side chain carboxylic acid functionalized P(MeOx$_{45}$-*co*-ButOx-COOH$_5$).

The resulting polymer was analysed by ^{1}H-NMR spectroscopy (see **figure 69**). While the broad signal at 3.48-3.46 ppm from the polymer *backbone* is still present and was used as intern reference, the characteristic signals from the educt allyl groups have disappeared due to the successful reaction. Instead, new signals from the formed alkyl chain as well as alkyl signals from the attached 3-mercaptopropionic acid appear at 2.75, 2.57, 2.41-2.28 and 1.65 ppm. The signal from the initiator methyl group can still be found at 3.04 ppm, as well as the broad side chain methyl group signal at 2.14-2.07 ppm and the terminating piperidine signals at 1.97-1.77 ppm. Further signals at 7.69, 7.19, 2.36 and 1.20 ppm stem from the tosylate counter ion and diethyl ether residues.

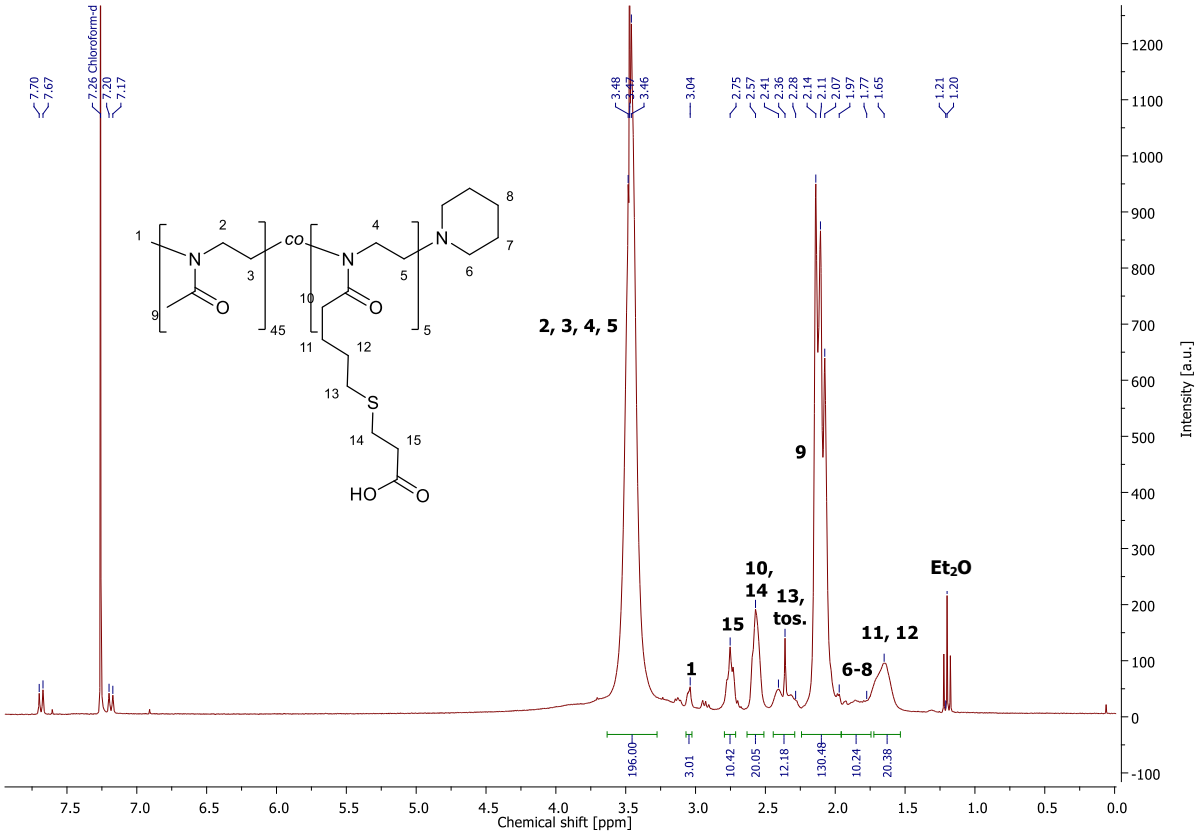

Figure 69: ^{1}H-NMR spectrum of side chain carboxylic acid functionalized P(MeOx$_{45}$-*co*-ButenOx-COOH$_5$) in $CDCl_3$.

At this stage of the reaction cascade, dialysis as an additional purification method was performed with a small fraction[1] of the product to demonstrate removal of tosylate and ethyl ether residues as well as the unidentified signal described in the previous chapter 4.3.1.2. An ^{1}H-NMR spectrum of the dialysed product, which shows the disappearance of the respective signals, yet some signal broadening due to a different (higher) polymer concentration in the sample, can be found in the appendix on page 249.

As it was already shown with telechelic polymers in chapter 4.2.1.2, IR spectroscopy can be performed in order to confirm the presence of carboxylic acid groups. The stretching vibration of C=O from the carboxylic acid group delivers a characteristic signal in the IR spectrum at 1720 cm^{-1} (see **figure 70**), which is not present in the IR spectrum of the precursor allyl functionalized polymer.

Since side chain functionalization is performed with manifold functional groups, the intensity of the signal is considerably stronger than it is with single telechelic functionalization.

Due to the inherent measuring method, quantitative statements concerning the rate of conjugation should still be made with caution. However, as already discussed in chapter 4.2.2.2, the degree of functionalization has a clear impact on the intensity of the characteristic carboxylic acid signal. To investigate this further, three copolymers with the same chain length of 50 repeating units, but a different ratio of methyl oxazoline to butenyl oxazoline (10 %, 20 % and 40 %) were synthesized: P($MeOx_{45}$-*co*-$ButOx_{5}$), P($MeOx_{40}$-*co*-$ButOx_{10}$) and P($MeOx_{30}$-*co*-$ButOx_{20}$). The three copolymers were then functionalized with carboxylic acid to yield P($MeOx_{45}$-*co*-ButOx-$COOH_{5}$) (10 %), P($MeOx_{40}$-*co*-ButOx-$COOH_{10}$) (20 %) and P($MeOx_{30}$-*co*-ButOx-$COOH_{20}$) (40 %). All copolymers display the same characteristic COOH signal in the IR spectrum (see **figure 70**). With the C=O stretching vibration of the polymer backbone taken as a reference, it is remarkable that the intensity of the COOH signal is relatively stronger, the higher the degree of functionalization is. In case of the copolymer with 10 % peptide conjugation, the characteristic signal is comparably weak, whereas with 40 % conjugation, the signal is relatively stronger. The matching intensities are an additional indication that on this stage of the reaction cascade, functionalization rates and reaction conversions are not impeded by a higher degree of functionalization, thus reaffirming the concrete numbers found by NMR spectroscopy and titration.

[1] to avoid losses in yield

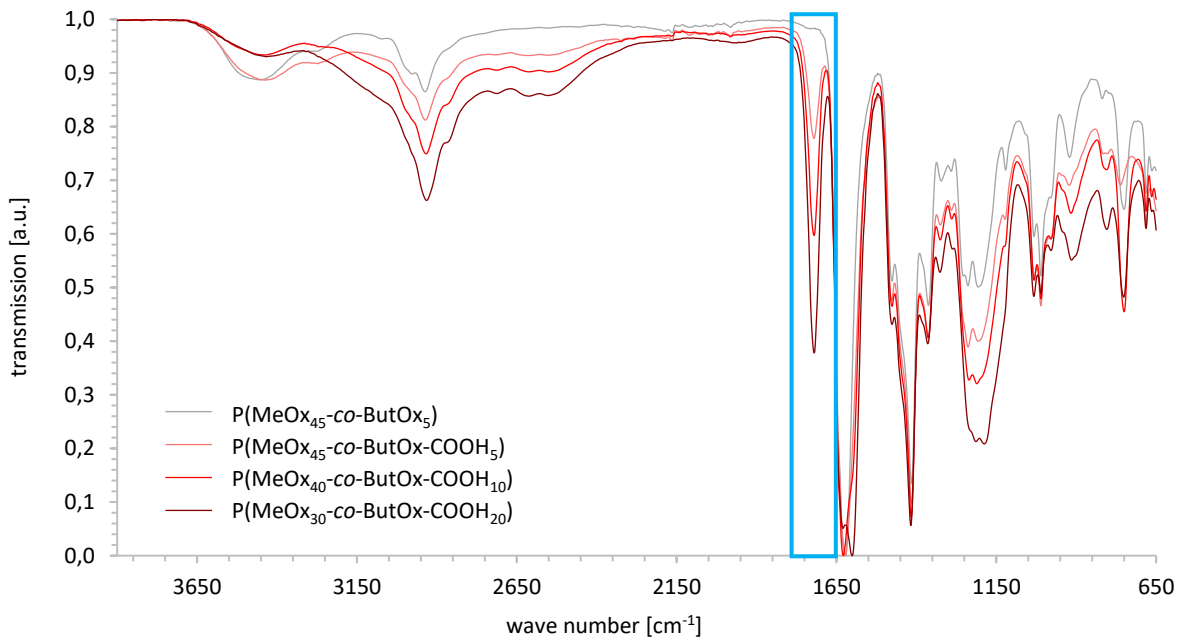

Figure 70: Superimposed IR spectra of 10 %, 20 % and 40 % carboxylic acid functionalized copolymers (light red: P(MeOx$_{45}$-*co*-ButOx-COOH$_5$), red: P(MeOx$_{40}$-*co*-ButOx-COOH$_{10}$), dark red: P(MeOx$_{30}$-*co*-ButOx-COOH$_{20}$)) as well as allyl functionalized precursor polymer P(MeOx$_{45}$-*co*-ButOx$_5$) (grey). The characteristic C=O stretching vibration of the carboxylic acid group at 1720 cm^{-1} is highlighted with a blue box. The strongest signal in each spectrum, the C=O stretching vibration of the polymer backbone, was taken as a reference.

Although no major changes in the molecular mass of the polymer are expected from functionalization, SEC measurements in DMF were performed on this stage of the reaction cascade as well. However, the strong interactions of the attached carboxylic acid groups with the column material lead to broad elution curves and therefore high dispersities as well as unexpectedly high molecular masses. This effect was already discussed thoroughly for telechelic polymers in chapter 4.2.1.1 and is significantly stronger for side chain functionalized polymers, since each polymer chain now bears multiple functional groups that can interact with column material. Therefore, SEC measurements are not unambiguous at this stage of the reaction cascade. The results from SEC measurements with various side chain carboxylic acid functionalized copolymers are listed in the experimental section in chapter 6.2.31.

Titration of Telechelic and Side Chain Carboxylic Acid Functionalized Polyoxazolines

As already mentioned earlier with telechelic functionalized polymers, the functionalization with carboxylic acid groups was verified by titration as an auxiliary analytical method. The measurement was performed with a pH electrode against a 0.01 M sodium hydroxide solution. **Figure 71** shows exemplary titration curves of telechelic and side chain carboxylic acid functionalized polyoxazolines.

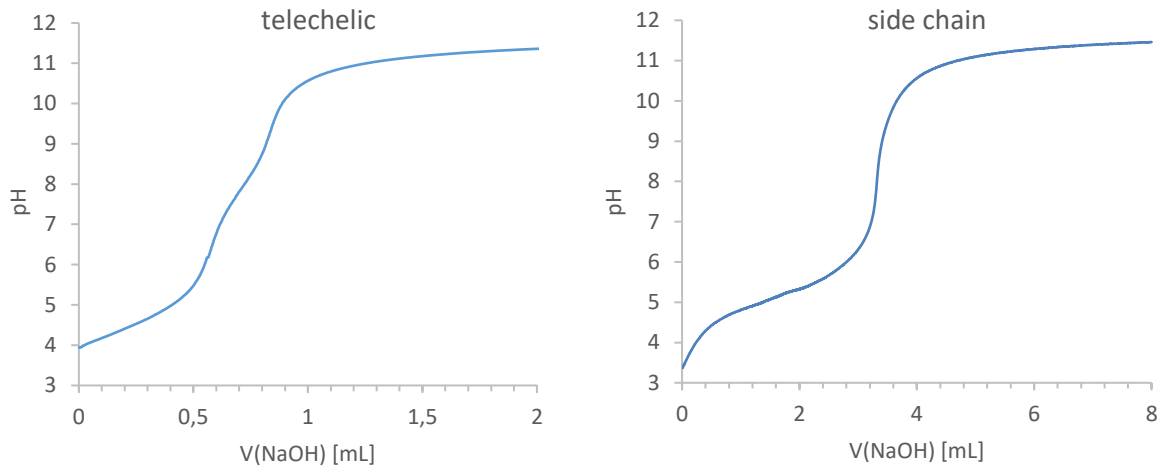

Figure 71: Titration curves of $PMeOx_{50}$-COOH (left) and $P(MeOx_{30}$-*co*-ButOx-$COOH_{20})$ (right) against 0.01 M NaOH solution.

In a work of Greß[615], side chain carboxylic acid functionalized polyoxazolines were titrated against 0.1 M NaOH. The curves and values of the equivalent points from literature are similar to the curves recorded in this work.

The titration gives information on the conversion rate of the thiol-ene reaction, provided that the correct molecular mass of the polymer is used for calculation. It indicates, how many of the polymer (side) chains were functionalized with carboxylic acid groups. In telechelic functionalized polyoxazolines, there is a maximum of one COOH group per polymer chain in case of complete conversion. For side chain functionalized copolymers, multiple COOH groups per polymer chain are introduced. In this work, carboxylic acid functionalized polymers with different chain lengths from 20 to 150 repeating units and functionalization rates of 10 % to 40 % were synthesized and analysed by titration.

However, several assumptions need to be made. The exact molecular mass of the polymer is needed for calculation and is usually determined from NMR and SEC. Although there is a slight deviation in the values depending on the method the molecular mass was determined from, both measuring techniques confirm that the desired molecular mass was achieved by the polymer synthesis (see chapter 4.2.1.2). Therefore, as an exact value, the theoretically expected molecular mass was used for calculations.

Also, depending on the strength of the acid, different measuring points can be used for calculation. For strong acids, the equivalence point (EP) is the same as the neutral point (NP) at a pH value of 7.[649] However, for weak acids or if the strength of the acid is unknown such as in this case, the EP can be derived from the point where the titration curve has its greatest gradient. It can be determined from complex calculation or graphic evaluation, whereby the latter method was used here.

Table 3 gives an overview over the experimental results. The functionalization rates are in good accordance with the theoretically expected values, especially for polymers up to 50 repeating units in size. With longer polymers, such as PMeOx$_{100}$-COOH and PMeOx$_{150}$-COOH, the number of COOH groups per chain is slightly lower than expected. This might be due to lower conversion rates in the thiol-ene reaction with long polymers.

Table 3: pH titration of carboxylic acid functionalized polymers against 0.01 M sodium hydroxide solution.

polymer	M_n theo. [g·mol^{-1}]	m [mg]	pH (EP)*	V (NaOH) [mL] **	№ COOH groups per chain (theo.)	№ COOH groups per chain (exp.)***
COOH-PMeOx$_{20}$ -SEt	1910	35.2	6.0	1.858	1	**1.01**
PMeOx$_{50}$-COOH	4433	24.6	6.2	0.554	1	**1.00**
		24.9	6.2	0.565		**1.01**
		24.7	6.2	0.567		**1.02**
PMeOx$_{100}$-COOH	8688	24.7	6.2	0.262	1	**0.92**
PMeOx$_{150}$-COOH ****	12943	25.3	6.2	1.487	1	**0.76**
P(MeOx$_{45}$-*co*-ButOx-COOH$_5$)	5086	24.6	7.0	1.977	5	**4.08**
P(MeOx$_{40}$-*co*-ButOx-COOH$_{10}$)	5817	25.0	7.5	4.534	10	**10.54**
P(MeOx$_{16}$-*co*-ButOx-COOH$_4$)	2386	12.6	7.0	2.235	4	**4.23**
P(MeOx$_{30}$-*co*-ButOx-COOH$_{20}$)	7279	12.7	8.2	3.335	20	**19.39**

*determined by graphic evaluation, **consumption to EP,
***calculated by NaOH consumption to EP, ****titration against 0.001 M NaOH.

It is noticeable, that the titration curves and the EP of side chain functionalized polymers resembles those of strong acids, whereas the titration curves of telechelic functionalized polymers with an EP around pH = 6.2 each resemble those of weak acids. This might be due to the fact that side chain functionalized polymers bear multiple COOH groups per polymer chain compared to telechelic polymers, where each molecule only bears one single COOH group.

The analytical results to side chain carboxylic acid functionalized polymers (NMR and titration) correspond well to findings for PButOx-COOH$_{21}$ and PButOx-COOH$_{26}$ polymers that have been described in literature[615].

Chapter 4.3.1.4 *Synthesis of Side Chain Thioester Functionalized Poly(2-Oxazoline)s*

The carboxylic acid group of side chain functionalized P(MeOx$_{45}$-*co*-ButOx-COOH$_5$) can be converted into a thioester functionality via thioesterification (see **scheme 35**), analogous to the reaction with telechelic functionalized polyoxazolines (see chapter 4.2.1.3). For this, P(MeOx$_{45}$-*co*-ButOx-COOH$_5$), together with *N*-methylmorpholine as a base, is dissolved in a mixture of chloroform and THF. After 90 min, isobutyl chloroformate as an activating agent for the carboxylic acid and thiophenol are added and the reaction is stirred overnight. In order to absorb water that is formed during the reaction, dry 4 Å molecular sieve is put into the reaction flask. The resulting thioester functionalized copolymer will be referred to as P(MeOx$_{45}$-*co*-ButOx-COSPh$_5$) and is obtained and purified via filtration and precipitation from cold diethyl ether.

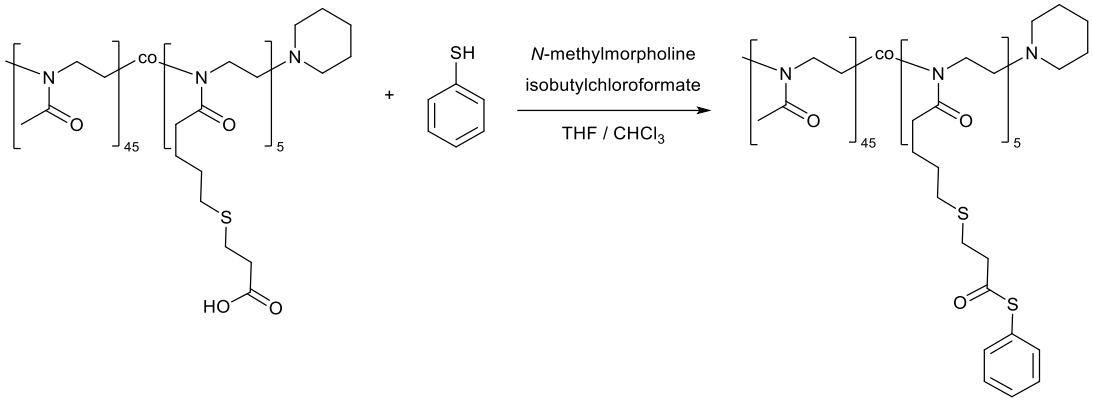

Scheme 35: Synthesis of side chain carboxylic acid functionalized P(MeOx$_{45}$-*co*-ButOx-COSPh$_5$).

The resulting polymer was analysed by ^{1}H-NMR spectroscopy (see **figure 72**). The most relevant signal can be found at 7.39 ppm and stems from the attached thiophenol. Interestingly, the aromatic ring does not yield multiple signals in the aromatic range as one would expect, but only one singlet signal with an integral of 20. This effect is already known, as it is also observed with telechelic functionalized polymers (see chapter 4.2.1.3) and in analogous reactions of peptides that were described in literature[225]. An integral of 20 (expected: 25) for this signal indicates that 80 % of the carboxylic acid groups were converted to thioester groups, which is in good accordance with conversions that were obtained in the low molecular model reaction.

The ^{1}H-NMR spectrum also exhibits three signals at 4.23-4.15, 3.98-3.94 and 2.91-2.89 ppm that do not belong to the copolymer, but stem from the isobutyl chloroformate by-product (bp) that was also observed and already extensively investigated with the telechelic functionalized polymer (see chapter 4.2.1.3). As it was described in the telechelic chapter, the by-product does not affect the NCL reaction, therefore the raw copolymer could be used in subsequent reactions without further purification.

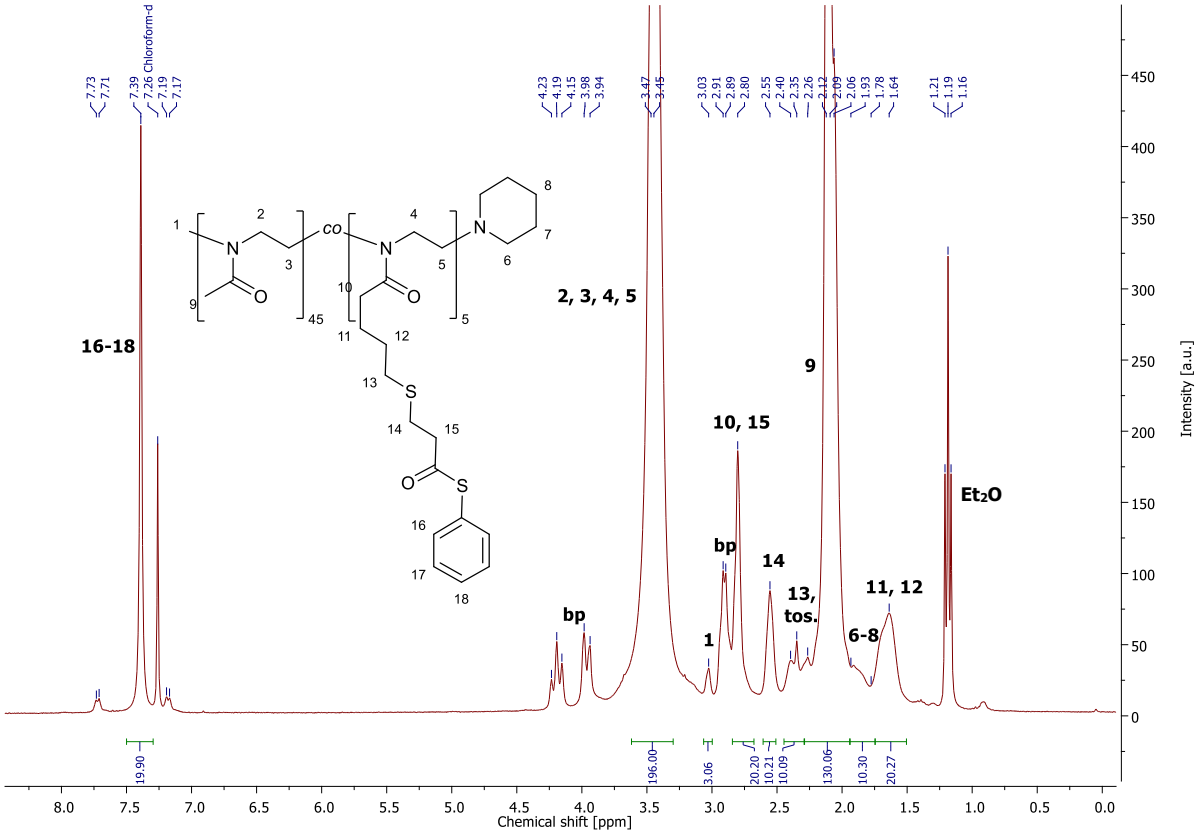

Figure 72: ^{1}H-NMR spectrum of side chain thioester functionalized P(MeOx$_{45}$-*co*-ButenOx-COSPh$_5$) in $CDCl_3$ with additional signals from an isobutyl chloroformate by-product (bp).

In analogy to the precursor carboxylic acid functionalized copolymer, the remaining signals can easily be assigned to the rest of the copolymer: Strongly present is the broad *backbone* signal at 3.47-3.45 ppm, which again was used as an internal reference. Also visible is the signal from the methyl initiator group at 3.03 ppm. The signals at 2.80, 2.55, 2.40-2.26 and 1.64 ppm stem from the alkyl side chain of the polymer, whereas the broad signal at 2.12-2.06 ppm stems from the methyl side chain. The piperidine end group yields a broad signal at 1.93-1.78 ppm. Further visible are tosylate counter ion and diethyl ether residue signals at 7.72, 7.18, 2.35 and 1.19 ppm.

Although no major changes in the molecular mass of the polymer are expected from functionalization, SEC measurements were performed on this stage of the reaction cascade as well. With M_n = 5367 g·mol^{-1}, M_w = 5577 g·mol^{-1} and a dispersity of $Đ$ = 1.04, the results correspond to the theoretically expected value of M_n = 5546 g·mol^{-1}. The elugram displays a symmetric curve (see **figure 73**).

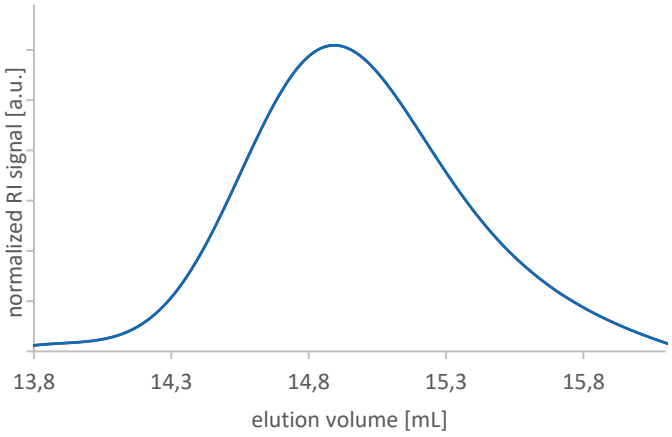

Figure 73: SEC elugram of side chain thioester functionalized P(MeOx$_{45}$-*co*-ButenOx-COSPh$_5$) in DMF.

Again, IR spectroscopy delivers information about this stage of the reaction cascade too. Just like the carboxylic acid group, the newly formed thioester group also delivers a characteristic signal in the IR spectrum (see **figure 74**). In comparison to the signal of the carboxylic acid group though, it is slightly shifted to 1703 cm^{-1} and comparably weaker.

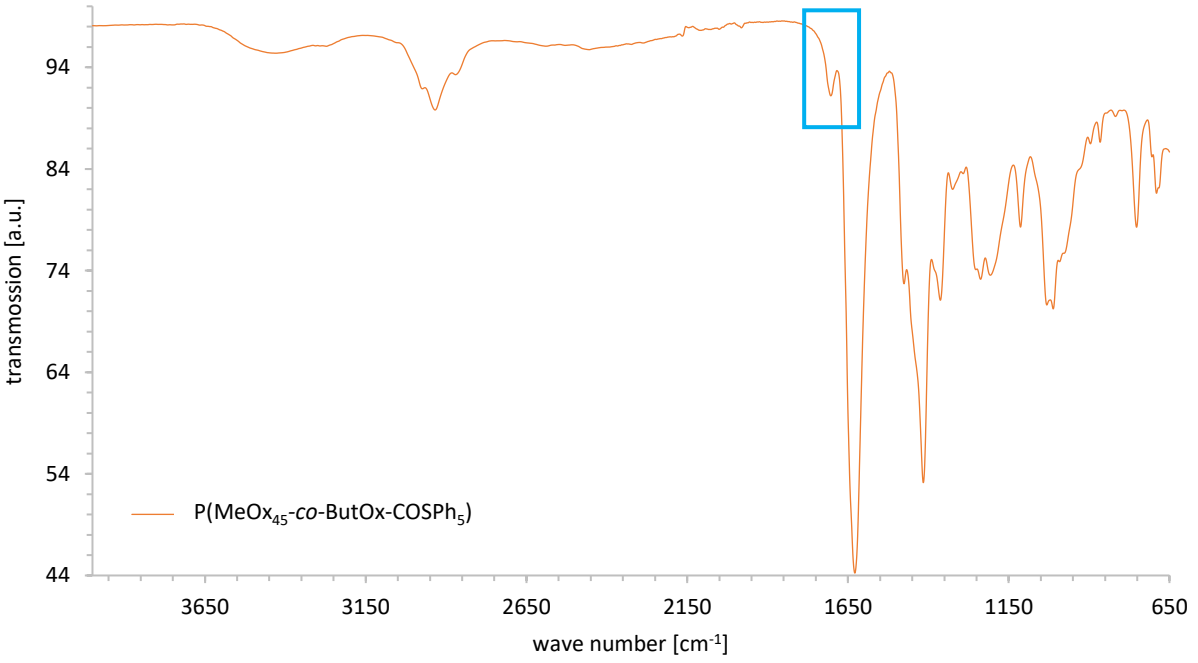

Figure 74: IR spectrum of thioester functionalized P(MeOx$_{45}$-*co*-ButenOx-COSPh$_5$) with characteristic C=O stretching vibration of the thioester group at 1703 cm^{-1} (highlighted with blue box).

Similarly to how it was described for the characteristic COOH signal (see **figure 70** in chapter 4.3.1.3), different intensities of this characteristic thioester signal are observed, depending relatively on the degree of functionalization. An IR spectrum with a comparison between side chain functionalized thioester polymers with different degree of functionalization can be found on page 249 in the appendix.

Figure 75 shows a comparison between IR spectra of telechelic thioester functionalized $PMeOx_{50}$-COSPh and side chain thioester functionalized polymer $P(MeOx_{45}$-*co*-ButenOx-$COSPh_5)$. Both the side chain functionalized polymer as well as the telechelic functionalized polymer display a signal at 1703 cm^{-1} that corresponds to the C=O stretching vibration of the thioester group. Since the ratio of functional groups per polymer chain is lower for telechelic polymers than for side chain functionalized polymers, the signal of telechelic polymers has a significantly diminished intensity. The analysis of side chain functionalized polymers, where multiple functional groups are responsible for a relative increase in intensity of characteristic signals, can therefore draw attention to signals that could have easily been underestimated in telechelic analytics.

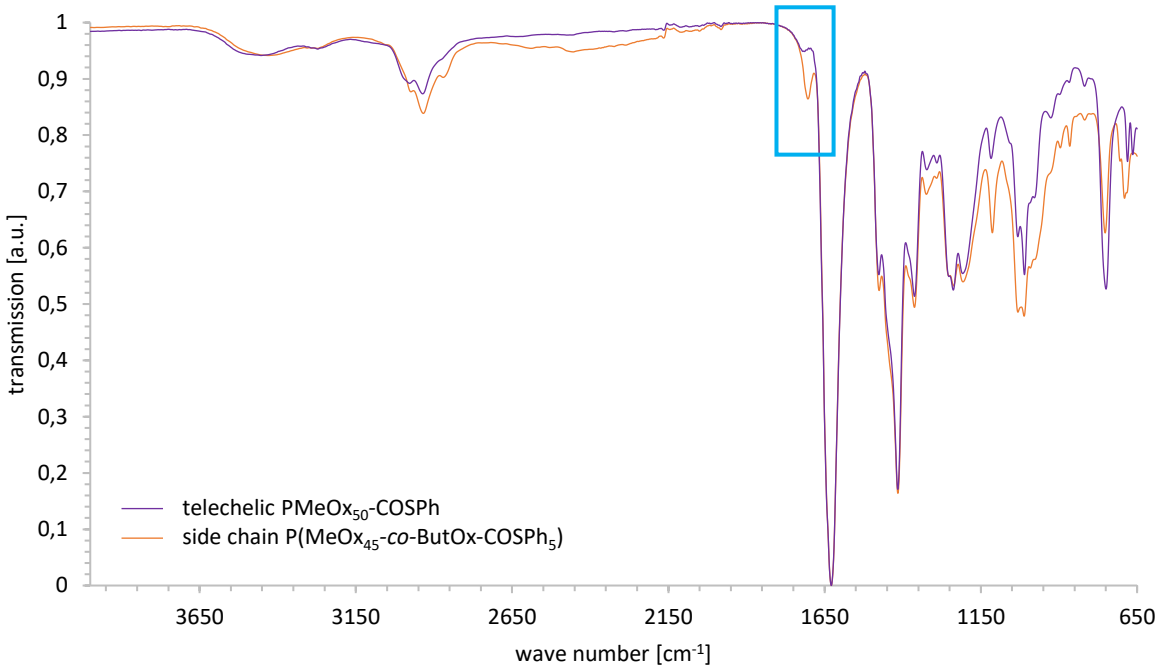

Figure 75: Superimposed IR spectra of telechelic thioester functionalized polymer $PMeOx_{50}$-COSPh (purple) and side chain thioester functionalized polymer $P(MeOx_{45}$-*co*-ButenOx-$COSPh_5)$ (orange) with characteristic C=O stretching vibration of the thioester group at 1703 cm^{-1} (highlighted with blue box). The intensity of the characteristic signal of the telechelic polymer is significantly lower than for the multiple side chain functionalized polymer.

Chapter 4.3.2 NCL

The resulting side chain thioester functionalized polymers from the preceding chapter were conjugated with three different peptides, CGGGF, CKFKFQF and CGGWYKYW (see **figure 34** on page 86 in chapter 4.2.2) in different degrees of functionalization. The subchapters are structured according to the respective peptide component used in the conjugation reaction.

Chapter 4.3.2.1 *NCL with Side Chain Functionalized Polymers and CGGGF*

Analogous to the reaction with telechelic functionalized polyoxazolines, side chain thioester functionalized polyoxazolines of various lengths and functionalization degrees were conjugated with the peptide CGGGF in a NCL (see **scheme 36**). In total, the reaction was performed 15 times with different derivates, yet similar outcomes for each experiment. Here, it will be described taking the example of P(MeOx$_{45}$-*co*-ButOx-COSPh$_5$) with 50 repetition units and a functionalization degree of 10 %. For the reaction, CGGGF was dissolved in methanol and sodium borohydride was added. P(MeOx$_{45}$-*co*-ButOx-COSPh$_5$) was added and the reaction was stirred for 24 h at room temperature. The resulting peptide functionalized polymer will be referred to as P(MeOx$_{45}$-*co*-ButOx-CGGGF$_5$) and was obtained and purified via precipitation from cold diethyl ether and dialysis against water (cut-off: 1000 g·mol^{-1}).

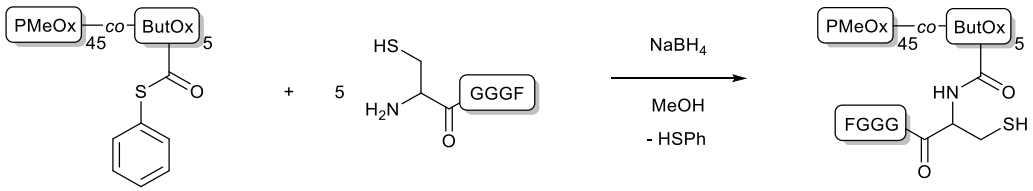

Scheme 36: Synthesis of side chain peptide functionalized P(MeOx$_{45}$-*co*-ButOx-CGGGF$_5$).

The reaction pathway is made visible in **figure 76** by comparing the educt and product ^{1}H-NMR spectra. The disappearance of the aromatic thioester signal at 7.30 ppm as well as the disappearance of the by-product signals at 4.19, 3.98 and 2.80 ppm can be clearly recognised. At the same time, characteristic signals from the peptide at 7.06, 4.48 and 3.80 ppm appear in the product spectrum.

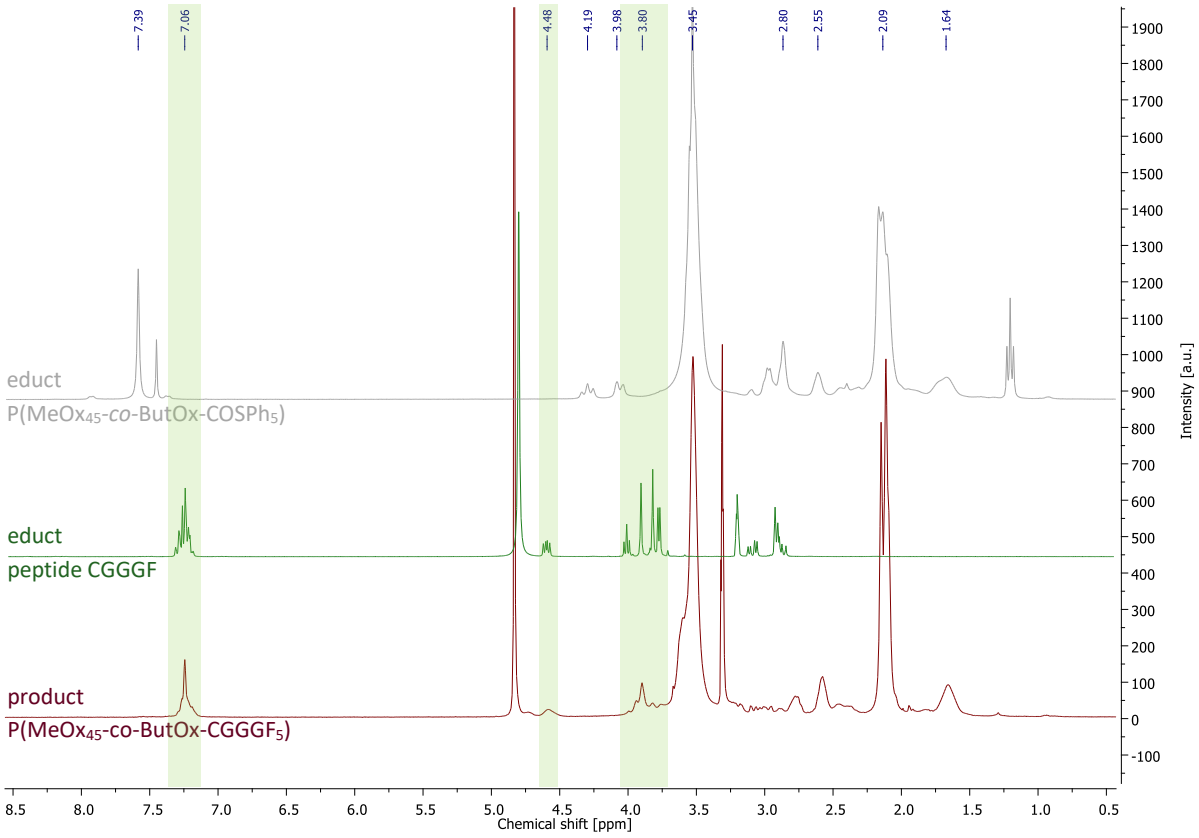

Figure 76: Stacked ^{1}H-NMR spectra of educt thioester functionalized P(MeOx$_{45}$-*co*-ButOx-COSPh$_5$) (grey, top) in $CDCl_3$, educt peptide CGGGF (green, middle) in MeOD and product peptide polymer conjugate P(MeOx$_{45}$-*co*-ButOx-CGGGF$_5$) (red, bottom) in MeOD with characteristic peptide signals highlighted in green.

Figure 77 shows the spectrum of the product in detail. The signal from the former thioester group at 7.30 ppm is no longer present, which is a first indicator for a successful reaction. The most relevant signal can be found at 7.24 ppm and stems from the aromatic ring of phenylalanine, which is one of the amino acids of the attached CGGGF peptide. The spectrum also exhibits a characteristic signal at 4.58 ppm that stems from the single phenylalanine proton right next to the carboxylic acid end group of the peptide. The integral values of these two characteristic peptide signals show that 4 of 5 binding sites for peptides have been conjugated with CGGGF, which corresponds to a conversion rate of 80 %. A more realistic notation of the conjugate would thus be P(MeOx$_{45}$-*co*-ButOx-**CGGGF$_4$**) instead of P(MeOx$_{45}$-*co*-ButOx-**CGGGF$_5$**). However, minor changes in conversion for each single experiment would require a different notation for otherwise analogous products. Therefore, for reasons of consistency, all conjugates will hereinafter be referred to with a notation that corresponds to the theoretically expected values of a complete conversion.

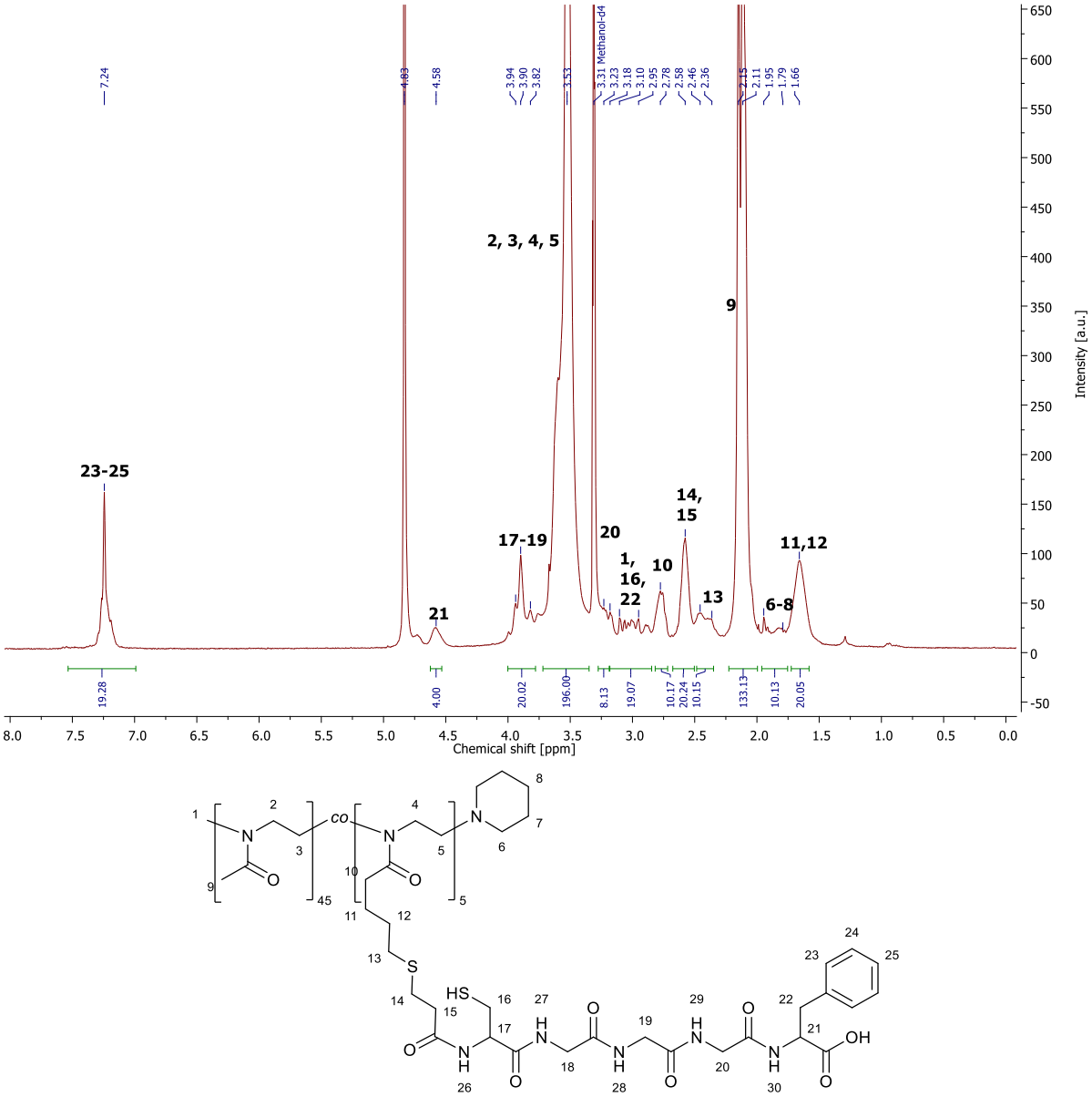

Figure 77: ^{1}H-NMR spectrum of side chain peptide functionalized P(MeOx$_{45}$-*co*-ButOx-CGGGF$_5$) in MeOD.

The remaining signals can either be assigned to the polymer or peptide part of the molecule. Strongly present is the broad *backbone* signal at 3.53 ppm which was again used as an internal reference and the broad signal at 2.15-2.11 ppm from the side chain methyl groups. Also visible are signals from the peptide backbone at 3.94-3.82 and 3.23-3.18 ppm, the methyl initiator group and the peptide side chain at 3.10-2.95 ppm, as well as the alkyl side chain of the polymer at 2.78, 2.58 and 2.46-2.36 ppm. Those signals can be identified by comparing both precursor spectra with the product spectrum (see **figure 76**). Diethyl ether residue signals and signals from the tosylate counter ion are not visible anymore, since those residues are removed by dialysis. The effectiveness of dialysis as a purification method is described in detail in chapter 4.2.4.

IR spectroscopy was performed in order to confirm the results from NMR spectroscopy. Compared to the educt polymer spectrum, a characteristic peptide signal from the N-H amide bond bending

vibration of the peptide is visible in the product spectrum after conjugation (see **figure 78**). This signal is present at 1531 cm^{-1} and is one of the strongest signals in the raw CGGGF peptide spectrum. While the mere educt P($MeOx_{45}$-*co*-ButOx-$COSPh_5$) polymer spectrum shows no signal at this position, the polymer-peptide conjugate P($MeOx_{45}$-*co*-ButOx-$CGGGF_5$) displays an apparent peak. Other works that utilized the same CGGGF peptide for conjugation with polyoxazoline polymers describe similar observations in IR spectroscopy.[601] Since the spectrum was taken after dialysis of the product, the findings affirm a qualitative conjugation of peptide to the polymer.

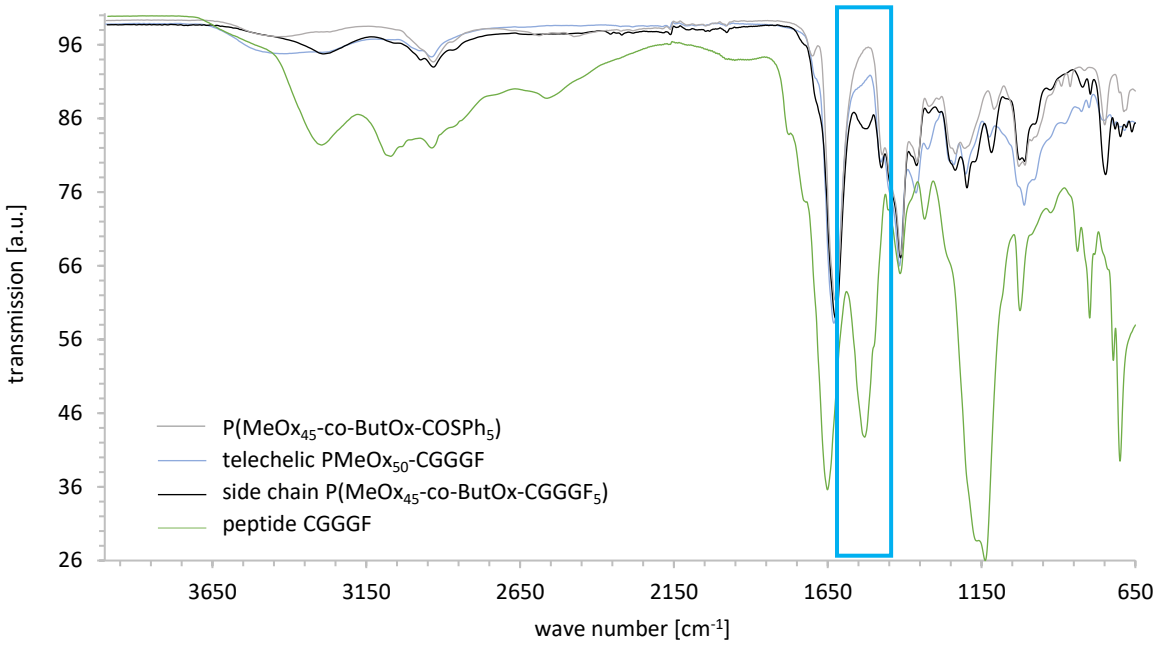

Figure 78: Superimposed IR spectra of educt polymer P($MeOx_{45}$-*co*-ButOx-$COSPh_5$) (grey), product polymer peptide conjugate P($MeOx_{45}$-*co*-ButOx-$CGGGF_5$) (black) and peptide CGGGF (green) with characteristic N-H amide bond bending vibration of CGGGF at 1531 cm^{-1} (highlighted with blue box). In the spectrum of the telechelic polymer peptide conjugate $PMeOx_{50}$-CGGGF (light blue), the same characteristic signal is significantly weaker and only appears as a shoulder.

The same characteristic peptide vibrational signal is also visible in the IR spectrum of telechelic conjugates with CGGGF. Of course, with telechelic conjugates, the intensity of the signal is much lower since there is only one instead of multiple conjugations. The signal therefore only appears as a shoulder.

For further investigation, three thioester functionalized copolymers with the same chain length of 50 repeating units, but a different degree of side chain functionalization were synthesized, conjugated with CGGGF and then analysed with IR spectroscopy. They will be referred to as P($MeOx_{45}$-*co*-ButOx-$CGGGF_5$) (10 % functionalization), P($MeOx_{40}$-*co*-ButOx-$CGGGF_{10}$) (20 %) and P($MeOx_{30}$-*co*-ButOx-$CGGGF_{20}$) (40 %). All copolymer conjugates display the characteristic peptide signal in the IR spectrum. It is remarkable that the intensity of this signal gets stronger with an increasing degree of functionalization (see **figure 79**). The rest of the signals that mainly stem from the polymer, display a comparable intensity. In case of a copolymer with 10 % peptide conjugation, the characteristic signal

is the weakest, whereas with 40 % conjugation, the signal is one of the strongest in the spectrum. The different intensities are an indication that the conversion rate of the NCL reaction is not impeded by a higher degree of functionalization and the findings give evidence that polymers with a high degree of functionalization are also conjugated with a congruently high number of peptide molecules.

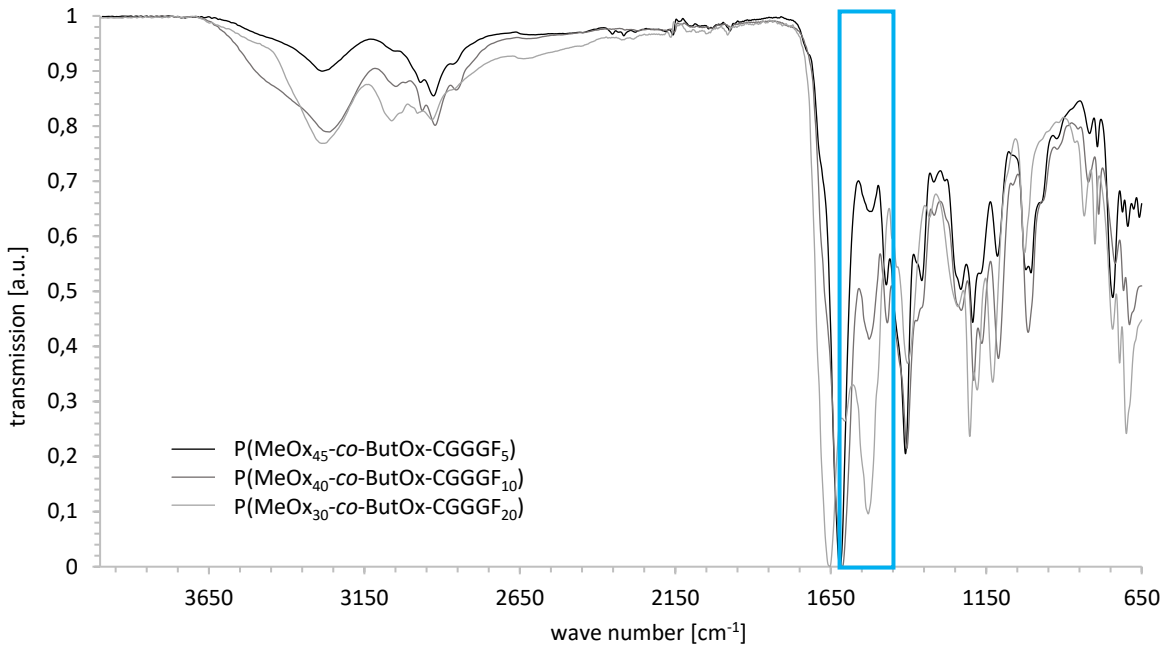

Figure 79: Superimposed IR spectra of copolymer conjugate P($MeOx_{45}$-*co*-ButOx-$CGGGF_5$) (black), P($MeOx_{40}$-*co*-ButOx-$CGGGF_{10}$) (grey) and P($MeOx_{30}$-*co*-ButOx-$CGGGF_{20}$) (light grey) with characteristic N-H amide bond bending vibration of the attached CGGGF at 1531 cm^{-1} (highlighted with blue box). The strongest signal in each spectrum, the C=O stretching vibration of the polymer backbone, was taken as a reference.

Material properties, such as the solubility of the conjugates vary drastically depending on the degree of functionalization. While conjugates with 10 % functionalization are fully soluble in methanol, water and dimethyl sulfoxide, conjugates with a functionalization degree of 20 % are only soluble in methanol and water to a certain extent and 40 % functionalized conjugates are exclusively soluble in dimethyl sulfoxide. It is conceivable that oxidation of the free thiol groups leads to intermolecular disulfide bridges, which in term would be responsible for a network formation and therefore also a decrease in solubility. However, the addition of TCEP as a reducing agent has only little influence on the material properties and thus it is assumed that other factors like entanglement of the polymer chains based on the brush-like polymer architecture, size of the macromolecules and non-covalent (peptide) interactions are mainly responsible for the differences in solubility.

SEC measurements were performed for all peptide polymer conjugates in water as well as in DMF as solvent but did not yield any reliable results due to either insolubilities of the conjugates in the SEC solvents or otherwise very strong interactions with column material. Reasons for this behaviour were already extensively discussed in chapter 4.2.1.1.

Although CGGGF as a model peptide exhibits good solubility properties – even in a conjugate with both telechelic and side chain functionalized polymers, with only one phenylalanine amino acid in the chain it offers only few characteristic side chain group functionalities that allow easy identification in both NMR and IR spectroscopy. Therefore, similar to how it was described in the telechelic chapter, CKFKFQF as a model peptide with multiple phenylalanine groups was used for further investigations.

Chapter 4.3.2.2 *NCL with Side Chain Functionalized Polymers and CKFKFQF*

For the NCL of peptide CKFKFQF with side chain thioester functionalized P(MeOx$_{45}$-*co*-ButOx-COSPh$_5$) (see **scheme 37**), the peptide is dissolved in DMSO and sodium borohydride is added. A solution of P(MeOx$_{45}$-*co*-ButOx-COSPh$_5$) in DMSO is added and the reaction mixture is stirred for 24 h at room temperature. The reaction was performed in analogy to the NCL with peptide CGGGF (see chapter 4.3.2.1), except DMSO was used as a solvent instead of MeOH. The resulting peptide functionalized polymer will be referred to as P(MeOx$_{45}$-*co*-ButOx-CKFKFQF$_5$) and was obtained and purified via dialysis against water (cut-off: 1000 g·mol^{-1}).

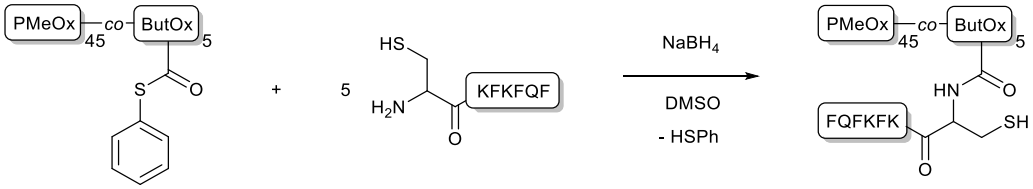

Scheme 37: Synthesis of side chain peptide functionalized P(MeOx$_{45}$-*co*-ButOx-CKFKFQF$_5$).

The resulting conjugate was analysed by ^{1}H-NMR spectroscopy (see **figure 80**). Because of the poor solubility of the conjugate, the spectrum was taken in deuterated DMSO. It displays similar results compared to the telechelic functionalized polymer (see chapter 4.2.2.2). The signal from the former thioester group at 7.39 ppm is no longer present, which is a first indicator for a successful reaction. Yet the most relevant signal can be found at 7.20 ppm. It stems from the aromatic rings of the three phenylalanine units of the attached peptide.

The remaining signals can either be assigned to the polymer or peptide part of the molecule. Strongly present is the broad polymer *backbone* signal at 3.35 ppm and the broad signal at 2.01-1.97 ppm from the side chain methyl groups. The latter one was used as internal reference, as the first one is overlaid by the DMSO solvent signal. Also visible are signals from the peptide backbone at 5.07-4.20 ppm. However, the integral values of those signals are higher than expected, since they are overlaid with signals from NH groups, which are also visible in DMSO spectra and deliver broad signals with only partial integral values. Further visible are signals from the methyl initiator group, polymer side chain and peptide side chain units. Those signals all overlap each other, which does not allow for specific assignment of each proton, therefore those signals are listed in clusters. Signals that were not present

in the educt polymer spectrum but are now clearly visible at 1.61-1.05 ppm stem from the lysine alkyl chains, but, similar to the spectrum of the telechelic conjugate, are overlaid by an artefact signal from labile carboxylic acid or thiol group protons, which occurs after dialysis. Diethyl ether residue signals and signals from the tosylate counter ion are not visible anymore, since those residues are removed by dialysis. The effectiveness of dialysis as a purification method is described in detail in chapter 4.2.4.

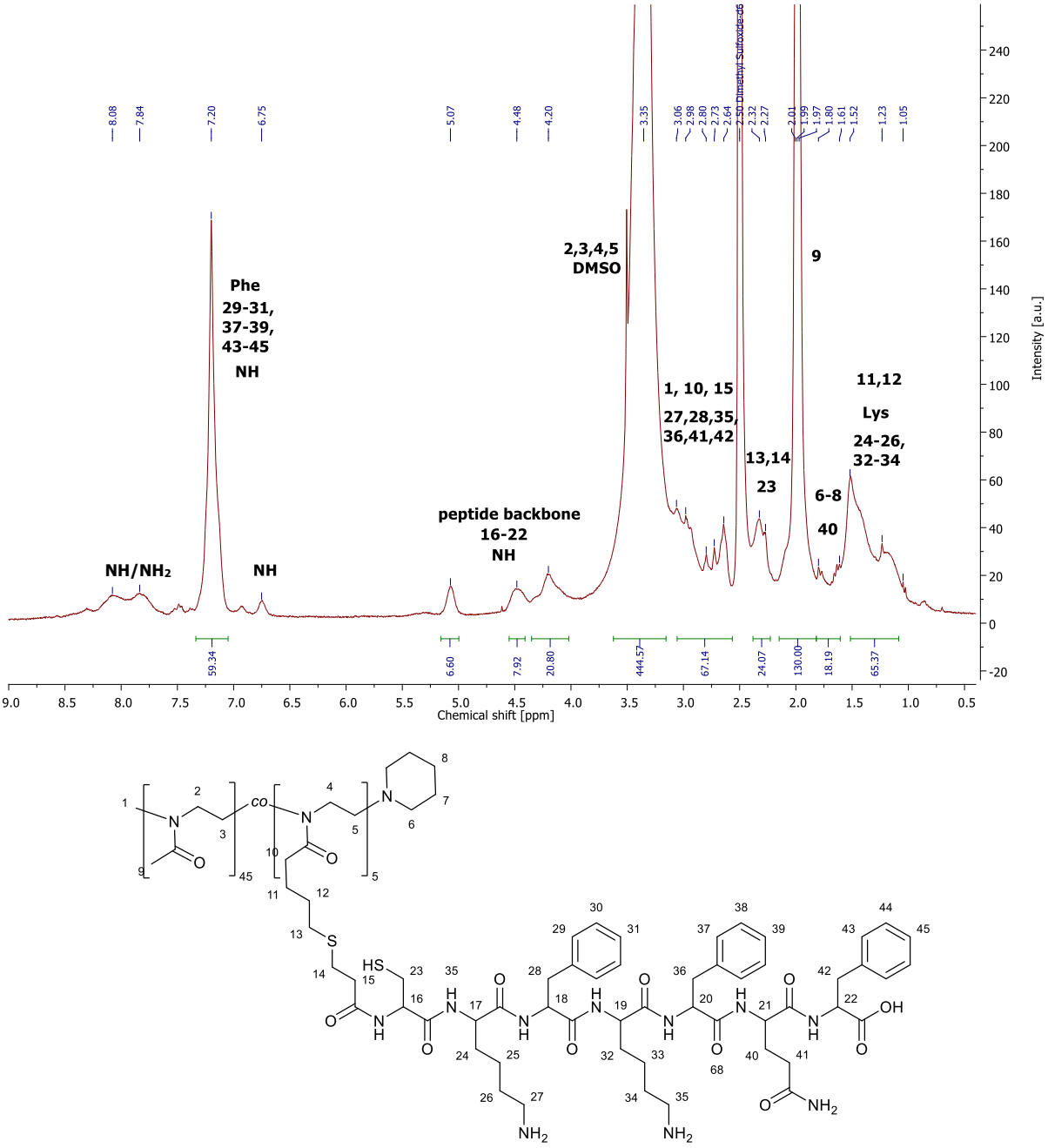

Figure 80: ^{1}H-NMR spectrum of side chain peptide functionalized P(MeOx$_{45}$-*co*-ButOx-CKFKFQF$_5$) in deuterated DMSO.

Although most of the polymer and peptide signals overlap each other, the total integral values of the combined signals can be used to calculate the amount of peptide that has been attached to the polymer. It shows that 4 of 5 binding sites for peptides have been conjugated with CKFKFQF, which is in good accordance with the rate that was also described for the short peptide CGGGF.

IR spectroscopy was performed in order to confirm the results from NMR spectroscopy. Compared to the educt polymer spectrum, the thioester C=O stretching vibration that was identified in chapter 4.3.1.4 is not present anymore and a characteristic signal from N-H amide bond bending vibration of the peptide is visible in the product spectrum at 1547 cm^{-1} after conjugation (see **figure 81**). While the mere educt P($MeOx_{45}$-*co*-ButOx-$COSPh_5$) polymer spectrum shows no signal at this position, the polymer-peptide conjugate P($MeOx_{45}$-*co*-ButOx-$CGGGF_5$) displays an apparent peak. The same characteristic signal was also observed with the telechelic conjugation of CKFKFQF to a polymer (see chapter 4.2.2.2). Since the spectrum was taken after dialysis of the product, the findings affirm a qualitative conjugation of peptide to the polymer.

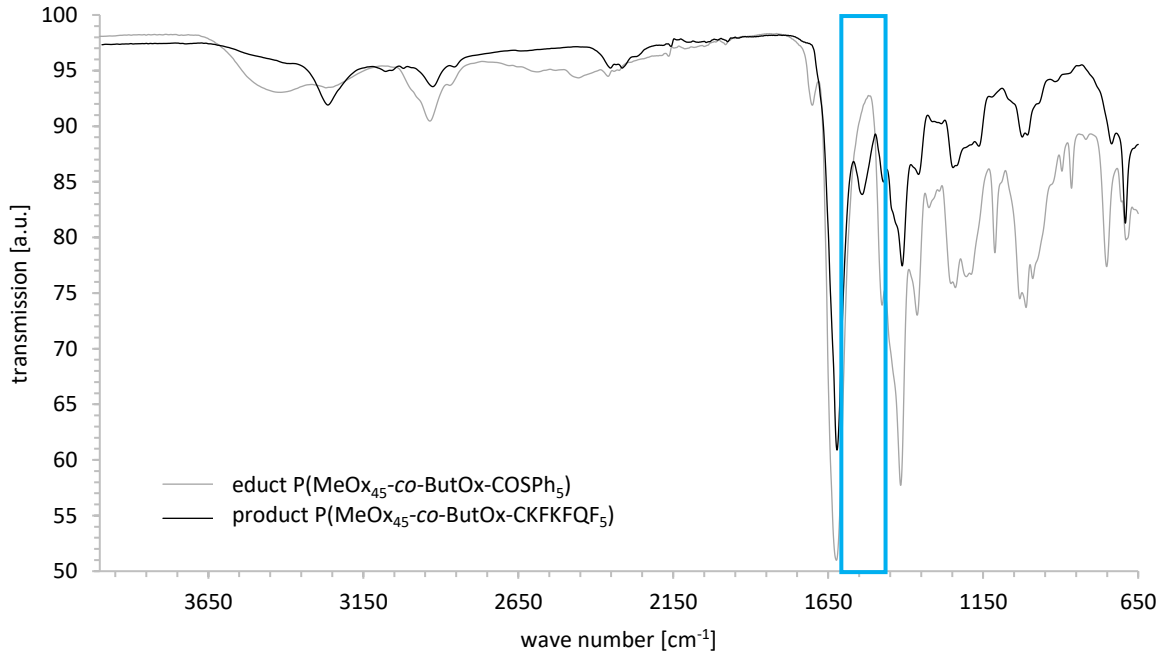

Figure 81: Superimposed IR spectra of educt polymer P($MeOx_{45}$-*co*-ButOx-$COSPh_5$) (grey) and product polymer peptide conjugate P($MeOx_{45}$-*co*-ButOx-$CKFKFQF_5$) (black) with characteristic N-H amide bond bending vibration of the attached CKFKFQF at 1547 cm^{-1} (highlighted with blue box).

Chapter 4.3.2.3 *NCL with Side Chain Functionalized Polymers and CGGWYKYW*

For the NCL of peptide CGGWYKYW with side chain thioester functionalized P($MeOx_{45}$-*co*-ButOx-$COSPh_5$) (see **scheme 38**), the peptide is dissolved in water and acetic acid is added to increase solubility. P($MeOx_{45}$-*co*-ButOx-$COSPh_5$) is dissolved separately and when it is added to the peptide solution, an immediate slight gel formation can be observed. This is already an indication for reaction, but to ensure complete conversion, more acetic acid is added and the reaction mixture is heated to 60 °C in order to dissolve the gel and prevent further precipitation. The reaction mixture is then stirred for 24 h at 60 °C. Purification via dialysis against water (cut-off: 1000 $g \cdot mol^{-1}$) was also performed at a

higher temperature of 60 °C and the resulting peptide functionalized polymer will be referred to as P(MeOx$_{45}$-*co*-ButOx-CGGWYKYW$_5$).

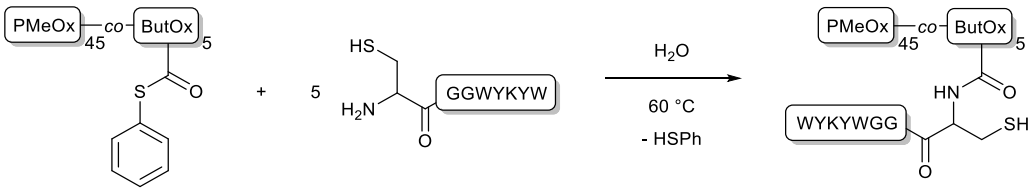

Scheme 38: Synthesis of side chain peptide functionalized P(MeOx$_{45}$-*co*-ButOx-CGGWYKYW$_5$).

The resulting polymer peptide conjugate showed similar material properties as the employed CGGWYKYW peptide. Like the pure peptide, the conjugate also forms thermoresponsive gels in methanol and water in high concentrations. It is remarkably, that the material properties of the sole peptide were therefore transferred to the polymer conjugate.

The product was analysed by ^{1}H-NMR spectroscopy (see **figure 82**). Because of the poor solubility of the conjugate, the spectrum was taken in deuterated DMSO. It displays similar results compared to the telechelic functionalized polymer (see chapter 4.2.2.3). In the NMR spectrum, some individual signals such as the tryptophan indole NH at 10.72 ppm, the aromatic ring signals of tyrosine and tryptophan at 7.56-6.56 ppm from the peptide part of the conjugate or the methyl side chain group at 2.01-1.91 ppm from the polymer part of the conjugate can be identified. Those signals are suitable for referencing. Concerning the rest of the signals, with so many protons contributing to the final spectrum and superimposing each other, it is not feasible to assign each signal individually. For those signals, the spectrum can be subdivided into different regions exactly like it was done for the educt peptide spectrum (see **figure 39**).

There is the 'NH and NH_2 region' and 'aromatic region' between 10.74 and 6.56 ppm, where signals from the amino groups of the conjugate as well as the aromatic rings of tyrosine and tryptophan can be found. The CH groups from each nodal point of the attached peptide are visible in the 'peptide backbone region' between 4.56 and 3.59 ppm. More specifically, the signals from the cysteine and glycine units can be found between 3.70 and 3.59 ppm, but are partly overlaid by the broad polymer *backbone* signal at 3.32 ppm, which in turn contains the DMSO water residue signal. Next, there is a 'side chain alkyl region' between 3.07 and 2.26 ppm, where signals from alkylic CH_2 groups of the amino acid residues and polymer side chain as well as the initiator group of the polymer are present. At 2.01-1.97 ppm, the methyl side chain groups of the polymer deliver a broad signal which was used as internal reference and at 1.91-1.84 ppm, the piperidine end group signal is present. Finally, there is a 'lysine region' between 1.51 and 0.87 ppm, where signals from the lysine and polymer side chain CH_2 groups can be found. At this stage of the reaction cascade, due to the size of the macromolecular conjugates, integration of single signals was not possible anymore, but the total integral values of each region match the expected number of protons of each part of the conjugate.

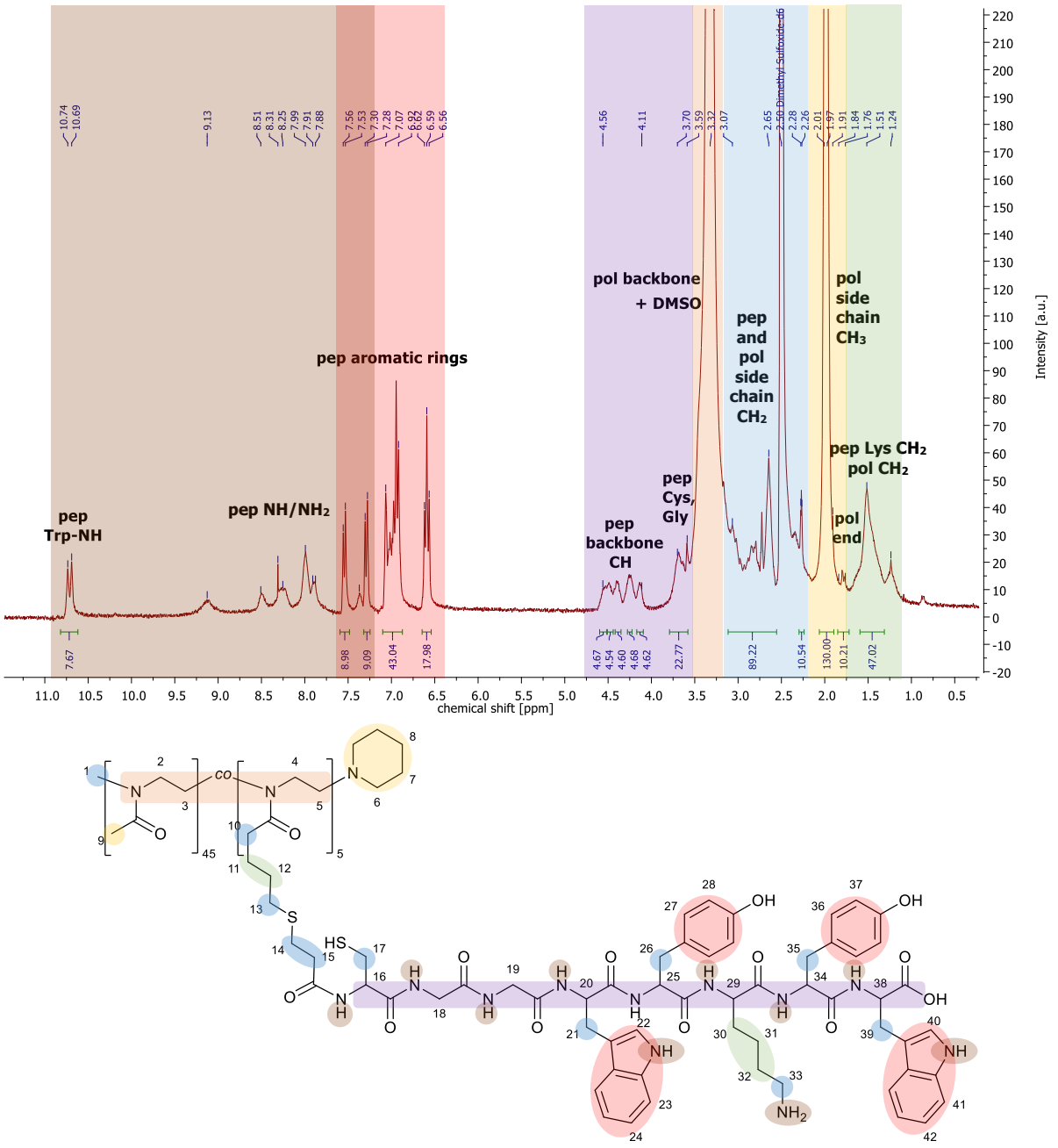

Figure 82: ^{1}H-NMR spectrum of side chain peptide functionalized P(MeOx$_{45}$-*co*-ButOx-CGGWYKYW$_5$) in deuterated DMSO with "pep" for signals that belong to the peptide part of the conjugate and "pol" for signals that belong to the polymer part. The spectrum is subdivided into different regions: 'NH and NH$_2$ region' (brown), 'aromatic region' (red), 'peptide backbone region' (purple), polymer backbone (orange), 'side chain alkyl region' (blue)), 'polymer region' (yellow) and 'lysine region' (green).

IR spectroscopy was performed in order to confirm the results from NMR spectroscopy. Compared to the educt polymer spectrum, a characteristic signal from the N-H amide bond bending vibration of the peptide is visible in the product spectrum after conjugation (see **figure 83**). This signal is present at 1514 cm^{-1} and is one of the strongest signals in the raw CGGWYKYW peptide spectrum. While the mere educt polymer spectrum of P(MeOx$_{45}$-*co*-ButOx-COSPh$_5$) shows no signal at this position, the polymer-peptide conjugate P(MeOx$_{45}$-*co*-ButOx-CGGWYKYW$_5$) displays an apparent peak. Since the spectrum

was taken after dialysis of the product, the findings affirm a qualitative conjugation of peptide to the polymer.

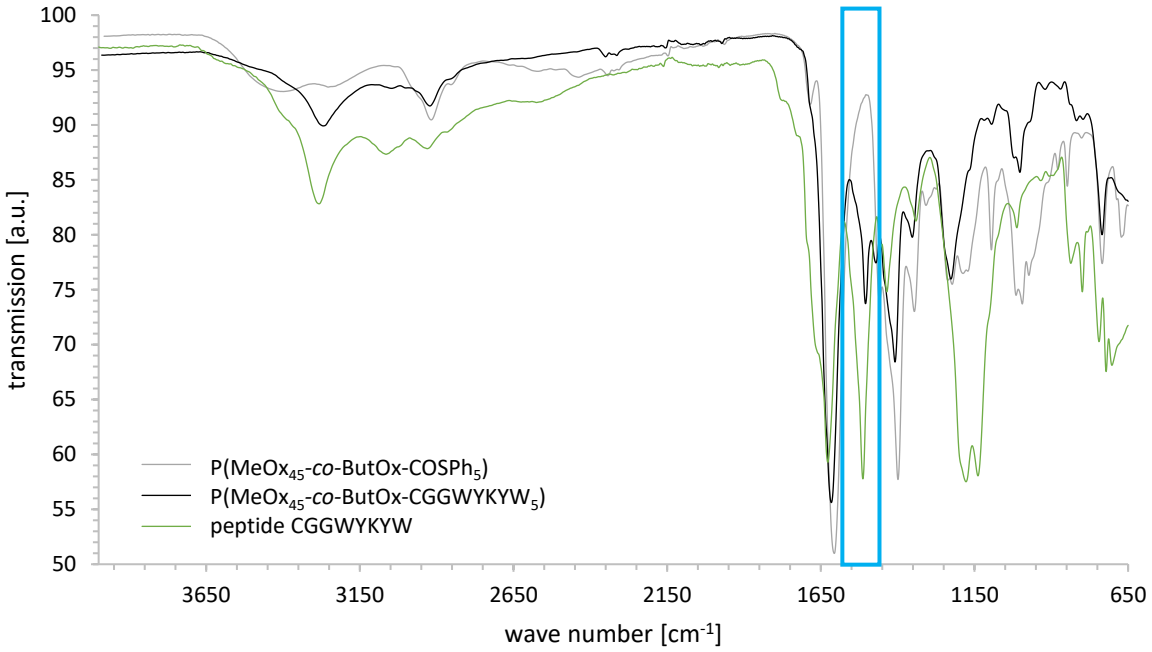

Figure 83: Superimposed IR spectra of educt polymer P(MeOx$_{45}$-*co*-ButOx-COSPh$_5$) (grey), product polymer peptide conjugate P(MeOx$_{45}$-*co*-ButOx-CGGWYKYW$_5$) (black) and peptide CGGWYKYW (green) with characteristic N-H amide bond bending vibration of CGGWYKYW at 1514 cm^{-1} (highlighted with blue box).

The same characteristic peptide vibrational signal is also visible in the IR spectrum of telechelic conjugates with CGGWYKYW (see chapter 4.2.2.3). Of course, with telechelic conjugates, the intensity of the signal is comparably lower since there is only one instead of multiple conjugations.

Chapter 4.3.3 Thiol-Ene

In chapter 4.2.3.2, the thiol-ene reaction between *telechelic* polymer peptide conjugates and an additional sugar moiety was displayed, covering the conjugates shown in the left column of **table 4**. Hereinafter, the transfer of the reaction to *side chain* functionalized conjugates, which are shown in the right column of **table 4**, will be discussed. The observations will be explained using the examples of the two highlighted conjugates that both have the same chain length of 50 repeating units and a functionalization degree of 10 %, but bear different peptide moieties. According to the respective peptide moiety, the first part of this chapter covers the thiol-ene reactions with CGGGF-functionalized conjugates and in the second part then depicts the thiol-ene reactions of CGGWYKYW-functionalized conjugates. In all reactions, the same sugar moiety, acetylated allyl mannose (AcMan), was used as a reaction partner.

Table 4: Overview of different polymer peptide sugar conjugates.

peptide moiety of the conjugate	telechelic functionalized conjugates	side chain functionalized conjugates (degree of funct., chain length)
CGGGF	PMeOx$_{50}$-CGGGF-AcMan Man-CGGGF-PMeOx$_{20}$-SEt	**P(MeOx$_{45}$-*co*-ButOx-CGGGF$_5$-AcMan$_5$) (10 %, 50)** P(MeOx$_{40}$-*co*-ButOx-CGGGF$_{10}$-AcMan$_{10}$) (20 %, 50) P(MeOx$_{30}$-*co*-ButOx-CGGGF$_{20}$-AcMan$_{20}$) (40 %, 50) P(MeOx$_{16}$-*co*-ButOx-CGGGF$_4$-AcMan$_4$) (20 %, 20)
CGGWYKYW	PMeOx$_{50}$-CGGWYKYW-AcMan AcMan-CGGWYKYW-PMeOx$_{20}$-SEt Man-CGGWYKYK-PMeOx$_{20}$-SEt	**P(MeOx$_{45}$-*co*-ButOx-CGGWYKYW$_5$-AcMan$_5$) (10 %, 50)** P(MeOx$_{16}$-*co*-ButOx-CGGWYKYW$_4$-AcMan$_4$) (20 %, 20)

Synthesis of the conjugates was always similar, oriented at the foregoing thiol-ene reactions. All reactions were, if not stated otherwise, performed under reductive conditions to ensure that the thiol group needed for the reaction is constantly and readily available for the reaction.

Chapter 4.3.3.1 *Thiol-Ene Reaction with CGGGF Polymer Conjugates*

In analogy to the thiol-ene reaction with telechelic conjugates (see chapter 4.2.3.2), the reaction was performed with side chain P(MeOx$_{45}$-*co*-ButOx-CGGGF$_5$) peptide conjugate (see **scheme 39**) under similar reaction conditions. Both educts were dissolved in water under the presence of TCEP to guarantee reductive conditions. Irgacure 2959 was added as initiator and the reaction mixture was stirred for 60 min under UV light irradiation. The resulting peptide and sugar functionalized polymer was purified via dialysis against water and will be referred to as P(MeOx$_{45}$-*co*-ButOx-CGGGF$_5$-AcMan$_5$).

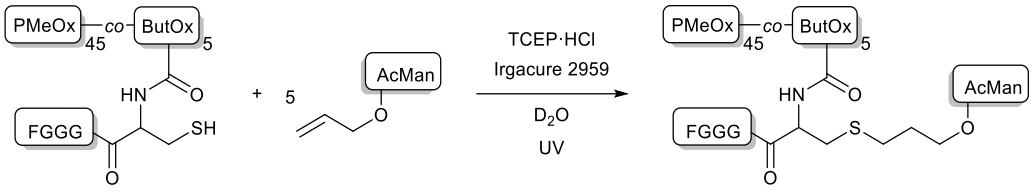

Scheme 39: Synthesis of side chain peptide and sugar functionalized P(MeOx$_{45}$-*co*-ButOx-CGGGF$_5$-AcMan$_5$).

The conjugate was analysed by ^{1}H-NMR spectroscopy (see **figure 84**).

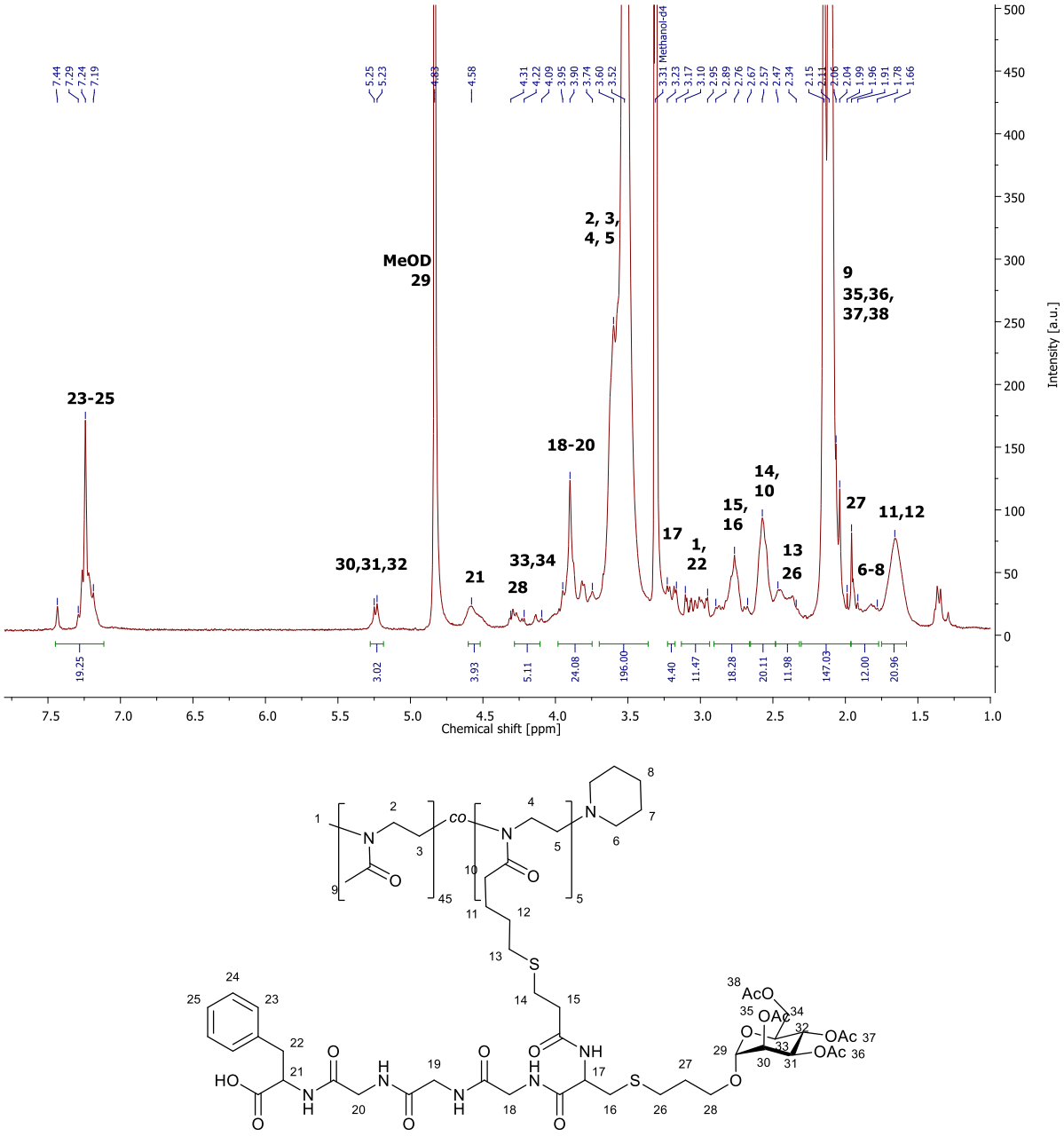

Figure 84: ^{1}H-NMR spectrum of side chain peptide and sugar functionalized P(MeOx$_{45}$-*co*-ButOx-CGGGF$_5$-AcMan$_5$) in MeOD.

In comparison to the telechelic conjugate, analogous signals appear in the spectrum: There is the characteristic peptide signal from the phenylalanine ring at 7.44-1.19 ppm. Further peptide signals appear at 4.58, 3.95-3.74, 3.23-3.17 and 2.89-2.67 ppm (the latter one being overlaid by polymer

signals) from the peptide backbone CH_2 groups and at 3.10-2.95 ppm for the peptide side chain CH_2 residue group.

The signal from three protons of the mannose ring at 5.25-5.23 ppm appears at the exact same position as the same group signal in the telechelic conjugate, with no allyl signals being present for the former allyl group of the acetylated allyl mannose educt. Other signals of the attached sugar ring are present at 4.22-4.09 ppm. An additional signal would be found at 4.83 ppm, but it is mostly overlaid by the MeOD / D_2O solvent signal. The alkyl chain that connects the sugar to the polymer backbone delivers a distinct signal at 4.31-4.22 ppm. The two other CH_2 groups at 2.47-2.34 and 1.99-1.91 ppm are overlaid by polymer signals, which is also the case for the acetyl group signals that appear together with the broad CH_3 side chain signal of the polymer at 2.15-2.06 ppm.

Further signals that are present are the broad polymer *backbone* signal at 3.60-3.52 ppm, that was used as internal reference, the initiator methyl group signal at 3.10-2.95 ppm, which is overlaid by peptide signals, as well as the polymer side chain CH_2 group signals at 2.89-2.67, 2.57, 2.47-2.34 and 1.66 ppm, which are also partly overlaid by peptide and sugar signals. The piperidine end group is visible with signals at 1.91-1.78 ppm.

Integration of the different signals reveals that of five possible conjugations with each the peptide and sugar, the peptide is attached four times, as already discussed in chapter 4.3.2.1 and mannose is attached only once per conjugate. As discussed earlier, this can be due to increasing steric or solvational factors of multiple side chain functionalized polymers that might limit conversion rates in the thiol-ene reaction.[602-605]

IR spectroscopy was performed as a supplementary analytic method. Compared to the educt polymer spectrum, a characteristic signal from the C=O stretching vibration of the sugar is visible in the product spectrum after conjugation (see **figure 85**). This signal is present at 1743 cm^{-1} and is one of the strongest signals in the raw acetylated allyl mannose spectrum. While the mere educt polymer spectrum of P($MeOx_{45}$-*co*-ButOx-$CGGGF_5$) shows no signal at this position, the polymer-peptide conjugate P($MeOx_{45}$-*co*-ButOx-$CGGGF_5$-$AcMan_5$) displays an apparent peak. Since the spectrum was taken after dialysis of the product, the findings affirm a qualitative conjugation of sugar to the conjugate.

The same characteristic vibrational signal is also visible in the IR spectrum of telechelic conjugates (see **figure 86, left**) . However, the intensity of the signal is much lower since there is only one instead of multiple conjugation sites and can, in some cases, only appear as a shoulder.

For further investigation, three copolymers with the same chain length of 50 repeating units, but a different degree of side chain functionalization that have already been conjugated with peptide and are described in detail in chapter 4.3.2.1 were now also conjugated with acetylated allyl mannose and

then analysed with IR spectroscopy (see **figure 86, right**). They will be referred to as P(MeOx$_{45}$-*co*-ButOx-CGGGF$_5$-AcMan$_5$) (10 % functionalization), P(MeOx$_{40}$-*co*-ButOx-CGGGF$_{10}$-AcMan$_{10}$) (20 %) and P(MeOx$_{30}$-*co*-ButOx-CGGGF$_{20}$-AcMan$_{20}$) (40 %). Those conjugates display the same characteristic sugar signal in the IR spectrum as well and it is noteworthy that the intensity of this signal increases with a higher degree of functionalization. The characteristic signal from the conjugated peptide at 1531 cm^{-1}, whose intensity varies with degree of functionalization, too, is also present in **figure 86, right**.

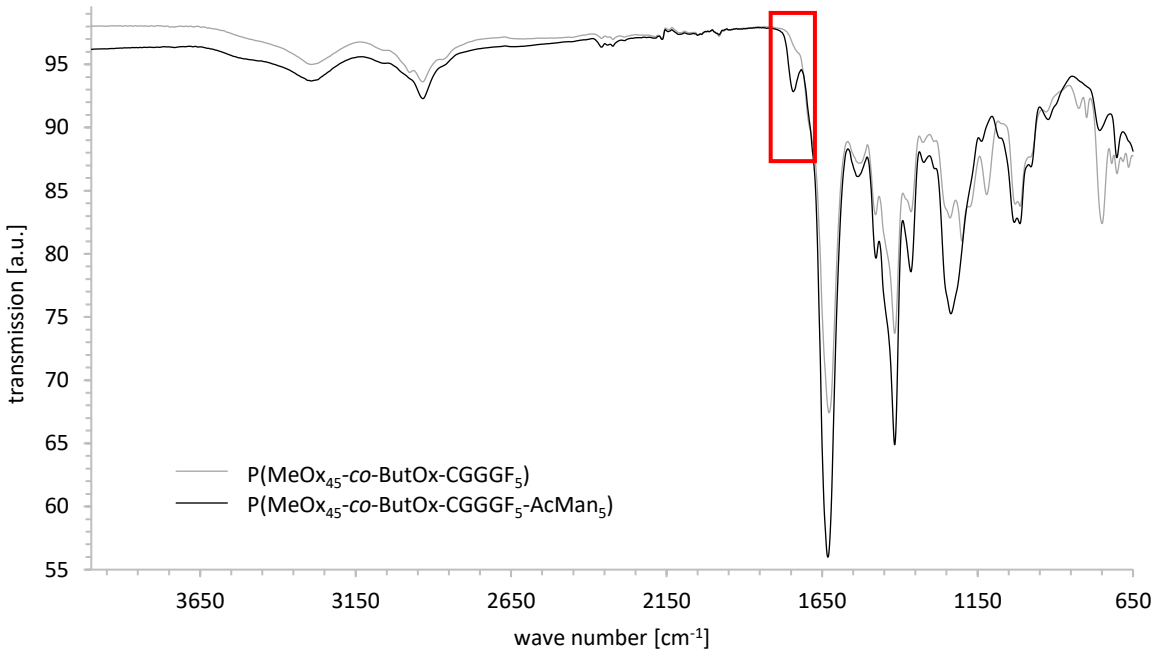

Figure 85: Superimposed IR spectra of educt polymer-peptide conjugate P(MeOx$_{45}$-*co*-ButOx-CGGGF$_5$) (grey), product polymer-peptide-sugar conjugate P(MeOx$_{45}$-*co*-ButOx-CGGGF$_5$-AcMan$_5$) (black) with characteristic C=O stretching vibration of the sugar acetyl groups at 1743 cm^{-1} (highlighted with red box).

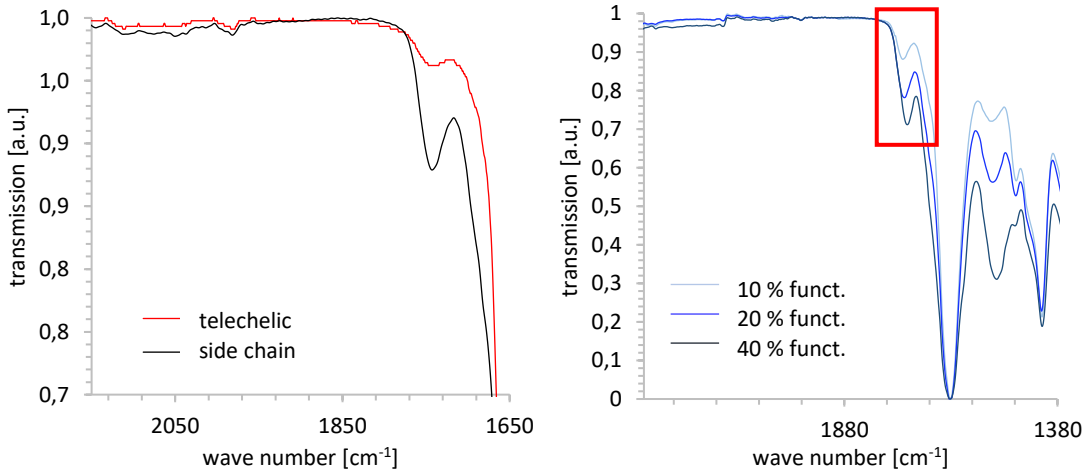

Figure 86: Left: Enlarged section of superimposed IR spectra of telechelic (red) and side chain (black) sugar functionalized conjugates (PMeOx$_{50}$-CGGGF-AcMan and P(MeOx$_{45}$-*co*-ButOx-CGGGF$_5$-AcMan$_5$)). The sugar signal in the telechelic conjugate is significantly weaker than that of the side chain functionalized conjugate. Right: Enlarged section of superimposed IR spectra of polymer conjugates with 10 % (light blue), 20 % (blue) and 40 % (dark blue) degree of functionalization (P(MeOx$_{45}$-*co*-ButOx-CGGGF$_5$-AcMan$_5$), P(MeOx$_{40}$-*co*-ButOx-CGGGF$_{10}$-AcMan$_{10}$) and P(MeOx$_{30}$-*co*-ButOx-CGGGF$_{20}$-AcMan$_{20}$)). The characteristic C=O stretching vibration of the sugar acetyl groups at 1743 cm^{-1} is highlighted with a red box.

Chapter 4.3.3.2 *Thiol-Ene Reaction with CGGWYKYW Polymer Conjugates*

In analogy to all previously described thiol-ene reactions between peptide conjugates and acetylated allyl mannose, the reaction was finally also performed with side chain P(MeOx$_{45}$-*co*-ButOx-CGGWYKYW$_5$) peptide conjugate (see **scheme 40**), employing the same reaction conditions that were utilized for the telechelic conjugate (see chapter 4.2.3.2b). Both educts were dissolved in water and DMSO under the presence of TCEP. Irgacure 2959 was added as initiator and the reaction mixture was stirred for 60 min under UV light irradiation. The product was purified via dialysis against water and will be referred to as P(MeOx$_{45}$-*co*-ButOx-CGGWYKYW$_5$-AcMan$_5$).

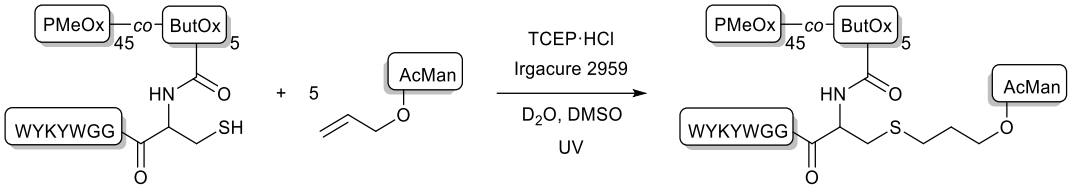

Scheme 40: Synthesis of side chain peptide and sugar functionalized P(MeOx$_{45}$-*co*-ButOx-CGGWYKYW$_5$-AcMan$_5$).

The resulting polymer was analysed by ^{1}H-NMR spectroscopy (see **figure 87**). The spectrum exhibits the same set of signals as the corresponding precursor spectrum (see **figure 82** in chapter 4.3.2.3). Those signals can be clustered in regions such as a 'NH and NH$_2$ region' and 'aromatic region' between 10.74 and 6.57 ppm, where signals from the amino groups of the conjugate as well as the aromatic rings of tyrosine and tryptophan can be found. Between 4.48 and 3.59 ppm, there is a 'peptide backbone region', where CH groups from each nodal point of the attached peptide are visible. There is the broad polymer *backbone* signal at 3.35 ppm, which in turn contains the DMSO water residue signal and a 'side chain alkyl region' between 3.07 and 2.27 ppm, where signals from alkylic CH$_2$ groups of the amino acid residues and polymer side chain as well as the initiator group of the polymer are present. The broad signal from the methyl side chain groups of the polymer can be found at 2.01-1.97 ppm, as well as the piperidine end group signal. Finally, there is a 'lysine region' between 1.51 and 1.19 ppm, where signals from the lysine and polymer side chain CH$_2$ groups can be detected.

On the one hand, the conjugation of the mannose sugar to the polymer leads to signals that fall into those already existing regions, which is the case for the alkylic sugar signals that appear in the 'peptide backbone region' and the 'alkyl side chain' region, as well as signals from the acetyl groups that add to the signal of the polymeric methyl side chain groups. On the other hand, the attachment of the sugar leads to distinct signals at 5.09-4.85 ppm, which stem from the protons at the positions 46 to 49 and define a new 'sugar ring' region. Although integration of all signals individually was not possible anymore due to the size of the macromolecular conjugates, the total integral values of each region still match the sum of protons for each part of the conjugate and it was possible to determine a conjugation of at least two sugar units per polymer chain. As it was also the case for other side chain functionalized

conjugates discussed in the previous chapter, steric hindrances in large macromolecules can be one of the reasons why in this case only two of the five possible conjugation sites are occupied by a sugar moiety.

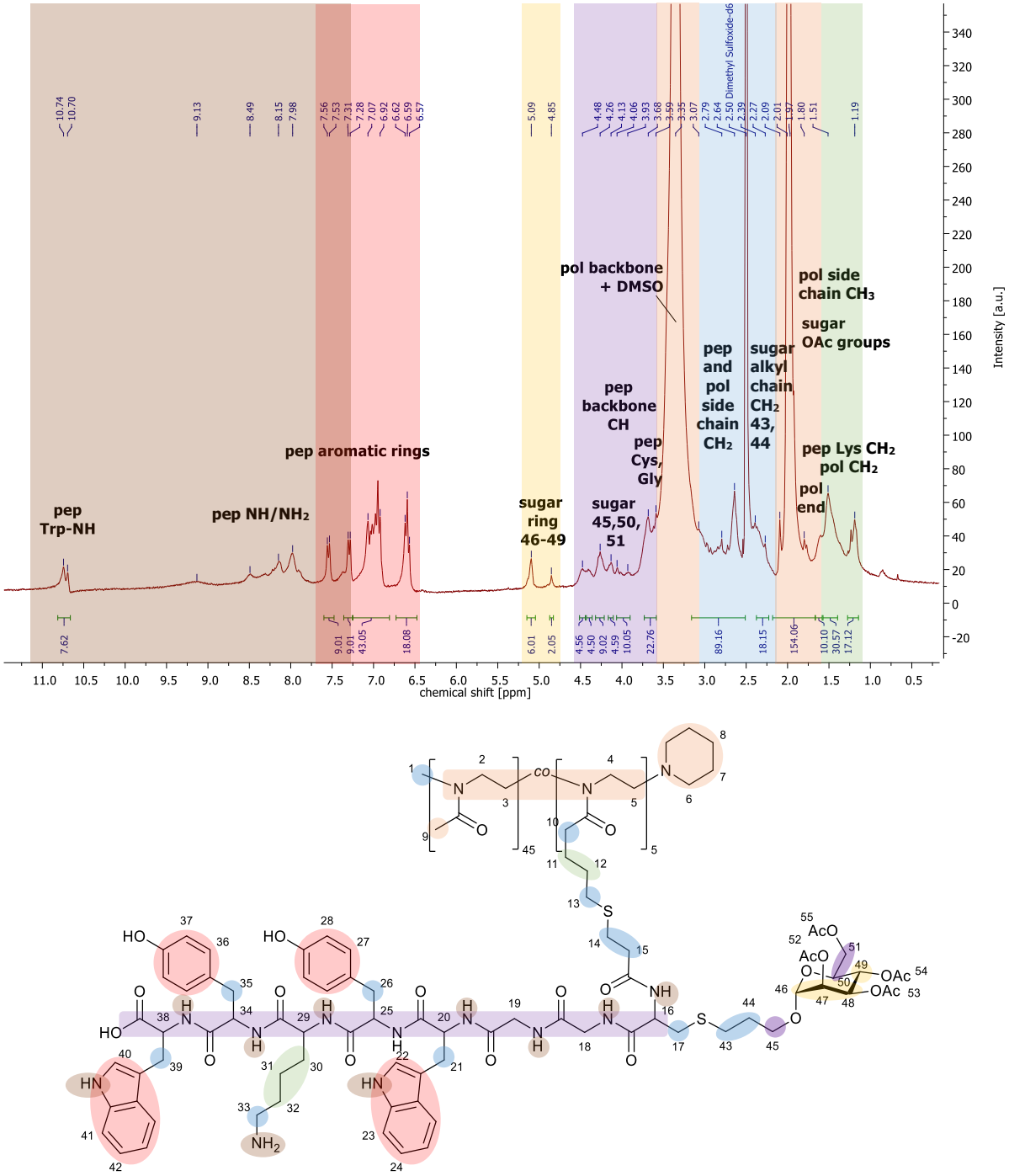

Figure 87: ^{1}H-NMR spectrum of side chain peptide and sugar functionalized P(MeOx$_{45}$-*co*-ButOx-CGGWYKYW$_5$-AcMan$_5$) in deuterated DMSO with "pep" for signals that belong to the peptide part of the conjugate and "pol" for signals that belong to the polymer part. The spectrum is subdivided into different regions: 'NH and NH$_2$ region' (brown), 'aromatic region' (red), 'sugar ring region' (yellow), 'peptide backbone region' (purple), polymer backbone (orange), 'side chain alkyl region' (blue), 'polymer region' (orange) and 'lysine region' (green).

IR spectroscopy was performed in order to confirm the results from NMR spectroscopy. Compared to the educt polymer spectrum, a characteristic signal from the C=O stretching vibration of the sugar is visible in the product spectrum at 1743 cm^{-1} after conjugation (see **figure 88**). This characteristic signal

has also been described in the previous chapter. While the mere educt P($MeOx_{45}$-*co*-ButOx-$CGGWYKYW_5$) polymer spectrum shows no signal at this position, the polymer-peptide conjugate P($MeOx_{45}$-*co*-ButOx-$CGGWYKYW_5$-$AcMan_5$) displays an apparent peak. Since the spectrum was taken after dialysis of the product, the findings affirm a qualitative conjugation of peptide to the polymer.

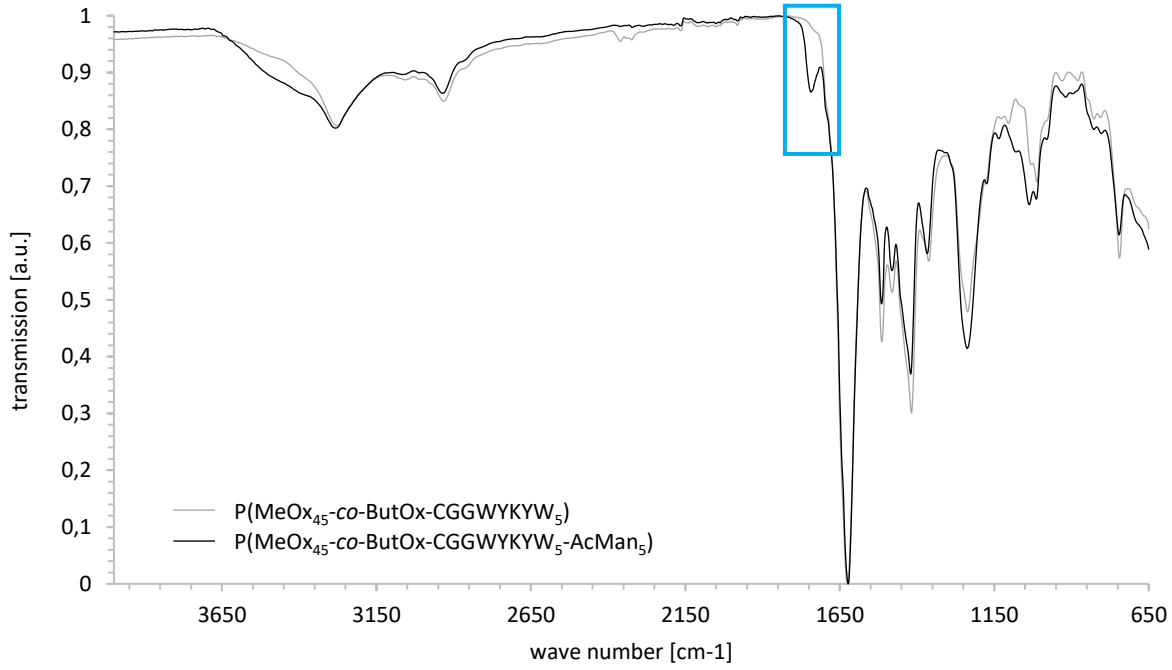

Figure 88: Superimposed IR spectra of educt polymer-peptide conjugate P($MeOx_{45}$-*co*-ButOx-$CGGWYKYW_5$) (grey), product polymer-peptide-sugar conjugate P($MeOx_{45}$-*co*-ButOx-$CGGWYKYW_5$-$AcMan_5$) (black) with characteristic C=O stretching vibration of the sugar acetyl groups at 1743 cm^{-1} (highlighted with blue box).

The same characteristic vibrational signal is also visible in the IR spectrum of telechelic conjugates (see **figure 89**). However, the intensity of the signal is much lower since there is only one instead of multiple conjugations and can, in some cases, only appear as a shoulder.

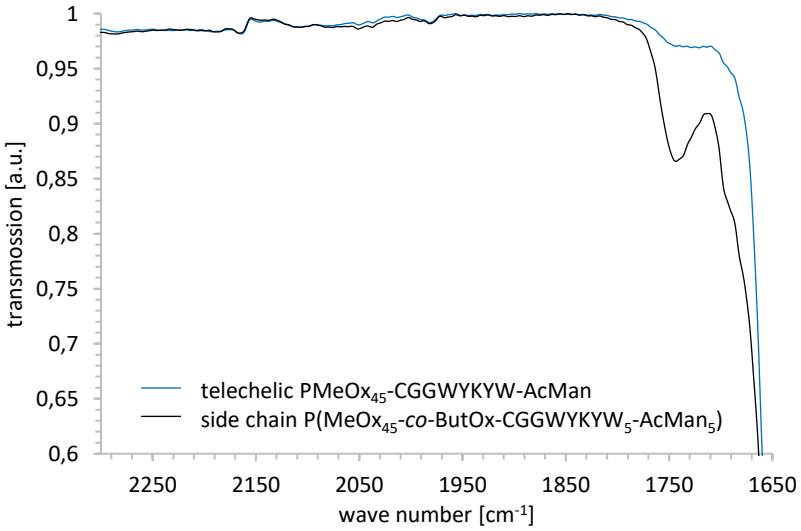

Figure 89: Enlarged section of superimposed IR spectra of telechelic (blue) and side chain (black) sugar functionalized conjugates ($PMeOx_{50}$-CGGWYKYW-AcMan and P($MeOx_{45}$-*co*-ButOx-$CGGWYKYW_5$-$AcMan_5$)). The sugar signal in the telechelic conjugate is significantly weaker than that of the side chain functionalized conjugate.

Chapter 5

Summary / Zusammenfassung

Chapter 5 Summary / Zusammenfassung

Chapter 5.1 Summary

In this work, a synthetic strategy was developed to chemoselectively couple three components at one binding site: POx polymer derivates as a basis plus different biomacromolecules, namely three different peptides CGGGF, CKFKFQF and CGGWYKYW and two saccharide molecules mannose and acetylated mannose.

Initially, all reaction steps were implemented on a low molecular level, both as a proof of principle, as well as a means of gaining specific analytical insights that would be intricate to obtain on a polymer level. A thoroughly characterized low molecular three-part conjugate was synthesized as a final product and in the course of conduct, the ideal reaction parameters that served as a guideline for all consecutive experiments were elaborated.

The gained expertise was then transferred to a more complex level. Thus, telechelic polyoxazoline polymers were utilized as educts for the reaction cascade. Via two different pathways, leading to both α as well as ω functionalized polyoxazolines, the polymer starting material was first synthesized.

The succeeding steps included a modification of the polyoxazoline end groups to carboxylic acids, which, in addition to the common analytical methods, were also thoroughly examined by means of titration before converting them into a thioester group via thioesterification. This route, leading to a various set of thioester functionalized polyoxazolines, therefore expands the spectrum of facilely available functional POx derivates. All stages of the reaction cascade were monitored by NMR, IR, SEC, as well as MALDI-TOF measurements.

Next, three peptides with different solubility and gelation properties were successfully conjugated to the thioester functionalized polymers in a NCL. Apart from NMR as the gold standard in polymer analytics and the observations in change of material behaviour, especially IR spectroscopy delivered distinct characteristic signals that allowed for the identification of the attached peptide compounds.

Despite drastic changes in solubility of the conjugates with increasing complexity of the system, the attachment of two different sugar derivates, acetylated mannose as a model saccharide as well as a deprotected mannose unit, was successful via the use of a thiol-ene click reaction. The viability of this reaction was once more fathomed by preceding model studies with less complex PEG- and POx-thiol model polymers, with the latter component being intentionally synthesized sole for this purpose.

In this last thiol-ene reaction step, NMR and IR spectroscopy studies again proved to be reliable means of analysis that allowed for the identification of easily recognizable and distinctive product signals. Moreover, dialysis turned out to be a reliable tool, not only for purification - but also to yield additional

information in characterizing the conjugates, which is explored in a special chapter dedicated to the uncommon use of this technique as an analytical method. In addition to this, SEC, MALDI-TOF, RAMAN and UV-Vis-spectroscopy were performed with the conjugates for the sake of completeness, however did not yield any subsidiary information on the systems.

The success of the last step and simultaneously implicating the success of the reaction cascade as a whole, was verified by ensuing biomacromolecular recognition experiments, consisting of SAW as well as complementary SPR affinity measurements. Those measurements demonstrated a biological interaction between ConA, a sugar-binding lectin and the conjugates bearing a saccharide unit. While other works that grafted saccharides to POx were only able to measure a *qualitative* interaction with ConA[37, 137, 650], in this work it was possible to measure *quantitative* values for the strength of the binding affinity, which constitutes a big advantage and was made feasible because a specific double telechelic design for the polymer conjugate systems was developed beforehand. It could be shown that POx-conjugated mannose showed a binding affinity to ConA in the range of literature values, with a K_D of 351 ± 77 nM (SAW), while protected mannose showed significantly lower binding affinities with a K_D of 1325 ± 97 nM (SAW). As expected, the peptide residue had no influence on the K_D value, which was proven in experiments with different pendant peptide moieties.

On the other hand, affinities between peptides with a specific amino acid sequence and the respective Gal1 lectin counterpart could not be observed, contrary to predictions from literature. Assumably, this was due to an insufficiently long peptide linker chain impeding the relevant sequence from interacting with the respective binding site of the biomacromolecule or the actual affinities being too small to be able to measure the weak intensities of those interactions, which could be enhanced by multivalent and/or synergistic effects.

First advances to multimeric polymer conjugates were already made in this work, as depicted in chapter 4.3, where the same components were grafted to multivalent, side chain functionalized polyoxazoline derivates. Once again, expertise from the preceding telechelic stage facilitated in implementing the same reaction cascade with these highly complex conjugate structures. Different degrees of functionalization were mirrored in different intensities of the respective characteristic signals of the functional groups in the applied measuring methods. Even though qualitative analysis showed success in all stages of the cascade, quantitative evaluation revealed that especially in the last step, only one of five possible reaction sites was conjugated with both components. This is probably due to steric hindrances in accessing the relevant functional groups.

In conclusion, it was shown that the NCL-thiol-ene reaction cascade of three components, bearing a thioester, a cysteine and an allyl groups, provides a versatile toolbox for the design of bioactive three-

part conjugates. The approach of this work, a stepwise increase in complexity of the investigated system, starting from low molecular model reactions to telechelic polymers through to side chain functionalized conjugates resulted in analytical findings that underpinned each consecutive step and led to profound conclusions on analytical statements that otherwise could not have been displayed with such a high level of certainty, especially in the field of complex and difficult to investigate macromolecular systems.

Together with the final affinity measurements that frame the whole cascade by proving positive the last of multiple reaction steps, this work contributes to overcome the challenges of the design of precise and defined polymer conjugates. At this point, it also seems conceivable to transfer this set of reactions to other specific and biologically relevant peptides and sugars that exhibit distinct interactions with tissues or proteins associated with certain autoimmune diseases, cancer or inflammation. The established system can furthermore serve as a targeting platform in future studies, providing a facile way to reliably determine biological interaction and corresponding affinity values of multivalent materials.

Chapter 5.2 Zusammenfassung

In der vorliegenden Arbeit wurde eine Synthesestrategie entwickelt, um drei makromolekulare Komponenten chemoselektiv an einer Bindungsstelle zu verknüpfen: POx-Polymer-Derivate dienten dabei als Basiskomponenten, an die jeweils zwei weitere makromolekulare Komponenten gebunden wurden. Im Wesentlichen waren das zum einen die Polymere CGGGF, CKFKFQF und CGGWYKYW sowie die beiden Zuckermoleküle Mannose und acetylierte Mannose.

Alle Reaktionsschritte wurden zunächst auf einem niedermolekularen Level durchgeführt. Zum einen als Machbarkeitsstudie, zum anderen um analytische Aussagen treffen zu können, die auf dem Größenordnungslevel von Polymeren nur eingeschränkt möglich sind. Das Reaktionsprodukt, ein drei-Komponenten-Konjugat wurde vollständig charakterisiert und im Verlauf der Modellreaktionen gleichzeitig die idealen Reaktionsparameter für die einzelnen Reaktionsschritte bestimmt, die später als Leitlinie für nachfolgende Experimente dienten.

Die so gewonnene Expertise wurde auf das nächsthöhere Komplexitätslevel übertragen, indem anschließend telechele Polymere als Edukte der Reaktionskaskade verwendet wurden. Ausgehend von zwei verschiedenen Syntheserouten wurden zunächst sowohl α als auch ω funktionalisierte POx-Polymere als Ausgangsmaterialien dargestellt.

Die nachfolgenden Schritte umfassten eine Modifizierung der Polymer-Endgruppen zu Säuregruppen, die neben den gängigen Analyseverfahren auch mittels Titration untersucht wurden, bevor sie durch eine Thioesterifizierung in Thioestergruppen umgewandelt wurden. Dieser Syntheseweg, mithilfe dessen eine Reihe Thioester-funktionalisierter Polyoxazolinderivate dargestellt werden konnte, erweitert somit das Spektrum leicht zugänglicher, funktioneller POx-Derivate. Der Erfolg aller Schritte der Reaktionskaskade wurde anhand von NMR, IR, GPC sowie MALDI-TOF-Messungen überprüft.

Anschließend wurden drei Peptide mit unterschiedlichen Löslichkeits- und Gelierungseigenschaften erfolgreich mit den Thioester-funktionalisierten Polymeren in einer NCL konjugiert. Neben NMR-Spektroskopie als Goldstandard in der Polymeranalytik und den Beobachtungen bei der Veränderung der Materialeigenschaften lieferte insbesondere die IR-Spektroskopie deutliche charakteristische Signale, die eine Identifizierung der angebundenen Peptidverbindungen ermöglichten.

Trotz drastischer Veränderungen der Löslichkeit der Konjugate mit zunehmender Komplexität des Systems gelang die Anbindung zweier verschiedener Zuckerderivate, der acetylierten Mannose als Modellsaccharid sowie einer entschützten Mannoseeinheit via Thiol-En-Klick-Reaktion. Die Durchführbarkeit dieser Reaktion wurde erneut durch vorgeschaltete Modellstudien mit weniger komplexen PEG- und POx-Thiol-Modellpolymeren belegt, wobei die letztere Komponente explizit zu diesem Zweck synthetisiert wurde.

NMR- und IR-Spektroskopie-Studien erwiesen sich als zuverlässige Analysemethoden, die es erlaubten, leicht erkennbare und unverwechselbare Produktsignale zu identifizieren. Darüber hinaus erwies sich die Dialyse als zuverlässiges Werkzeug - nicht nur zur Aufreinigung, sondern auch zur Gewinnung zusätzlicher Informationen bei der Charakterisierung der Konjugate. Der ungewöhnlichen Verwendung dieser Technik als Analysemethode ist ein eigenes Kapitel dieser Arbeit gewidmet. Darüber hinaus wurden SEC-, MALDI-TOF-, RAMAN- und UV-Vis-Spektroskopie mit den Konjugaten durchgeführt, die jedoch keinen zusätzlichen Informationsgewinn zu den untersuchten Systemen lieferten.

Die erfolgreiche Kopplung der drei beschriebenen makromolekularen Komponenten wurde durch anschließende biomakromolekulare Erkennungsexperimente, bestehend aus SAW- sowie komplementären SPR-Affinitätsmessungen, verifiziert. Diese Messungen zeigten eine Wechselwirkung zwischen ConA, einem zuckerbindenden Lektin und denjenigen Konjugaten, die eine Saccharideinheit tragen. Während in anderen Arbeiten[37, 137, 650], in denen Saccharide an POx angebunden wurden, nur eine *qualitative* Interaktion mit ConA gemessen werden konnte, konnten in dieser Arbeit *quantitative* Werte für die Stärke der Bindungsaffinität gemessen werden. Dies wurde dadurch ermöglicht, dass zuvor ein spezifisches, doppelt telechel funktionalisiertes Design für die Polymerkonjugatsysteme entwickelt worden war. Es konnte gezeigt werden, dass POx-konjugierte Mannose mit einem K_D-Wert von 351 ± 77 nM (SAW) eine Bindungsaffinität zu ConA im Bereich der Literaturwerte zeigte, während geschützte Mannose durch den Einfluss der Schutzgruppen mit einem K_D-Wert von 1325 ± 97 nM (SAW) signifikant geringere Bindungsaffinitäten aufweist. Wie erwartet, hatte der Peptidrest keinen Einfluss auf den K_D-Wert, was durch die Verwendung verschiedener Peptide in den Konjugaten nachgewiesen wurde.

Entgegen zu Feststellungen aus der Literatur konnten keine Affinitäten zwischen Peptiden mit einer spezifischen WYKYW-Aminosäuresequenz und dem jeweiligen Gal1-Lectin-Gegenstück beobachtet werden. Dies kann womöglich einer nicht ausreichend langen Peptid-Linkerkette zugeschrieben werden, die die relevante Sequenz daran hinderte, mit der jeweiligen Bindungsstelle des Biomakromoleküls zu interagieren. Es ist ebenfalls vorstellbar, dass die tatsächlichen Affinitäten zu klein sind, um die schwachen Intensitäten dieser Interaktionen messen zu können, die durch multivalente und/oder synergistische Effekte verstärkt werden könnten.

Wie im letzten Kapitel dargestellt, wurden in dieser Arbeit bereits erste Fortschritte zu multimeren Polymerkonjugaten gemacht, bei welchen die gleichen Komponenten mit multivalent seitenkettenfunktionalisierten Polyoxazolinderivaten konjugiert wurden. Auch hier erleichterte die Erfahrung aus den vorhergehenden telechelen Stufen eine Implementierung derselben Reaktionskaskade mit den nun entsprechend komplexeren Konjugatstrukturen. Unterschiedliche Funktionalisierungsgrade spiegelten sich in unterschiedlichen Intensitäten der jeweiligen

charakteristischen Signale der funktionellen Gruppen in den angewandten Messmethoden wider. Obwohl die qualitative Analyse in allen Stufen der Kaskade eine erfolgreiche Umsetzung zeigte, ergab eine quantitative Auswertung, dass insbesondere im letzten Schritt nur einer von fünf möglichen Reaktionsstellen mit beiden Komponenten konjugiert war. Dies ist sehr wahrscheinlich auf eine sterische Hinderung des Zugangs zu den jeweilig relevanten reaktiven funktionellen Gruppen zurückzuführen.

Zusammenfassend konnte gezeigt werden, dass die NCL-Thiol-En-Reaktionskaskade aus drei Komponenten, die jeweils eine Thioester-, Cystein- oder Allylgruppe tragen, einen vielseitigen ‚Werkzeugkasten' für das Design dreiteiliger, bioaktiver Konjugate darstellt. Die Herangehensweise in dieser Arbeit, eine schrittweise Erhöhung der Komplexität der untersuchten Systeme, angefangen von niedermolekularen Modellreaktionen, über telechele Polymere bis hin zu seitenkettenfunktionalisierten Konjugaten, konnte mit den jeweiligen analytischen Erkenntnissen die entsprechenden nachfolgenden Schritte untermauern und somit Schlussfolgerungen möglich machen, die andernfalls nicht mit einem so hohen Grad an Sicherheit hätten erbracht werden können, insbesondere im Bereich komplexer und schwer zu untersuchender makromolekularer Systeme.

Die abschließenden Affinitätsmessungen bestätigen den Erfolg der ganzen Reaktionskaskade insofern, als dass sie ein Gelingen des letzten Schritts von mehreren, aufeinander aufbauenden Reaktionsstufen nachweisen. Damit trägt diese Arbeit dazu bei, die Herausforderungen beim Design präziser und definierter Polymerkonjugate zu bewältigen und an diesem Punkt scheint es auch denkbar, diese Reihe von Reaktionen auf andere spezifische und biologisch relevante Peptide und Zucker zu übertragen, die ausgeprägte Wechselwirkungen mit Geweben oder Proteinen aufweisen und zum Beispiel mit bestimmten Autoimmunerkrankungen, Entzündungen oder Krebs assoziiert sein können. Das etablierte System kann darüber hinaus als Targeting-Plattform für zukünftige Interaktionsstudien dienen und bietet eine einfache Möglichkeit, biologische Wechselwirkungen und entsprechende Affinitätswerte von multivalenten Materialien zuverlässig zu bestimmen.

Chapter 6

Experimental Section

Chapter 6 Experimental Section

Chapter 6.1 Materials and Methods

Chapter 6.1.1 Chemicals

Reagents and solvents were, unless stated otherwise, commercially available as reagent grade and did not require further purification.

As solvents, acetic acid (AcOH) (30 %, *Sigma Aldrich*), acetone (≥99.5 %, *Sigma Aldrich*), acetonitrile (≥99.9 %, *Honeywell*), chloroform ($CHCl_3$) (≥99.8 %, *Fisher*), cyclohexane (≥98 %, *Fisher*), dichloromethane (DCM) (≥99.9 %, *Sigma Aldrich*), diethyl ether (Et_2O) (≥98 %, *Sigma Aldrich*), dimethyl sulfoxide (DMSO) (≥98 %, *Sigma Aldrich*), dimethylformamide (≥99.5 %, *Fisher*), ethyl acetate (EtOAc) (≥99.8 %, *Fisher*), hydrochloric acid (HCl) (32 %, *Merck*), isopropyl alcohol (≥99.9 %, *VWR chemicals),* methanol (MeOH) (≥98 %, *Sigma Aldrich*), tetrahydrofuran (THF) (≥98 %, *Sigma Aldrich*), deuterated acetonitrile (CD_3CN-*d3*) (≥99.8 % D, *Sigma Aldrich*), deuterated chloroform ($CDCl_3$) (≥99.8 % D, *Eurisotop*), deuterated dimethyl sulfoxide (DMSO-*d6*) (≥99.8 % D, *Deutero*), deuterated methanol (MeOD) (≥99.8 % D, *Deutero*), deuterated water (D_2O) (≥99.9 % D, *Deutero*), acetonitrile for MALDI (≥99.9 %, *Sigma Aldrich*), chloroform for MALDI (≥99.9 %, *Sigma Aldrich*), dimethylformamide for MALDI (≥99.8 %, *Sigma Aldrich*) and methanol for MALDI (≥99.8 %, *Sigma Aldrich*) were used as received.

As reagents, α-cyano-4-hydroxy cinnamic acid (≥99.0 %, *Fluka*), 1-ethyl-3-(3-dimethylaminopropyl) carbodiimide (EDC) (98 %, *Carbosynth*), 2,2-dimethoxy-2-phenylacetophenone (DMPA) (99 %, *Sigma Aldrich*), 2-hydroxy-4'-(2-hydroxyethoxy)-2-methylpropiophenone (Irgacure 2959) (98 %, *Sigma Aldrich, BASF*), 3-mercaptopropionic acid (≥99 %, *Sigma Aldrich*), 4 Å molecular sieve (*Sigma Aldrich*), 4-pentenoic acid (98 %, *Sigma Aldrich*), allyl alcohol (98 %, *Sigma Aldrich*), allylamine (98 %, *Sigma Aldrich*), allylpentafluorobenzene (98 %, *Sigma Aldrich*), benzyltrimethylammonium chloride (98 %, *Sigma Aldrich*), *Boc*-protected alanine (≥99 %, *Sigma Aldrich*), calcium hydride (92 %, *abcr GmbH),* cesium triiodide (99.999 %, *Sigma Aldrich*), chloroethyl amine hydrochloride (98 %, *AlphaAesar*), cysteamine hydrochloride (≥97 %, *Fluka*), cysteine hydrochloride monohydrate (≥98 %, *Sigma Aldrich*), cysteine methyl ester hydrochloride (≥98 %, *Sigma Aldrich*), dialysis membranes (*Spectrum Laboratories*), ethanethiol (98 %, *Sigma Aldrich*), isobutyl chloroformate (98 %, *Sigma Aldrich*), lithium bromide (98 %, *Sigma Aldrich*), magnesium sulfate (≥99.5 %, *Sigma Aldrich*), *N*-hydroxysuccinimide (NHS) (98 %, *Sigma Aldrich*), *N*-methylmorpholine (≥98.0 %, *Fluka*), piperidine (≥99.5 %, *Sigma Aldrich*), poly(ethylene glycol) methyl ether thiol (*Sigma Aldrich*), *p*-toluic acid (98 %, *Sigma Aldrich*), sinapic acid (≥99.0 %, *Fluka*), sodium azide (98 %, *Sigma Aldrich*), sodium borohydride (99 %, *Acros Organics*), sodium hydroxide (≥99 %, *Merck*), potassium hydroxide (≥99 %, *Merck*), sodium nitrate (98 %, *Sigma*

Aldrich), thioacetic acid (96 %, *Sigma Aldrich*), thiophenol (≥99 %, *Sigma Aldrich, AlphaAesar*), tosyl chloride (98 %, *Sigma Aldrich*), *trans*-2-[3-(4-tert-Butylphenyl)-2-methyl-2-propenylidene] malononitrile (DCTB) (≥99.0 %, *Fluka*), triazabicyclodecene (98 %, *Sigma Aldrich*), trifluoroacetic acid (TFA) (*Merck*), tris(2-carboxyethyl)phosphine (TCEP) (≥98 %, *Sigma Aldrich, Roth*) and tris(hydroxypropyl)phosphine (THPP) (80 %, *abcr GmbH*) were used as received.

All peptides (CGGGF, CKFKFQF and CGGWYKYW) were ordered from *GeneCust* and used as received. Recombinant Human Galectin-1 (Gal1) (≥ 98%, *PeproTech*) and Concanavalin A (ConA) (≥ 90 %, *Aldrich*) were used as received.

Acetylated allyl mannose and allyl mannose were synthesized by the working group of a cooperation partner Prof. Seibel (Julius-Maximilians-Universität Würzburg) and were used as received.

Acetonitrile (99.9 %, *Sigma-Aldrich*), 2-methyl-2-oxazoline (MeOx) (98 %, *Sigma-Aldrich*) and *p*-toluenesulfonate (98 %, *Sigma Aldrich*) for polymer synthesis were dried over CaH_2 and distilled before use.

Chapter 6.1.2 Column Chromatography

Material: *Merck* Geduran® silica gel 60 (0.040 - 0.063 mm)

Column chromatography was performed with silica gel by *Merck*. Length and diameter of the column were adapted to the reaction parameters. All solvent mixtures are given in volume fractions (V:V).

Chapter 6.1.3 Fourier-Transform-Infrared Spectroscopy with Attenuated Total Reflection (FT-IR ATR)

Instrument: *Thermo Scientific* Nicolet iS10 with Smart iTR diamond ATR

FT-IR spectroscopy was performed with an instrument by *Thermo Scientific*, carrying an ATR unit and a deuterated triglycine sulfate - potassium bromide (DTGS-KBr) detector, covering a wavenumber range from 4000 cm^{-1} to 650 cm^{-1}. Signal intensities were abbreviated with w (weak), m (medium), s (strong), vs (very strong) and br. (broad).

Chapter 6.1.4 Matrix-Assisted Laser Desorption Ionization – Time of Flight (MALDI-TOF) Mass Spectrometry

Instrument: *Bruker Daltonics* Autoflex II LRF, *Bruker Daltonics* MTP 384 massive target T

MALDI-TOF mass spectrometry measurements were performed on a time of flight mass spectrometer by *Bruker Daltonics*, equipped with a SCOUT TM MTP MALDI Ion Source. Reference standards were prepared by mixing a solution of CsI_3 (1 $mg{\cdot}mL^{-1}$ in acetonitrile) and DCTB (1 $mg{\cdot}mL^{-1}$ in chloroform) (1:1). 1 µL of the reference solution was spotted on the aluminium target (*Bruker Daltonics* MTP 384 massive target T). The polymer solution (10 $mg{\cdot}mL^{-1}$ in methanol with 1 % TFA) was mixed in volume ratios of 1:1, 1:2, 1:5 and 1:10 with the matrix solution (either 1 $mg{\cdot}mL^{-1}$ sinapic acid in methanol with

1 % TFA, respective 1 mg·mL^{-1} α-cyano-4-hydroxy cinnamic acid in methanol with 1 % TFA) and 1 µL of the mixture was also spotted on the target. 800 shots of a 337 nm nitrogen laser (laser power 70 %) at 20 Hz were applied and the spectra were accumulated with a cut off of 450 g·mol^{-1}.

Chapter 6.1.5 Microwave

Instrument: *CEM GmbH* Discover SP micowave (20-300°C, max. 300 watt)

Microwave reactions were performed with a microwave (20-300°C, max. 300 watt) by *CEM GmbH*. Depending on reaction mixture volume, either 10 mL or 35 mL glass vials with a silicone cap were used.

Chapter 6.1.6 Nuclear Magnetic Resonance (NMR) Spectroscopy

Instrument: *Bruker* Fourier 300 spectrometer

NMR spectroscopy was performed with an instrument by *Bruker* at 300 MHz with 128 scans. Chemical shifts δ are given in ppm. The ^{1}H resonance signal of the used solvent was used as internal reference for ^{1}H-NMR spectra (deuterated acetonitrile (CD_3CN-*d3*): 1.94 ppm; deuterated chloroform ($CDCl_3$): 7.26 ppm; deuterated dimethyl sulfoxide (DMSO-*d6*): 2.50 ppm; deuterated methanol (MeOD): 3.31 ppm; deuterated water (D_2O): 4.79 ppm). For all substances, the carbon bound protons were numbered consecutively. In some cases, individual carbon, nitrogen or fluorine atoms were also assigned numbers. Signal multiplicities were abbreviated with s (singlet), d (doublet), t (triplet), q (quartet), m (multiplet), dd (doublet of doublets), br. (broad) and app. (apparent).

Chapter 6.1.7 RAMAN Spectroscopy

Instrument: *Thermo Scientific* DXR Raman Microscope (excitation laser 780 nm)

RAMAN spectroscopy was performed with an instrument by *Thermo Scientific* with a special resolution of 540 nm and a confocal depth resolution of 1.7 µm, which includes an excitation laser of 780 nm and laser class 1 as well as an Olympus Optic (4x, 10x, 20x, 50x) and an *automatic fluorescence correction*.

Chapter 6.1.8 Size Exclusion Chromatography (SEC)

Instruments: *Viscotek* GPCmax (in-line degasser, 2-piston-pump and autosampler), *Viscotek* A-Columns A6000M for aqueus SEC (length = 300 mm, width = 8 mm, porous polyhydroxymethacrylate polymer, particle size = 13 µm), refractive index detector (*Viscotek VE3580*), viscosity detector (*Viscotek* 270), multiple angle light scattering detector (*Viscotek* SEC-MALS 20, laser wavelength 660 nm).

Malvern Instruments OmniSEC Resolve (*Agilent* high-pressure liquid chromatography pump, autosampler), SEC column D2000 for organic SEC (length: 300 mm, width: 7.8 mm, styrene-divinylbenzene (styrene-DVB) polymer, particle size: 6 µm,

exclusion limit: 5,000 g·mol^{-1}), SEC column D3000 for organic SEC (length: 300 mm, width: 7.8 mm, styrene-divinylbenzene (styrene-DVB) polymer, particle size: 6 µm, exclusion limit: 70,000 g·mol^{-1}), refractive index detector (*Agilent*), viscosity detector (*Agilent*), right-angle light scattering detector (*Agilent*), low-angle light scattering detector (*Agilent*).

SEC measurements in water were performed on an instrument by *Viscotek* with an oven temperature of 35 °C, water with 0.1 M $NaNO_3$ and 0.02 % NaN_3 as eluent and an applied flow rate of 0.7 mL·min^{-1}. The system includes an in-line degasser a 2-piston-pump and an autosampler as well as *Viscotek* A-Columns A6000M for aqueus SEC (length: 300 mm, width: 8 mm, porous polyhydroxymethacrylate polymer, particle size: 13 µm). As detectors, a refractive index detector (*Viscotek VE3580*), a viscosity detector (*Viscotek* 270) and a multiple angle light scattering detector (*Viscotek* SEC-MALS 20, laser wavelength 660 nm) are used. For calibration, PEG standards

by *Malvern* were used. For sample preparation, 3 mg of the samples were dissolved in 1 mL of the eluent and filtered with cellulose filters with a 0.2 µm pore size.

SEC measurements in DMF were performed on an instrument by *Malvern Instruments* with an oven temperature of 45 °C, DMF with 1 g·L^{-1} lithium bromide as eluent and an applied flow rate of 1.0 mL·min^{-1}. The system includes a high-pressure liquid chromatography pump (*Agilent*), an autosampler and a precolumn (Dguard, Organic Guard Column, length: 10 mm, width: 4.6 mm) as well as a SEC column D2000 for organic solvents, (length: 300 mm, width: 7.8 mm, styrene-divinylbenzene (styrene-DVB) polymer, particle size: 6 µm, exclusion limit: 5,000 g·mol^{-1}) respectively SEC column D3000 for organic solvents, (length: 300 mm, width: 7.8 mm, styrene-divinylbenzene (styrene-DVB) polymer, particle size: 6 µm, exclusion limit: 70,000 g·mol^{-1}). As detectors, a refractive index detector (*Agilent*), a viscosity detector (*Agilent*), a right-angle light scattering detector (*Agilent*) and a low-angle light scattering detector (*Agilent*) are used. For conventional calibration, 1-65 kDa PEG standards by *Malvern* were used. For triple detection calibration, 50 kDa PMMA standards by *Malvern* were used. For sample preparation, 5 mg of the samples were dissolved in 1 mL of the eluent and filtered with PTFE filters with a 0.2 µm pore size.

Chapter 6.1.9 Surface Acoustic Wave (SAW) Measurements

Instrument: *SAW Instruments GmbH* sam5 BLUE Surface Acoustic Wave biosensor

Surface Acoustic Wave (SAW) measurements were performed with an instrument by *SAW Instruments GmbH* which includes an autosampler and allows for measuring of protein adsorption and K_D value determination. Measurements were performed at 25 °C using phosphate-buffered saline (PBS) as running buffer. For immobilization of polymers containing a thioether group on the bare gold sensor

chip surface, respectively 30 µL of polymers per lane (concentration: 10 µg·mL^{-1} in PBS) were preincubated onto the sensor chip for 1 h with an external application mask. Remaining unspecific protein binding sites on the bare gold surface were saturated by injection of 500 µM BSA. Purified recombinant ConA was used as analyte at four concentrations, ranging from 118 to 944 nM. The flow rate for the acquisition of interaction data was set to 40 µL·min^{-1} in all experiments. Association was measured for 300 seconds, then dissociation was initiated by perfusing running buffer, and the dissociation phase was also monitored for 300 seconds. Regeneration of the chip surface was performed by injection of two 60 second pulses of 100 mM glycine (pH 2.5) at a flow rate of 100 µL·min^{-1}. Interaction data were analysed using the FitMaster add-in (*SAW Instruments GmbH*) of software Origin version 8.5 (*OriginLab Corporation*), applying a simple Langmuir-type 1:1 interaction model. Association rate constant k_{on} values and dissociation rates constant k_{off} values were obtained by fitting data of individual experiments. Equilibrium binding K_D values were deduced using the equation $K_D = k_{off}/k_{on}$. The sensor chips integrate 5 independent sensor elements (lanes) and allow for simultaneous analysis of different species or parameters and parallel references. All SAW experiments were performed in at least three independent experiments.

Chapter 6.1.10 Surface Plasmon Resonance (SPR) Spectroscopy

Instrument: REICHERT®4SPR, *Reichert Technologies*

Interactions between polymers and Concanavalin A (ConA) were measured by SPR using a REICHERT®4SPR system (*Reichert Technologies*). Measurements were performed at 25 °C using HBS150T [10 mM HEPES (pH 7.4), 150 mM NaCl, 3.4 mM EDTA, 0.005 % (v/v) Tween 20] as running buffer. For immobilization of polymers containing a thioether group on the bare gold sensor chip surface, the polymers were injected onto sensor for 8 min at a flow rate of 10 µL·min^{-1} to cause polymer coating to a final density of 1000 resonance units. Remaining unspecific protein binding sites on the bare gold surface were saturated by injection of 500 µM BSA. Purified recombinant ConA was used as analyte at four concentrations, ranging from 118 to 944 nM. The flowrate for the acquisition of interaction data was set to 25 µL·min^{-1} in all experiments. Association was measured for 180 seconds, then dissociation was initiated by perfusing running buffer, and the dissociation phase was monitored for 300 seconds. Regeneration of the chip surface was performed by injecting of two 60-second pulses of 100 mM glycine (pH 2.5) at a flow rate of 100 µL·min^{-1}. Interaction data were analysed using the software TraceDrawer version 1.8.1 (*Ridgeview Instruments AB*, Uppsala, Sweden), applying a simple Langmuir-type 1:1 interaction model and using global fitting for the rate constants. Association rate constant k_{on} values and dissociation rates constant k_{off} values were obtained by fitting data of individual experiments. Equilibrium binding K_D values were deduced using the equation $K_D = k_{off}/k_{on}$. All SPR experiments were performed in at least three independent experiments.

Chapter 6.1.11 Thin Layer Chromatography (TLC)

Material: *Macherey-Nagel* Alugram® Nano-Sil G/UV_{254} (20 x 20 cm foils)

Reaction control by TLC was performed on silica gel 60 G/UV_{254} coated aluminium plates by *Macherey-Nagel*. Visualization was done by fluorescence quenching of the indicator at 254 nm, fluorescence of the substances at 254 nm respective 365 nm under UV light irradiation or by dying with iodine. Composition of the solvent mixtures are always given in volume fractions (V:V).

Chapter 6.1.12 Titration

Instrument: *Metrohm* 905 Titrando

Titration experiments were performed with a titrator from *Metrohm* with two *Metrohm* 800 Dosino dosing units and a pH electrode for small sample volumes (*Metrohm* Biotrode). For each measurement, 25 mg sample were dissolved in 2 mL water and titrated against 0.01 M respective 0.001 M NaOH solution.

Chapter 6.1.13 UV Light Irradiation

Instruments: *A. Hartenstein Laborbedarf GmbH* UV lamp (230 V, 50 Hz, 4 W, 254/365 nm)

Polymerschmiede GmbH UV LED cubes (11 W, 365 nm)

TLC experiments were controlled by an UV lamp (230 V, 50 Hz, 4 W, 254/365 nm) by *A. Hartenstein Laborbedarf GmbH*. Photoinitiated reactions were performed with three UV LED cubes by *Polymerschmiede GmbH* with an output of 11 W (each) and a wavelength of 365 nm.

Chapter 6.1.14 UV-Vis Spectroscopy

Instrument: *Thermo Fisher Scientific* Genesys 10S Bio spectrophotometer

UV-Vis measurements were performed at room temperature on an instrument by *Thermo Fisher Scientific* with a xenon flash lamp, covering a wavelength range from 190 nm to 1100 nm.

Chapter 6.2 Synthesis

Chapter 6.2.1 Synthesis of 2-[(*tert*-Butyloxycarbonyl)amino]thiopropionic Acid *S*-Phenyl Ester

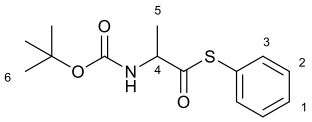

5.00 g (26.4 mmol, 1.00 eq.) *Boc*-protected alanine, 3.50 mL (3.20 g, 31.7 mmol, 1.20 eq.) *N*-methylmorpholine and 60 mL THF are put onto 4 Å molecular sieve under argon atmosphere. The solution is cooled to 0 °C and 3.77 mL (3.97 g, 29.1 mmol, 1.10 eq.) isobutyl chloroformate are added. A colourless solid precipitates. After 15 min, 3.26 mL (3.49 g, 31.7 mmol, 1.20 eq.) thiophenol and another 3.50 mL (3.20 g, 31.7 mmol, 1.20 eq.) *N*-methylmorpholine are added and the solution is warmed up to RT. After stirring for 18 h at RT, the colourless solid and the molecular sieve are filtered out and the solvent is removed in vacuo. The purple-black precipitate is taken up in DCM and washed with both a saturated solution of sodium hydrogencarbonate and a saturated solution of sodium chloride. The organic phase is dried over magnesium sulfate and the solvent is removed in vacuo. The raw product is purified via column chromatography using a mixture of cyclohexane and EtOAc (3:1).

Yield: (2.00 g, 7.11 mmol, 27 %, Lit.[225] 73 %);

R_f (Cyclohexane:EtOAc, 3:1): 0.80;

^{1}H-NMR ($CDCl_3$): δ = 7.41 (s, 5H, H-1/H-2/H-3), 4.98 (br. d, J = 5.8 Hz, 1H, N-H), 4.52 (br. app. t, ^3J = 6 Hz, 1H, H-4), 1.49 (s, 9H, H-6), 1.44 (d, J = 6 Hz , 3H, H-5) ppm.

Chapter 6.2.2 Synthesis of *p*-Toluic Acid *S*-Phenyl Ester

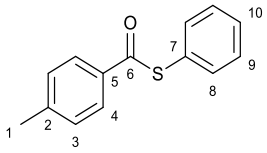

20.0 g (147 mmol, 1.00 eq.) *p*-toluic acid, 19.4 mL (17.9 g, 176 mmol, 1.20 eq.) *N*-methylmorpholine and 200 mL THF are put onto 4 Å molecular sieve and stirred for 2 h. 20.8 mL (22.1 g, 162 mmol, 1.10 eq.) isobutyl chloroformate are then added and a colourless solid precipitates. After 15 min, 18.1 mL (19.4 g, 176 mmol, 1.20 eq.) thiophenol and another 19.4 mL (17.9 g, 176 mmol, 1.20 eq.) *N*-methylmorpholine are added. After stirring at RT overnight, the colourless solid and the molecular sieve are filtered off and the solvent is removed in vacuo. The purple-black precipitate is taken up in 200 mL of DCM and washed three times with 150 mL water. The organic phase is dried over magnesium sulfate and the solvent is removed in vacuo. The ochre-coloured precipitate is washed multiple times with cold cyclohexane. Solid that remains from the washing phase can be washed again with cold cyclohexane to increase the yield.

Yield: 25.3 g (111 mmol, 76 %);

^{1}H-NMR ($CDCl_3$): δ = 7.59-7.92 (m, 2H, H-4), 7.51-7.44 (m, 5H, H-8/H-9/H-10), 7.30-7.27 (m, 2H, H-3), 2.44 (s, 3H, H-1) ppm;

^{13}C-NMR ($CDCl_3$): δ = 189.8 (C_q, C-6), 144.7 (C_q, C-5), 135.3 (C_q, C-7), 134.3 (C_q, C-2), 129.5 (C_t, C-8/C-9), 129.3 (C_t, C-3/C4), 127.7 (C_t, C-10), 21.8 (C_p, C-1) ppm;

FT-IR (ATR): $\tilde{\upsilon}$ = 3052 (w, ν(C-H_{arom})), 2911 (w), 1668 (vs, ν(C=O)), 1603 (m), 1574 (m), 1477 (w), 1441 (m), 1407 (w), 1308 (w), 1217 (s), 1207(s), 1173 (s), 1114 (w), 1022 (w), 906 (s), 821 (s), 788 (m), 748 (s), 717 (w), 689 (s) cm^{-1}.

Chapter 6.2.3 Synthesis of (4-Methylbenzoyl)cysteine

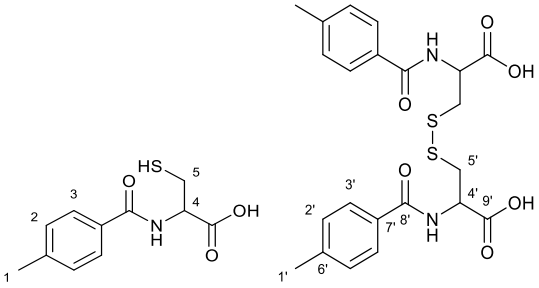

1.83 g (10.5 mmol, 1.00 eq.) of cysteine hydrochloride monohydrate are dissolved in 60 mL methanol and 663 mg (17.4 mmol, 2.00 eq.) sodium borohydride are added while stirring. Gas formation and heat development is observed. After 10 min, 2.40 g (10.5 mmol, 1.00 eq.) *p*-toluic acid *S*-phenyl ester are added and the reaction is stirred at RT overnight.

A strong characteristic odor of thiophenol emerges. 50 mL chloroform and 50 mL water are added. The aqueous phase is washed three times with 50 mL chloroform and water is removed in vacuo.

Yield: 1.91 g (8.30 mmol, 76 %);

^{1}H-NMR (MeOD): δ (monomer) = 7.78 (d, J = 8.3 Hz, 2H, H-3), 7.29 (d, J = 8.0 Hz, 2H, H-2), 4.59 (t, J = 4.7 Hz, 1H, H-4), 3.07 (d, J = 4.9 Hz, 2H, H-5), 2.40 (s, 3H, H-1) ppm;

δ (dimer) = 7.74 (d, J = 8.2 Hz, 2H, H-3'), 7.21 (d, J = 8.0 Hz, 2H, H-2'), 4.72-4.68 (m, 1H, H-4'), 3.47-3.19 (m, 2H, H-5'), 2.36 (s, 3H, H-1') ppm;

^{13}C-NMR (MeOD): δ (dimer) = 176.2 (C_q, C-9'), 169.3 (C_q, C-8'), 143.4 (C_q, C-7'), 132.7 (C_t, C-3'), 130.2 (C_t, C-2'), 128.3 (C_q, C-6'), 58.0 (C_t, C-4'), 27.9 (C_s, C-5'), 21.4 (C_t, C-1') ppm;

FT-IR (ATR): $\tilde{\upsilon}$ (dimer) = 3192 (br. m, v(C-OH)), 1607 (s, v(C=O)), 1529 (s), 1497 (s), 1392 (vs), 1300 (w), 1188 (m), 918 (w), 835 (w), 751 (s), 704 (w) cm^{-1}.

Chapter 6.2.4 Synthesis of (3-(Perfluorophenyl)propyl)-phenyl-thioether

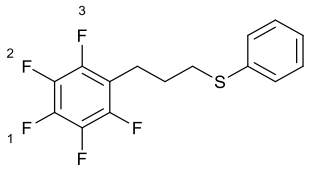

308 mg (1.20 mmol, 0.50 eq.) DMPA are dissolved in 368 µL (500 mg, 2.40 mmol, 1.00 eq.) allylpentafluorobenzene and 1.48 mL (1.59 g, 14.4 mmol, 6.00 eq.) thiophenol. The reaction mixture is stirred for 1 h under UV light irradiation.

The raw product is purified by two times column chromatography (*n*-hexane as solvent).

R_f (*n*-hexane): 0.25;

^{1}H-NMR (MeOD): δ = 7.35-7.26 (m, 4H, H-2/H-3), 7.21-7.16 (m, 1H, H-1), 2.97 (t, *J* = 7.0 Hz, 2H, H-4), 2.88 (t, *J* = 7.0 Hz, 2H, H-6), 1.88 (quintet, *J* = 7.0 Hz, 2H, H-5) ppm;

^{19}F-NMR (MeOD): δ = -146.36 (d, *J* = 13.4 Hz, 2F, F-3'), -161.09 (d, *J* = 20.0 Hz, 1F, F-1'), -165.94 (dd, *J* = 20.0, 13.4 Hz, 2F, F-2') ppm.

Chapter 6.2.5 Synthesis of *N*-(4-Methylbenzoyl)-*S*-(3-(Perfluorophenyl)propyl)cysteine

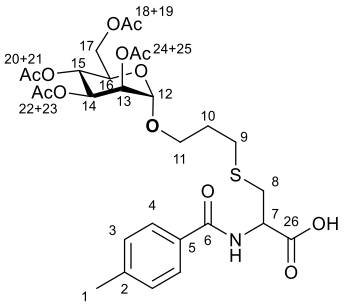

135 mg (0.35 mmol, 1.00 eq.) acetylated allyl mannose and 500 mg (2.09 mmol, 6.00 eq.) (4-methylbenzoyl)cysteine are dissolved in 1.00 mL MeOD. 44.6 mg (0.17 mmol, 0.50 eq.) DMPA are added. The reaction mixture is stirred for 60 min under UV light irradiation.

The raw product is purified by column chromatography (EtOAc as solvent). Column chromatography leads to high losses in yield, 50.0 mg of the final product were obtained.

Yield: 50.0 mg (0.08 mmol, 23 %);

R_f (EtOAc): 0.80;

^{1}H-NMR ($CDCl_3$): δ = 7.76-7.73 (m, 2H, H-4), 7.26-7.24 (m, 2H, H-3), 7.17-7.13 (m, 1H, N-H), 5.38-5.24 (m, 3H, H-13/H-14/H-15), 5.04-5.02 (m, 1H, H-7), 4.81 (s, 1H, H-12), 4.30-4.11 (m, 2H, H-17), 4.01-3.95 (m, 2H, H-16), 3.80-3.45 (m, 2H, H-11), 3.29-3.14 (m, 2H, H-8), 2.80-2.59 (m, 2H, H-9), 2.40 (s, 3H, H-1), 2.16-2.02 (m, 12H, H-19/H-21/H-23/H-25), 1.94-1.80 (m, 2H, H-10) ppm;

^{13}C-NMR ($CDCl_3$): δ = 172.9 (C_q, C-6), 171.1 (C_q, C-18), 170.7 (C_q, C-20), 170.4 (C_q, C-22), 170.0 (C_q, C-24), 167.6 (C_q, C-26), 142.7 (C_q, C-5), 130.7 (C_q, C-2), 129.4 (C_t, C-4), 127.4 (C_t, C-3), 97.5 (C_t, C-12), 69.7 (C_p, C-19), 69.6 (C_p, C-21), 68.7 (C_p, C-23), 66.5 (C_s, C-8), 66.2 (C_p, C-25), 62.7 (C_s, C-9), 52.1 (C_t, C-7), 33.9 (C_s, C-11), 29.3 (C_s, C-17), 29.1 (C_s, C-10), 23.2 (C_p, C-1), 21.6 (C_t, C-13), 21.0 (C_t, C-14), 20.9 (C_t, C-15), 20.8 (C_t, C-16) ppm;

FT-IR (ATR): $\tilde{\upsilon}$ = 2938 (w, ν(C-H)), 1742 (s, ν(C=O)), 1646 (m), 1532 (w), 1499 (w), 1427 (w), 1369 (m), 1221 (s), 1207(s), 1137 (w), 1083 (m), 1046 (m), 979 (w), 907 (s), 726 (vs) cm^{-1}.

Chapter 6.2.6 Synthesis of ω Telechelic Allyl Functionalized Poly(2-methyl-2-oxazoline)

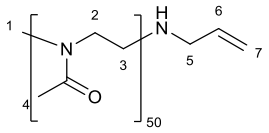

Under argon atmosphere, 300 mg (1.61 mmol, 1.00 eq.) dried methyl *p*-toluenesulfonate are dissolved in 20 mL dry acetonitrile and 6.82 mL (6.85 g, 80.5 mmol, 50.0 eq.) dry 2-methy-2-oxazoline are added. The reaction mixture is stirred for 90 min at 100 °C in a microwave reactor. Afterwards, 1.22 mL (0.92 g, 16.1 mmol, 10.0 eq.) allylamine are added and the reaction mixture is stirred at 40 °C for 48 h.

The raw product is precipitated three times in 200 mL cold diethyl ether. Between the precipitation steps, solvent is decanted and the residue is taken up in 5 mL MeOH/$CHCl_3$. After the last time precipitating, solvent is removed in vacuo.

^{1}H-NMR ($CDCl_3$): δ = 7.68 (d, tosylate counterion), 7.13 (d, tosylate counterion), 5.84-5.75 (m, 1H, H-6), 5.22 (m, 2H, H-7), 3.92 (m, 2H, H-5), 3.46-3.43 (br. m, 198H, H-2/H-3), 3.04-2.93 (m, 3H, H-1), 2.32 (s, tosylate counterion), 2.12-2.05 (br. m, 147H, H-4) ppm;

FT-IR (ATR): $\tilde{\upsilon}$ = 3449 (br. w), 2937 (w, ν(C-H)), 2937 (w, ν(C-H)), 1623 (vs, ν(C=O)), 1477 (w), 1415 (vs), 1362 (m), 1323 (w), 1291 (m), 1239 (m), 1207 (m), 1120 (w), 1032 (w), 1011 (m), 925 (w), 748 (m), 680 (w) cm^{-1}.

Table 5: Calculated and attained molecular weight of ω telechelic allyl functionalized polyoxazolines in experiment I-XI.

experiment	polymer	M_n (theo.) [g·mol^{-1}]	M_n (exp.)* [g·mol^{-1}]	M_n (exp.)** [g·mol^{-1}]	M_w (exp.)** [g·mol^{-1}]	Đ**
I	**PMeOx$_{15}$**	1348	1178	1281	1348	1.05
II	**PMeOx$_{25}$**	2199	2156	2154	2295	1.07
III	**PMeOx$_{30}$**	2624	2539	2503	2635	1.05
IV	**PMeOx$_{38}$**	3305	3305	3275	3452	1.05
V	**PMeOx$_{50}$**	4326	4284	4196	4413	1.05
VI	**PMeOx$_{50}$**	4326	4071	4236	4426	1.05
VII	**PMeOx$_{50}$**	4326	4241	4258	4415	1.04
VIII	**PMeOx$_{50}$**	4326	4199	4153	4339	1.05
IX	**PMeOx$_{60}$**	5177	4922	4968	5311	1.07
X	**PMeOx$_{100}$**	8582	8411	7982	8640	1.08
XI	**PMeOx$_{150}$**	12837	12752	12230	13590	1.11

*determined by ^{1}H-NMR-spectroscopy in $CDCl_3$, **determined by SEC in DMF (1 mL·min^{-1}, PEG standard).

As examples, the elugrams of experiment I, V, X and XI are shown:

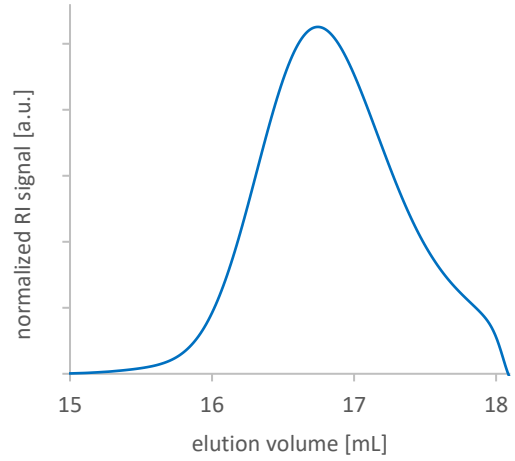

Figure 90: SEC elugram of experiment I.

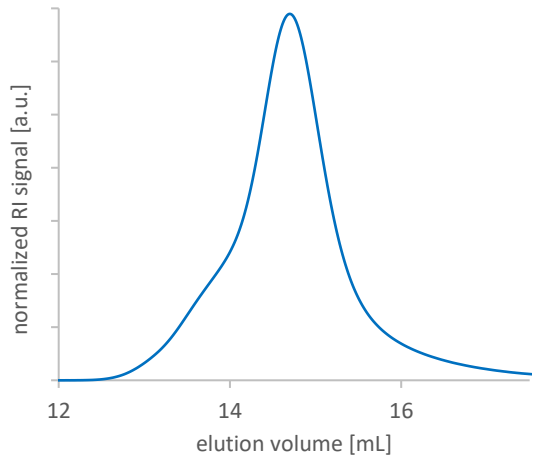

Figure 91: SEC elugram of experiment V.

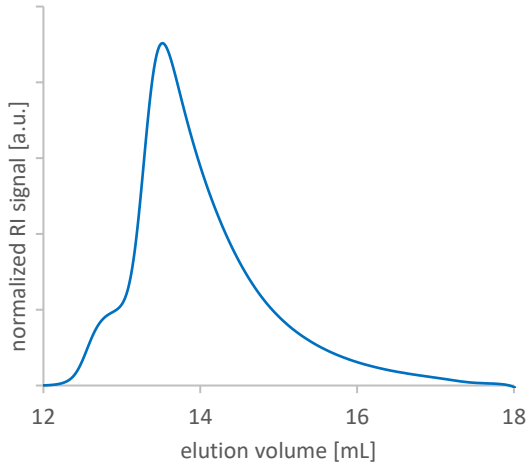

Figure 92: SEC elugram of experiment X.

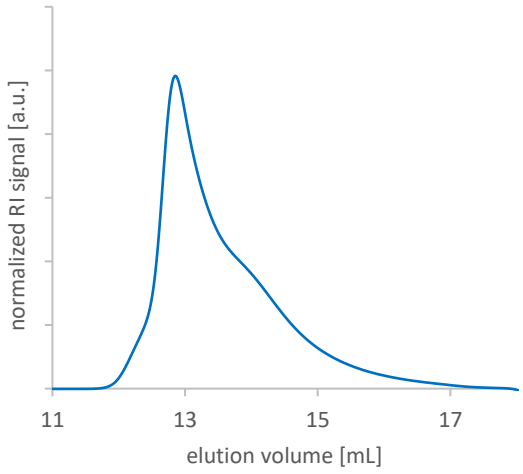

Figure 93: SEC elugram of experiment XI.

Chapter 6.2.7 Synthesis of Allyl *p*-Toluenesulfonate

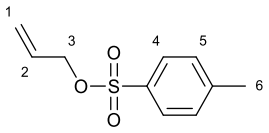

A solution of 20 mL THF and 20 mL 2.5 M NaOH is cooled to 0 °C and 836 mg (4.50 mmol, 0.13 eq.) benzyltrimethylammonium chloride are added. 2.50 mL (2.14 g, 36.8 mmol, 1.10 eq.) allyl alcohol are added and the solution is stirred for 30 min at 0 °C. 6.39 g (33.5 mmol, 1.00 eq.) tosyl chloride are dissolved in 20 mL THF and added to the reaction mixture. After stirring for 60 min at 0 °C, the aqueous phase is removed and washed with 80 mL EtOAc. The combined organic phases are then washed three times with 50 mL water, dried over $MgSO_4$ and solvent is removed in vacuo.

Yield: 4.79 g (22.6 mmol, 67 %, Lit. 36 %[616] 44 %[617] 77 %[618]);

^{1}H-NMR ($CDCl_3$): δ = 7.78 (d, J = 8.3 Hz, 2H, H-4), 7.33 (d, J = 8.0 Hz, 2H, H-5), 5.87-5.74 (m, 1H, H-2), 5.34-5.21 (m, 2H, H-1), 4.52 (d, J = 5.9 Hz, 2H, H-3), 2.43 (s, 3H, H-6) ppm.

Chapter 6.2.8 Synthesis of α Telechelic Allyl Functionalized Poly(2-methyl-2-oxazoline)

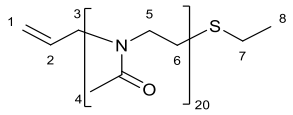

Under argon atmosphere, 424 µL (500 mg, 2.36 mmol, 1.00 eq.) dried allyl *p*-toluenesulfonate are dissolved in 10 mL acetonitrile and 3.99 mL (4.00 g, 80.5 mmol, 50.0 eq.) 2-methy-2-oxazoline are added. The reaction mixture is stirred for 1 h at 100 °C in a microwave reactor. Afterwards, 524 µL (440 mg, 7.08 mmol, 3.00 eq.) ethanethiol are added and the reaction mixture is stirred at 40 °C for 48 h.

The raw product is precipitated four times in 100 mL cold diethyl ether. Between the precipitation steps, solvent is decanted and the residue is taken up in 5 mL MeOH/$CHCl_3$. After the last time precipitating, solvent is removed in vacuo.

^{1}H-NMR ($CDCl_3$): δ = 7.62 (d, tosylate counterion), 7.13 (d, tosylate counterion), 5.79-5.68 (m, 1H, H-2), 5.22-5.07 (m, 2H, H-1), 3.92 (m, 2H, H-5), 4.28 (s, 2H, H-3), 3.87-3.41 (br. m, 80H, H-5/H-6/H-7), 2.82 (s, 4H, H-6/H-7), 2.31 (s, tosylate counterion), 2.09-1.99 (br. m, 63H, H-4/H-8) ppm;

FT-IR (ATR): $\tilde{\upsilon}$ = 3444 (br. w), 2937 (w, ν(C-H)), 1743 (w), 1626 (vs, ν(C=O)), 1477 (w), 1416 (vs), 1363 (m), 1235 (m), 1120 (w), 1032 (w), 1010 (m), 926 (w), 819 (w), 749 (m), 680 (w) cm^{-1}.

Table 6: Calculated and attained molecular weight of α telechelic allyl functionalized polyoxazolines in experiment I-III.

experiment	polymer	M_n (theo.) [g·mol^{-1}]	M_n (exp.)* [g·mol^{-1}]	M_n (exp.)** [g·mol^{-1}]	M_w (exp.)** [g·mol^{-1}]	Đ**
I	allyl-PMeOx$_{20}$-SEt	1804	1762	1722	1829	1.06
II	allyl-PMeOx$_{20}$-SEt	1804	1804	1759	1903	1.08
III	allyl-PMeOx$_{20}$-SEt	1804	1847	1759	1854	1.05

*determined by ^{1}H-NMR-spectroscopy in $CDCl_3$, **determined by SEC in DMF (1 mL·min^{-1}, PEG standard).

As an example, the elugram of experiment III is shown:

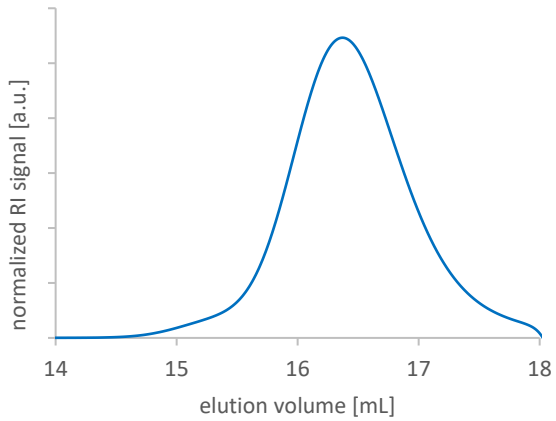

Figure 94: SEC elugram of experiment III.

Chapter 6.2.9 Synthesis of ω Telechelic Carboxylic Acid Functionalized Poly(2-methyl-2-oxazoline)

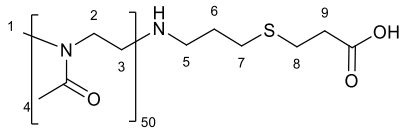

2.00 g (0.66 mmol, 1.00 eq.) allyl functionalized $PMeOx_{50}$ and 85.0 µL (104 mg, 0.98 mmol, 1.50 eq.) 3-mercaptopropionic acid are dissolved in 5 mL MeOH and the solution was flushed with argon. 42.0 mg (0.16 mmol, 0.25 eq.) DMPA are added and the reaction mixture is stirred for 60 min under UV light irradiation.

The raw product is precipitated four times in 100 mL cold diethyl ether. Between the precipitation steps, solvent is decanted and the residue is taken up in 5 mL MeOH/$CHCl_3$ (1:1). After the last time precipitating, solvent is removed in vacuo.

^{1}H-NMR ($CDCl_3$): δ = 7.67 (tosylate counter ion), 7.17 (tosylate counter ion), 3.46 (br. s, 4nmH, H-2/H-3), 3.03 (m, 3H, H-1), 2.94-2.90 (m, 2H, H-9), 2.78-2.69 (m, 4H, H-5/H-8), 2.65-2.57 (m, 4H, H-6/H-7), 2.35 (tosylate counter ion), 2.13-1.99 (br. m, 3nH, H-4) ppm;

FT-IR (ATR): $\tilde{\upsilon}$ = 3440 (br. w), 3272 (w, ν(N-H)), 2937 (w, ν(C-H)), 1721 (w, ν(C=O, COOH)), 1628 (vs, ν(C=O)), 1477 (w), 1416 (vs), 1362 (m), 1323 (w), 1238 (m), 1209 (m), 1121 (w), 1032 (w), 1010 (m), 925 (w), 818 (w), 749 (m), 681 (w) cm^{-1}.

Table 7: Calculated and determined mol. weight of telechelic carboxylic acid funct. $PMeOx_n$-COOH in experiment I-IX.

experiment	polymer	M_n (theo.) [g·mol^{-1}]	M_n (exp.)* [g·mol^{-1}]	M_n (exp.)** [g·mol^{-1}]	M_w (exp.)** [g·mol^{-1}]	Đ**
I	**$PMeOx_{15}$-COOH**	1454	1326	1524	1608	1.05
II	**$PMeOx_{25}$-COOH**	2305	2220	2329	2433	1.05
III	**$PMeOx_{25}$-COOH**	2305	2305	2288	2376	1.04
IV	**$PMeOx_{38}$-COOH**	3411	3496	2766	3038	1.10
V	**$PMeOx_{50}$-COOH**	4433	4390	2784	3092	1.11
VI	**$PMeOx_{50}$-COOH**	4433	4390	4208	4714	1.12
VII	**$PMeOx_{50}$-COOH**	4433	4433	4353	4793	1.10
VIII	**$PMeOx_{100}$-COOH**	8688	8688	8216	9199	1.12
IX	**$PMeOx_{150}$-COOH**	12943	12773	11630	13390	1.15

*determined by ^{1}H-NMR-spectroscopy in $CDCl_3$, **determined by SEC in DMF (1 mL·min^{-1}, PEG standard).

As examples, the elugrams of experiment III and VII are shown:

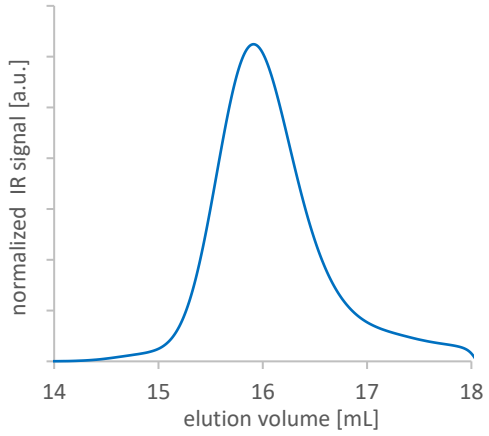

Figure 95: SEC elugram of experiment III.

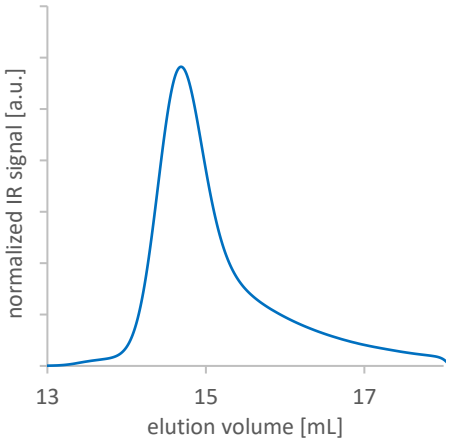

Figure 96: SEC elugram of experiment VII.

Chapter 6.2.10 Synthesis of α Telechelic Carboxylic Acid Functionalized Poly(2-methyl-2-oxazoline)

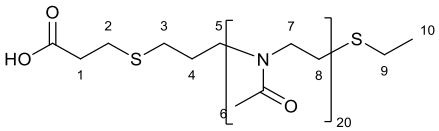

2.50 g (1.39 mmol, 1.00 eq.) allyl functionalized allyl-$PMeOx_{20}$-SEt and 362 µL (441 mg, 4.16 mmol, 3.00 eq.) 3-mercaptopropionic acid are dissolved in 5 mL MeOH. 178 mg (0.67 mmol, 0.50 eq.) DMPA are added and the reaction mixture is stirred for 60 min under UV light irradiation.

The raw product is precipitated three times in 100 mL cold diethyl ether. Between the precipitation steps, solvent is decanted and the residue is taken up in 5 mL MeOH/$CHCl_3$. After the last time precipitating, solvent is removed in vacuo.

^{1}H-NMR ($CDCl_3$): δ = 7.67 (tosylate counter ion), 7.18 (tosylate counter ion), 4.33 (s, 2H, H-1), 3.46 (br. m, 80H, H-7/H-8), 2.79-2.71 (m, 4H, H-2/H-5), 2.71-2.59 (m, 4H, H-3/H-9), 2.36 (s, tosylate counterion), 2.14-2.07 (br. m, 63H, H-6/H-10), 1.86 (s, 2H, H-4) ppm;

FT-IR (ATR): $\tilde{\upsilon}$ = 3439 (br. w , ν(N-H)), 2939 (w, ν(C-H)), 1735 (m, ν(C=O, COOH)), 1619 (vs, ν(C=O)), 1479 (w), 1417 (s), 1364 (m), 1212 (m), 1121 (w), 1032 (m), 1010 (m), 819 (w), 753 (m), 681 (w) cm^{-1}.

Table 8: Calculated and attained molecular weight of α telechelic functionalized COOH-PMeOxn-SEt in experiment I-II.

experiment	polymer	Mn (theo.) [g·mol^{-1}]	Mn (exp.)* [g·mol^{-1}]	Mn (exp.)** [g·mol^{-1}]	Mw (exp.)** [g·mol^{-1}]	Đ**
I	**COOH-$PMeOx_{20}$-SEt**	1910	1910	1871	1918	1.03
II	**COOH-$PMeOx_{20}$-SEt**	1910	1910	1930	1960	1.02

*determined by ^{1}H-NMR-spectroscopy in $CDCl_3$, **determined by SEC in DMF (1 mL·min^{-1}, PEG standard).

As an example, the elugram of experiment I is shown:

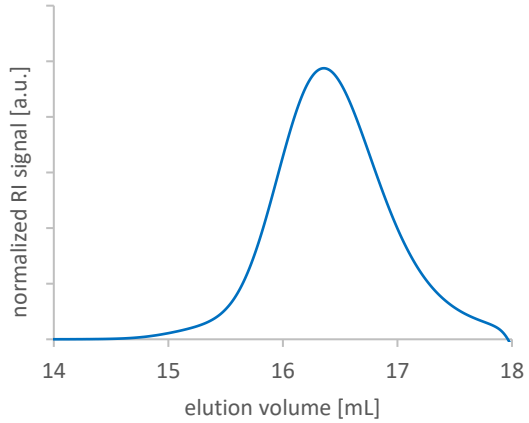

Figure 97: SEC elugram of experiment I.

Chapter 6.2.11 Synthesis of ω Telechelic Thioester Functionalized Poly(2-methyl-2-oxazoline)

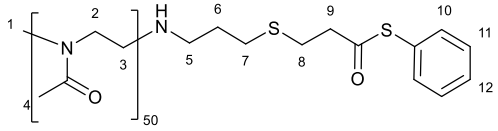

In a flame-dried flask, 1.46 g (0.46 mmol, 1.00 eq.) carboxylic acid functionalized PMeOx and 61.0 µL (56.2 mg, 0.56 mmol, 1.20 eq.) *N*-methylmorpholine are dried for 90 min over 4 Å molecular sieve in 10 mL chloroform and 5 mL THF. 66.2 µL (69.5 mg, 0.51 mmol, 1.10 eq.) isobutylchloroformate are added and the reaction mixture is stirred for another 15 min. 57.1 µL (61.1 mg, 0.56 mmol, 1.20 eq.) thiophenol are added, followed by another 61.0 µL (56.2 mg, 0.56 mmol, 1.20 eq.) *N*-methylmorpholine and the reaction mixture is stirred at RT overnight.

The reaction mixture is filtered to remove molecular sieves and the raw product is precipitated four times in 100 mL cold diethyl ether. Between the precipitation steps, solvent is decanted and the residue is taken up in 5 mL $CHCl_3$. After the last time precipitating, solvent is removed in vacuo.

^{1}H-NMR ($CDCl_3$): δ = 7.69 (tosylate counter ion), 7.41 (s, 5H, H-10/H-11/H-12), 7.18 (tosylate counter ion), 4.20 (t, isobutyl chloroformate by-product), 3.98 (d, isobutyl chloroformate by-product), 3.46 (br. s, 4nH, H-2/H-3), 3.04 (m, 3H, H-1), 2.94-2.92 (m, 4H, H-5/H-9), 2.83-2.81 (m, isobutyl chloroformate by-product), 2.70-2.55 (m, 4H, H-6/H-7/H-8), 2.36 (tosylate counter ion), 2.14-2.08 (br. m, 3nH, H-4) ppm;

FT-IR (ATR): $\tilde{\upsilon}$ = 3443 (br. w), 2936 (w, ν(C-H)), 1698 (w, ν(C=O, COSPh), 1628 (vs, C=O)), 1477 (w), 1416 (s), 1362 (m), 1239 (m), 1207 (m), 1116 (m), 1011 (m), 757 (w) cm^{-1}.

Table 9: Calculated and determined mol. weight of telechelic thioester functionalized $PMeOx_n$-COSPh in experiment I-IX.

experiment	polymer	M_n (theo.) [g·mol^{-1}]	M_n (exp.)* [g·mol^{-1}]	M_n (exp.)** [g·mol^{-1}]	M_w (exp.)** [g·mol^{-1}]	Đ**
I	**$PMeOx_{15}$-COSPh**	1546	1460	1467	1676	1.14
II	**$PMeOx_{25}$-COSPh**	2397	2312	2323	2454	1.06
III	**$PMeOx_{25}$-COSPh**	2397	2397	2329	2433	1.05
IV	**$PMeOx_{38}$-COSPh**	3503	3418	3433	3620	1.05
V	**$PMeOx_{50}$-COSPh**	4525	4440	4395	4649	1.06
VI	**$PMeOx_{50}$-COSPh**	4525	4440	4427	4672	1.06
VII	**$PMeOx_{50}$-COSPh**	4525	4525	4404	4638	1.05
VIII	**$PMeOx_{100}$-COSPh**	8780	8780	8612	8937	1.04
IX	**$PMeOx_{150}$-COSPh**	13035	12950	12650	13870	1.06

*determined by ^{1}H-NMR-spectroscopy in $CDCl_3$, **determined by SEC in DMF (1 mL·min^{-1}, PEG standard).

As examples, the elugrams of experiment II and VI are shown:

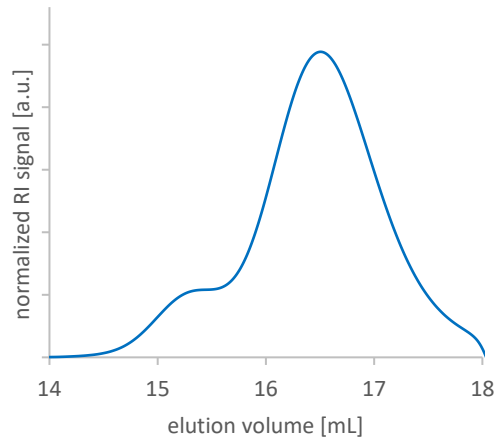

Figure 98: SEC elugram of experiment II.

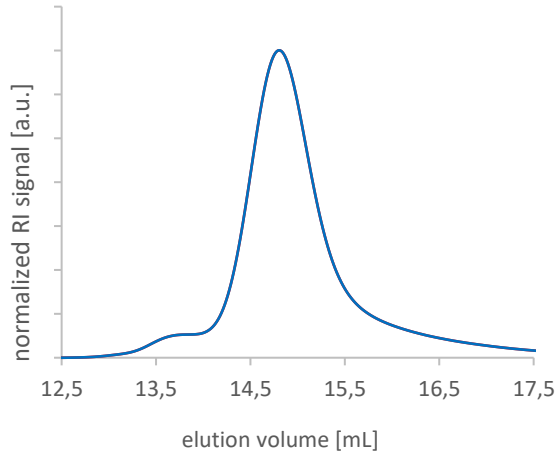

Figure 99: SEC elugram of experiment VI.

Chapter 6.2.12 Synthesis of α Telechelic Thioester Functionalized Poly(2-methyl-2-oxazoline)

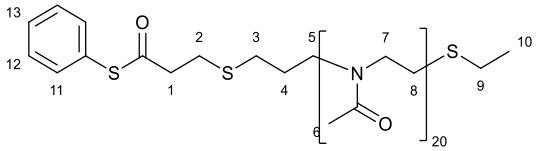

In a flame-dried flask, 2.00 g (1.05 mmol, 1.00 eq.) carboxylic acid functionalized COOH-PMeOx$_{20}$-SEt and 138 µL (127 mg, 1.26 mmol, 1.20 eq.) *N*-methylmorpholine are dried for 90 min over 4 Å molecular sieve in 15 mL chloroform and 5 mL THF. 150 µL (157 mg, 1.15 mmol, 1.10 eq.) isobutylchloroformate are added and the reaction mixture is stirred for another 15 min. 129 µL (138 mg, 1.26 mmol, 1.20 eq.) thiophenol are added, followed by another 138 µL (127 mg, 1.26 mmol, 1.20 eq.) *N*-methylmorpholine and the reaction mixture is stirred at RT overnight.

The reaction mixture is filtered to remove molecular sieves and the raw product is precipitated three times in 100 mL cold diethyl ether. Between the precipitation steps, solvent is decanted and the residue is taken up in 5 mL $CHCl_3$. After the last time precipitating, solvent is removed in vacuo.

^{1}H-NMR ($CDCl_3$): δ = 7.71 (tosylate counter ion), 7.40 (s, 5H, H-11/H-12/H-13), 7.18 (tosylate counter ion), 4.37 (s, 2H, H-1), 4.13 (t, isobutyl chloroformate by-product), 3.96 (d, isobutyl chloroformate by-product), 3.46 (br. s, 80H, H-7/H-8), 2.93-2.91 (m, 4H, H-2/H-5), 2.84 (s, isobutyl chloroformate by-product), 2.55-2.53 (m, 4H, H-3/H-5), 2.35 (tosylate counter ion), 2.13-2.06 (br. m, 63H, H-6/H-10), 1.85 (s, 2H, H-4) ppm;

FT-IR (ATR): $\tilde{\upsilon}$ = (br. w , ν(N-H)), 2939 (w, ν(C-H)), 1737 (w, (C=O), COSPh), (1621 (vs, ν(C=O)), 1478 (w), 1417 (vs), 1364 (m), 1237 (m), 1115 (m), 1032 (m), 1010 (m), 753 (w), 682 (w) cm^{-1}.

Table 10: Calculated and attained molecular weight of α telechelic functionalized COSPh-PMeOx$_n$-SEt in experiment I-V.

experiment	polymer	M_n (theo.) [g·mol^{-1}]	M_n (exp.)* [g·mol^{-1}]	M_n (exp.)** [g·mol^{-1}]	M_w (exp.)** [g·mol^{-1}]	Đ**
I	**COSPh-PMeOx$_{20}$-SEt**	2003	2003	1912	2170	1.14
II	**COSPh-PMeOx$_{20}$-SEt**	2003	2003	1954	2208	1.13
III	**COSPh-PMeOx$_{20}$-SEt**	2003	2003	1893	2142	1.13
IV	**COSPh-PMeOx$_{20}$-SEt**	2003	1960	-	-	-
V	**COSPh-PMeOx$_{20}$-SEt**	2003	2003	-	-	-

*determined by ^{1}H-NMR-spectroscopy in $CDCl_3$, **determined by SEC in DMF (1 mL·min^{-1}, PEG standard).

As an example, the elugram of experiment III is shown:

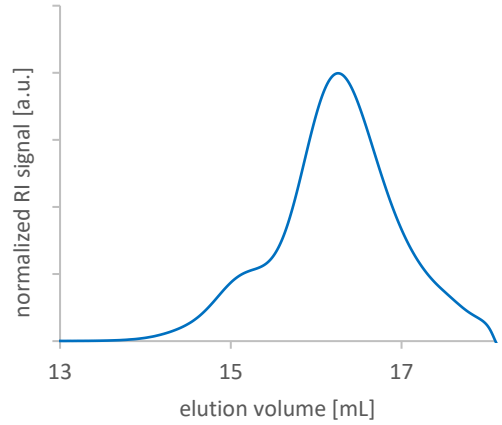

Figure 100: SEC elugram of experiment III.

Chapter 6.2.13 Synthesis of ω Telechelic $PMeOx_{50}$-CGGGF

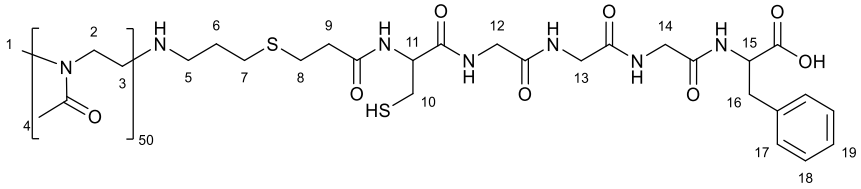

20.0 mg (45.5 µmol, 2.06 eq.) CGGGF peptide are dissolved in 1.5 mL MeOH and 5.00 mg (0.13 mmol, 5.88 eq.) sodium borohydride are added. Gas formation and heat development is observed. 100 mg (22.1 µmol, 1.00 eq.) thioester functionalized $PMeOx_{50}$-COSPh are dissolved in 1.5 mL MeOH and added to the peptide solution. The reaction mixture is stirred for 4 d at RT.

The raw product is precipitated three times in 50 mL cold diethyl ether. Between the precipitation steps, solvent is decanted and the residue is taken up in 2 mL MeOH/$CHCl_3$. After the last time precipitating, solvent is removed in vacuo.

^{1}H-NMR (MeOD): δ = 7.71 (d, tosylate counterion), 7.21 (s, H-17/H-18/H-19), 7.15 (tosylate counterion), 4.47 (s, H-15), 3.93-3.88 (m, H-12/H-13/H-14), 3.53 (br. s, 4nH, H-2/H-3), 3.22-3.17 (m, H-11), 3.11-3.07 (m, 3H, H-1), 3.00-2.95 (m, H-16), 2.79-2.62 (m, H-5/H-7/H-8/H-9/H-10), 2.37 (s, tosylate counterion), 2.15-2.11 (br. m, 3nH, H-4), 1.94-1.92 (m, 2H, H-6) ppm;

FT-IR (ATR): $\tilde{\upsilon}$ = 3271 (br. w, ν(O-H), peptide carboxylic acid), 2976 (w ν(C-H)), 2936 (w, ν(C-H)), 1628 (vs, ν(C=O)), 1541 (m, ν(N-H), peptide amide), 1478 (w), 1416 (vs), 1363 (m, ν(C-N) amide), 1324 (w), 1239 (m), 1199 (m), 1120 (m), 1031 (w), 1011 (m), 927 (w), 761 (w), 681 (w) cm^{-1}.

Chapter 6.2.14 Synthesis of α Telechelic CGGGF-PMeOx$_{20}$-SEt

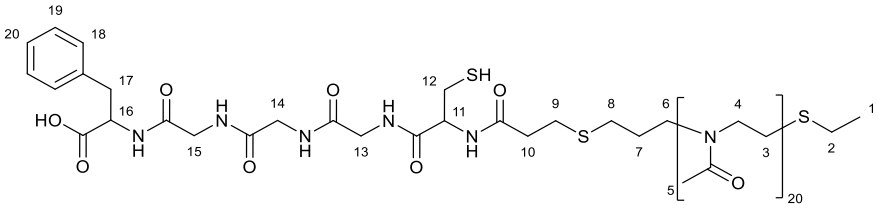

43.9 mg (100 µmol, 1.00 eq.) CGGGF peptide are dissolved in 1 mL MeOH. 200 mg (100 µmol, 1.00 eq.) thioester functionalized COSPh-PMeOx$_{20}$-SEt are dissolved in 1 mL MeOH and added to the peptide solution. 7.61 mg (0.20 mmol, 2.00 eq.) sodium borohydride are added. Gas formation and heat development is observed. The reaction mixture is stirred for 24 h at RT.

The raw product is precipitated three times in 40 mL cold diethyl ether. Between the precipitation steps, solvent is decanted and the residue is taken up in 2 mL MeOH/$CHCl_3$. After the last time precipitating, solvent is removed in vacuo.

The raw product is dialysed against water (cut-off: 1000 g·mol^{-1}) for 4 d. After dialysis, solvent is removed via lyophilisation.

^{1}H-NMR (DMSO-*d6*): δ = 8.10-7.29 (br. m, NH/NH_2), 7.19 (s, 5H, H-18/H-19/H-20), 4.55 (s, 1H, H-16), 4.32 (s, 2H, H-10), 4.09-3.70 (m, 6H, H-13/H-14/H-15), 3.35 (br. s, 4nH, H-3/H-4), 3.03-2.57 (m, 13H, H-2/H-6/H-8/H-9/H-11/H-12/H-17), 2.00-1.97 (br. m, 3nH+3, H-5/H-1), 1.80-1.77 (m, 2H, H-7) ppm;

FT-IR (ATR): $\tilde{\upsilon}$ = 3448 (br. w, ν(N-H)), 3305 (w, ν(O-H)), 2937 (w, ν(C-H)), 1736 (w), 1626 (vs, ν(C=O)), 1550 (w, (ν(N-H) peptide amide), 1478 (w), 1417 (s), 1364 (w), 1324 (w), 1240 (m), 1213 (w), 1013 (m), 980 (w), 928 (w), 758 (w), 702 (w) cm^{-1}.

Chapter 6.2.15 Synthesis of ω Telechelic PMeOx$_{50}$-CKFKFQF

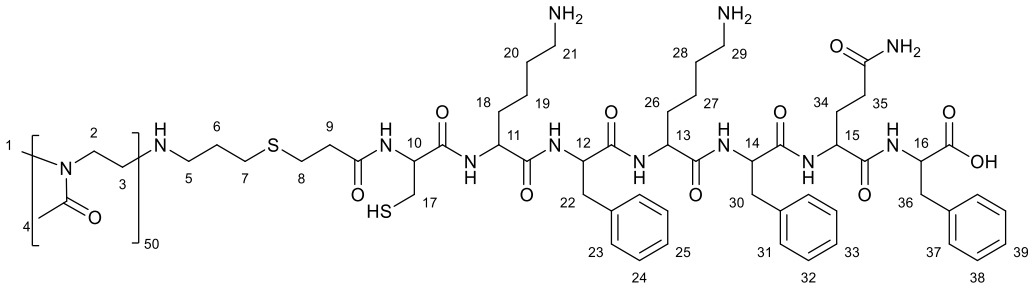

58.3 mg (61.6 µmol, 1.39 eq.) CKFKFQF peptide are dissolved in 1 mL DMSO and 4.69 mg (0.12 mmol, 2.71 eq.) sodium borohydride are added. Gas formation and heat development is observed. 200 mg (44.2 µmol, 1.00 eq.) thioester functionalized PMeOx$_{50}$-COSPh are dissolved in 1 mL DMSO and added to the peptide solution. The reaction mixture is stirred for 24 h at RT.

The raw product is precipitated three times in 50 mL cold diethyl ether. Between the precipitation steps, solvent is decanted and the residue is taken up in 3 mL DMSO. After the last time precipitating, solvent is removed in vacuo. The product is taken up in 9 mL water and dialysed against water (cut-off: 1000 g·mol^{-1}) for 6 d. After dialysis, solvent is removed via lyophilisation.

^{1}H-NMR (DMSO-*d6*): δ = 8.08-7.88 (br. m, NH/NH$_2$) 7.20 (s, phenylalanine aromatic ring), 6.75 (s, NH), 5.07-4.17 (m, NH, peptide backbone), 3.34 (br. s, DMSO, polymer backbone), 3.06-2.20 (m, initiator methyl group, polymer ω-terminal alkyl chain CH$_2$, peptide side chain CH$_2$), 2.01-1.97 (br. m, polymer side chain methyl groups), 1.80-1.77 (m, peptide side chain CH$_2$), 1.41 (br. s, dialysis artefact signal), 1.23-0.87 (m, lysine side chain CH$_2$) ppm;

FT-IR (ATR): $\tilde{\upsilon}$ = 3273 (br. w), 2935 (w, ν(C-H)), 2383 (w), 2316 (w), 1630 (vs, ν(C=O)), 1545 (m, ν(N-H) peptide amide), 1480 (w), 1416 (m), 1365 (w), 1239 (m, ν(C-N) peptide amide), 1169 (m), 1012 (m), 924 (w), 743 (w), 698 (m) cm^{-1}.

Chapter 6.2.16 Synthesis of ω Telechelic $PMeOx_{50}$-CGGWYKYW

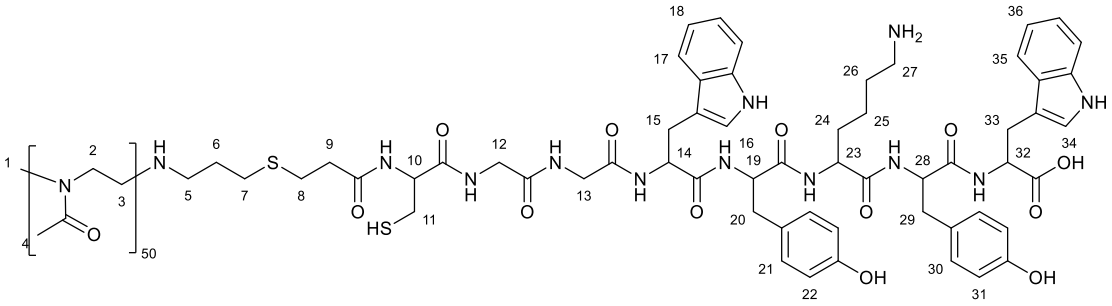

235 mg (221 µmol, 1.00 eq.) CGGWYKYW peptide are dissolved in 4 mL MeOH. 1.00 g (221 µmol, 1.00 eq.) thioester functionalized $PMeOx_{50}$-COSPh are dissolved in 4 mL MeOH and added to the peptide solution. The reaction mixture is stirred for 24 h at 65 °C.

The raw product is dialysed against water (cut-off: 1000 g·mol^{-1}) for 4 d. After dialysis, solvent is removed via lyophilisation.

^{1}H-NMR (DMSO-*d6*): δ = 10.73 (d, tryptophan NH), 9.11-7.86 (br. m, NH/NH_2), 7.56-6.56 (m, tryptophan and tyrosine aromatic rings), 4.44-3.70 (m, peptide backbone), 3.33 (br. s, DMSO, polymer backbone), 2.98-2.01 (m, initiator CH_3 group, polymer alkyl chain CH_2, peptide side chain CH_2), 2.01-1.97 (br. m, polymer side chain methyl groups), 1.44-0.89 (m, lysine side chain CH_2) ppm;

FT-IR (ATR): $\tilde{\upsilon}$ = 3416 (br. w, ν(N-H)), 3283 (w, ν(O-H)), 2939 (w, ν(C-H)), 1618 (vs, ν(C=O)), 1516 (w, ν(N-H) peptide amide), 1480 (w), 1417 (s), 1362 (w), 1325 (w), 1291 (w), 1242 (m), 1203 (w), 1123 (w), 1012(w), 1012 (m), 928 (w), 746 (w) cm^{-1}.

Chapter 6.2.17 Synthesis of α Telechelic CGGWYKYW-PMeOx$_{20}$-SEt

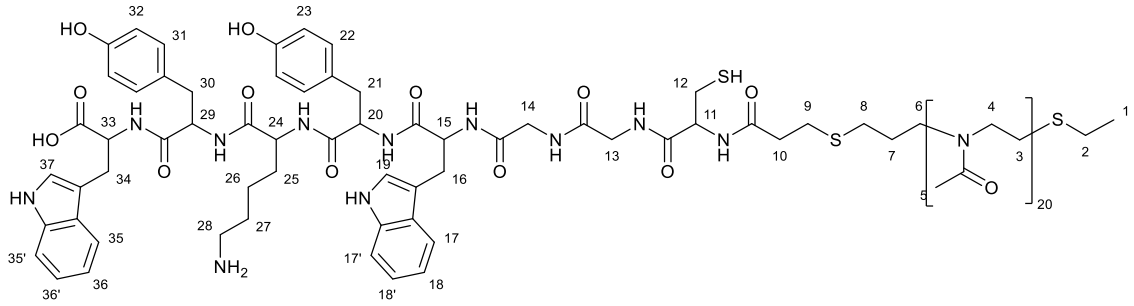

212 mg (200 µmol, 1.00 eq.) CGGWYKYW peptide are dissolved in 3 mL MeOH. 400 mg (200 µmol, 1.00 eq.) thioester functionalized COSPh-PMeOx$_{20}$-SEt are dissolved in 3 mL MeOH and added to the peptide solution. The reaction mixture is stirred for 24 h at 65 °C.

The raw product is dialysed against water (cut-off: 1000 g·mol^{-1}) for 4 d. After dialysis, solvent is removed via lyophilisation.

^{1}H-NMR (DMSO-*d6*): δ = 10.71 (d, tryptophan NH), 9.11-7.90 (br. m, NH/NH$_2$), 7.56-6.56 (m, tryptophan and tyrosine aromatic rings), 4.48-3.60 (m, peptide backbone), 3.34 (br. s, DMSO, polymer backbone), 3.07-2.66 (m, polymer alkyl chain CH$_2$, peptide side chain CH$_2$), 1.99-1.97 (br. m, polymer side chain methyl groups, polymer CH$_3$ ω end group), 1.77 (br. s, dialysis artefact signal), 1.41-0.87 (m, lysine side chain CH$_2$) ppm;

FT-IR (ATR): $\tilde{\upsilon}$ = 3282 (br. m, ν(O-H)), 2938 (w, ν(C-H)), 1732 (m), 1615 (vs, ν(C=O)), 1515 (m, ν(N-H) peptide amide), 1482 (w), 1419 (s), 1363 (m), 1238 (m), 1122 (w), 1033 (m), 1011 (m), 931 (w), 801 (w), 745 (m), 682 (m) cm^{-1}.

Chapter 6.2.18 Synthesis of Conjugate Between PEG-SH and Allylpentafluorobenzene

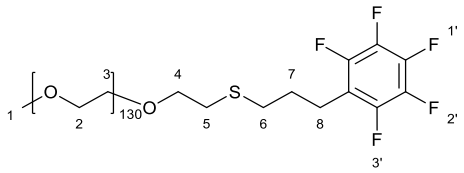

100 mg (16.7 µmol, 1.00 eq.) PEG-SH and 4.78 mg (16.7 µmol, 1.00 eq.) TCEP·HCl are dissolved in 200 µL MeOD and stirred at RT for 60 min. 2.56 µL (3.48 mg, 16.7 µmol, 1.00 eq.) allylpentafluorobenzene and 2.14 mg (8.33 µmol, 0.5 eq.) DMPA are added. The reaction mixture is stirred for 60 min under UV light irradiation.

10 mL water are added and the reaction mixture is dialysed against water for 5 d (cut-off: 1000 g·mol^{-1}) and dried via lyophilisation for 5 d.

^{1}H-NMR (D_2O): δ = 3.98 (satellite signal), 3.74 (br. m, 526H, H-2/H-3/H-4/H-7/H-8), 3.49 (satellite signal), 3.41 (s, 3H, H-1), 2.99 (t, *J* = 6.1 Hz, 4H, H-5/H-6) ppm;

^{19}F-NMR (MeOD): δ = -145.95 (d, *J* = 24.2 Hz, 2F, F-3'), -160.44 (m, 1F, F-1'), -165.54 (m, 2F, F-2') ppm.

Chapter 6.2.19 Synthesis of Conjugate Between PEG-SH and Acetylated Allyl Mannose

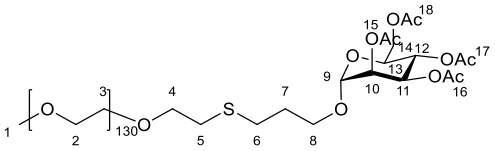

100 mg (16.7 µmol, 1.00 eq.) PEG-SH and 4.78 mg (16.7 µmol, 1.00 eq.) TCEP·HCl are dissolved in 200 µL D_2O and stirred at RT for 60 min. 6.47 mg (16.7 µmol, 1.00 eq.) acetylated allyl mannose and 2.14 mg (8.33 µmol, 0.5 eq.) DMPA are added. The reaction mixture is stirred for 60 min under UV light irradiation.

10 mL water are added and the reaction mixture is dialysed against water for 5 d (cut-off: 1000 $g \cdot mol^{-1}$) and dried via lyophilisation for 5 d.

^{1}H-NMR (D_2O): δ = 5.38-5.34 (m, 3nH, H-10/H-11/H-12), 5.26 (s, 1nH, H-9), 4.32-4.21 (m, 5nH H-8/H-13/H-14), 3.97 (satellite signal), 3.87 (m, 2H, H-4), 3.74 (br. s, 520H, H-2/H-3), 3.49 (satellite signal), 3.41 (s, 3H, H-1), 2.99 (m, 4nH, H-6/H-7), 2.83 (m, 2nH, H-5'), 2.79-2.74 (t, J = 6.1 Hz, 2-2nH, H-5), 2.24-1.07 (m, 12nH, H-15/ H-16/H-17/ H-18) ppm;

FT-IR (ATR): $\tilde{\upsilon}$ = 2881 (s, v(C-H)), 1979 (w, v(C-H)), 1749 (w, v(C=O) acetyl sugar), 1631 (br. w), 1467 (s), 1414 (w), 1359 (w), 1341 (s), 1279 (m), 1240 (m), 1146 (m), 1097 (vs, v(-C-O-C)), 1060 (m), 960 (s), 842 (s) cm^{-1}.

Chapter 6.2.20 Synthesis of Telechelic Thiol Functionalized Poly(2-methyl-2-oxazoline)

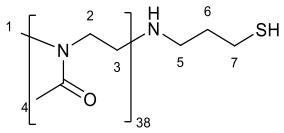

1.00 g (0.30 mmol, 1.00 eq.) allyl functionalized $PMeOx_{38}$ is dissolved in 1.00 mL MeOD. 97.3 µL (104 mg, 1.36 mmol, 4.50 eq.) thioacetic acid and 58.2 mg (0.23 mmol, 0.75 eq.) DMPA are added. The reaction mixture is stirred for 60 min under UV radiation.

The polymer is precipitated three times in 60 mL cold diethyl ether. Between the precipitation steps, solvent is decanted and the residue is taken up in 3 mL MeOH. After the last time precipitating, solvent is removed in vacuo and the yield of 530 mg raw product is redissolved in 5 mL MeOH.

40.9 mg (0.232 mmol, 0.23 mmol, 1.50 eq.) cysteine hydrochloride monohydrate and 17.7 mg (0.47 mmol, 3.00 eq.) sodium borohydride are added while stirring. Gas formation and heat development is observed. A strong characteristic odor of thiophenol emerges.

After 120 min, 10 mL water and 30 mg TCEP·HCl are added and the reaction mixture is dialysed for 2.5 d (cut-off: 1000 $g \cdot mol^{-1}$) against degassed water and dried via lyophilisation for 5 d.

^{1}H-NMR (MeOD): δ = 3.60-3.53 (br. m, 154H, H-2/H-3/H-5), 3.07-2.96 (m, 3H, H-1), 2.15-2.12 (br. m, 114H, H-4), 1.94 (m, 2H, H-7), 1.29 (m, 2H, H-6), 1.18 (m, 1H, S-H) ppm;

FT-IR (ATR): $\tilde{\upsilon}$ = 3440 (br. w, v(N-H)), 2938 (w, v(C-H)), 1620 (vs, v(C=O)), 1478 (w), 1416 (vs), 1362 (m), 1322 (w), 1291 (w), 1240 (m), 1205 (w), 1012 (m), 762 (w) cm^{-1}.

Chapter 6.2.21 Synthesis of Conjugate Between $PMeOx_{38}$-SH and Acetylated Allyl Mannose

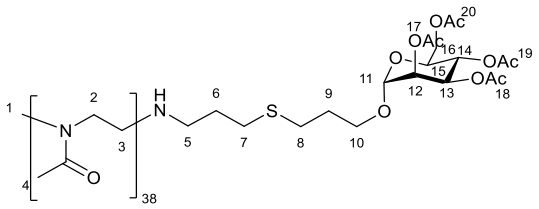

100 mg (33.4 µmol, 1.00 eq.) $PMeOx_{38}$-SH and 17.0 mg (59.3 µmol, 1.78 eq.) TCEP·HCl are dissolved in 700 µL D_2O. 17.4 mg (44.8 µmol, 1.34 eq.) acetylated allyl mannose and 6.00 mg (26.7 µmol, 0.80 eq.) Irgacure 2959 are added. The reaction mixture is stirred for 70 min under UV light irradiation.

The reaction mixture is dialysed against water for 3 d (cut-off: 1000 $g \cdot mol^{-1}$) and dried via lyophilisation.

^{1}H-NMR ($CDCl_3$): δ = 5.26-5.20 (m, 3nH, H-12/H-13/H-14), 4.86-4.79 (m, 1nH, H-11), 4.30-3.98 (m, 5nH, H-10/H-15/H-16), 3.45 (br. s, 154H, H-2/H-3/H-5), 3.04-2.95 (m, 3H, H-1), 2.10 (br. m, 114H+9nH, H-4/H-17/H-18/H-19/H-20), 2.35-2.29 (m, 2H+2nH, H-7/H-8), 1.20 (m, 2H+2nH, H-6/H-9) ppm;

FT-IR (ATR): $\tilde{\upsilon}$ = 3451 (br. w, ν(N-H)), 2937 (w, ν(C-H)), 1754 (w, ν(C=O) acetyl sugar), 1624 (vs, ν(C=O)), 1477 (w), 1416 (vs), 1363 (m), 1322 (w), 1291 (w), 1238 (m), 1012 (m), 925 (w), 763 (w) cm^{-1}.

Chapter 6.2.22 Synthesis of $PMeOx_{50}$-CGGGF-AcMan

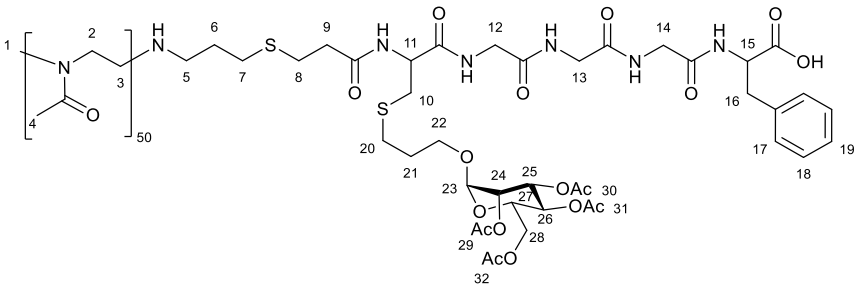

100 mg (20.6 µmol, 1.00 eq.) $PMeOx_{50}$-CGGGF and 9.63 mg (33.6 µmol, 1.63 eq.) TCEP·HCl are dissolved in 1.5 mL D_2O. 10.9 mg (28.0 µmol, 1.36 eq.) acetylated allyl mannose and 3.77 mg (16.8 µmol, 0.82 eq.) Irgacure 2959 are added. The reaction mixture is stirred for 60 min under UV light irradiation.

The reaction mixture is dialysed against water for 4 d (cut-off: 1000 $g \cdot mol^{-1}$) and dried via lyophilisation.

^{1}H-NMR (MeOD): δ = 7.23 (s, 5H, H-17/H-18/H-19), 5.27-5.23 (m, 3H, H-24/H-25/H-26), 4.83 (br. s, H-23/deuterated solvent signal), 4.47 (s, 2H, H-15), 4.26 (s, 2H, H-22), 4.13-3.95 (m, 3H, H-27/H-28), 3.93-3.85 (m, 6H, H-12/H-13/H-14), 3.62-3.53 (br. m, 4nH, H-2/H-3), 3.11-3.06 (m, 3H, H-1), 2.95 (m, 3H, H-16/H-11), 2.78-2.30 (m, 14H, H-5/H-6/H-7/H-8/H-9/H-10/H-21), 2.15-1.90 (br. m, 3nH+14H, H-4/H-20/ H-29/H-30/H-31/H-32) ppm;

FT-IR (ATR): $\tilde{\upsilon}$ = 3443 (br. w, ν(N-H)), 2937 (w, ν(C-H)), 1744 (w, ν(C=O) acetyl sugar), 1631 (vs, ν(C=O)), 1539 (w, ν(N-H) peptide amide), 1477 (w), 1417 (vs), 1364 (m), 1322 (w), 1291 (w), 1239 (m), 1211 (w), 1012 (m), 924 (w), 763 (m), 702 (w) cm^{-1}.

Chapter 6.2.23 Synthesis of Man-CGGGF-PMeOx$_{20}$-SEt

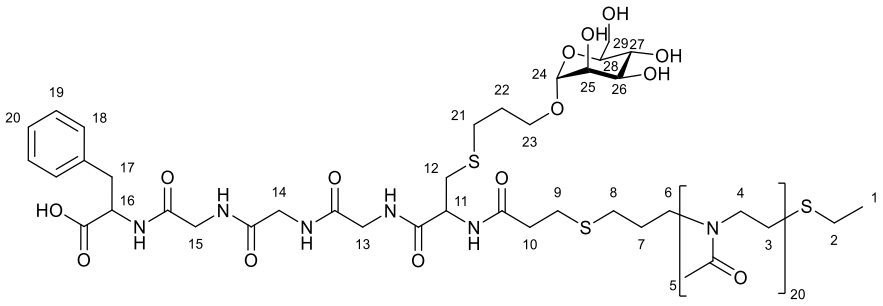

100 mg (42.6 µmol, 1.00 eq.) CGGGF-PMeOx$_{20}$-SEt and 10.0 mg (34.9 µmol, 0.82 eq.) TCEP·HCl are dissolved in 0.2 mL D_2O and 0.6 mL MeOD. 9.38 mg (42.6 µmol, 1.00 eq.) allyl mannose and 5.74 mg (25.6 µmol, 0.60 eq.) Irgacure 2959 are added. The reaction mixture is stirred for 60 min under UV light irradiation.

The reaction mixture is dialysed against water for 4 d (cut-off: 1000 g·mol^{-1}) and dried via lyophilisation.

^{1}H-NMR (MeOD): δ = 8.15-7.08 (br. m, H-18/H-19/H-20), 4.66 (m, H-24), 4.57 (s, H-16), 4.23-3.72 (m, H-10/H-13/H-14/H-15/H-25/H-26/H-27/H-28/H-29), 3.53 (br. s, H-3/H-4), 3.05-2.59 (m, H-2/H-6/H-8/H-9/H-11/H-12/H-17/H-21/H-23), 2.15-2.05 (br. m, H-5/H-1), 1.94-1.87 (m, H-7/H-22) ppm;

FT-IR (ATR): $\tilde{\upsilon}$ = 3425 (br. w, ν(N-H)), 2938 (w, ν(C-H)), 1734 (w), 1624 (vs, ν(C=O)), 1544 (w, ν(N-H) peptide amide), 1479 (w), 1418 (vs), 1364 (m), 1318 (w), 1241 (m), 1211 (w), 1083 (w), 1013 (m), 926 (w), 760 (w), 700 (m) cm^{-1}.

Chapter 6.2.24 Synthesis of PMeOx$_{50}$-CGGWYKYW-AcMan

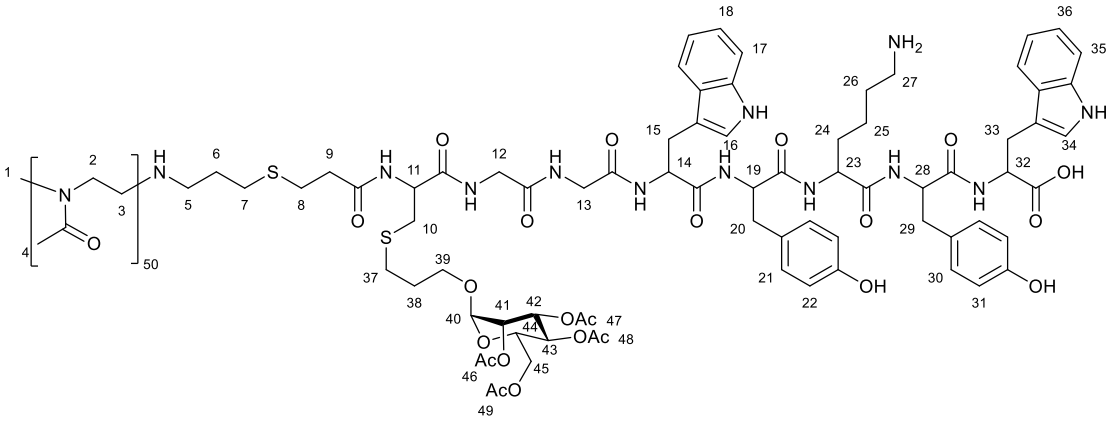

250 mg (45.5 µmol, 1.00 eq.) PMeOx$_{50}$-CGGWYKYW and 10.0 mg (34.9 µmol, 0.77 eq.) TCEP·HCl are dissolved in 0.5 mL D_2O and 0.8 mL DMSO. 17.7 mg (45.5 µmol, 1.00 eq.) acetylated allyl mannose and 6.13 mg (27.3 µmol, 0.60 eq.) Irgacure 2959 are added. The reaction mixture is stirred for 90 min under UV light irradiation.

The reaction mixture is dialysed against water for 4 d (cut-off: 1000 g·mol^{-1}) and dried via lyophilisation.

^{1}H-NMR (DMSO-*d6*): δ = 8.11-6.59 (m, tryptophan and tyrosine aromatic rings), 5.16-4.85 (m, sugar ring), 4.22-3.71 (m, peptide backbone, sugar ring), 3.32 (br. s, DMSO, polymer backbone), 2.92-2.24 (m, initiator CH_3 group, polymer alkyl chain CH_2, peptide side chain CH_2, sugar CH_2 chain), 2.05-1.92 (br. m, polymer side chain methyl groups, sugar acetyl signals), 1.36-0.80 (m, lysine side chain CH_2) ppm;

FT-IR (ATR): $\tilde{\upsilon}$ = 3452 (br. w, v(N-H)), 2941 (w, v(C-H)), 1743 (w, v(C=O) acetyl sugar)), 1623 (vs, v(C=O)), 1516 (w, v(N-H) peptide amide), 1478 (w), 1417 (vs), 1363 (m), 1291 (w), 1240 (m), 1209 (w), 1031 (w), 1012 (m), 926 (w), 761 (m) cm^{-1}.

Chapter 6.2.25 Synthesis of AcMan-CGGWYKYW-PMeOx$_{20}$-SEt

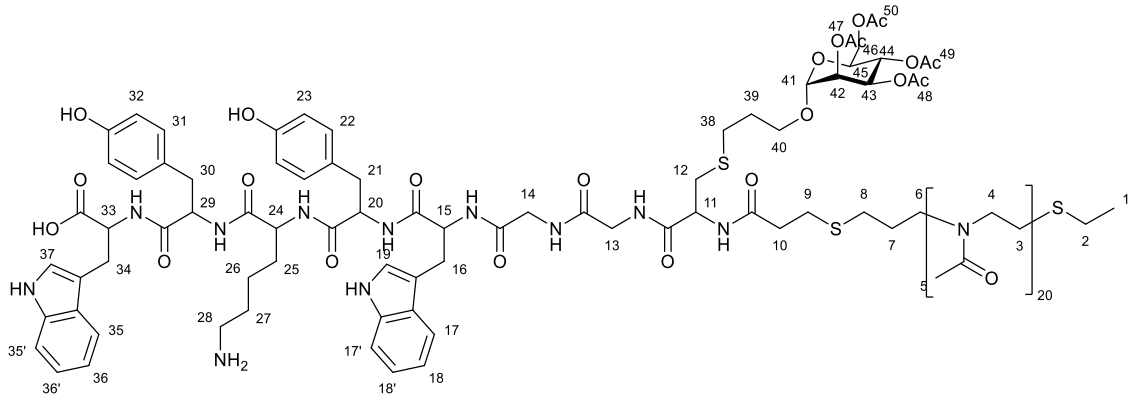

22.6 mg (7.65 µmol, 1.00 eq.) CGGWYKYW-PMeOx$_{20}$-SEt and 5.00 mg (17.5 µmol, 2.28 eq.) TCEP·HCl are dissolved in 0.6 mL D_2O and 0.4 mL DMSO. 2.97 mg (7.65 µmol, 1.00 eq.) acetylated allyl mannose and 1.03 mg (4.59 µmol, 0.60 eq.) Irgacure 2959 are added. The reaction mixture is stirred for 60 min under UV light irradiation.

The reaction mixture is dialysed against water for 3 d (cut-off: 1000 g·mol^{-1}) and dried via lyophilisation.

^{1}H-NMR (DMSO-*d6*): δ = 10.74 (s, tryptophan NH), 9.12-7.99 (br. m, NH/NH_2), 7.56-6.59 (m, tryptophan and tyrosine aromatic rings), 5.14-5.10 (m, sugar ring), 4.48-3.60 (m, peptide backbone), 3.33 (br. s, DMSO, polymer backbone), 2.83-2.60 (m, polymer alkyl chain CH_2, peptide side chain CH_2, sugar CH_2 chain), 1.99-1.78 (br. m, polymer side chain methyl groups, polymer CH_3 ω end group, sugar acetyl signals), 1.23-0.87 (m, lysine side chain CH_2) ppm;

FT-IR (ATR): $\tilde{\upsilon}$ = 3402 (br. w, ν(N-H)), 3291 (br. w, ν(O-H)), 2938 (w, ν(C-H)), 1736 (w, ν(C=O) acetyl sugar)), 1620 (vs, ν(C=O)), 1516 (w, ν(N-H) peptide amide), 1480 (w), 1419 (vs), 1365 (m), 1322 (w), 1241 (s), 1034 (w), 1014 (m), 927 (w), 751 (m) cm^{-1}.

Chapter 6.2.26 Synthesis of Man-CGGWYKYW-PMeOx$_{20}$-SEt

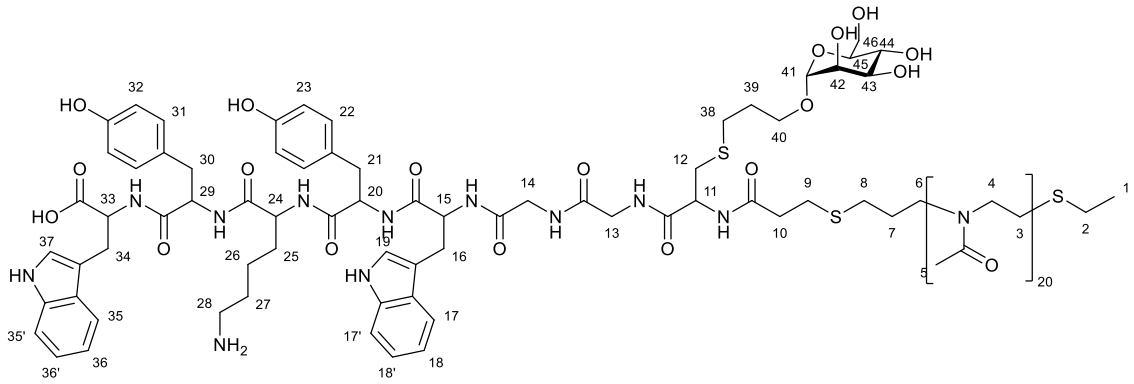

150 mg (50.8 µmol, 1.00 eq.) CGGWYKYW-PMeOx$_{20}$-SEt and 10.0 mg (34.9 µmol, 0.69 eq.) TCEP·HCl are dissolved in 0.6 mL D_2O and 0.4 mL DMSO. 11.2 mg (50.8 µmol, 1.00 eq.) allyl mannose and 6.84 mg (30.5 µmol, 0.60 eq.) Irgacure 2959 are added. The reaction mixture is stirred for 60 min under UV light irradiation.

The reaction mixture is dialysed against water for 4 d (cut-off: 1000 g·mol^{-1}) and dried via lyophilisation.

^{1}H-NMR (DMSO-*d6*): δ = 10.72 (s, tryptophan NH), 9.10-7.98 (br. m, NH/NH$_2$), 7.98-6.57 (m, tryptophan and tyrosine aromatic rings), 4.59 (anomeric sugar signal), 4.48-3.60 (m, peptide backbone), 3.91-3.77 (m, sugar ring), 3.34 (br. s, DMSO, polymer backbone), 2.86-2.61 (m, polymer alkyl chain CH$_2$, peptide side chain CH$_2$, sugar CH$_2$ chain), 2.01-1.97 (br. m, polymer side chain methyl groups, polymer CH$_3$ ω end group, sugar acetyl signals), 1.80-0.87 (m, lysine side chain CH$_2$) ppm;

FT-IR (ATR): $\tilde{\upsilon}$ = 3281 (br. w, ν(O-H)), 2938 (w, ν(C-H)), 1729 (w), 1622 (vs, ν(C=O)), 1516 (w, ν(N-H) peptide amide), 1480 (w), 1419 (s), 1364 (m), 1315 (w), 1240 (m), 1101 (w), 1032 (w), 1013 (m), 922 (w), 804 (w), 748 (m), 700 (w) cm^{-1}.

Chapter 6.2.27 Synthesis of *N*-Succinimidyl-4-pentenate

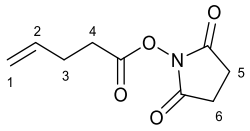

Following a procedure by Gress et al. [230], 15.0 mL (14.7 g, 147 mmol, 1.00 eq.) 4-pentenoic acid and 33.8 g (176 mmol, 1.20 eq.) 1-ethyl-3-(3-dimethylaminopropyl)carbodiimide are dissolved in 600 mL dichloromethane under argon atmosphere. After 10 minutes, 27.0 g (235 mmol, 1.60 eq.) *N*-hydroxysuccinimide are added and the reaction mixture is stirred at RT overnight.

Solvent is removed in vacuo and the residue is dissolved in 200 mL diethyl ether. The organic phase is washed five times with 60 mL water. The organic phase is dried over $MgSO_4$ and solvent is removed in vacuo. A colourless, low viscous liquid remains, which crystallizes while cooling to RT.

Yield: 28.6 g (145 mmol, 99 %, lit.[230] 88 %);

^{1}H-NMR ($CDCl_3$): δ = 5.88-5.75 (m, 1H, H-2), 5.13-3.02 (m, 2H, H-1), 2.79 (s, 4H, H-5/H-6), 2.70-2.65 (m, 2H, H-4), 2.48-2.38 (m, 2H, H-3) ppm.

Chapter 6.2.28 Synthesis of *N*-(2-Chloroethyl)-4-pentenamide

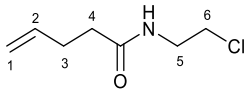

Following a procedure by Gress et al. [230], 27.2 g (138 mmol, 1.00 eq.) *N*-succinimidyl-4-pentenate are dissolved in 200 mL dichloromethane and cooled to 0 °C. In a second flask, 32.0 g (276 mmol, 2.00 eq.) chloroethyl amine hydrochloride are dissolved in 100 mL water, also cooled to 0 °C and 11.0 g (276 mmol, 2.00 eq.) sodium hydroxide are added. The solution is then dropwise added to the first flask and stirred at RT overnight.

The organic phase is washed four times with 80 mL water, dried over $MgSO_4$ and solvent is removed in vacuo. A colourless, low viscous liquid remains.

Yield: 19.7 g (122 mmol, 88 %, lit.[230] 88 %);

^{1}H-NMR ($CDCl_3$): δ = 6.00 (br. s, 1H, N-H), 5.88-5.75 (m, 1H, H-2), 5.11-4.99 (m, 2H, H-1), 3.63-3.55 (m, 4H, H-5/H-6), 2.43-2.27 (m, 4H, H-3/H-4) ppm.

Chapter 6.2.29 Synthesis of 2-(3-Butenyl)-2-oxazoline

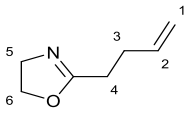

Under argon atmosphere, 36.9 g (228 mmol, 1.00 eq.) *N*-(2-chloroethyl)-4-pentenamide are dissolved in 60 mL dry methanol. In a second flask, 14.7 g (262 mmol, 1.15 eq.) ground potassium hydroxyde are dissolved in 60 mL dry methanol under argon atmosphere. Both solutions are flushed with argon for 10 minutes. The solutions are mixed and stirred at 100 °C under reflux overnight.

The reaction mixture is filtered and solvent is removed in vacuo. The residue is dissolved in 200 mL dichloromethane and washed four times with 80 mL water. The organic phase is dried over $MgSO_4$ and solvent is removed in vacuo. 20 mg of CaH_2 are added to the raw product and the reaction mixture is stirred at RT overnight. The product is purified via distillation and a colourless liquid remains.

Yield: 15.8 g (126 mmol, 55 %, lit.[230] 53 %);

^{1}H-NMR ($CDCl_3$): δ = 5.84-5.71 (m, 1H, H-2), 5.03-4.91 (m, 2H, H-1), 4.15 (t, *J* = 9.5 Hz, 2H, H-4), 3.72 (t, *J* = 9.4 Hz, 2H, H-3), 2.30 (s, 4H, H-5/H-6) ppm.

Chapter 6.2.30 Synthesis of Side Chain Allyl Functionalized P(MeOx$_{45}$-*co*-ButenOx$_5$)

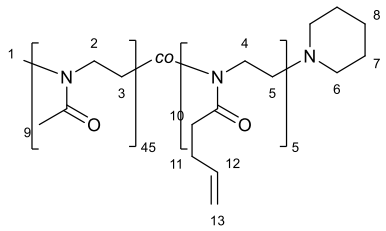

Under argon atmosphere, 150 mg (0.81 mmol, 1.00 eq.) dried methyl *p*-toluenesulfonate are dissolved in 10 mL acetonitrile and 3.08 g (3.07 mL, 36.2 mmol, 45.0 eq.) 2-methy-2-oxazoline and 504 mg (4.03 mmol, 5.00 eq.) 2-butenyl-2-oxazoline are added. The reaction mixture is stirred for 60 min at 100 °C in a microwave reactor. Afterwards, 206 mg (239 µL, 2.42 mmol, 3.00 eq.) piperidine are added and the reaction mixture is stirred at RT for 18 h.

The raw product is precipitated four times in 100 mL cold diethyl ether. Between the precipitation steps, solvent is decanted and the residue is taken up in 5 mL MeOH/$CHCl_3$. After the last time precipitating, solvent is removed in vacuo.

^{1}H-NMR ($CDCl_3$): δ = 7.70 (tosylate counter ion), 7.18 (tosylate counter ion), 5.81 (m, 1mH, H-12), 5.07-5.01 (m, 2mH, H-13), 3.44 (br. s, 4nmH, H-2/H-3/H-4/H-5), 3.03-2.94 (m, 3H, H-1), 2.45-2.35 (m, 4nH, H-10/H-11/tosylate counter ion), 2.13-2.06 (m, 3nH, H-9), 1.78 (m, 4H, H-6), 1.57 (m, 4H, H-7), 1.44 (m, 4H, H-8) ppm;

FT-IR (ATR): $\tilde{\upsilon}$ = 3454 (br. w), 2937 (w, ν(C-H)), 1622 (vs, ν(C=O)), 1476 (w), 1416 (vs), 1362 (m) 1322 (w), 1239 (m), 1206 (m), 1121 (w), 1032 (w), 1010 (m), 921 (w), 750 (m), 681 (w) cm^{-1}.

Table 11: Calculated and attained molecular weight of side chain allyl functionalized polyoxazolines in experiment I-VIII.

experiment	polymer	M_n (theo.) [g·mol^{-1}]	M_n (exp.)* [g·mol^{-1}]	M_n (exp.)** [g·mol^{-1}]	M_w (exp.)** [g·mol^{-1}]	Đ**
I	**P(MeOx$_{45}$-*co*-ButenOx$_5$)**	4555	4345	4526	4649	1.03
II	**P(MeOx$_{45}$-*co*-ButenOx$_5$)**	4555	4214	4417	4610	1.04
III	**P(MeOx$_{16}$-*co*-ButenOx$_4$)**	1962	1876	1885	2064	1.09
IV	**P(MeOx$_{40}$-*co*-ButenOx$_{10}$)**	4755	4630	4698	4874	1.04
V	**P(MeOx$_{30}$-*co*-ButenOx$_{20}$)**	5156	5093	5072	5196	1.02
VI	**P(MeOx$_{95}$-*co*-ButenOx$_5$)**	8810	8515	8654	9116	1.05
VII	**P(MeOx$_{475}$-*co*-ButenOx$_{25}$)**	43654	39399	38980	42350	1.09
VIII	**P(MeOx$_{475}$-*co*-ButenOx$_{25}$)**	43654	43228	41630	45010	1.08

*determined by ^{1}H-NMR-spectroscopy in $CDCl_3$, **determined by SEC in DMF (1 mL·min^{-1}, PEG standard).

As examples, the elugrams of experiment I, V, VI and VII are shown:

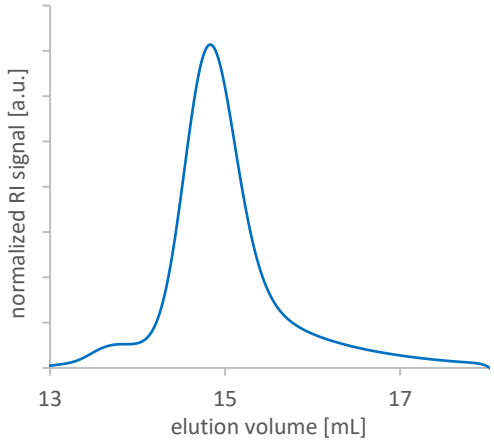

Figure 101: SEC elugram of experiment I.

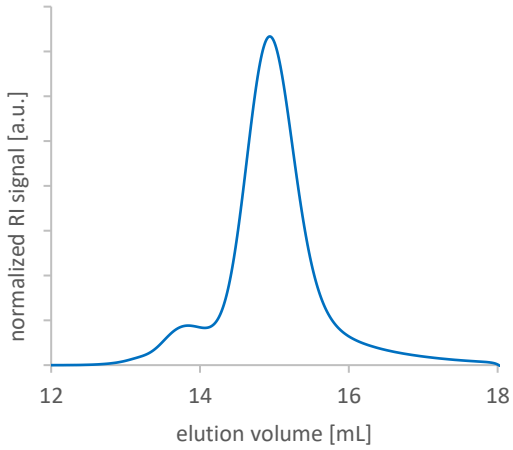

Figure 102: SEC elugram of experiment V.

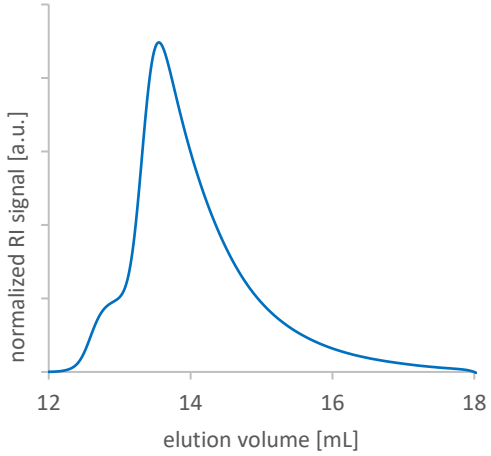

Figure 103: SEC elugram of experiment VI.

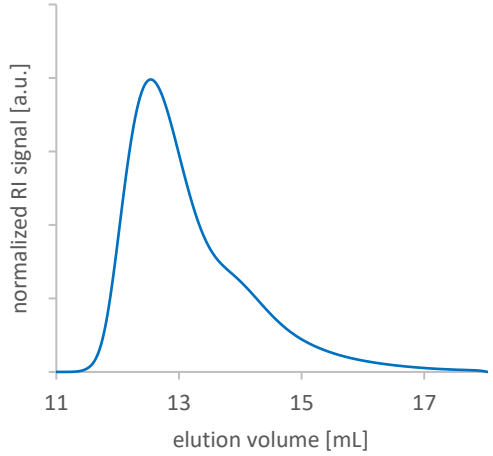

Figure 104: SEC elugram of experiment VII.

Chapter 6.2.31 Synthesis of Side Chain Carboxylic Acid Functionalized P(MeOx$_{45}$-*co*-ButOx-COOH$_5$)

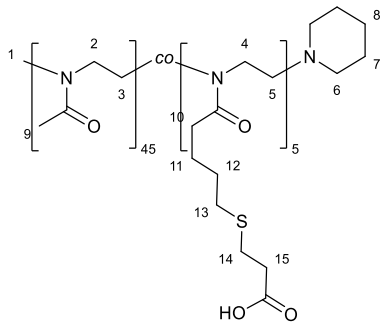

1.00 g (0.22×5 mmol, 1.00 eq.) allyl functionalized P(MeOx$_{45}$-*co*-ButenOx$_5$) and 350 mg (285 µL, 3.30 mmol, 3.00 eq.) 3-mercaptopropionic acid are dissolved in 2 mL MeOH and the solution was flushed with argon for 10 minutes. 141 mg (0.55 mmol, 0.50 eq.) DMPA are added and the reaction mixture is stirred for 90 min under UV light irradiation.

The raw product is precipitated four times in 100 mL cold diethyl ether. Between the precipitation steps, solvent is decanted and the residue is taken up in 5 mL MeOH/$CHCl_3$. After the last time precipitating, solvent is removed in vacuo.

^{1}H-NMR ($CDCl_3$): δ = 7.69 (tosylate counter ion), 7.19 (tosylate counter ion), 3.48-3.46 (br. m, 4nmH, H-2/H-3/H-4/H-5), 3.04 (m, 3H, H-1), 2.75 (m, 2mH, H-15), 2.57 (m, 4mH, H-10/H-14), 2.41-2.28 (m, 2mH, H-13/tosylate counter ion), 2.14-2.07 (br. m, 3nH, H-9), 1.97-1.77 (m, 10H, H-6/H-7/H-8), 1.65 (br. s, 4mH, H-11/H-12) ppm;

FT-IR (ATR): $\tilde{\upsilon}$ = 3440 (br. w, ν(N-H)), 2936 (w, ν(C-H)), 1720 (m, ν(C=O) carboxylic acid), 1622 (vs, ν(C=O)), 1477 (w), 1416 (vs), 1363 (m, ν(C-N) amide), 1325 (w), 1238 (m), 1206 (m), 1122 (w), 1032 (w), 1010 (m), 922 (w), 761 (m), 681 (w) cm^{-1}.

Table 12: Calculated and attained mol. weight of side chain carboxylic acid functionalized polyoxazolines in experiment I-VIII.

experiment	polymer	M_n (theo.) [g·mol^{-1}]	M_n (exp.)* [g·mol^{-1}]	M_n (exp.)** [g·mol^{-1}]	M_w (exp.)** [g·mol^{-1}]	Đ**
I	**P(MeOx$_{45}$-*co*-ButOx-COOH$_5$)**	5086	4660	4893	6914	1.41
II	**P(MeOx$_{45}$-*co*-ButOx-COOH$_5$)**	5086	5000	8344	8991	1.08
III	**P(MeOx$_{45}$-*co*-ButOx-COOH$_5$)**	5086	5086	8736	9547	1.09
IV	**P(MeOx$_{45}$-*co*-ButOx-COOH$_5$)**	5086	5086	8961	9598	1.07
V	**P(MeOx$_{16}$-*co*-ButOx-COOH$_4$)**	2386	2301	N/C	N/C	N/C
VI	**P(MeOx$_{40}$-*co*-ButOx-COOH$_{10}$)**	5817	5731	N/C	N/C	N/C
VII	**P(MeOx$_{30}$-*co*-ButOx-COOH$_{20}$)**	7279	7297	N/C	N/C	N/C
VIII	**P(MeOx$_{95}$-*co*-ButOx-COOH$_5$)**	9341	9341	N/C	N/C	N/C

*determined by ^{1}H-NMR-spectroscopy in $CDCl_3$, **determined by SEC in DMF (1 mL·min^{-1}, PEG standard).

As discussed in chapter 4.3.1.3, the strong interactions of the attached carboxylic acid groups with the column material lead to broad elution curves, severe tailing behaviour and unambiguous measuring results. As examples, the elugrams of experiment I, III and VIII are shown:

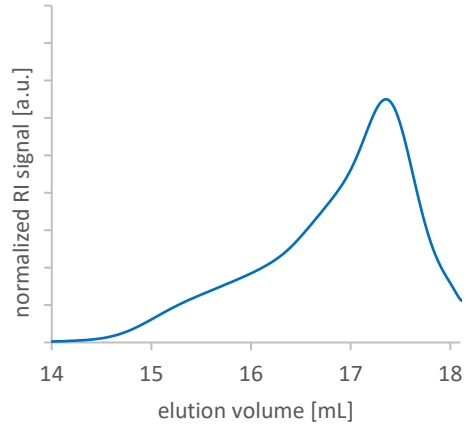

Figure 105: SEC elugram of experiment I.

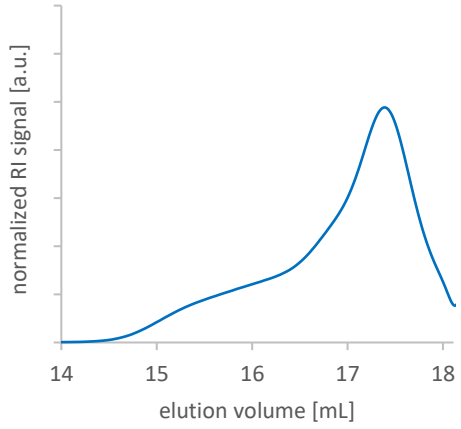

Figure 106: SEC elugram of experiment III.

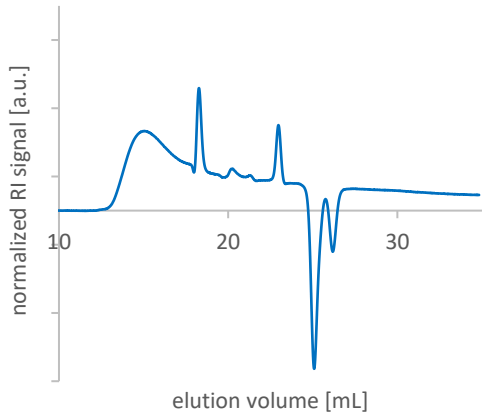

Figure 107: SEC elugram of experiment VIII.

Chapter 6.2.32 Synthesis of Side Chain Thioester Functionalized P(MeOx$_{45}$-*co*-ButenOx-COSPh$_5$)

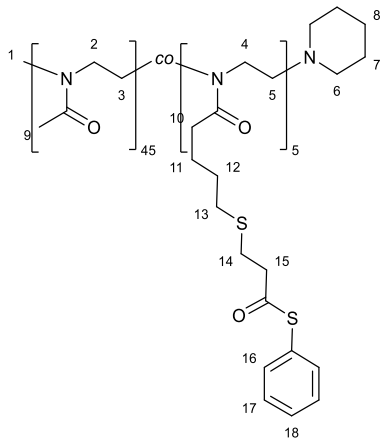

In a flame-dried flask, 0.83 g (0.21×5 mmol, 1.00 eq.) carboxylic acid functionalized P(MeOx$_{45}$-*co*-ButEnOx-COOH$_5$) and 137 µL (126 mg, 1.24 mmol, 1.20 eq.) *N*-methylmorpholine are stirred for 90 min over 4 Å molecular sieve in 10 mL chloroform and 5 mL THF. 148 µL (155 mg, 1.14 mmol, 1.10 eq.) isobutyl chloroformate are added and the reaction mixture is stirred for another 15 min. 128 µL (137 mg, 1.24 mmol, 1.20 eq.) thiophenol are added, followed by another 137 µL (126 mg, 1.24 mmol, 1.20 eq.) *N*-methylmorpholine and the reaction mixture is stirred at RT overnight.

The reaction mixture is filtered to remove molecular sieve and the raw product is precipitated four times in 100 mL cold diethyl ether. Between the precipitation steps, solvent is decanted and the residue is taken up in 5 mL $CHCl_3$, respectively MeOH. After the last time precipitating, solvent is removed in vacuo.

^{1}H-NMR ($CDCl_3$): δ = 7.72 (tosylate counter ion), 7.39 (s, 5mH, H-16/H-17/H-18), 7.18 (tosylate counter ion), 4.19 (t, isobutyl chloroformate by-product), 3.92 (d, isobutyl chloroformate by-product), 3.47-3.45 (br. m, 4nmH, H-2/H-3/H-4/H-5), 3.03 (m, 3H, H-1), 2.91-2.89 (m, isobutyl chloroformate by-product), 2.80 (m, 4mH, H-10/H-15), 2.55 (m, 4mH, H-14), 2.40-2.26 (m, 2mH, H-13/tosylate counter ion), 2.12-2.06 (br. m, 3nH, H-9), 1.93-1.78 (m, 10H, H-6/H-7/H-8), 1.64 (br. s, 4mH, H-11/H-12) ppm;

FT-IR (ATR): $\tilde{\upsilon}$ = 3428 (br. w, ν(N-H)), 2934 (w, ν(C-H)), 1703 (w, ν(C=O), COSPh), 1629 (vs, ν(C=O)), 1476 (w), 1416 (vs), 1363 (m), 1324 (w), 1237 (m , ν(C-N) amide), 1207 (m), 1113 (m), 1031 (w), 1012 (m), 865 (w), 752 (m), 690 (w) cm^{-1}.

Table 13: Calculated and attained mol. weight of side chain carboxylic acid functionalized polyoxazolines in experiment I-VIII.

experiment	polymer	M_n (theo.) [g·mol^{-1}]	M_n (exp.)* [g·mol^{-1}]	M_n (exp.)** [g·mol^{-1}]	M_w (exp.)** [g·mol^{-1}]	Đ**
I	P(MeOx$_{45}$-*co*-ButOx-COSPh$_5$)	5546	5461	5356	5673	1.05
II	P(MeOx$_{45}$-*co*-ButOx-COSPh$_5$)	5546	5546	5398	6177	1.14
III	P(MeOx$_{45}$-*co*-ButOx-COSPh$_5$)	5546	5223	5367	5577	1.04
IV	P(MeOx$_{45}$-*co*-ButOx-COSPh$_5$)	5546	5138	5473	5851	1.07
V	P(MeOx$_{16}$-*co*-ButOx-COSPh$_4$)	2755	2670	2553	2876	1.13
VI	P(MeOx$_{40}$-*co*-ButOx-COSPh$_{10}$)	6738	6330	6349	6854	1.08
VII	P(MeOx$_{30}$-*co*-ButOx-COSPh$_{20}$)	9122	8475	9007	9279	1.03
VIII	P(MeOx$_{95}$-*co*-ButOx-COSPh$_5$)	9802	9802	9592	9911	1.03

*determined by ^{1}H-NMR-spectroscopy in $CDCl_3$, **determined by SEC in DMF (1 mL·min^{-1}, PEG standard).

As examples, the elugrams of experiment I and VI are shown:

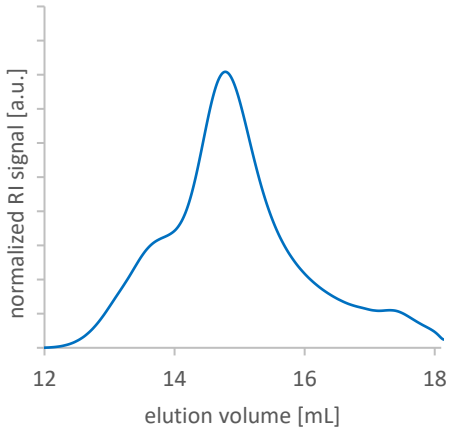

Figure 108: SEC elugram of experiment I.

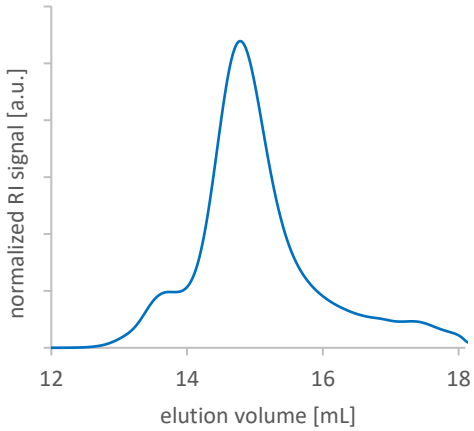

Figure 109: SEC elugram of experiment VI.

Chapter 6.2.33 Synthesis of Side Chain CGGGF Polymer Conjugates

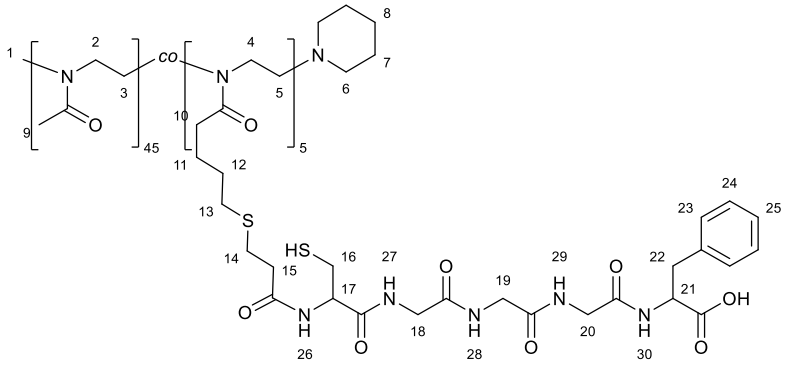

159 mg (0.36 mmol, 1.00 eq.) CGGGF peptide are dissolved in 1.5 mL MeOH and 27.5 mg (0.72 mmol, 2.00 eq.) sodium borohydride are added. Gas formation and heat development is observed. 400 mg (72.1×5 µmol, 1.00 eq.) thioester functionalized P($MeOx_{45}$-*co*-ButOx-$COSPh_5$) are dissolved in 3 mL MeOH and added to the peptide solution. The reaction mixture is stirred for 24 h at RT.

The raw product is precipitated three times in 100 mL cold diethyl ether. Between the precipitation steps, solvent is decanted and the residue is taken up in 5 mL MeOH/$CHCl_3$. After the last time precipitating, solvent is removed in vacuo. The product is taken up in 20 mL water and dialysed against water (cut-off: 1000 g·mol^{-1}) for 5 d. After dialysis, solvent is removed via lyophilisation.

^{1}H-NMR (MeOD): δ = 7.24 (s, 5mH, H-23/H-24/H-25), 4.58 (s, 1mH, H-21), 3.94-3.82 (m, 5mH, H-17/H-18/H-19), 3.53 (br. s, 4nmH, H-2/H-3/H-4/H-5), 3.23-3.18 (m, 2mH, H-20), 3.10-2.95 (m, 4mH+3, H-1/H-16/H-22), 2.78 (m, 2mH, H-10), 2.58 (m, 4mH, H-14/H-15), 2.46-2.36 (m, 2mH, H-13), 2.15-2.11 (br. m, 3nH, H-9), 1.95-1.79 (m, 10H, H-6/H-7/H-8), 1.66 (br. s, 4mH, H-11/H-12) ppm;

FT-IR (ATR): $\tilde{\upsilon}$ = 3293 (br. w, v(O-H), peptide carboxylic acid), 2934 (w, v(C-H)), 1627 (vs, v(C=O)), 1531 (m, v(N-H), peptide amide), 1478 (w), 1416 (vs), 1364 (m, v(C-N) amide), 1325 (w), 1238 (m), 1200 (m), 1121 (w), 1013 (w), 824 (w), 799 (w), 750 (m), 701 (w), 664 (w) cm^{-1}.

Chapter 6.2.34 Synthesis of Side Chain CKFKFQF Polymer Conjugates

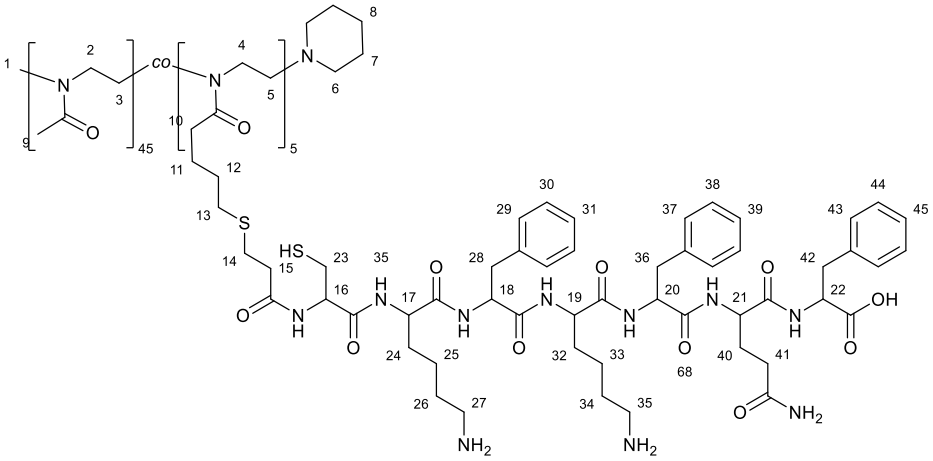

51.2 mg (54.1 µmol, 1.00 eq.) CKFKFQF peptide are dissolved in 2 mL DMSO and 4.11 mg (0.11 mmol, 2.00 eq.) sodium borohydride are added. Gas formation and heat development is observed. 60 mg (108×5 µmol, 1.00 eq.) thioester functionalized P(MeOx$_{45}$-*co*-ButOx-COSPh$_5$) are dissolved in 1 mL DMSO and added to the peptide solution. The reaction mixture is stirred for 24 h at RT.

The raw product is dialysed against water (cut-off: 1000 g·mol^{-1}) for 6 d. After dialysis, solvent is removed via lyophilisation.

^{1}H-NMR (DMSO-*d6*): δ = 8.08-6.75 (m, NH/NH$_2$/H-29/H-30/H-31/H-37/H-38/H-39/H-43/H-44/H-45), 5.07-4.20 (m, NH/H-16/H-17/H-18/H-19/H-20/H-21/H-22), 3.35 (br. s, DMSO, H-2/H-3/H-4/H-5), 3.06-2.64 (m, H-1/H-10/H-15/H-27/H-28/H-35/H-36/H-41/H-42), 2.32-2.27 (m, H-13/H-14/H-23), 2.01-1.97 (br. m, H-9), 1.80-1.61 (m, 10H, H-6/H-7/H-8/H-40), 1.52-1.05 (m, H-11/H-12/H-24/H-25/H-26/H-32/H-33/H-34) ppm;

FT-IR (ATR): $\tilde{\upsilon}$ = 3270 (br, w,), 2999 (w, ν(C-H)), 2916 (w, ν(C-H)), 2358 (w) , 2314 (w), 1631 (vs, ν(C=O)), 1547(m, ν(N-H), peptide amide), 1478 (w), 1417 (m), 1365 (m), 1313 (w), 1257 (w), 1201 (w), 1169 (m), 1125 (m), 1020 (vs), 953 (m), 823 (w), 800 (w), 745 (w), 700 (m) cm^{-1}.

Chapter 6.2.35 Synthesis of Side Chain CGGWYKYW Polymer Conjugates

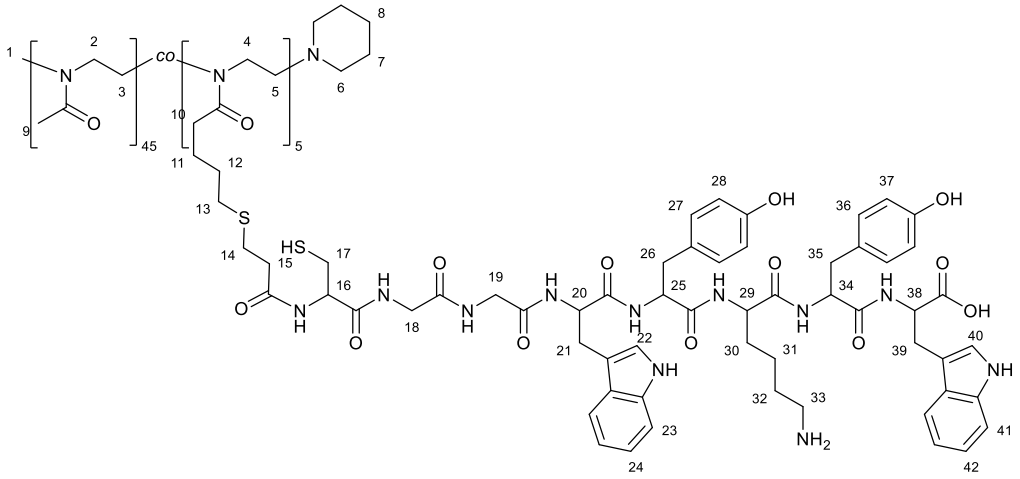

219 mg (206 µmol, 1.00 eq.) CGGWYKYW peptide are dissolved in 5 mL water and 2 mL acetic acid (30 %) are added. 200 mg (41.2×5 µmol, 1.00 eq.) thioester functionalized P(MeOx$_{45}$-*co*-ButOx-COSPh$_5$) are dissolved in 2 mL water and added to the peptide solution. Gel formation is observed. Another 0.5 mL acetic acid (30 %) are added and the gel dissolves. The reaction mixture is stirred for 24 h at 60 °C.

The raw product is dialysed against water (cut-off: 1000 g·mol^{-1}) for 3 d at 60 °C. After dialysis, solvent is removed via lyophilisation.

^{1}H-NMR (DMSO-*d6*): δ = 10.71 (d, tryptophan NH), 9.13-7.88 (br. m, NH/NH$_2$), 7.56-6.56 (m, tryptophan and tyrosine aromatic rings), 4.56-3.59 (m, peptide backbone), 3.32 (br. s, DMSO, polymer backbone), 3.07-2.66 (m, initiator methyl group, polymer alkyl chain CH$_2$, peptide side chain CH$_2$), 2.28-2.26 (polymer alkyl chain CH$_2$), 2.01-1.91 (br. m, polymer side chain methyl groups), 1.84-1.76 (m, piperidine ring CH$_2$), 1.51-1.24 (br. m, polymer alkyl chain CH$_2$, lysine side chain CH$_2$) ppm;

FT-IR (ATR): $\tilde{\upsilon}$ = 3279 (br. w, ν(O-H)), 2932 (w, ν(C-H)), 1625 (vs, ν(C=O)), 1541 (m, ν(N-H), peptide amide), 1480 (w), 1418 (vs), 1362 (m), 1236 (s, ν(C-N), amide), 1104 (w), 1012 (m), 930 (w), 880 (w), 827 (w), 744 (m) cm^{-1}.

Chapter 6.2.36 Synthesis of Side Chain CGGGF AcMan Polymer Conjugates

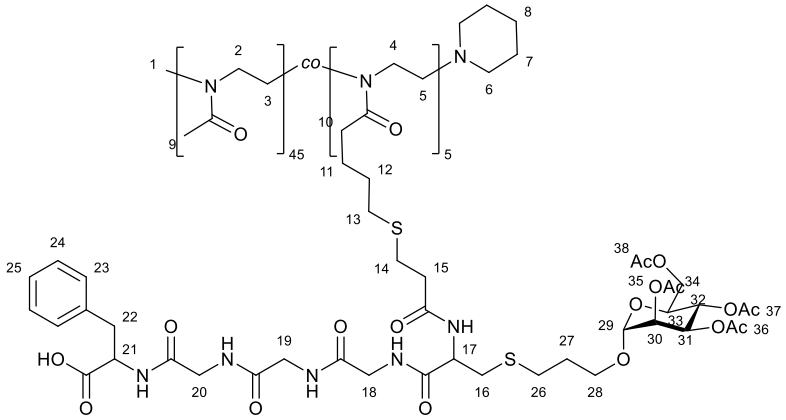

200 mg (139 µmol, 1.00 eq.) P(MeOx$_{45}$-*co*-ButOx-CGGGF$_5$) and 54.4 mg (190 µmol, 1.36 eq.) TCEP·HCl are dissolved in 1.0 mL D_2O. 61.4 mg (158 µmol, 1.14 eq.) acetylated allyl mannose and 21.3 mg (95.0 µmol, 0.68 eq.) Irgacure 2959 are added. The reaction mixture is stirred for 60 min under UV light irradiation.

The reaction mixture is dialysed against water for 4 d (cut-off: 1000 g·mol^{-1}) and dried via lyophilisation.

^{1}H-NMR (MeOD): δ = 7.44-7.19 (m, H-23/H-24/H-25), 5.25-5.23 (m, H-30/H-31/H-32), 4.83 (s, MeOD, H-29), 4.58 (s, H-21), 4.31-4.09 (H-28/H-33/H-34), 3.95-3.90 (m, H-18/H-19/H-20), 3.74-3.52 (br. m, H-2/H-3/H-4/H-5), 3.23-3.17 (m, H-17), 3.10-2.95 (m, H-1/H-22), 2.89-2.67 (m, H-15/H-16), 2.57 (m, H-10/H-14), 2.47-2.34 (m, H-13/H-26), 2.15-2.06 (br. m, H-9/H-35/H-36/H-37/H-38), 2.04-1.78 (m, H-6/H-7/H-8/H-27), 1.66 (br. s, H-11/H-12) ppm;

FT-IR (ATR): $\tilde{\upsilon}$ = 3293 (br. w, ν(O-H)), 2934 (w, ν(C-H)), 1743 (w, ν(C=O) acetyl sugar)), 1631 (vs, ν(C=O)), 1534 (m, ν(N-H) peptide amide), 1477 (w), 1416 (vs), 1364 (m), 1323 (w), 1236 (m), 1137 (w), 1032 (w), 1014 (m), 979 (w), 923 (w), 757 (m), 702 (m) cm^{-1}.

Chapter 6.2.37 Synthesis of Side Chain CGGWYKYW AcMan Polymer Conjugates

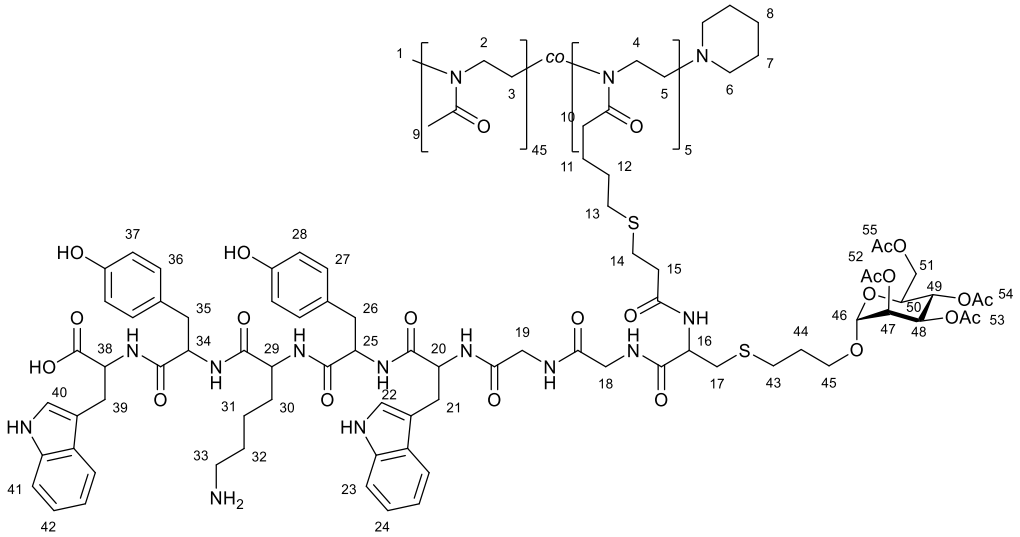

41.0 mg (19.9 µmol, 1.00 eq.) P(MeOx$_{45}$-*co*-ButOx-CGGWYKYW$_5$) and 10.0 mg (34.9 µmol, 1.76 eq.) TCEP·HCl are dissolved in 0.6 mL D_2O and 0.4 mL DMSO. 7.73 mg (19.9 µmol, 1.00 eq.) acetylated allyl mannose and 2.68 mg (11.9 µmol, 0.60 eq.) Irgacure 2959 are added. The reaction mixture is stirred for 60 min under UV light irradiation.

The reaction mixture is dialysed against water for 3 d (cut-off: 1000 g·mol^{-1}) and dried via lyophilisation.

^{1}H-NMR (DMSO-*d6*): δ = 10.72 (d, tryptophan NH), 9.13-7.98 (br. m, NH/NH_2), 7.56-6.57 (m, tryptophan and tyrosine aromatic rings), 5.09-4.85 (m, sugar ring), 4.48-3.59 (m, peptide backbone, sugar signals), 3.35 (br. s, DMSO, polymer backbone), 3.07-2.64 (m, initiator methyl group, polymer alkyl chain CH_2, peptide side chain CH_2), 2.39-2.27 (polymer and sugar alkyl chain CH_2), 2.01-1.97 (br. m, polymer side chain methyl groups, sugar acetyl groups), 1.89-1.51 (m, piperidine ring CH_2), 1.51-1.19 (br. m, polymer alkyl chain CH_2, lysine side chain CH_2) ppm;

FT-IR (ATR): $\tilde{\upsilon}$ = 3283 (br. w, ν(O-H)), 2935 (w, ν(C-H)), 1743 (w, ν(C=O) acetyl sugar)), 1623 (vs, ν(C=O)), 1515 (m, ν(N-H) peptide amide), 1481 (w), 1420 (vs), 1367 (m), 1238 (vs), 1175 (w), 1135 (w), 1037 (w), 1014 (w), 980 (w), 919 (w), 828 (w), 803 (w), 746 (m) cm^{-1}.

References

[1] D. F. Williams, *The Williams dictionary of biomaterials*, Liverpool University Press, **1999**.

[2] J. Park, R. S. Lakes, *Biomaterials: an introduction*, Springer Science & Business Media, **2007**.

[3] K. D. Jandt, *Advanced Engineering Materials* **2007**, *9*, 1035-1050.

[4] B. D. Ratner, A. S. Hoffman, F. J. Schoen, J. E. Lemons, *MRS Bull* **2006**, *31*, 59.

[5] G. T. Hermanson, *Bioconjugate techniques*, Academic press, **2013**.

[6] O. Koniev, A. Wagner, *Chemical Society Reviews* **2015**, *44*, 5495-5551.

[7] H.-A. Klok, *Macromolecules* **2009**, *42*, 7990-8000.

[8] M. A. Gauthier, H.-A. Klok, *Chemical Communications* **2008**, 2591-2611.

[9] D. Heinz, E. Amado, J. Kressler, *Polymers* **2018**, *10*, 960.

[10] B. V. K. J. Schmidt, *Polymers* **2019**, *11*, 693.

[11] S. Abbina, A. Parambath, in *Engineering of Biomaterials for Drug Delivery Systems* (Ed.: A. Parambath), Woodhead Publishing, **2018**, pp. 363-376.

[12] M. Barz, R. Luxenhofer, R. Zentel, M. J. Vicent, *Polymer Chemistry* **2011**, *2*, 1900-1918.

[13] M. Grube, M. N. Leiske, U. S. Schubert, I. Nischang, *Macromolecules* **2018**, *51*, 1905-1916.

[14] B. Gallot, *Progress in polymer science* **1996**, *21*, 1035-1088.

[15] R. Langer, D. A. Tirrell, *Nature* **2004**, *428*, 487.

[16] P. Bailon, W. Berthold, *Pharmaceutical Science & Technology Today* **1998**, *1*, 352-356.

[17] R. Duncan, *Nat Rev Drug Discov* **2003**, *2*, 347-360.

[18] A. S. Hoffman, P. S. Stayton, in *Macromolecular Symposia, Vol. 207*, Wiley Online Library, **2004**, pp. 139-152.

[19] P. Caliceti, F. M. Veronese, *Advanced drug delivery reviews* **2003**, *55*, 1261-1277.

[20] G. W. Vandermeulen, H. A. Klok, *Macromolecular Bioscience* **2004**, *4*, 383-398.

[21] A. S. Hoffman, *Clinical Chemistry* **2000**, *46*, 1478-1486.

[22] J. van Hest, B. Sumerlin, K. S. Anseth, M. Shoichet, S. Hammes-Schiffer, *Chemical Reviews* **2017**, *117*, 900-900.

[23] S. Zalipsky, *Bioconjugate chemistry* **1995**, *6*, 150-165.

[24] J. M. Harris, R. B. Chess, *Nature reviews Drug discovery* **2003**, *2*, 214-221.

[25] S. J. Bell, C. M. Fam, E. A. Chlipala, S. J. Carlson, J. I. Lee, M. S. Rosendahl, D. H. Doherty, G. N. Cox, *Bioconjugate chemistry* **2008**, *19*, 299-305.

[26] K. L. Heredia, H. D. Maynard, *Organic & Biomolecular Chemistry* **2007**, *5*, 45-53.

[27] J. Ohata, M. K. Miller, C. M. Mountain, F. Vohidov, Z. T. Ball, *Angewandte Chemie International Edition* **2018**, *57*, 2827-2830.

[28] B. A. Griffin, S. R. Adams, R. Y. Tsien, *Science* **1998**, *281*, 269-272.

[29] M. Fernández-Suárez, A. Y. Ting, *Nature reviews Molecular cell biology* **2008**, *9*, 929-943.

[30] H. G. Börner, *Progress in Polymer Science* **2009**, *34*, 811-851.

[31] Y. Miura, Y. Hoshino, H. Seto, *Chemical Reviews* **2016**, *116*, 1673-1692.

[32] S. S. Ting, G. Chen, M. H. Stenzel, *Polymer Chemistry* **2010**, *1*, 1392-1412.

[33] L. L. Kiessling, J. E. Gestwicki, L. E. Strong, *Current Opinion in Chemical Biology* **2000**, *4*, 696-703.

[34] M. Mammen, S.-K. Choi, G. M. Whitesides, *Angewandte Chemie International Edition* **1998**, *37*, 2754-2794.

[35] R. Haag, *Beilstein J. Org. Chem.* **2015**, *11*, 848-849.

[36] J.-F. Lutz, H. G. Börner, *Progress in Polymer Science* **2008**, *33*, 1-39.

[37] K. Kempe, C. Weber, K. Babiuch, M. Gottschaldt, R. Hoogenboom, U. S. Schubert, *Biomacromolecules* **2011**, *12*, 2591-2600.

[38] A. S. Hoffman, *Artificial Organs* **1995**, *19*, 458-467.

[39] M. A. van Dongen, C. A. Dougherty, M. M. Banaszak Holl, *Biomacromolecules* **2014**, *15*, 3215-3234.

[40] C. Chittasupho, *Therapeutic Delivery* **2012**, *3*, 1171-1187.

[41] B. Kang, T. Opatz, K. Landfester, F. R. Wurm, *Chemical Society Reviews* **2015**, *44*, 8301-8325.

[42] D. Pranantyo, L. Q. Xu, Z. Hou, E.-T. Kang, M. B. Chan-Park, *Polymer Chemistry* **2017**, *8*, 3364-3373.

[43] X. Yan, A. Sivignon, P. Alcouffe, B. Burdin, S. Favre-Bonté, R. Bilyy, N. Barnich, E. Fleury, F. Ganachaud, J. Bernard, *Chemical Communications* **2015**, *51*, 13193-13196.

[44] Z. Ma, X. X. Zhu, *Journal of Materials Chemistry B* **2019**, *7*, 1361-1378.

[45] F. Driessen, S. Martens, B. De Meyer, F. Du Prez, P. Espeel, *Macromolecular rapid communications* **2016**, *37*, 947-951.

[46] U. Tunca, *Macromolecular Chemistry and Physics* **2018**, *219*, 1800163.

[47] U. Tunca, *Journal of Polymer Science Part A: Polymer Chemistry* **2014**, *52*, 3147-3165.

[48] H. Durmaz, A. Sanyal, G. Hizal, U. Tunca, *Polymer Chemistry* **2012**, *3*, 825-835.

[49] P. Espeel, F. E. Du Prez, in *Multi-Component and Sequential Reactions in Polymer Synthesis*, Springer, **2014**, pp. 105-131.

[50] Y. Méndez, J. Chang, A. R. Humpierre, A. Zanuy, R. Garrido, A. V. Vasco, J. Pedroso, D. Santana, L. M. Rodríguez, D. García-Rivera, *Chemical science* **2018**, *9*, 2581-2588.

[51] L. Reguera, Y. Méndez, A. R. Humpierre, O. Valdés, D. G. Rivera, *Accounts of Chemical Research* **2018**, *51*, 1475-1486.

[52] A. E. de Nooy, G. Masci, V. Crescenzi, *Macromolecules* **1999**, *32*, 1318-1320.

[53] T. Ziegler, S. Gerling, M. Lang, *Angewandte Chemie International Edition* **2000**, *39*, 2109-2112.

[54] O. Kreye, T. Tóth, M. A. R. Meier, *Journal of the American Chemical Society* **2011**, *133*, 1790-1792.

[55] M. Schmitz, M. Kuhlmann, O. Reimann, C. P. R. Hackenberger, J. Groll, *Biomacromolecules* **2015**, *16*, 1088-1094.

[56] H. Schlaad, M. Antonietti, *The European Physical Journal E* **2003**, *10*, 17-23.

[57] H.-A. Klok, S. Lecommandoux, in *Peptide Hybrid Polymers*, Springer, **2006**, pp. 75-111.

[58] B. Le Droumaguet, K. Velonia, *Macromolecular Rapid Communications* **2008**, *29*, 1073-1089.

[59] H. Robson Marsden, A. Kros, *Macromolecular Bioscience* **2009**, *9*, 939-951.

[60] M. Morell, J. Puiggalí, *Polymers* **2013**, *5*, 188-224.

[61] P. Thordarson, B. Le Droumaguet, K. Velonia, *Applied microbiology and biotechnology* **2006**, *73*, 243-254.

[62] L. A. Canalle, D. W. P. M. Löwik, J. C. M. van Hest, *Chemical Society Reviews* **2010**, *39*, 329-353.

[63] J. Y. Shu, B. Panganiban, T. Xu, *Annual Review of Physical Chemistry* **2013**, *64*, 631-657.

[64] S. Slavin, J. Burns, D. M. Haddleton, C. R. Becer, *European Polymer Journal* **2011**, *47*, 435-446.

[65] H. Schlaad, in *Peptide hybrid polymers*, Springer, **2006**, pp. 53-73.

[66] G. Pasut, F. M. Veronese, *Progress in Polymer Science* **2007**, *32*, 933-961.

[67] H. Maeda, L. W. Seymour, Y. Miyamoto, *Bioconjugate chemistry* **1992**, *3*, 351-362.

[68] A. S. Hoffman, P. S. Stayton, V. Bulmus, G. Chen, J. Chen, C. Cheung, A. Chilkoti, Z. Ding, L. Dong, R. Fong, *Journal of Biomedical Materials Research* **2000**, *52*, 577-586.

[69] P. S. Stayton, A. S. Hoffman, M. El-Sayed, S. Kulkarni, T. Shimoboji, N. Murthy, V. Bulmus, C. Lackey, *Proceedings of the IEEE* **2005**, *93*, 726-736.

[70] C. De las Heras Alarcón, S. Pennadam, C. Alexander, *Chemical Society Reviews* **2005**, *34*, 276-285.

[71] M. S. Ganewatta, H. N. Lokupitiya, C. Tang, *Polymers* **2019**, *11*, 1176.

[72] H. Rettig, E. Krause, H. G. Börner, *Macromolecular rapid communications* **2004**, *25*, 1251-1256.

[73] M. L. Becker, J. Liu, K. L. Wooley, *Chemical Communications* **2003**, 180-181.

[74] H. Murata, F. Sanda, T. Endo, *Macromolecules* **1996**, *29*, 5535-5538.

[75] L. Ayres, K. Koch, P. H. H. Adams, J. C. van Hest, *Macromolecules* **2005**, *38*, 1699-1704.

[76] N. Budisa, *Angewandte Chemie International Edition* **2004**, *43*, 6426-6463.

[77] L. Wang, P. G. Schultz, *Angewandte Chemie International Edition* **2005**, *44*, 1-1.

[78] T. L. Schlick, Z. Ding, E. W. Kovacs, M. B. Francis, *Journal of the American Chemical Society* **2005**, *127*, 3718-3723.

[79] K. L. Heredia, D. Bontempo, T. Ly, J. T. Byers, S. Halstenberg, H. D. Maynard, *Journal of the American Chemical Society* **2005**, *127*, 16955-16960.

[80] I. Hamachi, S. Shinkai, *European journal of organic chemistry* **1999**, *1999*, 539-549.

[81] A. Bückmann, M. Kula, R. Wichmann, C. Wandrey, *J Appl Biochem* **1981**, *3*, 301-315.

[82] V. Bulmus, *Polymer Chemistry* **2011**, *2*, 1463-1472.

[83] R. Peltier, M. Hartlieb, S. Perrier, *Material Matters* **2017**, *12*, 53.

[84] A. Arsiwala, A. Castro, S. Frey, M. Stathos, R. S. Kane, *Chemistry – An Asian Journal* **2019**, *14*, 244-255.

[85] L. L. Kiessling, L. E. Strong, J. E. Gestwicki, in *Annual Reports in Medicinal Chemistry, Vol. 35*, Academic Press, **2000**, pp. 321-330.

[86] R. T. Lee, Y. C. Lee, *Glycoconjugate Journal* **2000**, *17*, 543-551.

[87] K. H. Mortell, R. V. Weatherman, L. L. Kiessling, *Journal of the American Chemical Society* **1996**, *118*, 2297-2298.

[88] L. L. Kiessling, N. L. Pohl, *Chemistry & Biology* **1996**, *3*, 71-77.

[89] D. A. Mann, M. Kanai, D. J. Maly, L. L. Kiessling, *Journal of the American Chemical Society* **1998**, *120*, 10575-10582.

[90] T. K. Dam, C. F. Brewer, *Chemical reviews* **2002**, *102*, 387-430.

[91] S. I. Rudnick, G. P. Adams, *Cancer Biotherapy and Radiopharmaceuticals* **2009**, *24*, 155-161.

[92] E. Walter, *Cambridge advanced learner's dictionary*, Cambridge University Press, **2008**.

[93] C. A. Hunter, H. L. Anderson, *Angewandte Chemie International Edition* **2009**, *48*, 7488-7499.

[94] A. Peselis, A. Gao, A. Serganov, *Biochimie* **2015**, *117*, 100-109.

[95] J. Berg, J. Tymoczko, L. Stryer, *Biochemistry (6th ed.), New York: Freeman WH and Co* **2007**, 428-429.

[96] M. F. Perutz, *Quarterly Reviews of Biophysics* **1989**, *22*, 139-237.

[97] J. Monod, F. Jacob, in *Cold Spring Harbor symposia on quantitative biology, Vol. 26*, Cold Spring Harbor Laboratory Press, **1961**, pp. 389-401.

[98] C. Fasting, C. A. Schalley, M. Weber, O. Seitz, S. Hecht, B. Koksch, J. Dernedde, C. Graf, E. W. Knapp, R. Haag, *Angewandte Chemie International Edition* **2012**, *51*, 10472-10498.

[99] J. J. Lundquist, E. J. Toone, *Chemical reviews* **2002**, *102*, 555-578.

[100] S. M. Dimick, S. C. Powell, S. A. McMahon, D. N. Moothoo, J. H. Naismith, E. J. Toone, *Journal of the American Chemical Society* **1999**, *121*, 10286-10296.

[101] M. Ambrosi, N. R. Cameron, B. G. Davis, *Organic & biomolecular chemistry* **2005**, *3*, 1593-1608.

[102] C. R. Becer, *Macromolecular rapid communications* **2012**, *33*, 742-752.

[103] S. Cecioni, J. P. Praly, S. E. Matthews, M. Wimmerová, A. Imberty, S. Vidal, *Chemistry–A European Journal* **2012**, *18*, 6250-6263.

[104] K. Kanazaki, K. Sano, A. Makino, T. Homma, M. Ono, H. Saji, *Scientific Reports* **2016**, *6*, 33798.

[105] K. Katagiri, A. Takasu, M. Higuchi, *Biomacromolecules* **2016**, *17*, 1902-1908.

[106] R. Luxenhofer, Dissertation thesis, Technische Universität (München), **2007**.

[107] L. L. Kiessling, J. C. Grim, *Chemical Society Reviews* **2013**, *42*, 4476-4491.

[108] K. Matyjaszewski, *Science* **2011**, *333*, 1104-1105.

[109] J. E. Gestwicki, L. E. Strong, L. L. Kiessling, *Angewandte Chemie International Edition* **2000**, *39*, 4567-4570.

[110] J. E. Gestwicki, C. W. Cairo, L. E. Strong, K. A. Oetjen, L. L. Kiessling, *Journal of the American Chemical Society* **2002**, *124*, 14922-14933.

[111] M. Kanai, K. H. Mortell, L. L. Kiessling, *Journal of the American Chemical Society* **1997**, *119*, 9931-9932.

[112] V. R. Pattabiraman, J. W. Bode, *Nature* **2011**, *480*, 471.

[113] B. D. Polizzotti, K. L. Kiick, *Biomacromolecules* **2006**, *7*, 483-490.

[114] B. D. Polizzotti, R. Maheshwari, J. Vinkenborg, K. L. Kiick, *Macromolecules* **2007**, *40*, 7103-7110.

[115] D. Ponader, F. Wojcik, F. Beceren-Braun, J. Dernedde, L. Hartmann, *Biomacromolecules* **2012**, *13*, 1845-1852.

[116] K. Gorska, K. T. Huang, O. Chaloin, N. Winssinger, *Angewandte Chemie International Edition* **2009**, *48*, 7695-7700.

[117] T. Hasegawa, S. Kondoh, K. Matsuura, K. Kobayashi, *Macromolecules* **1999**, *32*, 6595-6603.

[118] J. Kumar, L. McDowall, G. Chen, M. H. Stenzel, *Polymer Chemistry* **2011**, *2*, 1879-1886.

[119] L. Johannes, R. Jacob, H. Leffler, *Journal of Cell Science* **2018**, *131*, 208884.

[120] I. Camby, M. Le Mercier, F. Lefranc, R. Kiss, *Glycobiology* **2006**, *16*, 137-157.

[121] I. Goldstein, C. Hollerman, E. Smith, *Biochemistry* **1965**, *4*, 876-883.

[122] N. Sharon, *Trends in biochemical sciences* **1993**, *18*, 221-226.

[123] S. G. Spain, N. R. Cameron, *Polymer Chemistry* **2011**, *2*, 1552-1560.

[124] W. I. Weis, K. Drickamer, *Annual review of biochemistry* **1996**, *65*, 441-473.

[125] M. Monsigny, R. Mayer, A.-C. Roche, *Carbohydrate letters* **2000**, *4*, 35-52.

[126] R. Loris, *Biochimica et Biophysica Acta (BBA)-General Subjects* **2002**, *1572*, 198-208.

[127] A. Jack, J. Weinzierl, A. J. Kalb, *Journal of molecular biology* **1971**, *58*, 389-395.

[128] J. Greer, H. Kaufman, A. J. Kalb, *Journal of molecular biology* **1970**, *48*, 365-366.

[129] R. J. Pieters, *Organic & biomolecular chemistry* **2009**, *7*, 2013-2025.

[130] K. D. Hardman, C. F. Ainsworth, *Biochemistry* **1972**, *11*, 4910-4919.

[131] J. Becker, G. Reeke, B. Cunningham, G. Edelman, *Nature* **1976**, *259*, 406-409.

[132] T. K. Dam, R. Roy, S. K. Das, S. Oscarson, C. F. Brewer, *Journal of Biological Chemistry* **2000**, *275*, 14223-14230.

[133] C. R. Yonzon, E. Jeoung, S. Zou, G. C. Schatz, M. Mrksich, R. P. Van Duyne, *Journal of the American Chemical Society* **2004**, *126*, 12669-12676.

[134] T. Mori, M. Toyoda, T. Ohtsuka, Y. Okahata, *Analytical biochemistry* **2009**, *395*, 211-216.

[135] G. S. Chen, Gan, J.H., Hu, R.T., To be published.

[136] W. Humphrey, A. Dalke, K. Schulten, *Journal of molecular graphics* **1996**, *14*, 33-38.

[137] M. A. Mees, C. Effenberg, D. Appelhans, R. Hoogenboom, *Biomacromolecules* **2016**, *17*, 4027-4036.

[138] T. Lorson, M. M. Lübtow, E. Wegener, M. S. Haider, S. Borova, D. Nahm, R. Jordan, M. Sokolski-Papkov, A. V. Kabanov, R. Luxenhofer, *Biomaterials* **2018**, *178*, 204-280.

[139] M. F. López-Lucendo, D. Solís, S. André, J. Hirabayashi, K.-i. Kasai, H. Kaltner, H.-J. Gabius, A. Romero, *Journal of molecular biology* **2004**, *343*, 957-970.

[140] I. Camby, M. Le Mercier, F. Lefranc, R. Kiss, *Glycobiology* **2006**, *16*, 137R-157R.

[141] N. Bertleff-Zieschang, J. Bechold, C. Grimm, M. Reutlinger, P. Schneider, G. Schneider, J. Seibel, *ChemBioChem* **2017**, *18*, 1461-1461.

[142] K. Balestrieri, M. McDaniel, C. Shoopman, N. Vohra, K. Verbanac, AACR, **2019**.

[143] N. S. Goud, P. Soukya, M. Ghouse, D. Komal, R. Alvala, M. Alvala, *Mini reviews in medicinal chemistry* **2019**, *19*, 1369-1378.

[144] S. H. Barondes, V. Castronovo, D. Cooper, R. D. Cummings, K. Drickamer, T. Feizi, M. A. Gitt, J. Hirabayashi, C. Hughes, K.-i. Kasai, *Cell* **1994**, *76*, 597-598.

[145] N. Ahmad, H.-J. Gabius, S. Sabesan, S. Oscarson, C. F. Brewer, *Glycobiology* **2004**, *14*, 817-825.

[146] F. P. Schwarz, H. Ahmed, M. A. Bianchet, L. M. Amzel, G. R. Vasta, *Biochemistry* **1998**, *37*, 5867-5877.

[147] N. Bertleff-Zieschang, J. Bechold, C. Grimm, M. Reutlinger, P. Schneider, G. Schneider, J. Seibel, *ChemBioChem* **2017**, *18*, 1477-1481.

[148] B.-W. Kim, S. Beom Hong, J. Hoe Kim, D. Hoon Kwon, H. Kyu Song, *Nature Communications* **2013**, *4*, 1613.

[149] S. Li, M. P. Wandel, F. Li, Z. Liu, C. He, J. Wu, Y. Shi, F. Randow, *Sci. Signal.* **2013**, *6*, 9.

[150] S. André, C. J. Arnusch, I. Kuwabara, R. Russwurm, H. Kaltner, H.-J. Gabius, R. J. Pieters, *Bioorg Med Chem* **2005**, *13*, 563-573.

[151] D. G. Mullen, M. M. Banaszak Holl, *Accounts of chemical research* **2011**, *44*, 1135-1145.

[152] I. F. Hakem, A. M. Leech, J. D. Johnson, S. J. Donahue, J. P. Walker, M. R. Bockstaller, *Journal of the American Chemical Society* **2010**, *132*, 16593-16598.

[153] D. G. Mullen, M. Fang, A. Desai, J. R. Baker Jr, B. G. Orr, M. M. Banaszak Holl, *Acs Nano* **2010**, *4*, 657-670.

[154] D. G. Mullen, E. L. Borgmeier, A. M. Desai, M. A. Van Dongen, M. Barash, X. m. Cheng, J. R. Baker Jr, M. M. Banaszak Holl, *Chemistry–A European Journal* **2010**, *16*, 10675-10678.

[155] D. Casanova, D. Giaume, M. Moreau, J.-L. Martin, T. Gacoin, J.-P. Boilot, A. Alexandrou, *Journal of the American Chemical Society* **2007**, *129*, 12592-12593.

[156] C. Wängler, G. Moldenhauer, R. Saffrich, E. M. Knapp, B. Beijer, M. Schnölzer, B. Wängler, M. Eisenhut, U. Haberkorn, W. Mier, *Chemistry–A European Journal* **2008**, *14*, 8116-8130.

[157] E. M. Munoz, J. Correa, E. Fernandez-Megia, R. Riguera, *Journal of the American Chemical Society* **2009**, *131*, 17765-17767.

[158] D. J. Welsh, D. K. Smith, *Organic & biomolecular chemistry* **2011**, *9*, 4795-4801.

[159] Y. Wang, Y. Wang, D. R. Breed, V. N. Manoharan, L. Feng, A. D. Hollingsworth, M. Weck, D. J. Pine, *Nature* **2012**, *491*, 51-55.

[160] A. L. Martin, B. Li, E. R. Gillies, *Journal of the American Chemical Society* **2009**, *131*, 734-741.

[161] H. Luo, J. Yang, H. Jin, C. Huang, J. Fu, F. Yang, H. Gong, S. Zeng, Q. Luo, Z. Zhang, *The FASEB Journal* **2011**, *25*, 1865-1873.

[162] M. A. Kostiainen, G. R. Szilvay, J. Lehtinen, D. K. Smith, M. B. Linder, A. Urtti, O. Ikkala, *Acs Nano* **2007**, *1*, 103-113.

[163] J. Y. Axup, K. M. Bajjuri, M. Ritland, B. M. Hutchins, C. H. Kim, S. A. Kazane, R. Halder, J. S. Forsyth, A. F. Santidrian, K. Stafin, *Proceedings of the National Academy of Sciences* **2012**, *109*, 16101-16106.

[164] R. Burai, J. Chatwichien, B. R. McNaughton, *Organic & biomolecular chemistry* **2011**, *9*, 5056-5058.

[165] J. M. Holub, M. J. Garabedian, K. Kirshenbaum, *QSAR & Combinatorial Science* **2007**, *26*, 1175-1180.

[166] K. V. Kong, W. Chew, L. H. K. Lim, W. Y. Fan, W. K. Leong, *Bioconjugate Chemistry* **2007**, *18*, 1370-1374.

[167] J. M. McFarland, M. B. Francis, *Journal of the American Chemical Society* **2005**, *127*, 13490-13491.

[168] J. M. Antos, M. B. Francis, *Current Opinion in Chemical Biology* **2006**, *10*, 253-262.

[169] G. Levesque, P. Arsène, V. Fanneau-Bellenger, T.-N. Pham, *Biomacromolecules* **2000**, *1*, 400-406.

[170] G. Levesque, P. Arsène, V. Fanneau-Bellenger, T.-N. Pham, *Biomacromolecules* **2000**, *1*, 387-399.

[171] S.-J. Xiao, M. Wieland, S. Brunner, *Journal of Colloid and Interface Science* **2005**, *290*, 172-183.

[172] H.-A. Klok, *Journal of Polymer Science Part A: Polymer Chemistry* **2005**, *43*, 1-17.

[173] D. R. W. Hodgson, J. M. Sanderson, *Chemical Society Reviews* **2004**, *33*, 422-430.

[174] S. Balan, J.-w. Choi, A. Godwin, I. Teo, C. M. Laborde, S. Heidelberger, M. Zloh, S. Shaunak, S. Brocchini, *Bioconjugate Chemistry* **2007**, *18*, 61-76.

[175] J. Wilken, S. B. H. Kent, *Current Opinion in Biotechnology* **1998**, *9*, 412–426.

[176] P. E. Dawson, M. J. Churchill, M. R. Ghadiri, S. B. H. Kent, *Journal of the American Chemical Society* **1997**, *119*, 4325-4329.

[177] S.-Y. Chen, S. Cressman, F. Mao, H. Shao, D. W. Low, H. S. Beilan, E. N. Cagle, M. Carnevali, V. Gueriguian, P. J. Keogh, H. Porter, S. M. Stratton, M. C. Wiedeke, L. Savatski, J. W. Adamson, C. E. Bozzini, A. Kung, S. B. H. Kent, J. A. Bradburne, G. G. Kochendoerfer, *Chemistry & Biology* **2005**, *12*, 371-383.

[178] W. C. Chan, P. D. White, *Fmoc Solid Phase Peptide Synthesis: A Practical Approach*, Oxford University Press, New York, **2000**.

[179] L. C. Chan, B. G. Cox, *The Journal of Organic Chemistry* **2007**, *72*, 8863-8869.

[180] A. Tam, M. B. Soellner, R. T. Raines, *Journal of the American Chemical Society* **2007**, *129*, 11421-11430.

[181] D. R. Hodgson, J. M. Sanderson, *Chemical Society Reviews* **2004**, *33*, 422-430.

[182] W. Chan, P. White, *Fmoc solid phase peptide synthesis: a practical approach, Vol. 222*, OUP Oxford, **1999**.

[183] H. T. Ten Brink, J. T. Meijer, R. V. Geel, M. Damen, D. W. Löwik, J. C. van Hest, *Journal of peptide science: an official publication of the European Peptide Society* **2006**, *12*, 686-692.

[184] G. T. Dolphin, *Chemistry–A European Journal* **2006**, *12*, 1436-1447.

[185] P. J. Duggan, D. A. Offermann, *Australian Journal of Chemistry* **2007**, *60*, 829-834.

[186] U. Hoffmanns, N. Metzler-Nolte, *Bioconjugate chemistry* **2006**, *17*, 204-213.

[187] D. Crich, A. Banerjee, *Journal of the American Chemical Society* **2007**, *129*, 10064-10065.

[188] G. Moad, Y. Chong, A. Postma, E. Rizzardo, S. H. Thang, *Polymer* **2005**, *46*, 8458-8468.

[189] A. Hirao, M. Hayashi, *Acta polymerica* **1999**, *50*, 219-231.

[190] C. J. Waschinski, J. C. Tiller, *Biomacromolecules* **2005**, *6*, 235-243.

[191] T. Dispinar, R. Sanyal, A. Sanyal, *Journal of Polymer Science Part A: Polymer Chemistry* **2007**, *45*, 4545-4551.

[192] A. Godwin, M. Hartenstein, A. H. Müller, S. Brocchini, *Angewandte Chemie International Edition* **2001**, *40*, 594-597.

[193] M. J. Yanjarappa, K. V. Gujraty, A. Joshi, A. Saraph, R. S. Kane, *Biomacromolecules* **2006**, *7*, 1665-1670.

[194] J. Hwang, R. C. Li, H. D. Maynard, *Journal of Controlled Release* **2007**, *122*, 279-286.

[195] M. Malkoch, R. J. Thibault, E. Drockenmuller, M. Messerschmidt, B. Voit, T. P. Russell, C. J. Hawker, *Journal of the American Chemical Society* **2005**, *127*, 14942-14949.

[196] D. Hua, W. Bai, J. Xiao, R. Bai, W. Lu, C. Pan, *Chemistry of materials* **2005**, *17*, 4574-4576.

[197] B. S. Sumerlin, N. V. Tsarevsky, G. Louche, R. Y. Lee, K. Matyjaszewski, *Macromolecules* **2005**, *38*, 7540-7545.

[198] J. Qiu, K. Matyjaszewski, *Macromolecules* **1997**, *30*, 5643-5648.

[199] C. Cheng, G. Sun, E. Khoshdel, K. L. Wooley, *Journal of the American Chemical Society* **2007**, *129*, 10086-10087.

[200] R. C. Li, R. M. Broyer, H. D. Maynard, *Journal of Polymer Science Part A: Polymer Chemistry* **2006**, *44*, 5004-5013.

[201] G. Sun, C. Cheng, K. L. Wooley, *Macromolecules* **2007**, *40*, 793-795.

[202] M. Camail, A. Margaillan, J. Maesano, S. Thuret, J. Vernet, *Polymer* **1998**, *39*, 3187-3192.

[203] F. Sanda, T. Abe, T. Endo, *Journal of Polymer Science Part A: Polymer Chemistry* **1997**, *35*, 2619-2629.

[204] A. Bentolila, I. Vlodavsky, R. Ishai-Michaeli, O. Kovalchuk, C. Haloun, A. J. Domb, *Journal of medicinal chemistry* **2000**, *43*, 2591-2600.

[205] H. Mori, M. Matsuyama, K. Sutoh, T. Endo, *Macromolecules* **2006**, *39*, 4351-4360.

[206] T. M. Trnka, R. H. Grubbs, *Accounts of Chemical Research* **2001**, *34*, 18-29.

[207] C. W. Bielawski, R. H. Grubbs, *Progress in Polymer Science* **2007**, *32*, 1-29.

[208] A. Hirao, S. Loykulnant, T. Ishizone, *Progress in polymer science* **2002**, *27*, 1399-1471.

[209] R. Luxenhofer, R. Jordan, *Macromolecules* **2006**, *39*, 3509-3516.

[210] S. Cesana, J. Auernheimer, R. Jordan, H. Kessler, O. Nuyken, *Macromolecular Chemistry and Physics* **2006**, *207*, 183-192.

[211] C. Taubmann, R. Luxenhofer, S. Cesana, R. Jordan, *Macromolecular Bioscience* **2005**, *5*, 603-612.

[212] W. H. Binder, H. Gruber, *Macromolecular Chemistry and Physics* **2000**, *201*, 949-957.

[213] H.-J. Gabius, H.-C. Siebert, S. André, J. Jiménez-Barbero, H. Rüdiger, *ChemBioChem* **2004**, *5*, 740-764.

[214] R. Narain, S. P. Armes, *Biomacromolecules* **2003**, *4*, 1746-1758.

[215] V. Ladmiral, M. Semsarilar, I. Canton, S. P. Armes, *Journal of the American Chemical Society* **2013**, *135*, 13574-13581.

[216] C. Bonduelle, S. Lecommandoux, *Biomacromolecules* **2013**, *14*, 2973-2983.

[217] Q. Zhang, P. Wilson, A. Anastasaki, R. McHale, D. M. Haddleton, *ACS Macro Letters* **2014**, *3*, 491-495.

[218] C. S. Cho, S. J. Seo, I. K. Park, S. H. Kim, T. H. Kim, T. Hoshiba, I. Harada, T. Akaike, *Biomaterials* **2006**, *27*, 576-585.

[219] K. Aoi, H. Suzuki, M. Okada, *Macromolecules* **1992**, *25*, 7073-7075.

[220] C. Weber, J. A. Czaplewska, A. Baumgaertel, E. Altuntas, M. Gottschaldt, R. Hoogenboom, U. S. Schubert, *Macromolecules* **2012**, *45*, 46-55.

[221] A. Takasu, H. Kojima, *Journal of Polymer Science Part A: Polymer Chemistry* **2010**, *48*, 5953-5960.

[222] J. Geng, J. Lindqvist, G. Mantovani, D. M. Haddleton, *Angewandte Chemie International Edition* **2008**, *47*, 4180-4183.

[223] A. Dondoni, A. Marra, *Chemical Society Reviews* **2012**, *41*, 573-586.

[224] M. Ahmed, P. Wattanaarsakit, R. Narain, *European Polymer Journal* **2013**, *49*, 3010-3033.

[225] L. Markey, S. Giordani, E. M. Scanlan, *The Journal of Organic Chemistry* **2013**, *78*, 4270-4277.

[226] J. Huang, G. Habraken, F. Audouin, A. Heise, *Macromolecules* **2010**, *43*, 6050-6057.

[227] W. Shi, S. Dolai, S. Averick, S. S. Fernando, J. A. Saltos, W. L'Amoreaux, P. Banerjee, K. Raja, *Bioconjugate Chemistry* **2009**, *20*, 1595-1601.

[228] C. Diehl, H. Schlaad, *Macromolecular Bioscience* **2009**, *9*, 157-161.

[229] C. Diehl, H. Schlaad, *Polimery* **2013**, *58*, 650--653.

[230] A. Gress, A. Völkel, H. Schlaad, *Macromolecules* **2007**, *40*, 7928-7933.

[231] K. Kempe, T. Neuwirth, J. Czaplewska, M. Gottschaldt, R. Hoogenboom, U. S. Schubert, *Polymer Chemistry* **2011**, *2*, 1737-1743.

[232] A. F. Thünemann, R. Bienert, D. Appelhans, B. Voit, *Macromolecular Chemistry and Physics* **2012**, *213*, 2362-2369.

[233] Z. Zhang, B. Schepens, L. Nuhn, X. Saelens, M. Schotsaert, N. Callewaert, R. De Rycke, Q. Zhang, S. Moins, S. Benali, L. Mespouille, R. Hoogenboom, B. G. De Geest, *Chemical communications (Cambridge, England)* **2016**, *52*, 3352-3355.

[234] S. S. Park, H.-W. Hsieh, J. Gervay-Hague, *Molecules* **2018**, *23*, 1742.

[235] V. Dimakos, M. S. Taylor, *Chemical Reviews* **2018**, *118*, 11457-11517.

[236] J. Nicolas, G. Mantovani, D. M. Haddleton, *Macromolecular Rapid Communications* **2007**, *28*, 1083-1111.

[237] H. G. Börner, H. Schlaad, *Soft Matter* **2007**, *3*, 394-408.

[238] D. W. Löwik, L. Ayres, J. M. Smeenk, J. C. Van Hest, in *Peptide Hybrid Polymers*, Springer, **2006**, pp. 19-52.

[239] M. Pechar, J. Brus, L. Kostka, Č. Koňák, M. Urbanová, M. Šlouf, *Macromolecular bioscience* **2007**, *7*, 56-69.

[240] A. Rösler, H.-A. Klok, I. W. Hamley, V. Castelletto, O. O. Mykhaylyk, *Biomacromolecules* **2003**, *4*, 859-863.

[241] K. Kodama, S. Fukuzawa, H. Nakayama, K. Sakamoto, T. Kigawa, T. Yabuki, N. Matsuda, M. Shirouzu, K. Takio, S. Yokoyama, *ChemBioChem* **2007**, *8*, 232-238.

[242] H. Dibowski, F. P. Schmidtchen, *Angewandte Chemie International Edition* **1998**, *37*, 476-478.

[243] A. Ojida, H. Tsutsumi, N. Kasagi, I. Hamachi, *Tetrahedron Letters* **2005**, *46*, 3301-3305.

[244] C. S. Cazalis, C. A. Haller, L. Sease-Cargo, E. L. Chaikof, *Bioconjugate chemistry* **2004**, *15*, 1005-1009.

[245] A. D. De Araújo, J. M. Palomo, J. Cramer, M. Köhn, H. Schröder, R. Wacker, C. Niemeyer, K. Alexandrov, H. Waldmann, *Angewandte Chemie International Edition* **2006**, *45*, 296-301.

[246] A. T. Dirks, S. S. van Berkel, N. S. Hatzakis, J. A. Opsteen, F. L. van Delft, J. J. Cornelissen, A. E. Rowan, J. C. van Hest, F. P. Rutjes, R. J. Nolte, *Chemical communications* **2005**, 4172-4174.

[247] O. Kinstler, G. Molineux, M. Treuheit, D. Ladd, C. Gegg, *Advanced drug delivery reviews* **2002**, *54*, 477-485.

[248] J. M. Hooker, A. P. Esser-Kahn, M. B. Francis, *Journal of the American Chemical Society* **2006**, *128*, 15558-15559.

[249] B. Pons, L. Mouhoubi, A. Adib, P. Godzina, J. P. Behr, G. Zuber, *ChemBioChem* **2006**, *7*, 303-309.

[250] M. Lutolf, N. Tirelli, S. Cerritelli, L. Cavalli, J. Hubbell, *Bioconjugate chemistry* **2001**, *12*, 1051-1056.

[251] Y. Geng, D. E. Discher, J. Justynska, H. Schlaad, *Angewandte Chemie International Edition* **2006**, *45*, 7578-7581.

[252] J. Justynska, Z. Hordyjewicz, H. Schlaad, in *Macromolecular symposia, Vol. 240*, Wiley Online Library, **2006**, pp. 41-46.

[253] J. Justynska, Z. Hordyjewicz, H. Schlaad, *Polymer* **2005**, *46*, 12057-12064.

[254] S. Wang, C. Fu, Y. Wei, L. Tao, *Macromolecular Chemistry and Physics* **2014**, *215*, 486-492.

[255] S. Hassan, T. J. Mueller, *Advanced Synthesis & Catalysis* **2015**, *357*, 617-666.

[256] B. Yang, Y. Zhao, Y. Wei, C. Fu, L. Tao, *Polymer Chemistry* **2015**, *6*, 8233-8239.

[257] R. Kakuchi, *Angewandte Chemie International Edition* **2014**, *53*, 46-48.

[258] E. F. Freitas, R. Y. Souza, S. T. A. Passos, J. A. Dias, S. C. L. Dias, B. A. D. Neto, *RSC Advances* **2019**, *9*, 27125-27135.

[259] M. Benaglia, A. Alberti, L. Giorgini, F. Magnoni, S. Tozzi, *Polymer Chemistry* **2013**, *4*, 124-132.

[260] R. Kakuchi, P. Theato, *ACS Macro Letters* **2013**, *2*, 419-422.

[261] S. Reinicke, P. Espeel, M. M. Stamenović, F. E. Du Prez, *ACS Macro Letters* **2013**, *2*, 539-543.

[262] P. Espeel, F. Goethals, M. M. Stamenović, L. Petton, F. E. Du Prez, *Polymer Chemistry* **2012**, *3*, 1007-1015.

[263] V. Agouridas, O. El Mahdi, V. Diemer, M. Cargoët, J.-C. M. Monbaliu, O. Melnyk, *Chemical Reviews* **2019**, *119*, 7328-7443.

[264] T. Wieland, E. Bokelmann, L. Bauer, H. U. Lang, H. Lau, *Liebigs Ann. Chem.* **1953**, *583*, 129.

[265] M. Brenner, J. P. Zimmermann, J. Wehrmüller, P. Quitt, I. Photaki, *Experientia* **1955**, *11*, 397.

[266] M. Brenner, J. P. Zimmermann, *Helv. Chim. Acta* **1958**, *41*, 467.

[267] D. S. Kemp, F. Vellaccio, *J. Org. Chem.* **1975**, *40*, 3003.

[268] D. S. Kemp, J. A. Grattan, J. Reczek, *J. Org. Chem.* **1975**, *40*, 3465.

[269] N. Fotouhi, B. R. Bowen, D. S. Kemp, *Int. J. Pept. Protein Res.* **1992**, *40*, 141.

[270] M. Schnolzer, S. B. H. Kent, *Science* **1992**, *256*, 221.

[271] P. E. Dawson, T. W. Muir, I. Clark-Lewis, S. B. Kent, *Science* **1994**, *266*, 776-779.

[272] C. F. Liu, J. P. Tam, *Proc. Natl. Acad. Sci. U. S. A.* **1994**, *91*, 6584.

[273] J. P. Tam, Y. A. Lu, C. F. Liu, J. Shao, *Proc. Natl. Acad. Sci. U. S. A.* **1995**, *92*, 12485.

[274] C. P. R. Hackenberger, D. Schwarzer, *Angewandte Chemie* **2008**, *120*, 10182-10228.

[275] I. van Baal, H. Malda, S. A. Synowsky, J. L. J. van Dongen, T. M. Hackeng, M. Merkx, E. W. Meijer, *Angewandte Chemie International Edition* **2005**, *44*, 5052-5057.

[276] S. M. Chafekar, H. Malda, M. Merkx, E. W. Meijer, D. Viertl, H. A. Lashuel, F. Baas, W. Scheper, *ChemBioChem* **2007**, *8*, 1857-1864.

[277] N. Isahak, G. Gody, L. R. Malins, N. J. Mitchell, R. J. Payne, S. Perrier, *Chemical Communications* **2016**, *52*, 12952-12955.

[278] L. Moroder, *J. Pept. Sci.* **2005**, *11*, 187.

[279] L. B. Poole, *Free Radical Biol. Med.* **2015**, *80*, 148.

[280] R. E. Benesch, R. Benesch, *J. Am. Chem. Soc.* **1955**, *77*, 5877.

[281] R. L. Thurlkill, G. R. Grimsley, J. M. Scholtz, C. N. Pace, *Protein Sci.* **2006**, *15*, 1214.

[282] G. A. Bagiyan, I. K. Koroleva, N. V. Soroka, A. V. Ufimtsev, *Russ. Chem. Bull.* **2003**, *52*, 1135.

[283] T. J. Wallace, A. Schriesheim, H. Hurwitz, M. B. Glaser, *Ind. Eng. Chem. Process Des. Dev.* **1964**, *3*, 237.

[284] R. Stevens, L. Stevens, N. C. Price, *Biochem. Educ.* **1983**, *11*, 70.

[285] W. J. Lees, G. M. Whitesides, *J. Org. Chem.* **1993**, *58*, 642.

[286] E. C. Johnson, S. B. H. Kent, *J. Am. Chem. Soc.* **2006**, *128*, 6640.

[287] W. W. Cleland, *Biochemistry* **1964**, *3*, 480.

[288] J. M. Yost, Knight, J.D., Coltart, D.M. and Li, E.W., in *Encyclopedia of Reagents for Organic Synthesis*, **2018**, pp. 1-9.

[289] J. A. Burns, J. C. Butler, J. Moran, G. M. Whitesides, *J. Org. Chem.* **1991**, *56*, 2648.

[290] H. Rohde, J. Schmalisch, Z. Harpaz, F. Diezmann, O. Seitz, *ChemBioChem* **2011**, *12*, 1396.

[291] A. M. Faucher, C. Grand-Maître, *Synth. Commun.* **2003**, *33*, 3503.

[292] E. Herbst, D. Shabat, *Org. Biomol. Chem.* **2016**, *14*, 3715.

[293] F. Lynen, E. Reichert, *Angew. Chem.* **1951**, *63*, 47.

[294] K. V. Mills, M. A. Johnson, F. B. Perler, *J. Biol. Chem.* **2014**, *289*, 14498.

[295] W. P. Jencks, S. Cordes, J. Carriuolo, *J. Biol. Chem.* **1960**, *235*, 3608.

[296] K. A. Connors, M. L. Bender, *J. Org. Chem.* **1961**, *26*, 2498.

[297] R. E. Barnett, W. P. Jencks, *J. Am. Chem. Soc.* **1969**, *91*, 2358.

[298] D. J. Hupe, W. P. Jencks, *J. Am. Chem. Soc.* **1977**, *99*, 451.

[299] P. J. Bracher, P. W. Snyder, B. R. Bohall, G. M. Whitesides, *Origins Life Evol. Biospheres* **2011**, *41*, 399.

[300] W. Yang, D. G. Drueckhammer, *Org. Lett.* **2000**, *2*, 4133.

[301] W. Yang, D. G. Drueckhammer, *J. Am. Chem. Soc.* **2001**, *123*, 11004.

[302] C. O. Della Védova, R. M. Romano, H. Oberhammer, *J. Org. Chem.* **2004**, *69*, 5395.

[303] M. Kitano, T. Fukuyama, K. Kuchitsu, *Bull. Chem. Soc. Jpn.* **1973**, *46*, 384.

[304] L. Pauling, R. B. Corey, H. R. Branson, *Proc. Natl. Acad. Sci. U. S. A.* **1951**, *37*, 205.

[305] A. M. M. El-Assar, C. P. Nash, L. L. Ingraham, *Biochemistry* **1982**, *21*, 1972.

[306] I. H. Um, G. R. Kim, D. S. Kwon, *Bull. Korean Chem. Soc.* **1994**, *15*, 585.

[307] R. R. Flavell, T. W. Muir, *Acc. Chem. Res.* **2009**, *42*, 107.

[308] J. Kang, D. Macmillan, *Org. Biomol. Chem.* **2010**, *8*, 1993.

[309] F. Mende, O. Seitz, *Angew. Chem., Int. Ed.* **2011**, *50*, 1232.

[310] J. S. Zheng, S. Tang, Y. C. Huang, L. Liu, *Acc. Chem. Res.* **2013**, *46*, 2475.

[311] N. H. Shah, T. W. Muir, *Chem. Sci.* **2014**, *5*, 446.

[312] E. Boll, H. Drobecq, N. Ollivier, L. Raibaut, R. Desmet, J. Vicogne, O. Melnyk, *Chem. Sci.* **2014**, *5*, 2017.

[313] S. Song, Z. Zhang, X. Liu, Z. Fu, J. Xu, Z. Fan, *Journal of Polymer Science Part A: Polymer Chemistry* **2017**, *55*, 4027-4036.

[314] M. J. Roberts, Z. Fang, U. S. Patent Nr. 6,908,963, **2005**.

[315] R. Ingenito, E. Bianchi, D. Fattori, A. Pessi, *J. Am. Chem. Soc.* **1999**, *121*, 11369.

[316] Y. Shin, K. A. Winans, B. J. Backes, S. B. H. Kent, J. A. Ellman, C. R. Bertozzi, *J. Am. Chem. Soc.* **1999**, *121*, 11684.

[317] J. B. Blanco-Canosa, P. E. Dawson, *Angew. Chem., Int. Ed.* **2008**, *47*, 6851.

[318] J. B. Blanco-Canosa, B. Nardone, F. Albericio, P. E. Dawson, *J. Am. Chem. Soc.* **2015**, *137*, 7197.

[319] R. Quaderer, D. Hilvert, *Org. Lett.* **2001**, *3*, 3181.

[320] J. S. Zheng, S. Tang, Y. Guo, H. N. Chang, L. Liu, *ChemBioChem* **2012**, *13*, 542.

[321] J. S. Zheng, S. Tang, Y. K. Qi, Z. P. Wang, L. Liu, *Nat. Protoc.* **2013**, *8*, 2483.

[322] J. Meienhofer, E. Gross, J. Meienhofer, *The Peptides. Analysis, Synthesis, Biology, Vol. 1*, **1979**.

[323] D. T. Flood, J. C. J. Hintzen, M. J. Bird, P. A. Cistrone, J. S. Chen, P. E. Dawson, *Angew. Chem., Int. Ed.* **2018**, *57*, 11634.

[324] D. A. Ryan, D. Y. Gin, *Journal of the American Chemical Society* **2008**, *130*, 15228-15229.

[325] B. Neises, W. Steglich, *Angewandte Chemie International Edition in English* **1978**, *17*, 522-524.

[326] K. Jeyakumar, D. K. Chand, *Journal of Molecular Catalysis A: Chemical* **2006**, *255*, 275-282.

[327] M. M. Mojtahedi, S. Samadian, *Journal of Chemistry* **2013**, *2013*, 7.

[328] M. Kazemi, H. Kohzadi, Z. Noori, *Iran. Chem. Commun.* **2014**, *2*, 39-47.

[329] S. T. Kadam, H. Lee, S. S. Kim, *Bull Korean Chem Soc.* **2009**, *30*, 1071–1076.

[330] R. Ghorbani-Vaghei, Z. Toghraei-Semiromi, *Phosphorus, Sulfur, and Silicon and the Related Elements* **2010**, *185*, 1701-1707.

[331] N. Iranpoor, H. Firouzabadi, D. Khalili, S. Motevalli, *The Journal of Organic Chemistry* **2008**, *73*, 4882-4887.

[332] M. Kazemi, L. Shiri, *Journal of Sulfur Chemistry* **2015**, *36*, 613-623.

[333] S. Schweinitzer, S. & C. Belger, K. Bauder, in *Watch Out, the Tiger is Coming!, Vol. 8, 40, 99, 111, 115* (Eds.: Hufnagel, Langmann, Pickert, Ötsch), **2019**, pp. 14-07.

[334] Y. Ohta, S. Itoh, A. Shigenaga, S. Shintaku, N. Fujii, A. Otaka, *Org. Lett.* **2006**, *8*, 467.

[335] W. Hou, X. Zhang, F. Li, C. F. Liu, *Org. Lett.* **2011**, *13*, 386.

[336] F. Burlina, G. Papageorgiou, C. Morris, P. D. White, J. Offer, *Chem. Sci.* **2014**, *5*, 766.

[337] C. Wang, Q. X. Guo, Y. Fu, *Chem. - Asian J.* **2011**, *6*, 1241.

[338] E. A. Castro, *Chem. Rev.* **1999**, *99*, 3505.

[339] B. Cowper, T. M. Sze, B. Premdjee, A. F. Bongat White, A. Hacking, D. Macmillan, *Chem. Commun.* **2015**, *51*, 3208.

[340] M. L. Bender, B. W. Turnquest, *J. Am. Chem. Soc.* **1957**, *79*, 1656.

[341] L. R. Fedor, T. C. Bruice, *J. Am. Chem. Soc.* **1964**, *86*, 4117.

[342] E. Vedejs, S. T. Diver, *J. Am. Chem. Soc.* **1993**, *115*, 3358.

[343] S. Tsuda, T. Yoshiya, M. Mochizuki, Y. Nishiuchi, *Org. Lett.* **2015**, *17*, 1806.

[344] D. H. Lee, J. R. Granja, J. A. Martinez, K. Severin, M. R. Ghadiri, *Nature* **1996**, *382*, 525.

[345] S. Yao, I. Ghosh, R. Zutshi, J. Chmielewski, *J. Am. Chem. Soc.* **1997**, *119*, 10559.

[346] G. S. Beligere, P. E. Dawson, *J. Am. Chem. Soc.* **1999**, *121*, 6332.

[347] L. Zhao, C. Ehrt, O. Koch, Y. W. Wu, *Angew. Chem., Int. Ed.* **2016**, *55*, 8129.

[348] T. Wieland, H. Hornig, *Liebigs Ann. Chem.* **1956**, *600*, 12.

[349] T. Sheradsky, *The Thiol Group (1974)*, **1974**.

[350] B. Kwon, D. Tietze, P. B. White, S. Y. Liao, M. Hong, *Protein Sci.* **2015**, *24*, 1087.

[351] Y. Sohma, H. Kitamura, H. Kawashima, H. Hojo, M. Yamashita, K. Akaji, Y. Kiso, *Tetrahedron Lett.* **2011**, *52*, 7146.

[352] M. Dittmann, J. Sauermann, R. Seidel, W. Zimmermann, M. Engelhard, *J. Pept. Sci.* **2010**, *16*, 558.

[353] M. S. Gill, A. A. Neverov, R. S. Brown, *J. Org. Chem.* **1997**, *62*, 7351.

[354] L. R. Malins, N. J. Mitchell, R. J. Payne, *J. Pept. Sci.* **2014**, *20*, 64.

[355] J. Vizzavona, F. Dick, T. Vorherr, *Bioorg. Med. Chem. Lett.* **2002**, *12*, 1963.

[356] K. Nakamura, T. Kanao, T. Uesugi, T. Hara, T. Sato, T. Kawakami, S. Aimoto, *J. Pept. Sci.* **2009**, *15*, 731.

[357] C. Marinzi, S. J. Bark, J. Offer, P. E. Dawson, *Bioorg. Med. Chem.* **2001**, *9*, 2323.

[358] C. P. R. Hackenberger, D. Schwarzer, *Angewandte Chemie International Edition* **2008**, *47*, 10030-10074.

[359] Y. G. Gololobov, I. N. Zhmurova, L. F. Kasukhin, *Tetrahedron* **1981**, *37*, 437-472.

[360] S. Sato, T. Sakamoto, E. Miyazawa, Y. Kikugawa, *Tetrahedron* **2004**, *60*, 7899-7906.

[361] T. Posner, *Berichte der deutschen chemischen Gesellschaft* **1905**, *38*, 646-657.

[362] A. B. Lowe, *Polymer Chemistry* **2010**, *1*, 17-36.

[363] C. Nilsson, N. Simpson, M. Malkoch, M. Johansson, E. Malmström, *Journal of Polymer Science Part A: Polymer Chemistry* **2008**, *46*, 1339-1348.

[364] A. Gress, A. Völkel, H. Schlaad, *Macromolecules* **2007**, *40*, 7928.

[365] R. L. A. David, J. A. Kornfield, *Macromolecules* **2008**, *41*, 1151-1161.

[366] L. M. Campos, K. L. Killops, R. Sakai, J. M. J. Paulusse, D. Damiron, E. Drockenmuller, B. W. Messmore, C. J. Hawker, *Macromolecules* **2008**, *41*, 7063-7070.

[367] C. Boyer, A. Granville, T. P. Davis, V. Bulmus, *Journal of Polymer Science Part A: Polymer Chemistry* **2009**, *47*, 3773-3794.

[368] J. M. Spruell, B. A. Levy, A. Sutherland, W. R. Dichtel, J. Y. Cheng, J. F. Stoddart, A. Nelson, *Journal of Polymer Science Part A: Polymer Chemistry* **2009**, *47*, 346-356.

[369] M. J. Kade, D. J. Burke, C. J. Hawker, *Journal of Polymer Science Part A: Polymer Chemistry* **2010**, *48*, 743-750.

[370] J. Justynska, H. Schlaad, *Macromolecular Rapid Communications* **2004**, *25*, 1478-1481.

[371] N. ten Brummelhuis, C. Diehl, H. Schlaad, *Macromolecules* **2008**, *41*, 9946-9947.

[372] T. Y. Lee, T. M. Roper, E. S. Jonsson, C. A. Guymon, C. E. Hoyle, *Macromolecules* **2004**, *37*, 3606-3613.

[373] J. Shin, S. Nazarenko, C. E. Hoyle, *Macromolecules* **2008**, *41*, 6741-6746.

[374] A. F. Senyurt, H. Wei, C. E. Hoyle, S. G. Piland, T. E. Gould, *Macromolecules* **2007**, *40*, 4901-4909.

[375] H. Wei, A. F. Senyurt, S. Jönsson, C. E. Hoyle, *Journal of Polymer Science Part A: Polymer Chemistry* **2007**, *45*, 822-829.

[376] N. B. Cramer, S. K. Reddy, M. Cole, C. Hoyle, C. N. Bowman, *Journal of Polymer Science Part A: Polymer Chemistry* **2004**, *42*, 5817-5826.

[377] K. L. Killops, L. M. Campos, C. J. Hawker, *Journal of the American Chemical Society* **2008**, *130*, 5062-5064.

[378] C. Rissing, D. Y. Son, *Organometallics* **2009**, *28*, 3167-3172.

[379] C. R. Nuttelman, M. A. Rice, A. E. Rydholm, C. N. Salinas, D. N. Shah, K. S. Anseth, *Progress in Polymer Science* **2008**, *33*, 167-179.

[380] C. N. Salinas, K. S. Anseth, *Macromolecules* **2008**, *41*, 6019-6026.

[381] M. C. Cushing, K. S. Anseth, *Science* **2007**, *316*, 1133-1134.

[382] G. Triola, L. Brunsveld, H. Waldmann, *The Journal of Organic Chemistry* **2008**, *73*, 3646-3649.

[383] S. Wittrock, T. Becker, H. Kunz, *Angewandte Chemie International Edition* **2007**, *46*, 5226-5230.

[384] H. C. Kolb, M. G. Finn, K. B. Sharpless, *Angewandte Chemie International Edition* **2001**, *40*, 2004-2021.

[385] R. Huisgen, *Proceedings of the Chemical Society* **1961**, 357-396.

[386] R. A. Evans, *Australian Journal of Chemistry* **2007**, *60*, 384-395.

[387] D. Fournier, R. Hoogenboom, U. S. Schubert, *Chemical Society Reviews* **2007**, *36*, 1369-1380.

[388] J. E. Moses, A. D. Moorhouse, *Chemical Society Reviews* **2007**, *36*, 1249-1262.

[389] T. Katsuki, K. B. Sharpless, *Journal of the American Chemical Society* **1980**, *102*, 5974-5976.

[390] Y. Gao, J. M. Klunder, R. M. Hanson, H. Masamune, S. Y. Ko, K. B. Sharpless, *Journal of the American Chemical Society* **1987**, *109*, 5765-5780.

[391] O. Diels, K. Alder, *Justus Liebigs Annalen der Chemie* **1928**, *460*, 98-122.

[392] S. Sinnwell, C. V. Synatschke, T. Junkers, M. H. Stenzel, C. Barner-Kowollik, *Macromolecules* **2008**, *41*, 7904-7912.

[393] C. E. Hoyle, T. Y. Lee, T. Roper, *Journal of Polymer Science Part A: Polymer Chemistry* **2004**, *42*, 5301-5338.

[394] A. B. Lowe, C. E. Hoyle, C. N. Bowman, *Journal of Materials Chemistry* **2010**, *20*, 4745-4750.

[395] H. Bader, L. C. Cross, I. Heilbron, E. R. H. Jones, *Journal of the Chemical Society (Resumed)* **1949**, 619-623.

[396] A. B. Lowe, *Polymer* **2014**, *55*, 5517-5549.

[397] J. Shin, H. Matsushima, J. W. Chan, C. E. Hoyle, *Macromolecules* **2009**, *42*, 3294-3301.

[398] B. M. Rosen, G. Lligadas, C. Hahn, V. Percec, *Journal of Polymer Science Part A: Polymer Chemistry* **2009**, *47*, 3931-3939.

[399] B. H. Northrop, R. N. Coffey, *Journal of the American Chemical Society* **2012**, *134*, 13804-13817.

[400] C. E. Hoyle, C. N. Bowman, *Angewandte Chemie International Edition* **2010**, *49*, 1540-1573.

[401] A. B. Lowe, *Polymer Chemistry* **2014**, *5*, 4820-4870.

[402] A. K. Sinha, D. Equbal, *Asian Journal of Organic Chemistry* **2019**, *8*, 32-47.

[403] E. Scanlan, V. Corcé, A. Malone, *Molecules (Basel, Switzerland)* **2014**, *19*, 19137-19151.

[404] A. Dondoni, *Angewandte Chemie International Edition* **2008**, *47*, 8995-8997.

[405] B. D. Mather, K. Viswanathan, K. M. Miller, T. E. Long, *Progress in Polymer Science* **2006**, *31*, 487-531.

[406] I. C. Stewart, R. G. Bergman, F. D. Toste, *Journal of the American Chemical Society* **2003**, *125*, 8696-8697.

[407] M. G. Voronkov, E. N. Deryagina, *Russian Chemical Reviews* **1990**, *59*, 778-791.

[408] M. Uygun, M. A. Tasdelen, Y. Yagci, *Macromolecular Chemistry and Physics* **2010**, *211*, 103-110.

[409] C. R. Morgan, F. Magnotta, A. D. Ketley, *Journal of Polymer Science: Polymer Chemistry Edition* **1977**, *15*, 627-645.

[410] K. Griesbaum, *Angewandte Chemie International Edition in English* **1970**, *9*, 273-287.

[411] A. A. Oswald, W. Naegele, *Die Makromolekulare Chemie: Macromolecular Chemistry and Physics* **1966**, *97*, 258-266.

[412] M. Claudino, M. Johansson, M. Jonsson, *European Polymer Journal* **2010**, *46*, 2321-2332.

[413] L. M. Stock, *Journal of Chemical Education* **1972**, *49*, 400.

[414] H. Kakwere, S. Perrier, *Journal of the American Chemical Society* **2009**, *131*, 1889-1895.

[415] J. R. Winther, C. Thorpe, *Biochim Biophys Acta* **2014**, *1840*, 838-846.

[416] R. Vestberg, A. M. Piekarski, E. D. Pressly, K. Y. Van Berkel, M. Malkoch, J. Gerbac, N. Ueno, C. J. Hawker, *Journal of Polymer Science Part A: Polymer Chemistry* **2009**, *47*, 1237-1258.

[417] Q. Chen, B.-H. Han, *Journal of Polymer Science Part A: Polymer Chemistry* **2009**, *47*, 2948-2957.

[418] E. Gungor, C. Bilir, H. Durmaz, G. Hizal, U. Tunca, *Journal of Polymer Science Part A: Polymer Chemistry* **2009**, *47*, 5947-5953.

[419] T. Miyadera, E. M. Kosower, *Journal of medicinal chemistry* **1972**, *15*, 534-537.

[420] L. C. Radu, J. Yang, J. Kopeček, *Macromolecular bioscience* **2009**, *9*, 36-44.

[421] R. Singh, *Bioconjugate chemistry* **1994**, *5*, 348-351.

[422] T. P. Kogan, *Synthetic communications* **1992**, *22*, 2417-2424.

[423] B. D. Fairbanks, T. F. Scott, C. J. Kloxin, K. S. Anseth, C. N. Bowman, *Macromolecules* **2009**, *42*, 211-217.

[424] J. W. Chan, H. Zhou, C. E. Hoyle, A. B. Lowe, *Chemistry of Materials* **2009**, *21*, 1579-1585.

[425] K. Knop, R. Hoogenboom, D. Fischer, U. S. Schubert, *Angewandte Chemie International Edition* **2010**, *49*, 6288-6308.

[426] J. Willersinn, A. Bogomolova, M. B. Cabré, B. V. K. J. Schmidt, *Polymer Chemistry* **2017**, *8*, 1244-1254.

[427] V. Hildebrand, M. Heydenreich, A. Laschewsky, H. M. Möller, P. Müller-Buschbaum, C. M. Papadakis, D. Schanzenbach, E. Wischerhoff, *Polymer* **2017**, *122*, 347-357.

[428] Y. Mai, A. Eisenberg, *Chemical Society Reviews* **2012**, *41*, 5969-5985.

[429] B. V. K. J. Schmidt, *Macromolecular Chemistry and Physics* **2018**, *219*, 1700494.

[430] Z. Ge, D. Xie, D. Chen, X. Jiang, Y. Zhang, H. Liu, S. Liu, *Macromolecules* **2007**, *40*, 3538-3546.

[431] Y. Jiang, H. Lu, F. Chen, M. Callari, M. Pourgholami, D. L. Morris, M. H. Stenzel, *Biomacromolecules* **2016**, *17*, 808-817.

[432] P. Heller, N. Mohr, A. Birke, B. Weber, A. Reske-Kunz, M. Bros, M. Barz, *Macromolecular Bioscience* **2015**, *15*, 63-73.

[433] J. Kopeček, *Biomaterials* **2007**, *28*, 5185-5192.

[434] J. Groll, T. Boland, T. Blunk, J. A. Burdick, D.-W. Cho, P. D. Dalton, B. Derby, G. Forgacs, Q. Li, V. A. Mironov, L. Moroni, M. Nakamura, W. Shu, S. Takeuchi, G. Vozzi, T. B. F. Woodfield, T. Xu, J. J. Yoo, J. Malda, *Biofabrication* **2016**, *8*, 013001.

[435] A. M. Kelly, F. Wiesbrock, *Macromolecular Rapid Communications* **2012**, *33*, 1632-1647.

[436] T. R. Dargaville, B. G. Hollier, A. Shokoohmand, R. Hoogenboom, *Cell Adhesion & Migration* **2014**, *8*, 88-93.

[437] J. Han, D. Zhao, D. Li, X. Wang, Z. Jin, K. Zhao, *Polymers* **2018**, *10*, 31.

[438] O. Koshkina, T. Lang, R. Thiermann, D. Docter, R. H. Stauber, C. Secker, H. Schlaad, S. Weidner, B. Mohr, M. Maskos, A. Bertin, *Langmuir* **2015**, *31*, 8873-8881.

[439] G. Morgese, E. M. Benetti, *European Polymer Journal* **2017**, *88*, 470-485.

[440] L. Tauhardt, K. Kempe, M. Gottschaldt, U. S. Schubert, *Chemical Society Reviews* **2013**, *42*, 7998-8011.

[441] F. Fuertges, A. Abuchowski, *Journal of controlled release* **1990**, *11*, 139-148.

[442] P. K. Working, M. S. Newman, J. Johnson, J. B. Cornacoff, ACS Publications, **1997**.

[443] R. I. Mahato, *Biomaterials for delivery and targeting of proteins and nucleic acids*, CRC Press, **2004**.

[444] H. Hatakeyama, H. Akita, H. Harashima, *Biological and Pharmaceutical Bulletin* **2013**, *36*, 892-899.

[445] F. M. Veronese, A. Mero, *BioDrugs* **2008**, *22*, 315-329.

[446] T. Gao, H. Uludag, *Journal of Biomedical Materials Research* **2001**, *57*, 92-100.

[447] V. B. Damodaran, C. Fee, *European Pharmaceutical Review* **2010**, *15*, 18-26.

[448] F. Zhang, M.-r. Liu, H.-t. Wan, *Biological and Pharmaceutical Bulletin* **2014**, *37*, 335-339.

[449] B. Guillerm, S. Monge, V. Lapinte, J. J. Robin, *Macromol Rapid Commun* **2012**, *33*, 1600-1612.

[450] M. Hartlieb, K. Kempe, U. S. Schubert, *Journal of Materials Chemistry B* **2015**, *3*, 526-538.

[451] M. M. Bloksma, U. S. Schubert, R. Hoogenboom, *Macromolecular Rapid Communications* **2011**, *32*, 1419-1441.

[452] R. Hoogenboom, *Angewandte Chemie International Edition* **2009**, *48*, 7978-7994.

[453] H. Schlaad, C. Diehl, A. Gress, M. Meyer, A. L. Demirel, Y. Nur, A. Bertin, *Macromol Rapid Commun* **2010**, *31*, 511-525.

[454] R. Hoogenboom, in *Handbook of Ring-Opening Polymerization*, **2009**, pp. 141-164.

[455] O. Sedlacek, B. D. Monnery, S. K. Filippov, R. Hoogenboom, M. Hruby, *Macromol. Rapid Commun.* **2012**, *33*, 1648.

[456] E. Rossegger, V. Schenk, F. Wiesbrock, *Polymers* **2013**, *5*, 956-1011.

[457] K. Aoi, M. Okada, *Progress in Polymer Science* **1996**, *21*, 151-208.

[458] B. Verbraeken, B. D. Monnery, K. Lava, R. Hoogenboom, *European Polymer Journal* **2017**, *88*, 451-469.

[459] S. Kobayashi, *Progress in Polymer Science* **1990**, *15*, 751-823.

[460] J. I. Kroschwitz, *Encyclopedia of polymer science and engineering, Vol. 17*, John Wiley & Sons New York, **1990**.

[461] B. M. Culbertson, *Progress in polymer science* **2002**, *27*, 579-626.

[462] R. Hoogenboom, H. Schlaad, *Polymer Chemistry* **2017**, *8*, 24-40.

[463] M. Glassner, M. Vergaelen, R. Hoogenboom, *Polymer International* **2018**, *67*, 32-45.

[464] N. Adams, U. S. Schubert, *Advanced Drug Delivery Reviews* **2007**, *59*, 1504-1520.

[465] R. Luxenhofer, Y. Han, A. Schulz, J. Tong, Z. He, A. V. Kabanov, R. Jordan, *Macromolecular rapid communications* **2012**, *33*, 1613-1631.

[466] V. R. de la Rosa, *Journal of Materials Science: Materials in Medicine* **2014**, *25*, 1211-1225.

[467] E. Vlassi, A. Papagiannopoulos, S. Pispas, *European Polymer Journal* **2017**, *88*, 516-523.

[468] T. X. Viegas, M. D. Bentley, J. M. Harris, Z. Fang, K. Yoon, B. Dizman, R. Weimer, A. Mero, G. Pasut, F. M. Veronese, *Bioconjugate Chemistry* **2011**, *22*, 976-986.

[469] P. Wilson, P. C. Ke, T. P. Davis, K. Kempe, *European Polymer Journal* **2017**, *88*, 486-515.

[470] D. A. Tomalia, D. P. Sheetz, *Journal of Polymer Science Part A-1: Polymer Chemistry* **1966**, *4*, 2253-2265.

[471] W. Seeliger, E. Aufderhaar, W. Diepers, R. Feinauer, R. Nehring, W. Thier, H. Hellmann, *Angewandte Chemie International Edition in English* **1966**, *5*, 875-888.

[472] T. Kagiya, S. Narisawa, T. Maeda, K. Fukui, *Journal of Polymer Science Part B: Polymer Letters* **1966**, *4*, 441-445.

[473] T. G. Bassiri, A. Levy, M. Litt, *Journal of Polymer Science Part B: Polymer Letters* **1967**, *5*, 871-879.

[474] R. Hoogenboom, *European Polymer Journal* **2017**, *88*, 448-450.

[475] M. Bauer, C. Lautenschlaeger, K. Kempe, L. Tauhardt, U. S. Schubert, D. Fischer, *Macromol. Biosci.* **2012**, *12*, 986.

[476] M. Bauer, S. Schroeder, L. Tauhardt, K. Kempe, U. S. Schubert, D. Fischer, *Journal of Polymer Science Part A: Polymer Chemistry* **2013**, *51*, 1816-1821.

[477] M. N. Leiske, A.-K. Trützschler, S. Armoneit, P. Sungur, S. Hoeppener, M. Lehmann, A. Traeger, U. S. Schubert, *Journal of Materials Chemistry B* **2017**, *5*, 9102-9113.

[478] D. L. Kyluik-Price, L. Li, M. D. Scott, *Biomaterials* **2014**, *35*, 412-422.

[479] P. Goddard, L. E. Hutchinson, J. Brown, L. J. Brookman, *J. Controlled Release* **1989**, *10*, 5.

[480] F. C. Gaertner, R. Luxenhofer, B. Blechert, R. Jordan, M. Essler, *J. Controlled Release* **2007**, *119*, 291.

[481] L. Wyffels, T. Verbrugghen, B. D. Monnery, M. Glassner, S. Stroobants, R. Hoogenboom, S. Staelens, *Journal of Controlled Release* **2016**, *235*, 63-71.

[482] Z. He, X. Wan, A. Schulz, H. Bludau, M. A. Dobrovolskaia, S. T. Stern, S. A. Montgomery, H. Yuan, Z. Li, D. Alakhova, M. Sokolsky, D. B. Darr, C. M. Perou, R. Jordan, R. Luxenhofer, A. V. Kabanov, *Biomaterials* **2016**, *101*, 296-309.

[483] H. P. C. Van Kuringen, J. Lenoir, E. Adriaens, J. Bender, B. G. De Geest, R. Hoogenboom, *Macromolecular Bioscience* **2012**, *12*, 1114-1123.

[484] K. L. Eskow Jaunarajs, D. G. Standaert, T. X. Viegas, M. D. Bentley, Z. Fang, B. Dizman, K. Yoon, R. Weimer, P. Ravenscroft, T. H. Johnston, M. P. Hill, J. M. Brotchie, R. W. Moreadith, *Movement Disorders* **2013**, *28*, 1675-1682.

[485] R. W. Moreadith, T. X. Viegas, M. D. Bentley, J. M. Harris, Z. Fang, K. Yoon, B. Dizman, R. Weimer, B. P. Rae, X. Li, C. Rader, D. Standaert, W. Olanow, *European Polymer Journal* **2017**, *88*, 524-552.

[486] M. W. M. Fijten, J. M. Kranenburg, H. M. L. Thijs, R. M. Paulus, B. M. van Lankvelt, J. de Hullu, M. Springintveld, D. J. G. Thielen, C. A. Tweedie, R. Hoogenboom, K. J. Van Vliet, U. S. Schubert, *Macromolecules* **2007**, *40*, 5879-5886.

[487] E. F.-J. Rettler, J. M. Kranenburg, H. M. L. Lambermont-Thijs, R. Hoogenboom, U. S. Schubert, *Macromolecular Chemistry and Physics* **2010**, *211*, 2443-2448.

[488] M. Baumert, J. Zimmermann, J. Scherble, R. Mülhaupt, J. Kressler, *Macromolecules* **1999**, *32*, 2503-2510.

[489] H. Malz, H. Komber, D. Voigt, I. Hopfe, J. Pionteck, *Macromolecular Chemistry and Physics* **1999**, *200*, 642-651.

[490] H. Malz, J. Pionteck, P. Pötschke, H. Komber, D. Voigt, J. Lustoň, F. Böhme, *Macromolecular Chemistry and Physics* **2001**, *202*, 2148-2154.

[491] T. Saegusa, H. Ikeda, *Macromolecules* **1973**, *6*, 808-811.

[492] M. Miyamoto, K. Aoi, M. Morimoto, Y. Chujo, T. Saegusa, *Macromolecules* **1992**, *25*, 5878-5885.

[493] T. Saegusa, H. Ikeda, H. Fujii, *Polymer Journal* **1973**, *4*, 87-92.

[494] F. Wiesbrock, R. Hoogenboom, M. Leenen, S. F. G. M. van Nispen, M. van der Loop, C. H. Abeln, A. M. J. van den Berg, U. S. Schubert, *Macromolecules* **2005**, *38*, 7957-7966.

[495] V. V. Jerca, K. Lava, B. Verbraeken, R. Hoogenboom, *Polymer Chemistry* **2016**, *7*, 1309-1322.

[496] J.-S. Park, K. Kataoka, *Macromolecules* **2007**, *40*, 3599-3609.

[497] S. Huber, R. Jordan, *Colloid and Polymer Science* **2008**, *286*, 395-402.

[498] M. Talelli, W. E. Hennink, *Nanomedicine* **2011**, *6*, 1245-1255.

[499] R. Luxenhofer, A. Schulz, C. Roques, S. Li, T. K. Bronich, E. V. Batrakova, R. Jordan, A. V. Kabanov, *Biomaterials* **2010**, *31*, 4972-4979.

[500] M. Beck, P. Birnbrich, U. Eicken, H. Fischer, W. E. Fristad, B. Hase, H. J. Krause, *Die Angewandte Makromolekulare Chemie* **1994**, *223*, 217-233.

[501] H. Wenker, *Journal of the American Chemical Society* **1935**, *57*, 1079-1080.

[502] K. Kempe, M. Lobert, R. Hoogenboom, U. S. Schubert, *Journal of Combinatorial Chemistry* **2009**, *11*, 274-280.

[503] H. Witte, W. Seeliger, *Justus Liebigs Annalen der Chemie* **1974**, *1974*, 996-1009.

[504] T. R. Dargaville, K. Lava, B. Verbraeken, R. Hoogenboom, *Macromolecules* **2016**, *49*, 4774-4783.

[505] S. Aoshima, S. Kanaoka, *Chemical Reviews* **2009**, *109*, 5245-5287.

[506] M. Szwarc, *Nature* **1956**, *178*, 1168-1169.

[507] T. Bodner, L. Ellmaier, V. Schenk, J. Albering, F. Wiesbrock, *Polymer International* **2011**, *60*, 1173-1179.

[508] R. Hoogenboom, M. W. Fijten, H. M. Thijs, B. M. van Lankvelt, U. S. Schubert, *Designed monomers and polymers* **2005**, *8*, 659-671.

[509] H. Goossens, S. Catak, M. Glassner, V. R. de la Rosa, B. D. Monnery, F. De Proft, V. Van Speybroeck, R. Hoogenboom, *ACS Macro Letters* **2013**, *2*, 651-654.

[510] K. Matyjaszewski, J. Xia, *Chemical Reviews* **2001**, *101*, 2921-2990.

[511] M. Litt, A. Levy, J. Herz, *Journal of Macromolecular Science: Part A - Chemistry* **1975**, *9*, 703-727.

[512] A. Levy, M. Litt, *Journal of Polymer Science Part A-1: Polymer Chemistry* **1968**, *6*, 1883-1894.

[513] A. Levy, M. Litt, *Journal of Polymer Science Part A-1: Polymer Chemistry* **1968**, *6*, 63-72.

[514] A. Baumgaertel, C. Weber, K. Knop, A. Crecelius, U. S. Schubert, *Rapid Communications in Mass Spectrometry* **2009**, *23*, 756-762.

[515] B. D. Monnery, S. Shaunak, M. Thanou, J. H. G. Steinke, *Macromolecules* **2015**, *48*, 3197-3206.

[516] R. Hoogenboom, B. Monnery, U.S. Patent Nr. 10,118,991, **2018**.

[517] J. M. G. Cowie, V. Arrighi, *Polymers: chemistry and physics of modern materials*, CRC press, **2007**.

[518] T. B. Bonné, K. Lüdtke, R. Jordan, C. M. Papadakis, *Macromolecular Chemistry and Physics* **2007**, *208*, 1402-1408.

[519] T. Bonné, K. Lüdtke, R. Jordan, P. Štěpánek, C. Papadakis, *Colloid Polym Sci* **2004**, *282*, 833-843.

[520] F. Wiesbrock, R. Hoogenboom, M. A. M. Leenen, M. A. R. Meier, U. S. Schubert, *Macromolecules* **2005**, *38*, 5025-5034.

[521] K. Kempe, *Macromolecular Chemistry and Physics* **2017**, *218*, 1700021.

[522] C. Ebner, T. Bodner, F. Stelzer, F. Wiesbrock, *Macromolecular Rapid Communications* **2011**, *32*, 254-288.

[523] R. Hoogenboom, F. Wiesbrock, H. Huang, M. A. M. Leenen, H. M. L. Thijs, S. F. G. M. van Nispen, M. van der Loop, C.-A. Fustin, A. M. Jonas, J.-F. Gohy, U. S. Schubert, *Macromolecules* **2006**, *39*, 4719-4725.

[524] R. Hoogenboom, F. Wiesbrock, M. A. M. Leenen, H. M. L. Thijs, H. Huang, C.-A. Fustin, P. Guillet, J.-F. Gohy, U. S. Schubert, *Macromolecules* **2007**, *40*, 2837-2843.

[525] R. Hoogenboom, M. A. M. Leenen, F. Wiesbrock, U. S. Schubert, *Macromol. Rapid Commun.* **2005**, *26*, 1773.

[526] M. G. Alemseghed, J. Servello, N. Hundt, P. Sista, M. C. Biewer, M. C. Stefan, *Macromolecular Chemistry and Physics* **2010**, *211*, 1291-1297.

[527] R. Weberskirch, J. Preuschen, H. W. Spiess, O. Nuyken, *Macromolecular Chemistry and Physics* **2000**, *201*, 995-1007.

[528] M. Reif, R. Jordan, *Macromolecular Chemistry and Physics* **2011**, *212*, 1815-1824.

[529] R. Hoogenboom, M. W. M. Fijten, U. S. Schubert, *Journal of Polymer Science Part A: Polymer Chemistry* **2004**, *42*, 1830-1840.

[530] P. Buzin, G. Schwarz, H. R. Kricheldorf, *Journal of Polymer Science Part A: Polymer Chemistry* **2008**, *46*, 4777-4784.

[531] M.-E. Kourti, G. C. Vougioukalakis, N. Hadjichristidis, M. Pitsikalis, *Journal of Polymer Science Part A: Polymer Chemistry* **2011**, *49*, 2520-2527.

[532] R. M. Paulus, C. R. Becer, R. Hoogenboom, U. S. Schubert, *Macromolecular Chemistry and Physics* **2008**, *209*, 794-800.

[533] M. W. M. Fijten, C. Haensch, B. M. van Lankvelt, R. Hoogenboom, U. S. Schubert, *Macromolecular Chemistry and Physics* **2008**, *209*, 1887-1895.

[534] J. C. Rueda, H. Komber, J. C. Cedrón, B. Voit, G. Shevtsova, *Macromolecular Chemistry and Physics* **2003**, *204*, 947-953.

[535] A. Cirpan, S. Alkan, L. Toppare, G. David, Y. Yagci, *European Polymer Journal* **2001**, *37*, 2225-2229.

[536] S. Zalipsky, C. B. Hansen, J. M. Oaks, T. M. Allen, *Journal of Pharmaceutical Sciences* **1996**, *85*, 133-137.

[537] B. Guillerm, S. Monge, V. Lapinte, J.-J. Robin, *Macromolecules* **2010**, *43*, 5964-5970.

[538] T. Saegusa, H. Ikeda, H. Fujii, *Polym J* **1972**, *3*, 176-180.

[539] G. Volet, V. Chanthavong, V. Wintgens, C. Amiel, *Macromolecules* **2005**, *38*, 5190-5197.

[540] R. Jordan, K. Martin, H. J. Räder, K. K. Unger, *Macromolecules* **2001**, *34*, 8858-8865.

[541] C. J. Waschinski, V. Herdes, F. Schueler, J. C. Tiller, *Macromolecular Bioscience* **2005**, *5*, 149-156.

[542] Y. Chujo, E. Ihara, H. Ihara, T. Saegusa, *Macromolecules* **1989**, *22*, 2040-2043.

[543] S. Kobayashi, H. Uyama, Y. Narita, J. Ishiyama, *Macromolecules* **1992**, *25*, 3232-3236.

[544] P. D. Trivedi, D. N. Schulz, *Polymer Bulletin* **1980**, *3*, 37-44.

[545] B. Guillerm, V. Darcos, V. Lapinte, S. Monge, J. Coudane, J.-J. Robin, *Chemical Communications* **2012**, *48*, 2879-2881.

[546] K. Shiro, U. Hiroshi, M. Toshild, N. Yutaka, *Chemistry Letters* **1991**, *20*, 1771-1774.

[547] C. Giardi, V. Lapinte, F. Nielloud, J.-M. Devoisselle, J.-J. Robin, *Journal of Polymer Science Part A: Polymer Chemistry* **2010**, *48*, 4027-4035.

[548] M. Einzmann, W. H. Binder, *Journal of Polymer Science Part A: Polymer Chemistry* **2001**, *39*, 2821-2831.

[549] C. Giardi, V. Lapinte, C. Charnay, J. J. Robin, *Reactive and Functional Polymers* **2009**, *69*, 643-649.

[550] J. S. Hrkach, K. Matyjaszewski, *Macromolecules* **1992**, *25*, 2070-2075.

[551] K. Król-Morkisz, K. Pielichowska, in *Polymer Composites with Functionalized Nanoparticles*, Elsevier, **2019**, pp. 405-435.

[552] B. Brissault, C. Guis, H. Cheradame, *European Polymer Journal* **2002**, *38*, 219-228.

[553] O. Nuyken, G. Maier, A. Groß, H. Fischer, *Macromolecular Chemistry and Physics* **1996**, *197*, 83-95.

[554] S. Kobayashi, E. Masuda, S. Shoda, Y. Shimano, *Macromolecules* **1989**, *22*, 2878-2884.

[555] J.-S. Park, Y. Akiyama, F. M. Winnik, K. Kataoka, *Macromolecules* **2004**, *37*, 6786-6792.

[556] G. Volet, A.-C. L. Deschamps, C. Amiel, *Journal of Polymer Science Part A: Polymer Chemistry* **2010**, *48*, 2477-2485.

[557] Y. Chujo, Y. Yoshifuji, K. Sada, T. Saegusa, *Macromolecules* **1989**, *22*, 1074-1077.

[558] S. Kobayashi, M. Kaku, S. Sawada, T. Saegusa, *Polymer Bulletin* **1985**, *13*, 447-451.

[559] A. Förtig, R. Jordan, K. Graf, G. Schiavon, O. Purrucker, M. Tanaka, *Macromolecular Symposia* **2004**, *210*, 329-338.

[560] R. Hoogenboom, M. W. M. Fijten, M. A. R. Meier, U. S. Schubert, *Macromolecular Rapid Communications* **2003**, *24*, 92-97.

[561] P. Van Caeter, E. J. Goethals, V. Gancheva, R. Velichkova, *Polymer Bulletin* **1997**, *39*, 589-596.

[562] M. Adeli, Z. Zarnegar, R. Kabiri, *European Polymer Journal* **2008**, *44*, 1921-1930.

[563] Y. Chujo, E. Ihara, S. Kure, T. Saegusa, *Macromolecules* **1993**, *26*, 5681-5686.

[564] G. Volet, T.-X. Lav, J. Babinot, C. Amiel, *Macromolecular Chemistry and Physics* **2011**, *212*, 118-124.

[565] C. Guis, H. Cheradame, *European Polymer Journal* **2000**, *36*, 2581-2590.

[566] T. Loontjens, L. Rique-Lurbet, *Designed Monomers and Polymers* **1999**, *2*, 217-229.

[567] A. Mero, Z. Fang, G. Pasut, F. M. Veronese, T. X. Viegas, *Journal of Controlled Release* **2012**, *159*, 353-361.

[568] M. C. Woodle, C. M. Engbers, S. Zalipsky, *Bioconjugate Chemistry* **1994**, *5*, 493-496.

[569] D. Christova, R. Velichkova, E. J. Goethals, *Macromolecular Rapid Communications* **1997**, *18*, 1067-1073.

[570] M. Miyamoto, K. Naka, M. Tokumizu, T. Saegusa, *Macromolecules* **1989**, *22*, 1604-1607.

[571] C. Weber, A. Krieg, R. M. Paulus, H. M. L. Lambermont-Thijs, C. R. Becer, R. Hoogenboom, U. S. Schubert, *Macromolecular Symposia* **2011**, *308*, 17-24.

[572] G. David, A. Ioanid, *Journal of Applied Polymer Science* **2001**, *80*, 2191-2199.

[573] G. David, V. Alupei, B. C. Simionescu, *European Polymer Journal* **2001**, *37*, 1353-1358.

[574] G. Cai, M. H. Litt, *Journal of Polymer Science Part A: Polymer Chemistry* **1992**, *30*, 649-657.

[575] K. Kempe, S. Jacobs, H. M. L. Lambermont-Thijs, M. M. W. M. Fijten, R. Hoogenboom, U. S. Schubert, *Macromolecules* **2010**, *43*, 4098-4104.

[576] K. Kempe, M. Lobert, R. Hoogenboom, U. S. Schubert, *Journal of Polymer Science Part A: Polymer Chemistry* **2009**, *47*, 3829-3838.

[577] P. Persigehl, R. Jordan, O. Nuyken, *Macromolecules* **2000**, *33*, 6977-6981.

[578] K. Aoi, A. Takasu, M. Okada, T. Imae, *Macromolecular Chemistry and Physics* **1999**, *200*, 1112-1120.

[579] N. t. Brummelhuis, H. Schlaad, *Polymer Chemistry* **2011**, *2*, 1180-1184.

[580] M. A. Cortez, S. M. Grayson, *Macromolecules* **2010**, *43*, 4081-4090.

[581] M. Lobert, H. M. L. Thijs, T. Erdmenger, R. Eckardt, C. Ulbricht, R. Hoogenboom, U. S. Schubert, *Chemistry – A European Journal* **2008**, *14*, 10396-10407.

[582] P. J. M. Bouten, D. Hertsen, M. Vergaelen, B. D. Monnery, M. A. Boerman, H. Goossens, S. Catak, J. C. M. van Hest, V. Van Speybroeck, R. Hoogenboom, *Polymer Chemistry* **2015**, *6*, 514-518.

[583] P. J. M. Bouten, K. Lava, J. C. M. Van Hest, R. Hoogenboom, *Polymers* **2015**, *7*, 1998-2008.

[584] K. Lüdtke, R. Jordan, P. Hommes, O. Nuyken, C. A. Naumann, *Macromolecular Bioscience* **2005**, *5*, 384-393.

[585] M. Hartlieb, D. Pretzel, K. Kempe, C. Fritzsche, R. M. Paulus, M. Gottschaldt, U. S. Schubert, *Soft Matter* **2013**, *9*, 4693-4704.

[586] S. Cesana, A. Kurek, M. A. Baur, J. Auernheimer, O. Nuyken, *Macromolecular Rapid Communications* **2007**, *28*, 608-615.

[587] C. A. Naumann, O. Prucker, T. Lehmann, J. Rühe, W. Knoll, C. W. Frank, *Biomacromolecules* **2002**, *3*, 27-35.

[588] M. B. Foreman, J. P. Coffman, M. J. Murcia, S. Cesana, R. Jordan, G. S. Smith, C. A. Naumann, *Langmuir* **2003**, *19*, 326-332.

[589] R. M. England, J. I. Hare, J. Barnes, J. Wilson, A. Smith, N. Strittmatter, P. D. Kemmitt, M. J. Waring, S. T. Barry, C. Alexander, M. B. Ashford, *Journal of Controlled Release* **2017**, *247*, 73-85.

[590] M. Schmidt, S. Harmuth, E. R. Barth, E. Wurm, R. Fobbe, A. Sickmann, C. Krumm, J. C. Tiller, *Bioconjugate Chemistry* **2015**, *26*, 1950-1962.

[591] L. Tauhardt, D. Pretzel, S. Bode, J. A. Czaplewska, K. Kempe, M. Gottschaldt, U. S. Schubert, *Journal of Polymer Science Part A: Polymer Chemistry* **2014**, *52*, 2703-2714.

[592] B. Trzebicka, R. Szweda, D. Kosowski, D. Szweda, Ł. Otulakowski, E. Haladjova, A. Dworak, *Progress in Polymer Science* **2017**, *68*, 35-76.

[593] H. Bludau, A. E. Czapar, A. S. Pitek, S. Shukla, R. Jordan, N. F. Steinmetz, *European Polymer Journal* **2017**, *88*, 679-688.

[594] S. Konieczny, C. P. Fik, N. J. H. Averesch, J. C. Tiller, *Journal of Biotechnology* **2012**, *159*, 195-203.

[595] T. Lühmann, M. Schmidt, M. N. Leiske, V. Spieler, T. C. Majdanski, M. Grube, M. Hartlieb, I. Nischang, S. Schubert, U. S. Schubert, L. Meinel, *ACS Biomaterials Science & Engineering* **2017**, *3*, 304-312.

[596] L. K. Kostanski, D. M. Keller, A. E. Hamielec, *Journal of Biochemical and Biophysical Methods* **2004**, *58*, 159-186.

[597] S. Harcum, in *Biologically Inspired Textiles* (Eds.: A. Abbott, M. Ellison), Woodhead Publishing, **2008**, pp. 26-43.

[598] P. Yu, X. Li, X. Li, X. Lu, G. Ma, Z. Su, *Bioorganic & Medicinal Chemistry Letters* **2007**, *17*, 5605-5609.

[599] F. Pinzner, master thesis, Julius-Maximilians-Universität (Würzburg), **2015**.

[600] B. Böhm, master thesis, Julius-Maximilians-Universität (Würzburg), **2019**.

[601] J. Liebscher, Dissertation thesis, Julius-Maximilians-Universität (Würzburg), **2019**.

[602] H. Morawetz, *Journal of Macromolecular Science—Chemistry* **1979**, *13*, 311-320.

[603] H. Morawetz, *Macromolecules in solution, Vol. 21*, Wiley-Interscience, **1975**.

[604] A. Ravve, *Principles of polymer chemistry*, Springer Science & Business Media, **2013**.

[605] K. Ito, H. Tsuchida, A. Hayashi, T. Kitano, E. Yamada, T. Matsumoto, *Polymer journal* **1985**, *17*, 827-839.

[606] B. D. Monnery, V. V. Jerca, O. Sedlacek, B. Verbraeken, R. Cavill, R. Hoogenboom, *Angewandte Chemie International Edition* **2018**, *57*, 15400-15404.

[607] O. Sedlacek, B. D. Monnery, R. Hoogenboom, *Polymer Chemistry* **2019**, *10*, 1286-1290.

[608] R. Hoogenboom, R. M. Paulus, M. W. Fijten, U. S. Schubert, *Journal of Polymer Science Part A: Polymer Chemistry* **2005**, *43*, 1487-1497.

[609] M. Schmitz, Dissertation thesis, Julius-Maximilians-Universität (Würzburg), **2016**.

[610] I. Paulus, master thesis, Julius-Maximilians-Universität (Würzburg), **2017**.

[611] D. Held, *The Column* **2017**, *13*, 14-18.

[612] D. Held, *The Column* **2017**, *13*, 18-23.

[613] J. W. Sons, *Characterization and Analysis of Polymers*, Arza Seidel, **2008**.

[614] B. R. Line, A. Mitra, A. Nan, H. Ghandehari, *Journal of Nuclear Medicine* **2005**, *46*, 1552-1560.

[615] A. Greß, Dissertation thesis, Universität Potsdam (Golm), **2008**.

[616] Y. Chujo, E. Ihara, H. Ihara, T. Saegusa, *Polymer Bulletin* **1988**, *19*, 435-440.

[617] K. Asano, S. Matsubara, *Organic Letters* **2009**, *11*, 1757-1759.

[618] D. W. MacDowell, J. M. Purpura, *The Journal of Organic Chemistry* **1986**, *51*, 183-188.

[619] O. Ceyhun, Diploma thesis, Johannes Gutenberg Universität (Mainz), **2018**.

[620] C. Schilling, T. Mack, S. Lickfett, S. Sieste, F. S. Ruggeri, T. Sneideris, A. Dutta, T. Bereau, R. Naraghi, D. Sinske, *Advanced Functional Materials* **2019**, *29*, 1809112.

[621] L. H. Cohen, A. I. Gusev, *Analytical and bioanalytical chemistry* **2002**, *373*, 571-586.

[622] P. O. Danis, D. E. Karr, F. Mayer, A. Holle, C. H. Watson, *Organic Mass Spectrometry* **1992**, *27*, 843-846.

[623] K. J. Wu, R. W. Odom, *Anal Chem* **1998**, *70*, 456A-461A.

[624] M. W. F. Nielen, *Mass Spectrometry Reviews* **1999**, *18*, 309-344.

[625] G. Montaudo, F. Samperi, M. S. Montaudo, *Progress in Polymer Science* **2006**, *31*, 277-357.

[626] S. F. Macha, P. A. Limbach, *Current Opinion in Solid State and Materials Science* **2002**, *6*, 213-220.

[627] A. J. Hoteling, W. J. Erb, R. J. Tyson, K. G. Owens, *Anal Chem* **2004**, *76*, 5157-5164.

[628] C. M. Guttman, S. J. Wetzel, W. R. Blair, B. M. Fanconi, J. E. Girard, R. J. Goldschmidt, W. E. Wallace, D. L. VanderHart, *Anal Chem* **2001**, *73*, 1252-1262.

[629] H. Günzler, H.-U. Gremlich, *IR-Spektroskopie: Eine Einführung*, John Wiley & Sons, **2012**.

[630] M. D. Krahling, R. Eliason, *Journal of Chemical Education* **1985**, *62*, 886.

[631] Z. Liu, M. D. Amiridis, *The Journal of Physical Chemistry B* **2005**, *109*, 16866-16872.

[632] I. M. Barszczewska-Rybarek, *Journal of Applied Polymer Science* **2012**, *123*, 1604-1611.

[633] J. L. Koenig, D. Kormos, *Applied Spectroscopy* **1979**, *33*, 349-350.

[634] M. Jöhnck, L. Müller, A. Neyer, J. Hofstraat, *Polymer* **1999**, *40*, 3631-3639.

[635] F. Dywan, B. Hartmann, S. Klauer, M. D. Lechner, R. A. Rupp, M. Wöhlecke, *Die Makromolekulare Chemie: Macromolecular Chemistry and Physics* **1993**, *194*, 1527-1536.

[636] E. K. Viljanen, M. Skrifvars, P. K. Vallittu, *Journal of applied polymer science* **2004**, *93*, 1908-1912.

[637] J. Blöhbaum, I. Paulus, A.-C. Pöppler, J. Tessmar, J. Groll, *Journal of materials chemistry B* **2019**, *7*, 1782-1794.

[638] C. H. H. Neufeld, C. S. Marvel, *Journal of Polymer Science Part A-1: Polymer Chemistry* **1966**, *4*, 2907-2908.

[639] K. Stancheva, *Oxidation Communications* **2008**, *31*, 758-775.

[640] P. Haney, K. Herting, S. Smith, *Separation Characteristics of Dialysis Membranes* **2013**.

[641] S. Feineis, Dissertation thesis, Julius-Maximilians-Universität (Würzburg), **2018**.

[642] S. Feineis, J. Lutz, L. Heffele, E. Endl, K. Albrecht, J. Groll, *Advanced Materials* **2018**, *30*, 1704972.

[643] E. A. Smith, W. D. Thomas, L. L. Kiessling, R. M. Corn, *Journal of the American Chemical Society* **2003**, *125*, 6140-6148.

[644] R. V. Weatherman, K. H. Mortell, M. Chervenak, L. L. Kiessling, E. J. Toone, *Biochemistry* **1996**, *35*, 3619-3624.

[645] F. S. Coulibaly, B.-B. C. Youan, *Biosens Bioelectron* **2014**, *59*, 404-411.

[646] A. Kussrow, E. Kaltgrad, M. L. Wolfenden, M. J. Cloninger, M. G. Finn, D. J. Bornhop, *Anal Chem* **2009**, *81*, 4889-4897.

[647] D. Diwan, K. Shinkai, T. Tetsuka, B. Cao, H. Arai, T. Koyama, K. Hatano, K. Matsuoka, *Molecules* **2017**, *22*, 157.

[648] R. Ramkumar, S. Chandrasekaran, *ChemistrySelect* **2018**, *3*, 2306-2310.

[649] P. W. Atkins, L. Jones, *Chemie-einfach alles*, Wiley-VCH, **2006**.

[650] G. Yilmaz, V. Uzunova, M. Hartweg, V. Beyer, R. Napier, C. R. Becer, *Polymer Chemistry* **2018**, *9*, 611-618.

Danksagung

Zu guter Letzt möchte ich mich ganz herzlich bei all denjenigen bedanken, die zum Gelingen der vorliegenden Arbeit beigetragen haben.

Großer Dank gebührt in erster Linie meinem Doktorvater Prof. Dr. Jürgen Groll, der mir überhaupt erst die Möglichkeit zur Durchführung dieser Doktorarbeit gegeben hat. Ich bin beeindruckt, welche großartigen Arbeitsbedingungen und eine außergewöhnliche Kommunikations- und Wertekultur er an unserem Institut geschaffen hat, bin dankbar für die beachtliche und ausgezeichnete Infrastruktur, von der ich profitieren durfte und dafür, dass mir die Teilnahme an Konferenzen und Kommunikations-/ Führungs-Seminaren ermöglicht wurde. Ich freue mich, dass ich meine Arbeit bei solch einem hervorragenden und reflektierenden Chef habe durchführen können, der mir nicht nur mit seiner fachlichen Kompetenz weiterhelfen konnte, sondern durch dessen Einflussnahme ich mich auch stets persönlich enorm weiterentwickelt habe. Vielen Dank für das interessante Thema der Arbeit, die entwickelnden Meetings und Gespräche sowie die professionelle, faire und sehr unterstützende Atmosphäre, die diese Promotion möglich gemacht hat.

Ebenfalls bedanken möchte ich mich bei meinen Kooperationspartnern Prof. Dr. Jürgen Seibel, Jürgen Mut und Julian Bechold für die innovativen Inputs und Ideen, den fachlichen Beistand und die gelungene und aussichtsreiche Zusammenarbeit, bei Ann-Christin Pöppler für die Hilfestellung in der NMR-Spektroskopie, sowie bei Thorsten Keller für all die großartige Hilfe und Unterstützung bei den SAW und SPR-Messungen. Mein Dank gilt außerdem auch Matze Stolte, der bei einem der vielfältigen Treffen auf und neben dem Lacrossefeld den Anstoß dazu gegeben hat, meine Arbeit in diesem AK aufzunehmen.

Ich möchte mich sehr bedanken bei dem herzlichen und aufgeschlossenen Führungskreis um Jörg, Andrea und Uwe, der Werkstatt mit Toni & Harald, bei Isabell und insbesondere bei dem jederzeit behilflichen Sekretariat mit Tanja, Eva und Birgit. Und nicht zuletzt auch bei meinen Laborpartnern/-innen, der Mittwochs-Burger-Crew, der Metttagessen-Runde, all den Arbeits- und Bürokollegen/-innen und dem Rest der FMZ-Mitarbeiter/innen, bei Jan, Jessi, Friederike, Franzi, Annika, Ilona, Johanna, Manuel, meiner Masterandin Bettina, Jean, Naomi, Viktoria, Leo, Jun, Christoph, Katrin, Michael, Alex, Berat, Carina, Jodie, Matze, Kai, meinem alten Masterarbeitsbetreuer Michi, Julia, Michaela und Willi, von denen ich einige unter anderem durch das PONTEA-Seminar noch einmal etwas besser kennenlernen durfte und die mir nicht nur den Arbeitsalltag schöner oder abwechslungsreicher gestaltet haben, sondern die auch an vielen Stellen zu meiner fachlichen und persönlichen Weiterentwicklung beigetragen haben.

Besonders bedanken möchte ich mich aber bei Ib, mit dem ich so viele perfekt kurze Mittagspausen genießen konnte, so viel Spaß bei fantastischen Inselverteidigungs- und League-of-Legends-Gelegenheiten hatte, der mich (vielleicht ohne es zu wissen) aufbauend und unterstützend durch einige schwierige oder anstrengende Phasen getragen hat, immer ein offenes Ohr hatte und mit dem ich viele spannende Diskussionen und Gespräche führen konnte. Danke dir, dass du dazu beigetragen hast, meine Zeit am FMZ noch um ein Erhebliches schöner zu gestalten!

Und selbstverständlich gilt mein Dank all den Menschen, die außerhalb des Instituts für mich da waren:

Bei meiner Familie, die bei jeder meiner Entscheidungen stets voll und vertrauensvoll hinter mir gestanden ist. Danke an Mama, dass ich darauf zählen kann, dass du jederzeit für mich da warst und sein wirst, an Papa, dass du mich immer bei all meinen Vorhaben unterstützt und unterstützt hast und an Anika, dass du mich immer wieder durch deine außergewöhnlichen Abenteuer überraschst - und dass ihr alle drei, jeder auf seine Weise, immer große und beeindruckende Vorbilder für mich wart und seid und mich so sehr auf meinem Weg geprägt habt. Danke auch an Susanne: Jedes Mal aufs Neue mit so viel Begeisterung bei gemeinsamen Unternehmungen empfangen worden zu sein, war immer etwas Besonderes.

Ich möchte mich bei Annika bedanken, die bei den vielen tiefsinnigen Gesprächen und Weinabenden den Anstoß dazu gegeben hat, parallel zu der Promotion eine Mediationsausbildung zu beginnen. Bei all den Freunden, den WueLAX-Unicorns und den Lamas, mit denen ich so unzählbar viele herrliche und außergewöhnliche Momente außerhalb des Labors erleben konnte[333],

und ohne Frage bei Anna,

die meine Arbeit vermutlich so gut kennt wie keine Zweite, mit der ich all die tollen, neuen, interessanten, wohltuenden, spannenden und grandiosen Erfahrungen gemacht habe, so viele Gespräche geführt, so viele Erlebnisse geteilt, so viel schöne Zeit verbracht habe, die mich beeindruckt, begeistert und unterstützt und immer für mich da ist und einfach eine unvergleichliche, wunderbare und einzigartige Person an meiner Seite ist.

Appendix

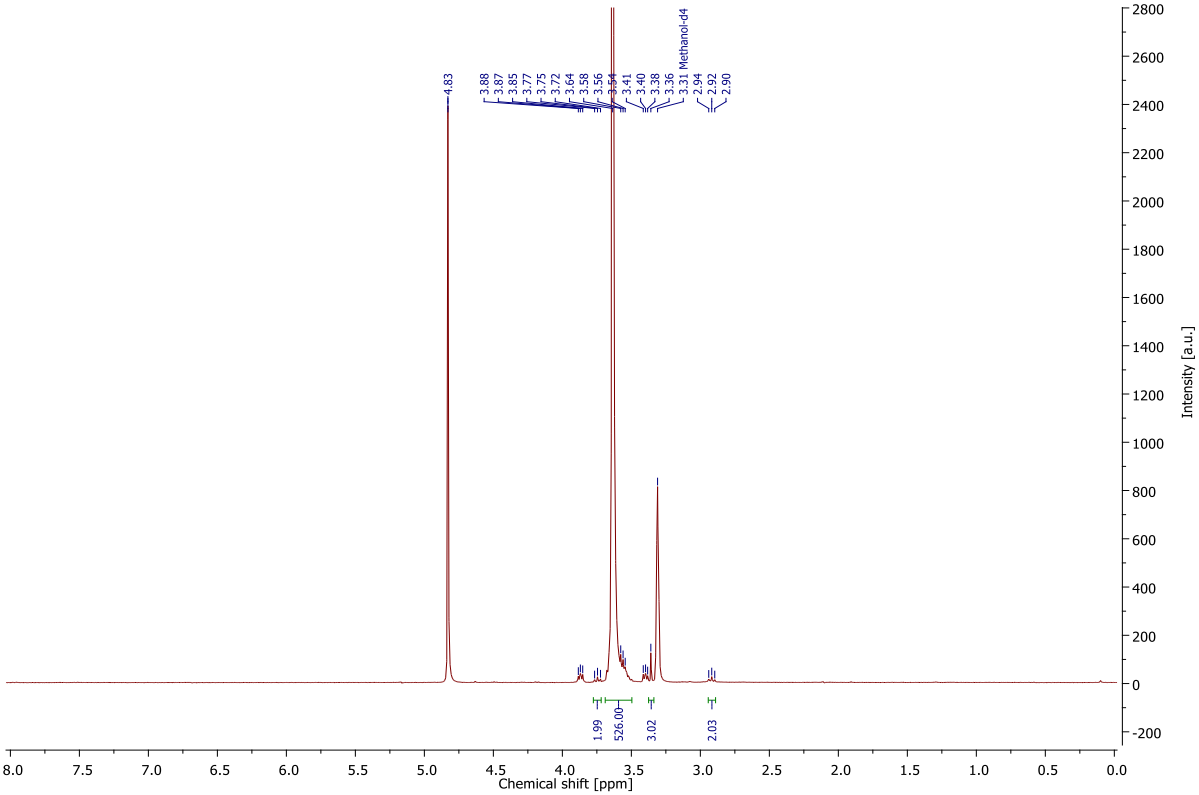

Figure 110: ^{1}H-NMR spectrum of conjugate between PEG-SH and allylpentafluorobenzene in MeOD.

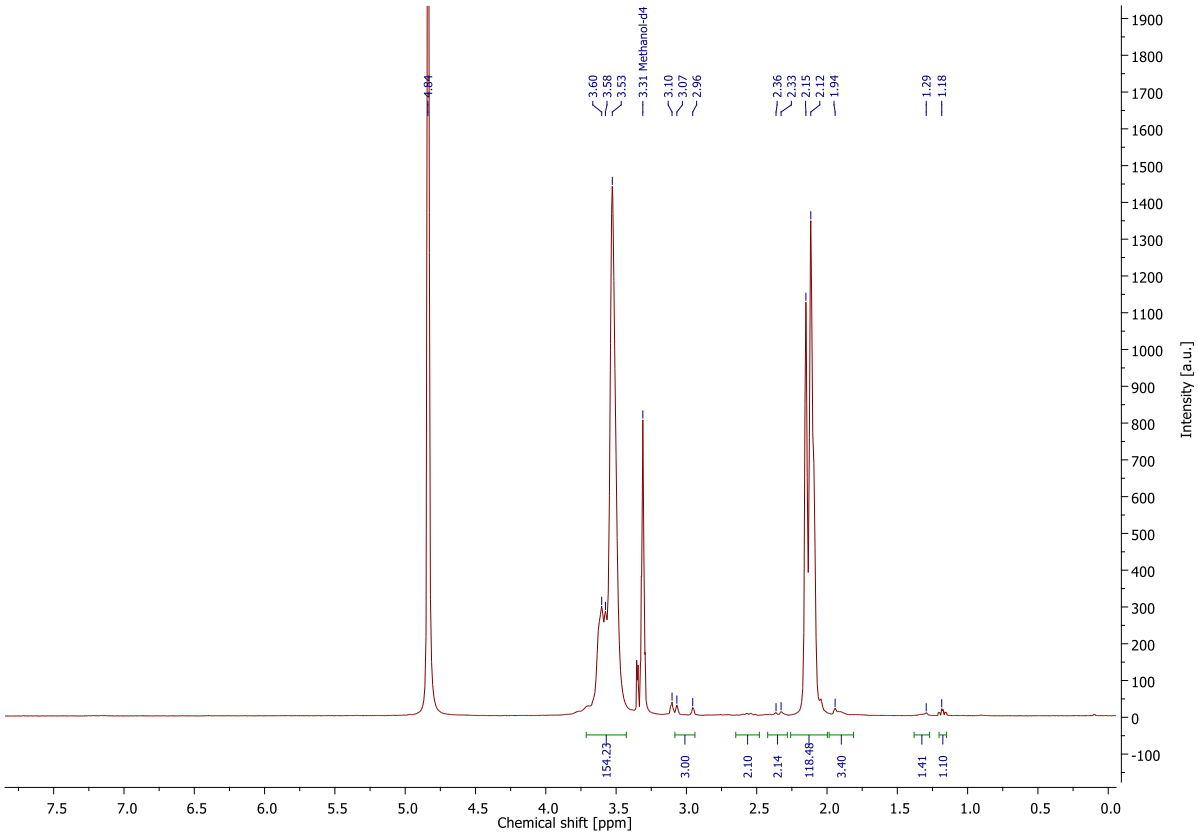

Figure 111: ^{1}H-NMR spectrum of PMeOx$_{38}$-SH in MeOD.

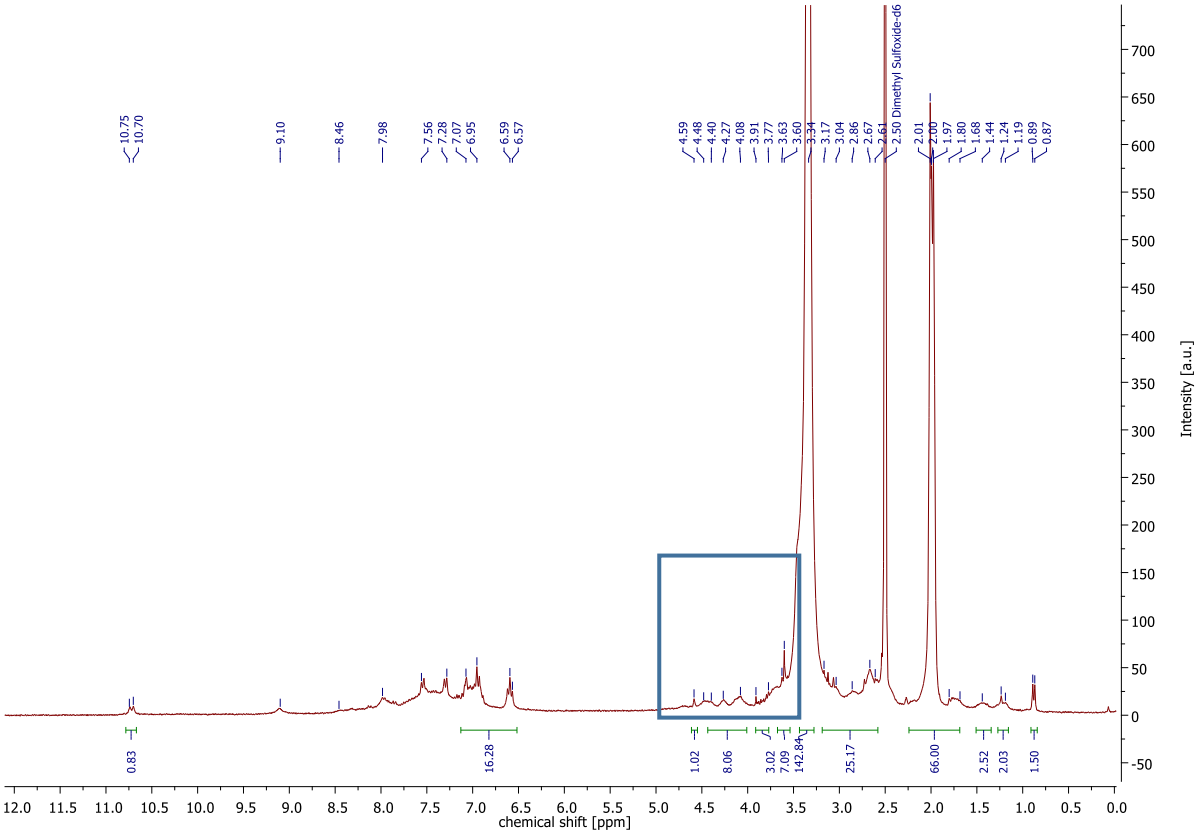

Figure 112: ^{1}H-NMR spectrum of Man-CGGWYKYW-PMeOx$_{20}$-SEt after dialysis in deuterated DMSO. The section discussed in chapter 4.2.5.1 is highlighted with a blue box.

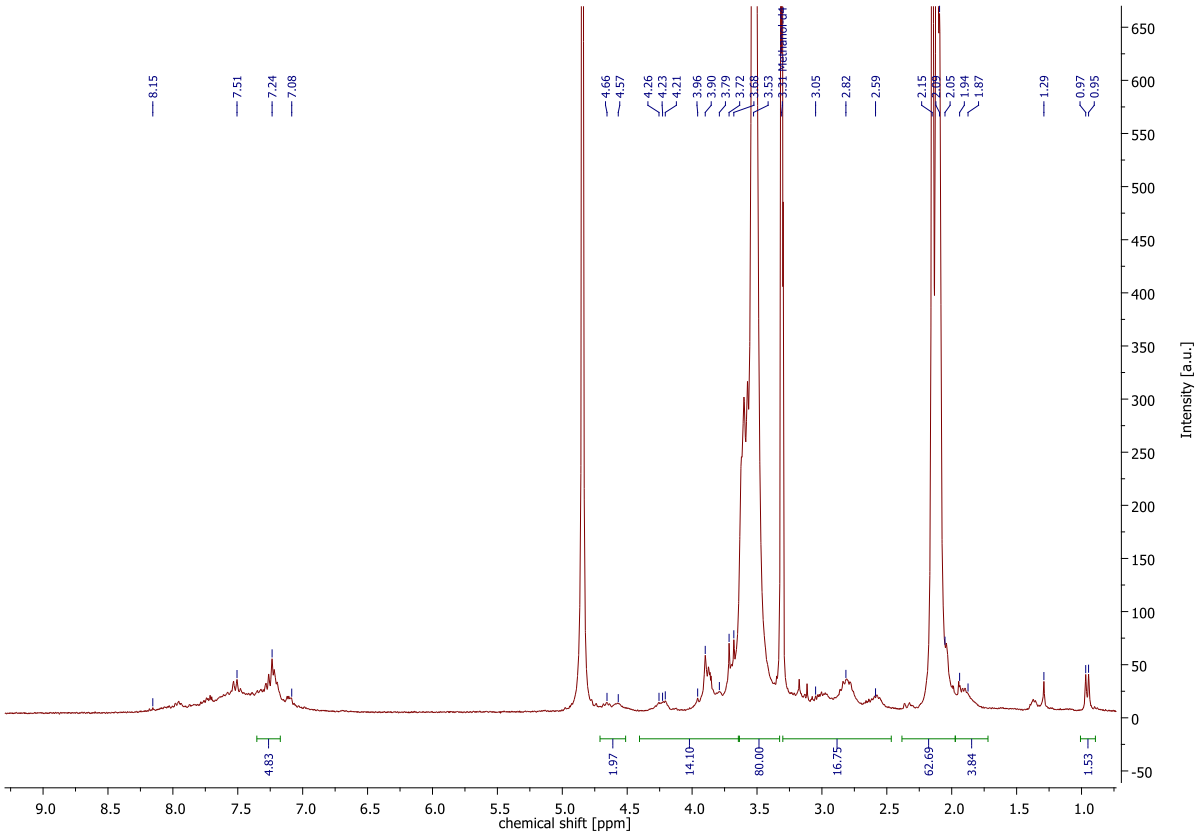

Figure 113: ^{1}H-NMR spectrum of Man-CGGGF-PMeOx$_{20}$-SEt after dialysis in MeOD.

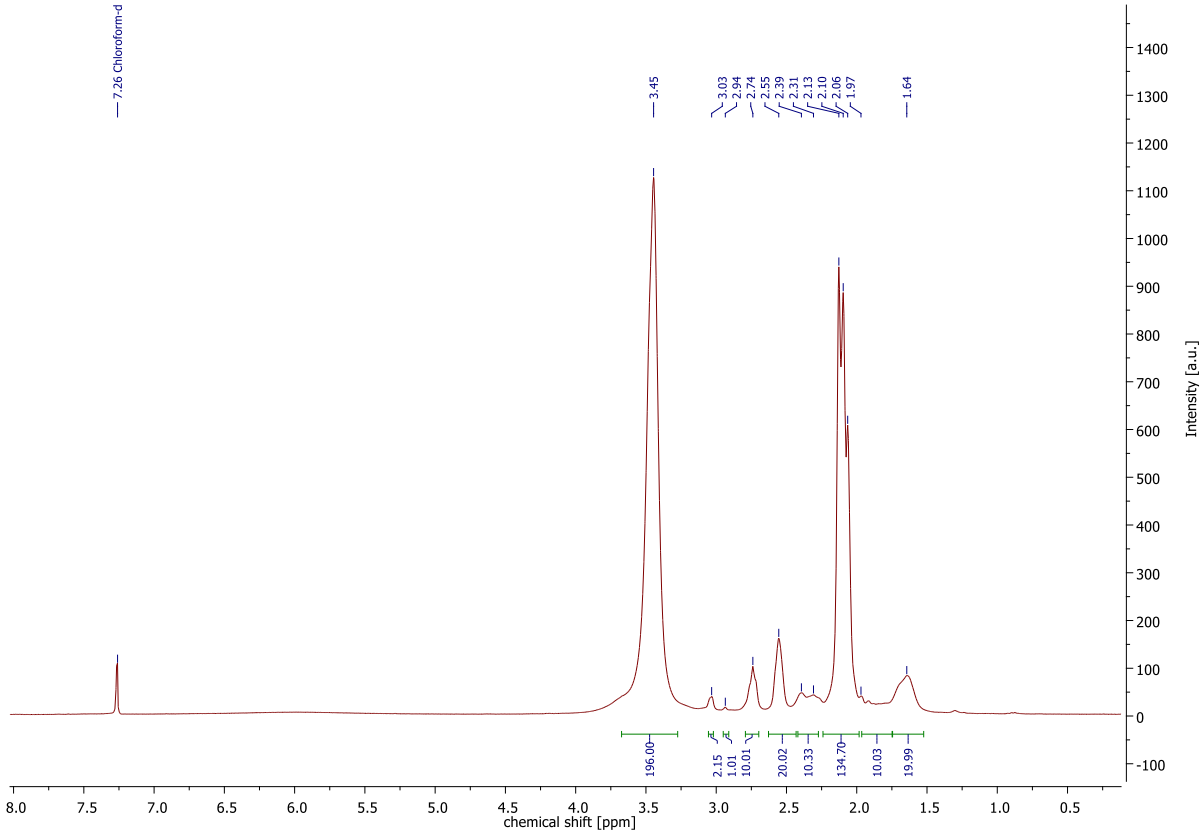

Figure 114: ^{1}H-NMR spectrum of P(MeOx$_{45}$-*co*-ButOx-COOH$_5$) after dialysis in $CDCl_3$.

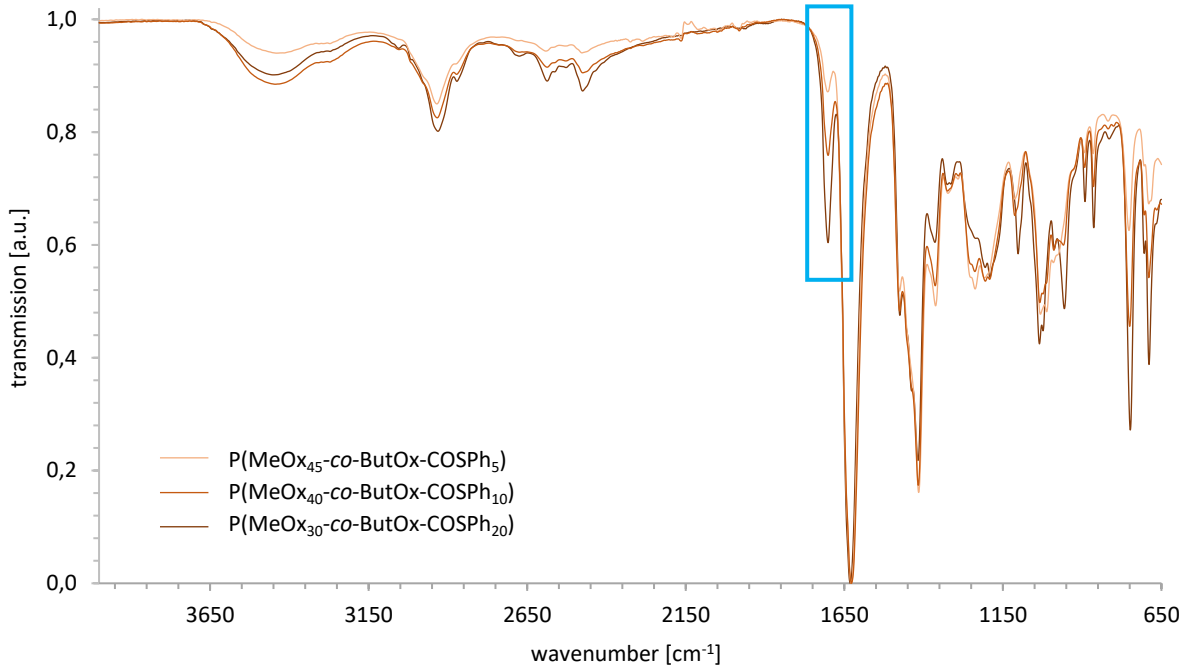

Figure 115: Superimposed IR spectra of 10 %, 20 % and 40 % thioester functionalized copolymers (light brown: P(MeOx$_{45}$-*co*-ButOx-COSPh$_5$), brown: P(MeOx$_{40}$-*co*-ButOx-COSPh$_{10}$), dark brown: P(MeOx$_{30}$-*co*-ButOx-COSPh$_{20}$)). The characteristic C=O stretching vibration of the thioester group at 1703 cm^{-1} is highlighted with a blue box. The strongest signal in each spectrum, the C=O stretching vibration of the polymer backbone, was taken as a reference.

q.e.d.